Functional Characterisation of *SLC2A3* and *PFKP* in t(8;21)-positive Acute Myeloid Leukaemia

Asmida Isa

089096958

Doctor of Philosophy

Wolfson Childhood Cancer Research Centre

Northern Institute for Cancer Research

Faculty of Medical Sciences, Newcastle University

June 2019

ABSTRACT

The translocation t(8;21) is the most prevalent chromosomal rearrangement in acute myeloid leukaemia (AML) and results in the expression of the oncogenic fusion protein RUNX1/ETO. The fusion protein is required for maintaining the leukaemic phenotype. Previous *in vivo* work identified genes related to glycolysis, namely *SLC2A3* and *PFKP* as potential transcriptional targets for RUNX1/ETO.

This project aimed to functionally investigate the role of *SLC2A3* and *PFKP* in RUNX1/ETO-driven leukaemia both *in vivo* and *in vitro.*

SLC2A3 significantly maintained the fitness of leukaemic cells under limited glucose and hypoxic conditions in the RUNX1/ETO-expressing Kasumi-1 cell line. Notably, *SLC2A3* knockdown impaired the competitive fitness of patient-derived xenograft (PDX) cells in high glucose and oxygen condition. Furthermore, *PFKP* knockdown results in loss of populations both *in vitro* and *in vivo*. Besides, double knockdown of *SLC2A3* and *PFKP* caused G1 cell cycle arrest and had a greater effect in impairing leukaemic cell propagation and fitness when compared to the single knockdowns.

Moreover, RUNX1/ETO-expressing cells showed to have a high sensitivity towards 2-deoxyglucose (2DG). 2DG is an analogue of glucose molecule that blocks glycolysis upstream of PFKP. RUNX1/ETO cells treated with this inhibitor undergo apoptosis associated with the overall decrease in cell number. The combination of 2DG and cell cycle inhibitor, palbociclib led to an additive effect and severely impaired expressions of genes in the glycolysis pathway.

Collectively, the oncogenic fusion protein, RUNX1/ETO shows dependency on glycolysis through *SLC2A3* and *PFKP*. Targeting these two genes may instruct new treatment strategies with reduced toxicity in t(8;21) leukaemia.

DEDICATION

To

My husband,

my parents

and

my siblings.

ACKNOWLEDGEMENTS

First and foremost, I would like to express my sincere gratitude to Professor Dr Olaf Heidenreich, my academic supervisor, for his continuous support, patience, motivation and immense knowledge. Without his supervision, this thesis would not have been completed. His guidance and scientific mentorship during this PhD journey will always be a life-long example and inspiration to me.

Secondly, my thanks go to Natalia. Although Natalia is not in the OTH group anymore, she helped me massively at the beginning of my candidature.

Next, I want to thank the key OTH members who have helped me in so many ways: Helen, who had helped me with the *in vivo* work, as well as helping me checked the relevant chapters in my thesis; Hesta, from whom I learnt a lot about flow cytometry, and for telling me stories about Jack, Japhy, Kip, Gus and Bear to boot; Ed for kindly and swiftly checking and correcting my chapters, and for all his suggestions too; Deepali who taught me about the feeder cells as well as reviewing my chapters; Kasia who checked my chapters and gave me a lot of suggestions; and Mojgan who have helped me check through my chapter even though she was on leave. I would also like to thank Lynsey for the support during the hard time.

Likewise, I would like to give my thanks to Yuzhe, Hasan, Ricky, Melanie (she checked a chapter too!) and Milene for those discussions during our late tea time and for their continuous encouragement. Moreover, I also would like to thank Saimir and Jill who have assisted me with the *in vivo* work.

Finally, thanks to all the current and past members of the OTH group.

"Jadilah seperti padi, semakin tunduk semakin berisi,

semakin berilmu, semakin merendah diri"

TABLE OF CONTENTS

LIST OF FIGURES

LIST OF TABLES

LIST OF ABBREVIATIONS

2DG	2-deoxyglucose
AML	Acute Myeloid Leukaemia
ATP	Adenosine triphosphate
cDNA	complementary DNA
CI	Combination Index
CLPs	Common lymphoid progenitors
CMPs	Common myeloid progenitors
EC	Effective concentration
F-1,6-BP	Fructose-1,2-biphosphate
F-1-P	Fructose-6-phosphate
F-2,6-BP	Fructose-2,6-biphosphate
FDG-PET	Fluorodeoxyglucose positron emission tomography
Fwd	Forward
GI	Growth inhibition
HK	Hexokinase
HSCs	Haematopoietic stem cells
IF	Intrafemoral
IP	Intraperitoneal
IV	Intravenous
IVIS	In vivo imaging
LB	Lysogeny broth
LDH	Lactate dehydrogenase
LSCs	Leukaemia initiating cells
LT-HSCs	Long-term haematopoietic stem cells
miRNA	micro-RNA
MPPs	Multipotent progenitors
MRC	Medical Research Council
NEAA	Non-essential amino acid
O-GlcNAc	O-linked β-N-acetylglucosamine
OS	Overall survival
OXPHOS	oxidative phosphorylation
PBS	Phosphate buffer saline
PDX	Patients derived xenograft
PFA	Paraformaldehyde
PFK-1	Phosphofructokinase-1
PFK2/FBPases	Fructose-2,6-biphospahatases
PI	Propidium iodide
PPP	Pentose phosphate pathway
PS	phosphatidylserine
RHD	Runt homology domain
RISC	RNA induced silencing complex
RNAi	RNA interference
ROS	Reactive oxygen species
RT-PCR	Real-time polymerase chain reaction
Rv	Reverse

SCID	Severe combined immunodeficiency
SDS-PAGE	Sodium dodecyl sulfate polyacrylamide gel electrophoresis
shRNA	short-hairpin RNA
siRNA	small interfering RNA
ST-HSCs	Short-term haematopoietic stem cells
TBHP	tert-butyl hydrogen proxide
TCA	Tricarboxylic acid
TKD	Tyrosine kinase domain

Chapter 1 : Introduction

1.1 Haematopoiesis

Haematopoiesis is the process of blood cell formation from the haematopoietic stem cells (HSCs), to provide 10^{12} new blood cells each day in an average human adult. The process begins in the yolk sac and progresses temporarily to the liver, before finally residing in the bone marrow and thymus (Huyhn et al., 1995). During embryonic development, there are two waves of haematopoiesis that take place. The first wave is called primitive haematopoiesis, which involves the development of erythroid progenitors to erythrocytes and macrophages in the yolk sac. The early rise of erythrocytes is to provide tissue oxygenation during the rapid growth of an embryo. The second wave is known as definitive haematopoiesis, which involves the generation of mature blood cell types from HSCs. The early experiments with human embryos confirm HSCs originate from haemangioblast precursor cells in the Aorta-Gonad-Mesonephros, that move toward the ventral aorta and give rise to the haematopoietic progenitor cells and endothelial cells (Tavian M., 2010, Huyhn et al., 1995, Ivanovs et al., 2011).

HSCs constitute only 0.05% to 0.1% of total bone marrow cells (Yang et al., 2005) and are maintained by long-term HSCs (LT-HSCs) that have the ability to self-renew and maintain pluripotency. This sub-population of HSCs remains quiescent and dormant throughout the lifetime of an organism (Ito and Suda, 2014).

The second sub-population of HSCs is short-term HSCs (ST-HSCs) that have restricted self-renewal capacity. ST-HSCs give rise to multipotent progenitors (MPPs) cells for 4-12 weeks before senescence (Colvin et al., 2009).

MPPs are described as highly proliferative, exhibit more robust differentiation activity (Morrison et al., 1997) and lack of self-renewal capacity. MPPs differentiate into two types of multipotent cells; common myeloid progenitors (CMPs) and common lymphoid progenitors (CLPs). CLPs give rise to restricted lymphoid lineages, while CMPs differentiate into a more morphologically, functionally and phenotypically distinct subset of cell types that include granulocytes, monocytes, macrophages, erythrocytes, megakaryocytes and mast cells.

In contrast to the classical model of haematopoiesis, recent studies revealed that HSCs are heterogeneous: they have continuous lineage segregation characteristics. HSC heterogeneity is described as a single cell of HSCs exhibits diverse molecular signatures, cellular fate and functional outcome to preferentially produce specific

lineage (Copley et al., 2012, Crisan and Dzierzak, 2016, Zhang et al., 2018b). This new concept proposes the origin of leukaemia to be from HSCs as well as disease resistance and relapse.

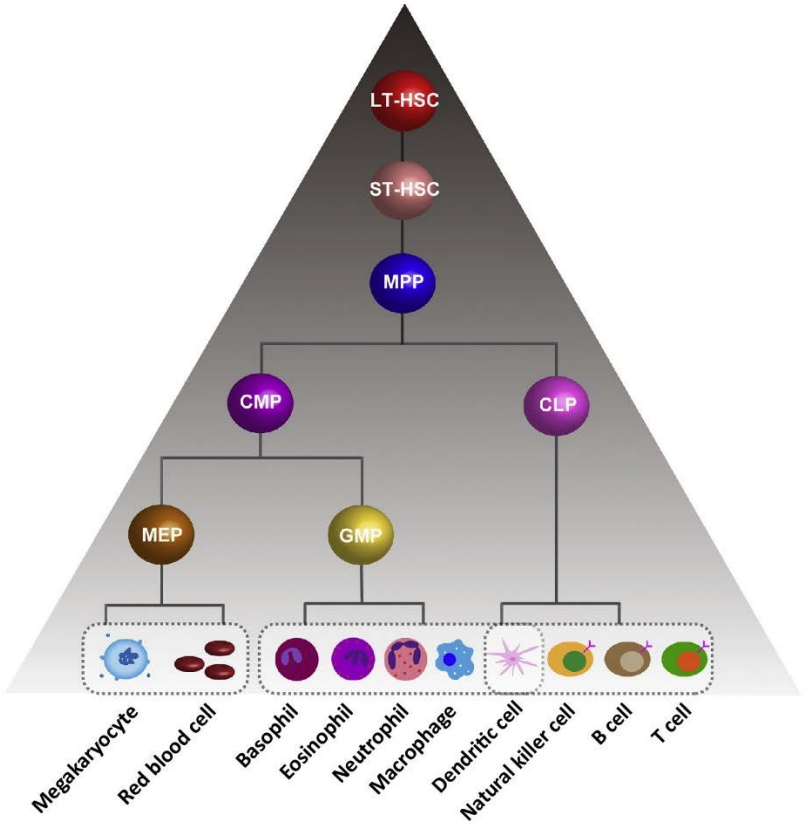

Figure 1-1: Hierarchical organisation of the haematopoietic system. Long-term haematopoietic stem cell (LT-HSC) resides at the peak of the system and undergoes self-renewal or sequential multilineage differentiation to produce lineage-specific blood cells in the body. Adapted from Zhang et al. (2018b).

1.2 Acute Myeloid Leukaemia (AML)

Acute myeloid leukaemia (AML), also called acute myelogenous leukaemia and acute myeloblastic leukaemia, is an aggressive malignancy of myeloid progenitor cells. It is highly heterogeneous with respect to the chromosomal abnormalities, gene mutations and changes in expression of genes and microRNAs. AML starts with the clonal transformation of defective myeloid precursor cells in the bone marrow. These cells lose their ability to differentiate but manifest the proliferative and survival ability. The abnormal differentiation of myeloid cells results in an immature population of marrow elements in the bone marrow and peripheral blood, thus increasing the risk

of fatal infection, severe bleeding and other symptoms such as anaemia. The development of AML is fast and fatal within a short period if no treatment is provided.

1.3 Epidemiology

In 2013 to 2015, approximately 3000 new cases of AML and 2600 deaths were reported every year in the UK with higher incidence observed in male (Figure 1-2) (Cancer Research UK). The incidence of AML increases with age and ranges from 0.7% to 3.9% cases per 100,000 between 0-60 years old. Whereas, for people aged 60 years and above, the incidence increases to between 6.7 and 19.2 cases in 100 000 people (Schoch et al., 2001).

Childhood AML constitutes 15 to 20% of paediatric leukaemia cases (Reedijk et al., 2018). The five-year overall survival (OS) for childhood AML has improved greatly from 40% in the early 1990s to more than 70% in 2010-2015 (Kaspers et al., 2013). However, a significant 30 to 40 percent of patients relapse and within this patient subgroup, the five-year OS is 16-34% (Kaspers et al., 2013, Abrahamsson et al., 2007).

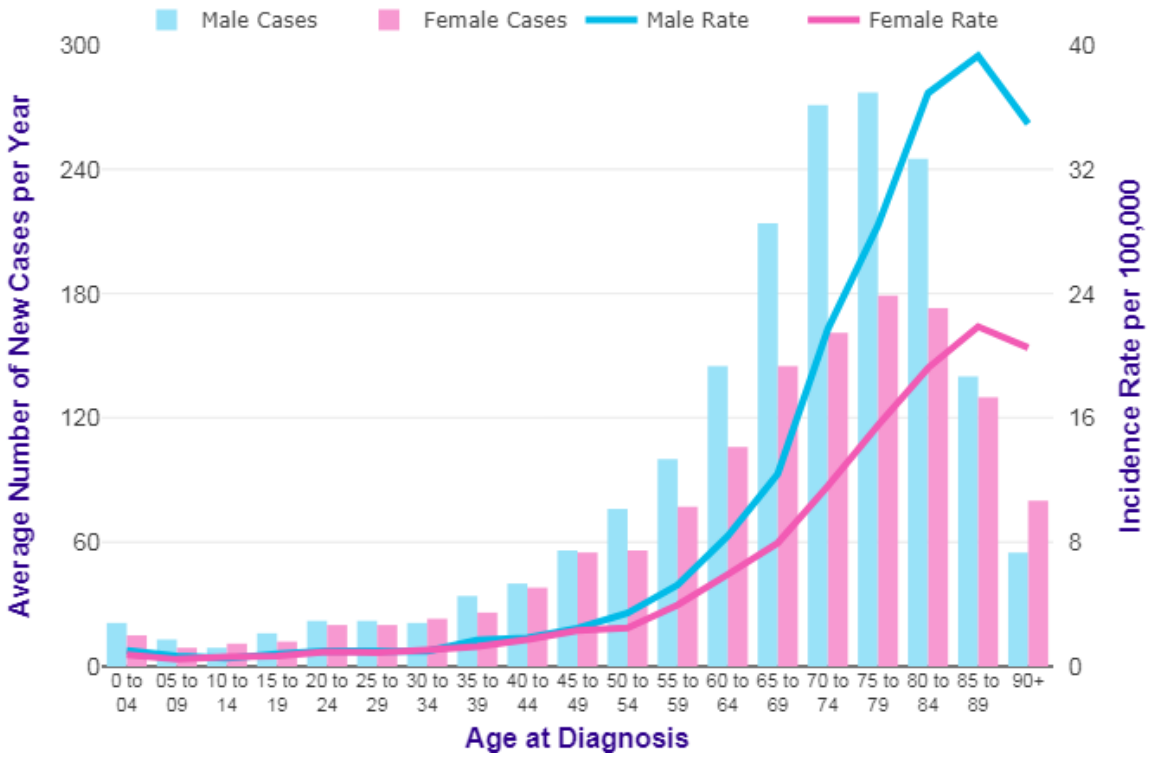

Figure 1-2: Incidence of AML in the UK per year. The average number of new cases detected per year and age-related incidence rate in 100 000 population. Adapted from Cancer Research UK.

1.4 AML and cytogenetics abnormalities

Cytogenetic abnormalities can be detected in 50-60% of newly diagnosed AML patients (Kumar, 2011). This feature remains the most important prognostic indicator for remission rate, relapse and OS. The most recurrent cytogenetic abnormality in AML is the t(8;21), which is found in 15-20% of AML patients and is considered to have a favourable prognosis. Other karyotypic abnormalities that are in the favourable prognostic group are t(15;17), inv(16) and t(16;16) (Grimwade et al., 2010, Mrózek and Bloomfield, 2012).

Based on the Medical Research Council (MRC) classification, complex karyotype abnormalities that contain more than four unrelated abnormalities are considered as poor prognosis group (Grimwade et al., 2010). Among the poor prognostic groups are monosomies of chromosome 5, 7 and 17. Abnormalities related to chromosome 3, which are inv(q21;q26.2) and t(q21;q26.1) are also associated with the adverse risk (Yi et al.). However, a balanced rearrangement of t(3;5)(q21~25;q31~35) and the normal karyotype are classified into intermediate risk group (Grimwade et al., 2010).

1.5 The mutational landscape of AML

Approximately 40% to 50% of AML patients present with a normal karyotype (Kumar, 2011). This subgroup of AML is classified into the intermediate-risk group, but not all patients have the same response to treatment. This is likely due to the large variabilities in gene mutations and expression in this subset of patients. Recent advanced genetic screens have allowed the detection of mutations that could be the driver of AML. These alterations were classified into two categories, Class I and II.

1.5.1 *Class I*

Class I is comprised of mutations that modulate signal transduction pathways and result in increased proliferation and survival of leukaemia. Class I mutations include *KIT, FLT3* and *RAS.*

KIT mutation. The *KIT* gene, located on chromosome 4q11-12, encodes a 145 kD type III receptor tyrosine kinase. The KIT protein has five extracellular-kinase domains, a juxtamembrane domain and an intracellular kinase domain. Activation of its ligand by stem cell factors sends proliferative signals and is important in haematopoiesis (Wakita et al., 2011) (Rönnstrand, 2004). In the t(8;21) patients, *KIT*

activating mutation contributed to significantly lower 5-year OS than patients without *KIT* mutation (P-value < 0.001, 5-year, 26.5%-with *KIT* vs 60.9%-non *KIT*) (Park et al., 2011). The same observations were also seen in favourable prognosis group inv(16). *KIT* activating mutation caused higher incidence of relapse (P = 0.05; 5 year, 56%-*KIT* v 29%-non *KIT*) and significantly lower survival (P=0.009; 5 year, 36%-*KIT* vs 62%-non *KIT*) (Paschka et al., 2006).

FLT3 mutation. Fms-like tyrosine kinase 3 (FLT3) is a receptor tyrosine kinase that functions in cell survival, proliferation and differentiation of haematopoietic cells. There are two major activating mutations which are internal tandem duplication (ITD) mutations of the juxtamembrane region and point mutations in the tyrosine kinase domain (TKD). Both mutations cause constitutive tyrosine kinase activity in the absence of ligand. *FLT3* mutations occur in approximately 30% of AML and the incidence increases with age. *FLT3* mutations confer poor prognosis in AML patients (Kumar, 2011).

RAS mutation. Mutations in NRAS present in 8-13% of AML cases, while *KRAS* can be found in 2% of adult AML and 9% in children with AML (Al-Issa and Nazha, 2016). Both *NRAS* and *KRAS* mutations did not show any impact on OS of AML patients (Al-Issa and Nazha, 2016, Bowen et al., 2005).

1.5.2 *Class II*

The Class II comprises mutations that affect the transcription factors or components of the cell cycle machinery which include *RUNX1, CEBP-α* mutations and MLL rearrangement.

RUNX1 mutation. RUNX1 is a transcription factor that plays critical roles in haematopoiesis. *RUNX1* mutations are found in 6% to 30% of AML cases (Schnittger et al., 2011, Zhang and Rowley, 2013). Mutations in the RUNX1 gene bestows an unfavourable prognosis (Takahashi, 2011).

CEBP-α mutation. CEBP-α is a transcription factor that is crucial for the differentiation of granulocytes. Mutations in the *CEBP-α* gene are found in 5% to 14% of AML cases (Lin et al., 2005). *CEBP-α* mutations are considered to impart a good prognosis even when associated with FLT3-ITD positive patients (Marcucci et al., 2008, Takahashi, 2011). When compared with wild-type *CEBP-α*, mutations in *CEBP-α* seem to have an improved rate of complete remission (p = 0.06, 5-year,

93% vs. 77%) and OS (p = 0.002, 5-year, 58% vs. 27%). However, hitherto it is still unclear the reason why *CEBP-α* mutation confers a good prognosis.

Recently, new mutations were discovered that did not fit in either Class I or II, thus making the classification of AML mutations and genomic abnormalities even more complex (Figure 1-3). For example, mutations in *Tp53* are strongly correlated with complex karyotypes (Ferrari et al., 2014) and drug resistance (Kadia et al., 2016). p53 is related to stress-inducing signals to different anti-proliferative cellular responses such as DNA damage (Zilfou and Lowe, 2009). Another example, a *DNMT* activating mutation that results in substitution of the amino acid arginine with histidine (R882H) is found in 60% of AML cases (Kim et al., 2013). The mutation leads to a lower OS in AML patients with mutant *DNMT* compared to patients without the mutation (median: 7.0 months vs 19.5 months, P = 0.004)(Yan et al., 2011).

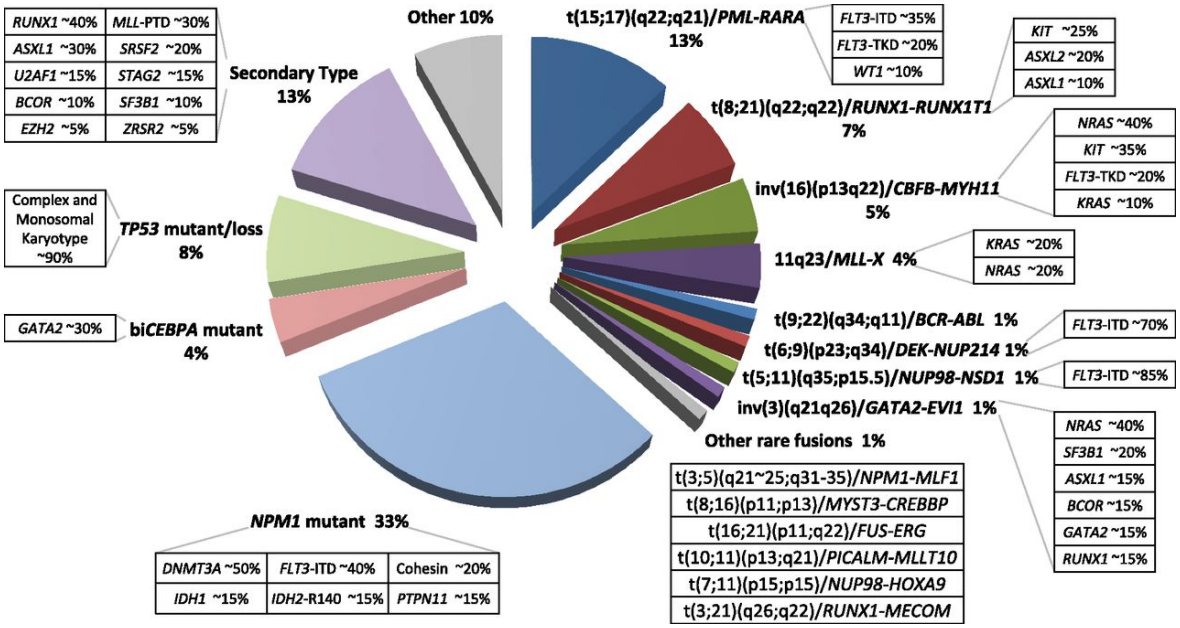

Figure 1-3: Distribution of cytogenetically and molecular subsets of AML. For each cytogenetically defined subset of AML denoted in the pie chart, frequent associated cooperating mutations are shown in the respective boxes. Mutational frequencies are derived from the integration of data from previous studies. Adapted from (Grimwade et al., 2016).

1.6 AML with t(8;21)

The translocation in t(8;21)(q22;q22) was first discovered by (Rowley) in 1973, and is the most common karyotypic abnormality, presenting in 15-20% of all AML cases (Figure 1-4) (Lam and Zhang, 2012, Miyoshi et al., 1993). It is usually reported as core-binding factor (CBF) AML and is closely associated with the AML-M2 subtype (French-American-British Classification). This subtype of AML is generally associated with a better clinical outcome; but, the prognosis worsens with age (Reikvam et al., 2011, Vardiman et al., 2002). Ten-year survival rates for this subtype of leukaemia are more than 70% when using standard chemotherapy treatments (Thomas and Majeti, 2017).

In this chromosomal rearrangement *RUNX1* (also known as *AML1*), which is originally located on chromosome 21, fuses to the *ETO* gene (also known as *RUNX1T1* or *MTG8)* on chromosome 8 and vice versa (Figure 1-4). However, only *RUNX1/ETO* expression is detectable in t(8;21) patients (Peterson et al., 2007a). The breakpoints occur in intron 5 of the *RUNX1* gene locus and either intron 1a or 1b of the *ETO* gene (Miyoshi et al., 1991, Lam and Zhang, 2012). This chimeric gene generates a fusion protein, RUNX1/ETO, containing 752 amino acids: 128 amino acids found on the N-terminal of Runt domain of RUNX1 and almost the entire ETO protein.

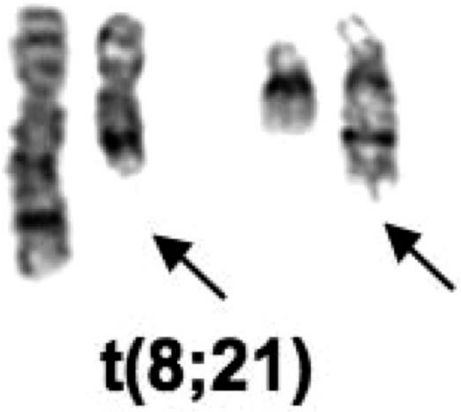

Figure 1-4: Chromosomal rearrangement involving chromosome 8 and 21 discovered by Rowley (1973). The q22 arm of chromosome 21 translocates to q22 arm of chromosome 8.

1.6.1 *RUNX1*

RUNX1 is a transcription factor that belongs to the Runt-related transcription factor family. From twelve currently identified RUNX1 isoforms resulting from alternative splicing, there are three that are well-described; RUNX1A consists of 250 amino acids, RUNX1B consists of 453 amino acids and RUNX1C consists of 480 amino acids (Figure 1-5-A). Both RUNX1A and RUNX1B have the same proximal start but differ in the carboxyl terminal. RUNX1C has the same carboxyl terminus with RUNX1B but has 32 amino acids encoded by an alternative exon at the distal N-terminus. Each isoform functions in different tissues and haematopoietic stages. For instance, RUNX1A is primarily found in CD34+ progenitor populations in human cord blood and are able to potentiate engraftment in mice (Tsuzuki et al., 2007). While RUNX1B drives neutrophil proliferation and differentiation, RUNX1C functions in lymphocytes definitive differentiations (Telfer and Rothenberg, 2001).

These three isoforms share the same N-terminal region that contains 128 amino acids: Runt Homology Domain (RHD) (Figure 1-5-B) (Sood et al., 2017). The RHD is required to facilitate binding of RUNX1 to DNA and interacts with its heterodimerisation partner, core-binding factor beta (CBFβ) (Lam and Zhang, 2012). The heterodimerisation complex of RUNX1-CBFβ increases the DNA-binding affinity of RUNX1 (Lam and Zhang, 2012). Besides the complex formation with CBFβ, RUNX1 also co-operates with other transcription factors and transcriptional co-regulators.

RUNX1B and RUNX1C share another domain, namely TAD, which contains activating and inhibitory domains that interact with several activator and repressor proteins (Sood et al., 2017). Moreover, RUNX1 mediates transcriptional activation through a 31 amino acid region namely nuclear matrix targeting signal (NMTS) located at the C-terminal region (Lam and Zhang, 2012, Sood et al., 2017). Furthermore, VWRPY motifs are conserved in Runt family members at the last 5 amino acids of the C-terminus (Sood et al., 2017).

RUNX1 is essential in determining the fate of HSCs in haematopoiesis. In mouse development, *Runx1* was detected in both primitive and definitive haematopoiesis (North et al., 1999). Further studies also showed that *Runx1*-deficiency shortened the lives of mice and caused severe haemorrhaging along the central nervous system when compared to healthy heterozygous mice (Wang et al., 1996, Okuda et al.,

1996). The extreme haemorrhaging may be caused by a lack of angiopoietin-1 expression, as the *ANGPT1* gene is one of the genes regulated by RUNX1 (Takakura et al., 2000).

In adults, RUNX1 plays a role in both haematopoiesis and HSC-niche interaction. *Runx1*-knockout mice display an accumulation of a putative HSC population, myeloid progenitors but a lack of thrombocytes and lymphocytes (Ichikawa et al., 2004, Growney et al., 2005, Ichikawa et al., 2008). Furthermore, Runx1 is required to maintain *Cxcr4*, a gene involved in stem cell homing and niche interactions in HSCs (Jacob et al., 2010). Notably, there are two RUNX1 binding sites in the *CXCR4* promoter region (Jacob et al., 2010). RUNX1 interacts with target genes in various blood types. In the myeloid lineage, RUNX1 directly interacts with the promoters of genes related to myeloid growth factor signalling; *IL-3, GM-CSF, M-CSF* and *c-MPL* (Lam and Zhang, 2012, Satoh et al., 2008, Cameron et al., 1994, Takahashi et al., 1995) as well as to the enzyme involved with myeloid functions such as myeloperoxidase, neutrophil elastase and mast cell protease 6 (Ogihara et al., 1999, Nuchprayoon et al., 1994, Lam and Zhang, 2012). In the T-cell lineage, RUNX1 directly binds to the promoters and enhancers of T-cell receptors (Ryuji Uchino)(Sun et al., 1995). In the B-cell lineage, RUNX1 interacts with B-cell specific src family tyrosine kinase promoters known as *blk and Iga* and the immunoglobulin antigen receptor enhancers (Lam and Zhang, 2012, Erman et al., 1998, Zhang and Derynck, 2000).

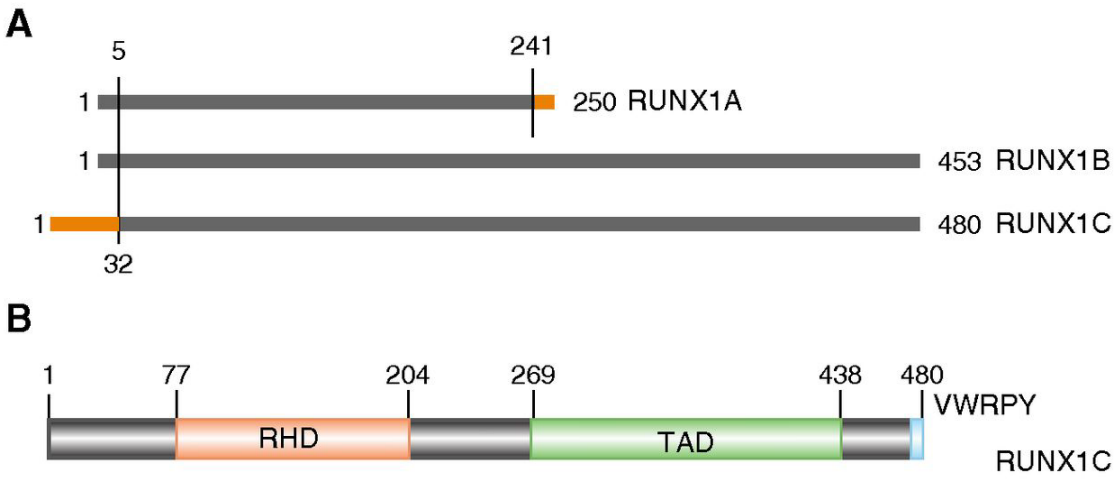

Figure 1-5: RUNX1 isoforms. A) The three major isoforms of RUNX1 (1A, 1B and IC). B) The domains of RUNX1C. The three isoforms share an RHD domain at the N-terminal, but only RUNX1B and RUNX1C have the TAD and VWPRY motif at C-terminal. Adapted from Sood et al., (2017).

1.6.2 *ETO*

ETO (Eight-twenty-one), also known as MTG8 or CBFA2T1, was first identified in translocation breakpoints in t(8;21) acute myeloid leukaemia (Miyoshi et al., 1993, Miyoshi et al., 1991). *ETO* expression is relatively low in haematopoietic tissues as *ETO-RUNX1* transcripts are not detectable in t(8;21) patient samples (Peterson et al., 2007b). Mice with *Eto* knockout showed normal haematopoiesis and no expression was detected in hematopoietic cells (Calabi et al., 2001). Instead, *Eto* is found highly expressed in the gut, as well as in the brain, suggesting important roles for ETO within these two organs (Sacchi et al., 1998, Calabi et al., 2001). ETO expression is also detected in the heart, pancreas and skin (Nathan Davis, 2003).

ETO shares 50-70% of Nervy homology region (NHR) similarities with *Drosophila* numbered 1 through 4 (Figure 1-6) (Davis et al., 2003). Briefly, NHR1 has sequence similarities with TATA-binding protein-associated factors, including human TAF105 and TAF130 and Drosophila TAF110 (Lam and Zhang, 2012). Similarities of these NHR1 domains gave rise to an early idea that ETO functions as a transcription factor. NHR2 is often referred to as a hydrophobic heptad repeat (HHR) due to an amphipathic amino acid sequence (Liu et al., 2006). It can mediate both alpha-helical tetramer formation and homo- and hetero-oligomerisation of ETO and its other family members, including ETO2 (MTG16) and MTGR1 (Liu et al., 2006). The alpha-helices align in a head to tail manner to form an anti-parallel dimer, through hydrophobic and ionic interactions and positioned on top of each other like a sandwich. This structure produces an extremely stable ETO tetramer and is thought to contribute to RUNX1/ETO stability (Liu et al., 2006). NHR2 was also shown to contain histone deacetylases (HDAC) contact site (Amann et al., 2001, Hildebrand et al., 2001, Lutterbach et al., 1998). NHR3 contains a coiled-coil motif, which has structural homology with PKA anchoring proteins and binds to a regulatory subunit of type II cyclic AMP-dependent protein kinase (PKA RIIalpha). NHR3 may interact with subsequent adjacent NHR domains (Lam and Zhang, 2012). NHR4, also known as the myeloid-Nervy-DEAF1 (MYND) domain, has zinc chelating motif (Lam and Zhang, 2012).

These NHR domains have in common the ability to interact with other proteins and thus define the function of ETO. For example, NHR1 facilitates binding with E proteins and inhibits the ability for E proteins to recruit co-activator molecules like p300/CBP (Lam and Zhang, 2012). Furthermore, both NHR2 and NHR4 interact with

co-repressors NCOR/SMRT (Zhang et al., 2004a). NHR2 also binds with other co-repressors such as mSin3a and HDACs (Kitabayashi et al., 1998).

ETO also contains a nuclear localisation signal (NLS) within amino acids 241-280, located between NHR1 and 2 domains. A NLS is required for nuclear localisation; however, no functional roles have been defined thus far (Davis et al., 2003).

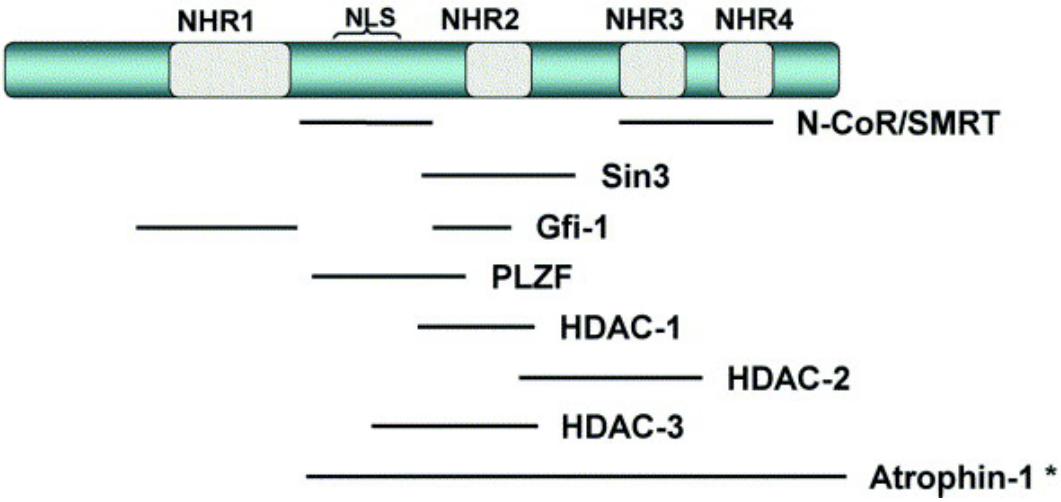

Figure 1-6: Schematic depiction of ETO and its protein interaction domains. A map of ETO is shown with NHR1–4 indicated as shaded regions. Some of the interacting corepressors are listed with the corresponding ETO-interaction domains underlined. Adapted from Davis, 2003 #614.

1.6.3 *RUNX1/ETO*

As a result of the translocation, almost the entire ETO protein replaces the C-terminal RUNX1 domains, creating a large 752 amino acid sequence. The RUNX1/ETO fusion protein keeps the N-terminal DNA-binding RHD domain of RUNX1 and loses the C-terminal of RUNX1, which is then replaced by C-terminal functional domains of the ETO protein. As in normal function of RUNX1, the resulting RUNX1/ETO fusion protein also binds to DNA through RHD, but interferes with transcriptional activation through ETO's interaction with co-repressors.

There are several isoforms of *RUNX1/ETO* transcripts detected in t(8;21) patient samples, but most studies focus on the full-length RUNX1/ETO. RUNX1/ETO on its own cannot induce leukaemia, as shown in several models. RUNX1/ETO expression in human CD34+ cells did not cause leukaemia in mice (Mulloy et al., 2002, Mulloy et al., 2003). This was also demonstrated in patients' samples who had RUNX1/ETO

transcripts in their neonatal blood, but did not develop leukaemia until after several years (Wiemels et al., 2002, Burjanivova et al., 2006, Mulloy et al., 2003). Instead, RUNX1/ETO positive cells require additional genetic alterations to develop into leukaemia. Association of RUNX1/ETO with *KIT, FLT3-ITD, NRAS* or *KRAS* mutations in mouse haematopoietic progenitors was able to produce *in vivo* leukaemia. In one mouse study, induction of RUNX1/ETO and mutated *KIT* on the exon 7 resulted in lethal haematopoietic neoplasms, and the mice died within 2 to 4 months after transplantation: mice without additional mutations but expressing RUNX1/ETO rarely progressed to lethal disease within a year (Nick et al., 2012a). *KIT* mutations on the loop of the kinase domain results in D816V or N822K amino acid alterations and are found in approximately 11% to 44% cases of t(8;21) positive AML (Jiao et al., 2009, Nick et al., 2012a). These activating mutations are associated with a high incidence of relapse and poor survival in t(8;21) patients (Jiao et al., 2009, Wichmann et al., 2015).

Two isoforms of truncated RUNX1/ETO that lack the NHR3 and NHR4 domains have been reported (Yan et al., 2004, Wolford and Prochazka, 1998). Mice transplanted with RUNX1/ETO-transduced-bone marrow cells were reported to have developed aggressive leukaemia. The leukaemic cells of these mice contained a mutated *RUNX1/ETO* cDNA, which resulted in a 552 amino acid fusion protein (Yan et al., 2004). Another isoform harbours an extra ETO exon which is widely detected in t(8;21) patients. This transcript produces a shorter C-terminal region of the RUNX1/ETO protein, known as RUNX1/ETO9a (Wolford and Prochazka, 1998). RUNX1/ETO9a has 572 amino acids, which is almost identical to the truncated isoform and both of these isoforms rapidly induces leukaemia in mice models.

Mice with heterozygous RUNX1/ETO allele died at an early embryonic stage and displayed haematopoietic defects similar to mice with homozygous RUNX1 deletion (Yergeau et al., 1997, Okuda et al., 1998). Interestingly, RUNX1/ETO requires the normal function of RUNX1 for leukaemic survival. Depletion of RUNX1 inhibits the growth and survival of RUNX1/ETO leukaemia cells in CD34+ cord blood cells and t(8;21)-positive cell line (Ben-Ami et al., 2013, Goyama et al., 2013).

Co-repressor recruitment through the ETO moiety defines a dominant inhibition role of RUNX1/ETO-induced leukaemia. Given that RUNX1/ETO shares 60% of binding sites with RUNX1 (Ptasinska et al., 2014), RUNX1/ETO blocks RUNX1 binding to DNA and interferes with normal haematopoietic maturation, inducing a pre-leukaemic

condition. In myeloid differentiation, RUNX1/ETO binds to haematopoietic transcription factors such as CEBPA, PU.1 and GATA1 (Vangala et al., 2003, Pabst et al., 2001b, Choi et al., 2006, Ptasinska et al., 2014, Ptasinska et al., 2012). RUNX1/ETO abolishes CEBPA self-activation on *CEBPA* by direct interaction with the promoter site; thus inhibiting granulocytic differentiation (Pabst et al., 2001a). RUNX1/ETO also represses the expression of *UBP43*, which functions in cytokine-induced monocytic differentiation (Liu et al., 1999). Moreover, GATA-1 requires p300 for transcriptional activity and programming of erythroid differentiation. However, RUNX1/ETO indirectly interferes with GATA-1 by forming an inhibitory complex with p300 and inhibits erythroid lineage commitment.

Despite well-established repressor roles in transcriptional activities, RUNX1/ETO was also shown to increase the expression of RUNX1 target genes in order to promote leukaemogenesis (Martinez-Soria et al., 2018). Recent findings have shown that RUNX1/ETO directly regulates high expression of *CCND2* through co-operation with AP-1 (Martinez-Soria et al., 2018), a transcription factor that is involved in cell proliferation and differentiation (Bakiri et al., 2002). Knockdown of *RUNX1/ETO* reduces AP-1 binding to the *CCND2* promoter region and lowers *CCND2* expression. Furthermore, to enhance leukaemic clonogenicity, RUNX1/ETO binds directly to the promoter of telomerase (*TERT*), leading to constitutive expression of *TERT* (Martinez et al., 2004, Ptasinska et al., 2014). In addition, RUNX1/ETO forms a pre-initiation complex with p300 to drive the expression of downstream target genes such as *Id1, p21* and *Egr1* that function in self-renewal activity (Wang et al., 2011a). Moreover, RUNX1/ETO was shown to inhibit senescence and increase stem cell marker, CD34, indicating that RUNX1/ETO is indeed essential for leukaemic maintenance (Martinez et al., 2004).

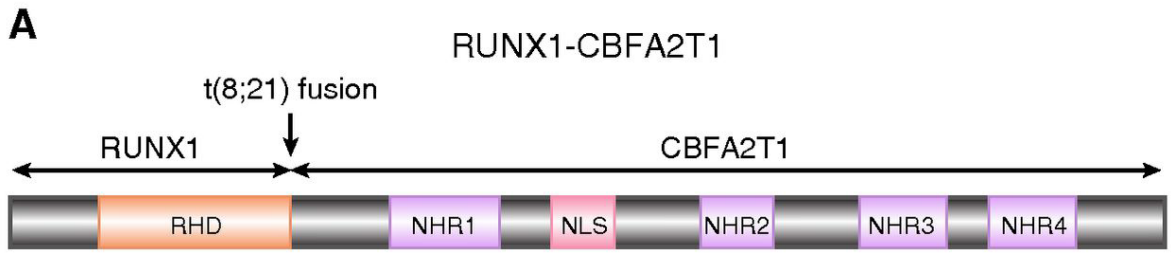

Figure 1-7: Scheme of RUNX1/ETO fusion protein. The full length of RUNX1/ETO fusion protein. RUNX1/ETO comprises the RHD domain from RUNX1 and 4 Nervy homology regions from ETO. Adapted from (Lam and Zhang, 2012).

1.7 Animal models of t(8;21) AML

Generation of t(8;21) AML animal models has been challenging over the years. Early work involved knock-in of *RUNX1/ETO* into the *RUNX1* locus to produce heterozygous *RUNX1/ETO* mice (Yergeau et al., 1997, Okuda et al., 1998). The experiment resulted in embryonic fatalities which occurred around embryonic stage 12.5 to 13.5 days (Okuda et al., 1998). These embryos failed to establish normal mature blood cells and presented with a severe haemorrhage phenotype which was also seen in homozygous deletion of *RUNX1* (Okuda et al., 1996) or *CBFβ* mice (Wang et al., 1996). However, in contrast to *RUNX1*- or *CBFβ*- deficient embryos, cells from *RUNX1/ETO* knock-in mice were able to generate a mix of abnormal myeloid lineage cells including erythroid precursors, monocytes, megakaryocytes and hypergranular cells that have a higher self-renewal capacity (Okuda et al., 1998).

An attempt was made to evade the RUNX1/ETO *in vivo* lethal effects by introducing a controlled expression of RUNX1/ETO using a tetracycline-inducible transgenic model (Rhoades et al., 2000). Interestingly, while RUNX1/ETO expression was detected in the bone marrow cells and macrophages, the mice did not show any onset of leukaemia. Furthermore, a primary colony formation assay from bone marrow cells showed no differences between control and RUNX1/ETO-expressing cells. Conversely, a serial replating of RUNX1/ETO-expressing cells resulted in block of myeloid differentiation, causing the cells to pause at an immature stage (Rhoades et al., 2000). Rhoades' study has made an important observation of RUNX1/ETO's capacity to induce self-renewal *ex vivo*; however, the inducible animal models did not exhibit haematopoietic abnormalities or tendency to develop leukaemia. These observations were also seen in knock-in of RUNX1/ETO cDNA that expressed the protein in the marrow of adult mice. The progenitors from these mice were able to be serially transplanted *in vivo*, but the mice did not develop leukaemia (Higuchi, 2000). Instead, treatment with a mutagen in these mice actuated leukaemia and granulocytic sarcoma which is similar to the clinical observation seen in patients with t(8;21) translocation. This notion was also supported in a transgenic mouse study, in which expression of RUNX1/ETO was under the control of human myeloid *MRP8* promoter (Yuan et al., 2001). The mice were healthy during their life-span, but treatment with DNA-alkylating mutagen (*N*-ethyl-*N*-nitrosourea) caused the mice to develop leukaemia. These studies suggest that RUNX1/ETO alone is insufficient to

develop leukaemia and secondary mutation(s) is required to induce disease progression.

Severe immunocompromised (*Scid*)-based mouse strains have been used to study HSCs and AML *in vivo* (Bhatia et al., 1997, Pearce et al., 2006); however, hitherto, there is no suitable animal model for the RUNX1/ETO human leukaemia background. Established cell lines as well as patient-derived t(8;21) leukaemic blasts do not or rarely engraft *in vivo* (Pearce et al., 2006, Soria et al., 2008). A study on RUNX1/ETO-transduced HSCs described the stemness property, marked by CD34 expression, as a prerequisite for successful RUNX1/ETO-leukaemia *in vivo* engraftment (Mulloy et al., 2003). However, one study showed that CD34 expression did not correlate with engraftment capability in t(8;21) leukaemia blasts (Pearce et al., 2006). Additionally, we have reported a successful RUNX1/ETO-positive cell line xenotransplantation model in *Rag2*$^{-/-}\gamma c^{-/-}$ mouse strain that lacks B, T and natural killer cells (Soria et al., 2008). This model was shown to promote CD34+ cord blood cell development towards adaptive immune system in newborn mice (Traggiai et al., 2004).

1.8 Therapeutic strategies for RUNX1/ETO-leukaemia

The t(8;21) AML rearrangement is grouped with inversion 16 (inv(16)) AML in the CBF leukaemia subset, which has favourable prognosis. Standard treatment for this group involves the induction chemotherapy with cytarabine for seven days in combination with three daily doses of anthracycline. The mode of action of cytarabine involves phosphorylation into its triphosphate form: mimicking native deoxycytidine triphosphate. This drug competitively incorporates into DNA and blocks synthesis of DNA by inhibiting DNA and RNA polymerase (Hatlen et al., 2012, Veuger et al., 2002). Whereas, anthracycline forms a complex with DNA and the topoisomerase 2α enzyme, which is highly expressed in proliferating and tumour cells, thereby causing double-stranded DNA breaks. The complex inhibits DNA replication, disrupts the cell cycle and finally induces apoptosis (McGowan et al., 2017, Stojak et al., 2014). Furthermore, if complete remission is achieved, a consolidation high-dose cytarabine is incorporated into the regimen for t(8;21) AML patients.

Consolidation of 3 to 4 cycles of high-dose cytarabine has been shown to improve cure rates of t(8;21) patients to 80% when compared to 40% of patients with one

cycle of high-dose cytarabine (Kantarjian, 2016, Byrd et al., 1999, Byrd et al., 2004). Recent studies demonstrated the use of fludarabine in combination with high-dose cytarabine and gemtuzumab ozogamicin or idarubicin have remarkably improved cure rates to 80 to 90% of patients in the CBF group (Borthakur et al., 2008, Burnett et al., 2010). The addition of gemtuzumab ozogamicin to the therapy regimen was reported to be the factor for improved survival (Burnett et al., 2010). Gemtuzumab ozogamicin is a drug-linked monoclonal antibody that targets CD33; however, it is reported to cause severe veno-occlusive disease and higher fatality rates in when in the combination group versus the group receiving chemotherapy alone (16/283=5.7% vs 4/281=1.4%; *P* = .01) (Nelson, 2010). Although it was once withdrawn from the market in 2010, gemtuzumab ozogamicin was approved again for adults with newly diagnosed AML, as well as patients 2 years of age and older with relapsed/refractory disease (**https://clinicaltrials.gov**). The new approval includes changes in the administered schedule and a lower dose than was initially approved (Rowe and Löwenberg, 2013).

1.9 Cancer and Metabolism

Cancer cells are characterised by accelerated proliferation, increased self-renewal capacity and an altered metabolism. These features require pathway reprogramming of nutrient acquisition and metabolism in order to support the accelerated bioenergetic demands. The reprogramming activity is now recognised as a hallmark of cancer, as recent works have uncovered plasticity of the pathways regulated by tumour cells to support these key functions.

The first metabolic reprogramming pathway was established by Otto Warburg, who observed abnormal glucose uptake and lactate production in the presence of oxygen, which is in contrast to the normal physiological function (Warburg, 1956b). The increased rate of glycolysis in cancer cells renders metabolic intermediates supplication to fulfil metabolic demand. Recent findings showed that dysregulation of oncogene/tumour suppressors and up-regulation of several key pathways are the reasons for the metabolic reprogramming.

1.9.1 *Glycolysis*

Glycolysis is a metabolic process of converting 1 mole of glucose into 2 moles of pyruvate, producing in a net gain of two moles of ATP and two moles of NADH. Glucose is transported into the cells through glucose transporters. There are five glucose transporters that are expressed in the mammalian system; SLC2A1 and SLC2A3, which are expressed in most tissues; SLC2A2, SLC2A4 and SLC2A5 conversely show tissue-specific expressions. Upon entry into the cells, glucose is phosphorylated by hexokinase (HK), trapped within the cells and then undergoes a series of transformations to produce pyruvate (Figure 1-8). Depending on the environmental condition, pyruvate has two fates; either to enter the mitochondria for the tricarboxylic cycle (TCA) to allow efficient ATP production or to divert to a less energy efficient process by converting to lactate. In normal oxygen conditions, pyruvate enters the mitochondria and is completely oxidised to CO_2. This process yields 36 moles of ATP from one mole of glucose. Under oxygen limitation, pyruvate is converted to lactic acid by lactate dehydrogenase (LDH) and mediates the conversion of NADH to NAD^+. Furthermore, lactate generated during anaerobic exercise is converted back to pyruvate and glucose in the liver, in a process called the Cori Cycle.

Pyruvate also provides the carbon backbone for the synthesis of amino acids (Figure 1-9). Pyruvate enters mitochondria to provide a carbon precursor for the synthesis of asparagine. The glucose by-products in glycolysis donate the carbon backbone for the synthesis of cysteine and glycine. Pyruvate can also be converted to alanine which provides the carbon backbone for amino acid synthesis Figure 1-9.

In cancer cells, increased glucose uptake is due to the upregulation of glucose transporters. For example, SLC2A3 has been reported to be upregulated in many cancer types and correlated to poor clinical outcome (Cosset et al., 2017, Starska et al., 2015, Flavahan et al., 2013). Upregulation of SLC2A3 is associated with accelerated glucose uptake and drives cancer proliferation (Hou et al., 2017) as well as inhibiting apoptosis in breast cancer cell lines (Wahdan-Alaswad et al., 2013).

Moreover, one of the key enzymes in glycolysis is phosphofructokinase-1 (PFK1) which catalyses the irreversible conversion of fructose-6-phosphate (F-6-P) to fructose-1,6-biphosphate (F-1,6-BP). There are three isoforms of PFK1 which are PFKP, PFKL and PFKM. PFKP is highly expressed in cancer cells in comparison to

the other two isoforms (Thakkar et al., 2010). PFKP activity is tightly regulated through several allosteric mechanisms. For example, high levels of ATP inhibits PFKP activity and blocks the production of F-1,6-BP. The intermediates upstream of PFKP can be used for other biosynthesis pathways such as the pentose phosphate pathway (PPP). Another allosteric regulator for PFK1 activity is fructose-2,6-biphosphate (F-2,6-BP) which is the product of 6-phosphofructo-2-kinase/fructose-2,6-biphospahatases (PFK2/FBPases2) activity. F-2,6-BP is a potent activator for glycolysis and degradation of this molecule by TP53-inducible glycolysis and apoptosis (TIGAR) inhibits PFKP activity (Bensaad et al., 2006). A recent study showed reduced PFK1 activity by O-linked β-N-acetylglucosamine (O-GlcNAc) transferase is detected in many cancer cell lines (Yi et al., 2012). This resulted in decreased glycolytic flux and redirected the intermediates to the PPP, allowing a growth advantage to cancer cells.

Furthermore, cancer cells preferentially transport lactate out to the extracellular environment, making it more acidic. This acidic environment mediates tumour invasion, angiogenesis and immune evasion (Nagarajan et al., 2016). For example, activation of the sodium-proton exchanger (NHE1) by the E7 oncogene is shown to cause gradual acidification of the extracellular microenvironment, which is associated with malignant transformation in human papilloma virus-transformed fibroblasts cells (Reshkin et al., 2000, Nagarajan et al., 2016).

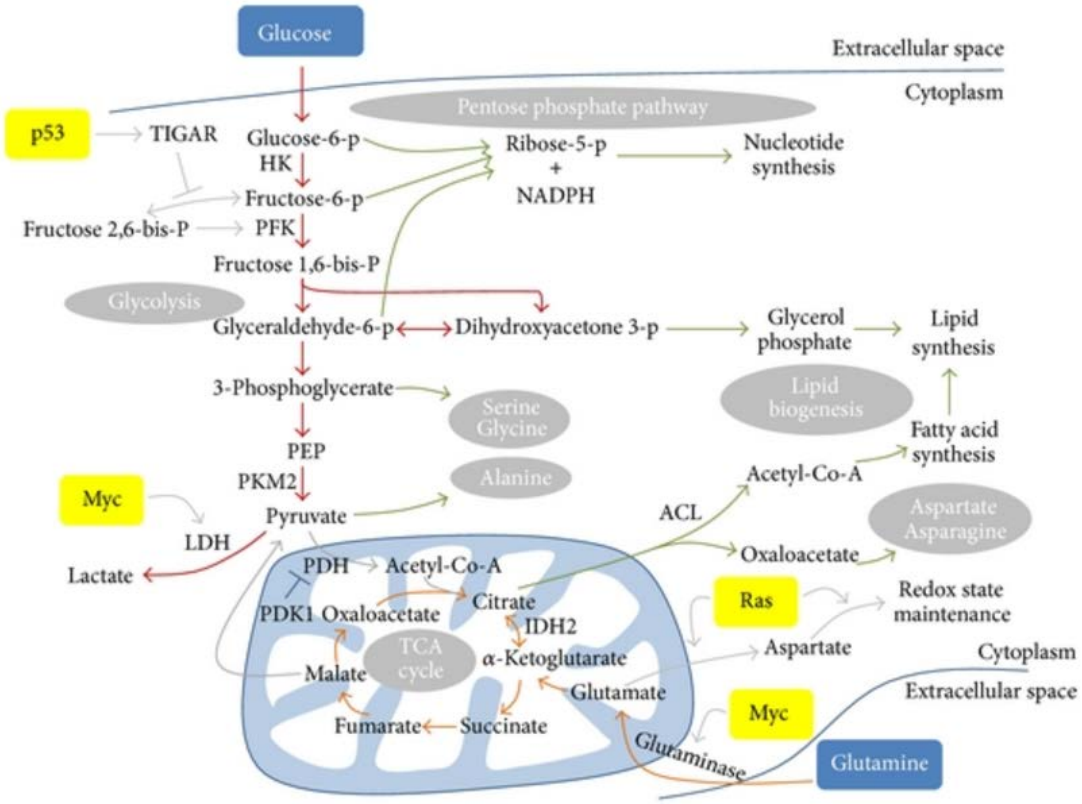

Figure 1-8: Metabolic pathways involving glycolysis and glutaminolysis. Glucose uptake results in the production of pyruvate which could either enter TCA cycle or converted into lactate. Upon entry into the cells, glutaminase converts glutamine to glutamate and then is converted into α-ketoglutarate in mitochondria. Both glucose and glutamine are required for the synthesis of amino acids, nucleotides and lipids. Metabolic changes in cancer cells are driven dysregulation of oncogenes (Myc and Ras) and tumour suppressor (p53). Glycolysis is indicated in red arrow. Glutaminolysis is indicated in orange. Biosynthetic pathway is shown in green (Adapted from Joshi, 2015 #601).

1.9.2 *Glutaminolysis*

Glutaminolysis is a metabolic process to convert glutamine into α-ketoglutarate (αKG) via glutamate. It is an important molecule required as a carbon and nitrogen backbone donor in the synthesis of micromolecules such as nucleotides and nonessential amino acids (NEAA). Glutamine enters the cell via its specific transporter and is converted to glutamate by glutaminase (GLS) in the cytoplasm. GLS1, which is the kidney-type of glutaminase is overexpressed in many types of cancer and reported to be associated with poor prognosis (Li et al., 2018). Glutamate is then converted to αKG and provides its nitrogen compound (amine group) to glucose- or glutamine-derived carbon compound to produce NEAA (glucose-derived; alanine, serine and aspartate; glutamine-derived; ornithine). Glutamine also donates its carbon skeleton and nitrogen to the synthesis of proline (Wise and Thompson, 2010, Young and Ajami, 2001). Moreover, glutamine can also replenish metabolites of the TCA cycle, a process called anaplerosis. Glutamine can also generate lactate via oxidative carboxylation of malate to pyruvate, thereby increasing NADPH production.

Studies have shown that glutamine is the essential amino acid required for tumour growth and some cancer cells exhibited higher glutamine uptake (R Wise et al., 2008). Cancer cells such as non-small cell lung cancer (NSCLC), breast cancer and brain tumours, exhibit a high dependency on glutamine for their growth and survival (Choi and Park, 2018, Márquez et al., 2017).

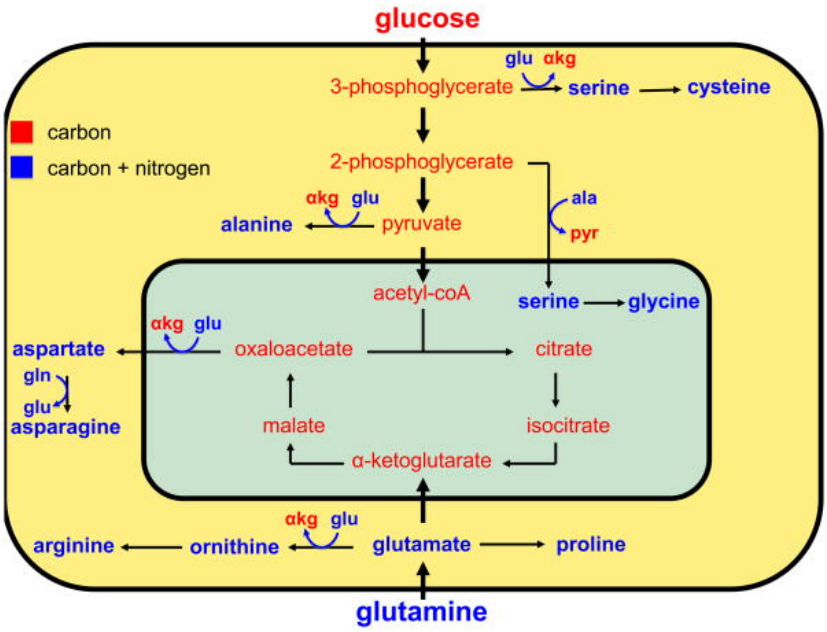

Figure 1-9: Glutamine and glucose as a nitrogen and carbon donor for the synthesis of non-essential amino acid. Glutamine, as well as glucose, provides carbon and nitrogen for the synthesis of nonessential amino acids (NEAA). Compounds containing carbon are shown in red, whereas compounds containing both carbon and nitrogen are shown in blue. Glycolysis and glutaminolysis provide carbon precursors for amino acid biosynthesis. (Glycolysis; 3-phosphoglycerate, 2-phosphoglycerate and pyruvate; Glutaminolysis; oxaloacetate, glutamic acid γ-semialdehyde). Glutamic acid derived from glutamine (glu) donates its amine group to these carbon substrates to produce NEAA (serine, alanine, aspartate, ornithine) and α-ketoglutarate (αKG). Alanine (ala) serves as the amine donor to produce serine and pyruvate in mitochondria for the production of glycine. Glutamine provides both carbon and nitrogen sources for the synthesis of proline, ornithine and arginine as well as a direct nitrogen donor in the synthesis of asparaginase from aspartic acid. Adapted from Wise et al. (2010).

1.9.3 *Hypoxia*

Low levels of oxygen is one of the common features for many tumours (Muz et al., 2015). In highly proliferative tumour tissue, oxygen demand exceeds oxygen supply and the distance between the cells from existing vascular tissues increases, thus restricting oxygen diffusion and creating an even more hypoxic microenvironment. The average oxygen level in the hypoxic tumour environment including in the bone marrow was reported to be between 1%-2% (Muz et al., 2015) (Spencer et al., 2014).

Hypoxia activates several complex intracellular signalling pathways such as hypoxia-inducible factor-1 (HIF-1). HIF is a family of transcriptional regulators that are regulated by oxygen sensors, including prolyl-4-hydroxylase domain (PHD) and factor inhibiting HIF1 (FIH-1). In normoxia, HIF1-α subunits are hydroxylated by PHD which requires oxygen as well as iron. The complex mediates binding of von Hippel-Lindau (VHL) tumour suppressor protein and results in proteasomal degradation. When the oxygen level reduces, the PHD enzymes lose the activity, leading to stabilisation of HIF1-α and translocation to the nucleus. In the nucleus, HIF1-α dimerises with constitutively expressed HIF1-β subunits, binds to DNA and initiates transcription.

Hypoxia is known to increase the expression of glucose transporters SLC2A1 and SLC2A3, as well as glycolytic enzymes such as ALDA and PGK1 (Iyer et al., 1998). Furthermore, studies have shown that decreasing oxygen tension would also accelerate glycolysis, as this is associated with a higher expression of *SLC2A3* (Yu et al., 2012, Christensen et al., 2015). Moreover, hypoxia is associated with resistance to chemotherapy and poor patient survival. Chemotherapy-resistant AML cells preferentially localised to the hypoxic endosteal niche in the bone marrow (Ishikawa et al., 2007). Several reports have shown therapeutic advantage of targeting HIF-1 in leukaemia (Wang et al., 2011b, Rouault-Pierre et al., 2013); however, several studies demonstrated contradictory evidence (Velasco-Hernandez et al., 2019, Vukovic et al., 2015). For instance, a study demonstrated deletion of *Hif-1a* led to a more aggressive phenotype in a MLL-AF9 mouse model (Velasco-Hernandez et al.,2018). One possibility of this is the enrichment of PTEN/PI3K/AKT pathway which induces *Hif-a* activation (Zundel et al., 2000) and at the same time promotes AML cell proliferation (Griessinger et al., 2014). Furthermore, HIF-1 stabilisation promotes the release of proangiogenic cytokines such as vascular endothelial growth factor (VEGF) (Moeller et al., 2004). In addition to promoting new

blood vessel formation, VEGF secretion enhances the protection of tumour blood vessels from radiotherapy, hence tumour resistance (Gorski et al., 1999).

1.10 Regulation of metabolism by tumour suppressors or oncogenes

1.10.1 *Tp53*

The tumour suppressor p53 regulates many of the proteins involved in metabolic pathways such as: cytochrome C oxidase (SCO2), TP53-induced glycolysis and apoptosis regulator (TIGAR), glucose transporters and phosphoglycerate mutase (PGM) (Harami-Papp et al., 2016, Bensaad et al., 2006). p53 induces the expression of an assembly factor SCO2 in the nucleus. SCO2 is an important regulator of the complex IV mitochondria, which is part of the respiratory chain for oxidative phosphorylation. p53 has also been shown to regulate glycolysis by suppressing it through induction of *TIGAR*, which shares similarity to Phosphofructokinase-2/fructose biphosphatase-2 (PFK-2/FBPase-2) (Bensaad et al., 2006). However, only the catalytic unit of the biphosphatase domain is well-conserved in TIGAR, suggesting that TIGAR may function similarly to FBPase-2 (Bensaad et al., 2006). FBPase-2 degrades fructose-2-6-biphosphate, a potent activator of PFK-1 and inhibits glycolysis. This inhibition results in increased flux of glucose-6-phosphate to the PPP pathway and consequently increases the synthesis of ribose sugars for nucleotide biosynthesis and NADPH for cellular antioxidants. However, p53 can also function as a negative regulator for PPP through direct inhibition of glucose-6-phosphate dehydrogenase (G6PD), the first rate-limiting enzyme in the PPP pathway. This results in decrease of NADPH generations and affects overall cellular reactive oxygen species (ROS) levels.

Another direct target of p53 is glutaminase 2 (GLS2), which catalyses the conversion of glutamate from glutamine in the mitochondria. This enzyme promotes antioxidant glutathione (GSH), thereby blocking ROS productions and act as a defence mechanism.

Tp53 mutation is the most common mutation found in cancers and more than 75% of the mutations result in the loss of p53 function (Kawauchi et al., 2008). Mutant p53 has been implicated in loss of mitochondrial respiration and supports a glycolytic phenotype (Kawauchi et al., 2008). Mutation in the DNA-binding domain of p53

abolishes the p53 repressor effect on glucose transporters and PFKP, thereby increasing glucose metabolism and cell energy supply in osteosarcoma cell lines (Schwartzenberg-Bar-Yoseph et al., 2004, Harami-Papp et al., 2016). The mechanism on how mutant p53 increases the expression of glucose transporters is through activation of NFKB. Wild-type p53 inhibits the activity of IκB kinases (IKK) that are required for NFKB activation and therefore suppresses glucose transporter expression (Kawauchi et al., 2008).

1.10.2 *IDH*

Isocitrate dehydrogenase (Thakkar et al.) 1 and 2 catalyse the oxidation of isocitrate to α-ketoglutarate (αKG). These enzymes also function in epigenetic regulation, redox states and DNA repair and are among many dysregulated oncogenes that are detected in glioma and AML patients (Parsons et al., 2008, Mardis et al., 2009, DiNardo et al., 2015). In AML, mutations in *IDH1* and *IDH2* present in about 6-19% and 8-34% of patients respectively, and is commonly found in adult patients (Im et al., 2014, DiNardo et al., 2015, Mardis et al., 2009). IDH1 is localised primarily in the cytoplasm and IDH2 is localised in the mitochondria. The mutations lead to the absence of a β-carboxyl group which is present in wild type IDH. These result in the neomorphic enzyme activity of IDH and favours irreversible conversion of αKG to an oncometabolite, 2-hydroxyglutarate (2HG). 2HG has an identical chemical backbone as isocitrate but lacks the carboxyl group (Figure 1-10) (Molenaar et al., 2018). As a consequence, IDH mutated cells impair TCA cycle metabolism, thus shifting the dependency towards glutaminolysis, which provides anaplerosis to the TCA at the level of αKG. 2HG accumulation elevates the risk of *in vivo* malignant brain tumours as shown in a study (Dang et al., 2009).

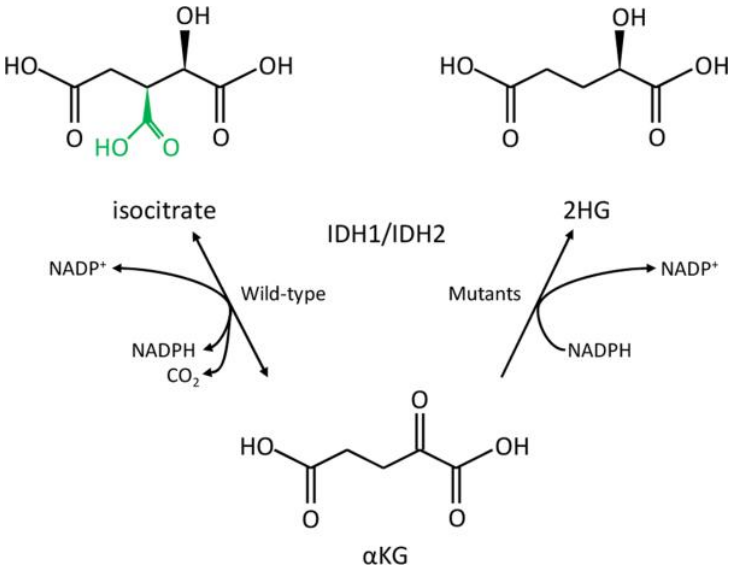

Figure 1-10: Mutations in the active carboxyl site of IDH1 and IDH2 result in neomorphic enzymatic activity. Wild-type IDH catalyse the reversible conversion of isocitrate to α-ketoglutarate (αKG) (left reaction) and at the same time reduce NADP+ to NADPH and produce CO_2. Mutations in IDH result in neomorphic enzymes that catalyse irreversible αKG to 2-hydroxyglutarate (2HG) and oxidised NADPH to NADP+ (Ward et al., 2010, Reitman et al., 2010).

1.10.3 *PI3K/AKT pathway*

PI3K/AKT signalling is one of the important pathways in the regulation of metabolic processes. This pathway is triggered in many cancers through abnormal activation of receptor tyrosine kinases, loss of PTEN or by activating mutations in *PIK3CA, AKT* or *RAS.* Activation of this pathway has been implicated in metabolic reprogramming in cancer cells. For instance, AKT has been suggested as a “Warburg kinase” as it promotes cancerous glycolysis (Robey and Hay, 2009). AKT upregulates the glycolytic enzyme PFK-2 and thus increases glycolytic flux through increased activity of PFK-1 (Deprez et al., 1997). Glucose transporters were also shown to be upregulated upon activation of AKT and are associated with radioresistance (Fang, 2015). In a study, constitutive activation of AKT by myristoylation caused glucose transporter-1 localisation to the cell surface, thus increasing uptake and phosphorylation of glucose (Rathmell et al., 2003). Aberrant expression of AKT also promotes localisation of HK2 to the mitochondrial membrane for direct access of ATP from ATP synthase and this accelerates glycolysis (Mathupala et al., 2006). Interestingly, high AKT activity protects prostate cancer cell lines from TRAIL-induced apoptosis (Nesterov et al., 2001). This protective mechanism is consistent with the

loss of PTEN function that is frequently observed in many cancers (Nesterov et al., 2001, Hollander et al., 2011).

1.11 Targeting altered cellular metabolism in cancer

Altered metabolism in cancer cells could be used to establish new therapeutic strategies to improve the outcome of patients. As cells depend on the synthesis of macromolecules such as nucleotides, amino acids and fatty acids to promote rapidly proliferating transformed cells, one could, therefore, take advantage of this loophole.

1.11.1 *Targeting glucose metabolism*

Tumour cells exhibit accelerated glucose uptake which can be imaged by fluorodeoxyglucose positron emission tomography (FDG-PET). 2-deoxyglucose (2DG), an inhibitor for glycolysis, was developed in the 1950s (Wick et al., 1957) and suppresses glycolysis by its disability to convert to fructose-6-phosphate. Initially, 2DG showed promising effects both *in vitro* and *in vivo,* but 2DG alone is insufficient for therapeutic benefit (Maschek et al., 2004). Another inhibitor in glucose metabolism is lonidamine, which inhibits glycolysis at the level of hexokinase 2,but has limited anti-tumour activity as a monotherapy agent (Nancolas et al., 2016). Despite restricted therapeutic values as a single agent, 2DG and lonidamine showed a promising effect when in combination with other chemotherapy agents (Maschek et al., 2004, Nancolas et al., 2016).

1.11.2 *Targeting amino acid metabolism*

Currently, the only anticancer agent that targets amino acid metabolism is L-asparaginase. This drug is FDA-approved for paediatric and adult ALL. Normal cells can produce asparagine, a non-essential amino acid, from aspartate and glutamine via asparagine synthetase. However, some cancer cells such as leukaemic lymphoblasts, do not express asparagine synthetase and therefore rely on the blood serum for asparagine supply. Asparaginases degrade asparagine resulting in the quick depletion of this amino acid in serum. Asparaginases also catalyse deamidation of glutamine, thus suppressing glutamine-derived asparagine. Since the 1950s, treatment of ALL patients with asparaginases and standard chemotherapy drugs has aided the in 5-year OS rate, to be more than 90% in the present day (Pui et al., 2009). Asparaginases showed a mix of antineoplastic effects on AML cell lines

(Jun et al., 2011). Although, asparaginases inhibited growth and induced apoptosis in some of the cell lines, there was no strong correlation between asparaginase sensitivity to asparagine synthetase expression in asparaginase-resistant cell lines (Jun et al., 2011).

1.11.3 *Targeting nucleotide metabolism*

Gemcitabine, cytarabine and 5-fluorouracil are three antimetabolite chemotherapeutics targeting nucleotide biosynthesis. Although these drugs do not display tumour specificity, they cause improved patient survival in many different types of cancers. These agents target all actively dividing cells, thus explaining the frequent observation of side effects such as hair loss and nausea.

1.11.4 *Targeting lactate metabolism*

Increased flux of glycolysis and concomitant lactate production is one of the characteristics of cancer cells (Nagarajan et al., 2016). Blocking the lactate transporters using a small molecule inhibitor (AZD3965) (Curtis et al., 2017) is currently in a phase I clinical trial in the UK for diffuse large B cell lymphoma and Burkitt lymphoma (https://www.cancerresearchuk.org/). AZD3965 selectively inhibits monocarboxylate transporter-1 (MCT-1), resulting in intratumoral lactate accumulation, and significantly inhibits tumour growth *in vivo* (Noble et al., 2017). Another putative target in lactate metabolism is lactate dehydrogenase (LDH), an enzyme that converts pyruvate to lactate. However, hitherto the inhibitor development remains a challenge as LDH has a small size of its substrate site (Zhang et al., 2018a).

1.11.5 *Mutated enzyme*

As described previously, mutations in IDH1 and IDH2 enzymes result in the failure of normal αKG functions and leads to accumulation of the oncometabolite 2HG. 2HG is secreted into the serum and urine and has become one of the predictive biomarkers for AML (Mondesir et al., 2016, Fathi et al., 2012). Both IDH1 and IDH2 inhibitors (Ivosidenib and enasidenib mesylate) are currently in clinical trial phases I and II in a biomarker-based treatment of AML in the United States (https://www.cancer.gov/). These drugs lower 2HG levels both *in vitro* and xenograft models (Hansen et al., 2014, Yen et al., 2017).

1.12 Identification of *SLC2A3* and *PFKP* as partner genes in RUNX1/ETO-driven leukaemia

The oncogenic transcription factor RUNX1/ETO drives a complex transcriptional network, hence its perturbation affects the expression of many genes that is being bound by the fusion protein (Ben-Ami et al., 2013, Ptasinska et al., 2012, Ptasinska et al., 2014). We predicted that such a transcriptional network would contain crucial elements relaying the oncogenic function of the fusion protein, which could be exploited for potential pharmacological inhibition. RNA sequencing, Chip-sequencing and microarray data were intersected to identify a set of 110 RUNX1/ETO-bound genes that are responsive to RUNX1/ETO depletion. These genes are down-regulated upon RUNX1/ETO knockdown, and therefore potentially required for RUNX1/ETO maintenance. A total of 374 shRNA constructs were produced using a pTRIPZ doxycycline (dox)-inducible vector and transduced on two RUNX1/ETO positive cell lines, Kasumi-1 and SKNO-1 (Figure 1-11-A). The screen was divided into two arms; dox-induced and a no-dox arm for both *in vitro* and *in vivo,* with the differentially expressed shRNA constructs being identified by comparison between the two corresponding arms. For the *in vitro* screen, the changes in shRNA pool compositions were determined after prolonged suspension culture for up to 56 days or in colony forming assay after three platings. To screen for genes relevant to leukaemogenesis *in vivo,* the shRNA library was intrafemorally transplanted in NOD.Cg-Prkdc^{scid} Il2rg^{tm1Wjl}/SzJ (NSG) mice with a total of 5x10^5 and 1x10^5 cells for both SKNO-1 and Kasumi-1. The screen results revealed that shSLC2A3 and shPFKP were significantly depleted *in vivo* in both of the cell lines; however, these two genes did not score *in vitro* (Figure 1-11-B).

Further analysis of the corresponding shRNAs present in the pool showed that two of three SLC2A3 shRNAs were at least two-fold significantly depleted *in vivo* in both of the cell lines; however, there was no change *in vitro* (Figure 1-11-C). This was also the case for PFKP shRNA, where two constructs were depleted *in vivo;* however, there was no variation in long-term suspension culture and replating assays (Table 1-1). As described in section 1.9.1, these two genes function in glycolysis and their overexpression is often associated with cancer (Thakkar et al., 2010, Cosset et al., 2017). The screen was carried out by Dr Natalia Martinez Soria and Dr Lynsey McKenzie, and the analysis was done by Dr Sirintra Nakjang.

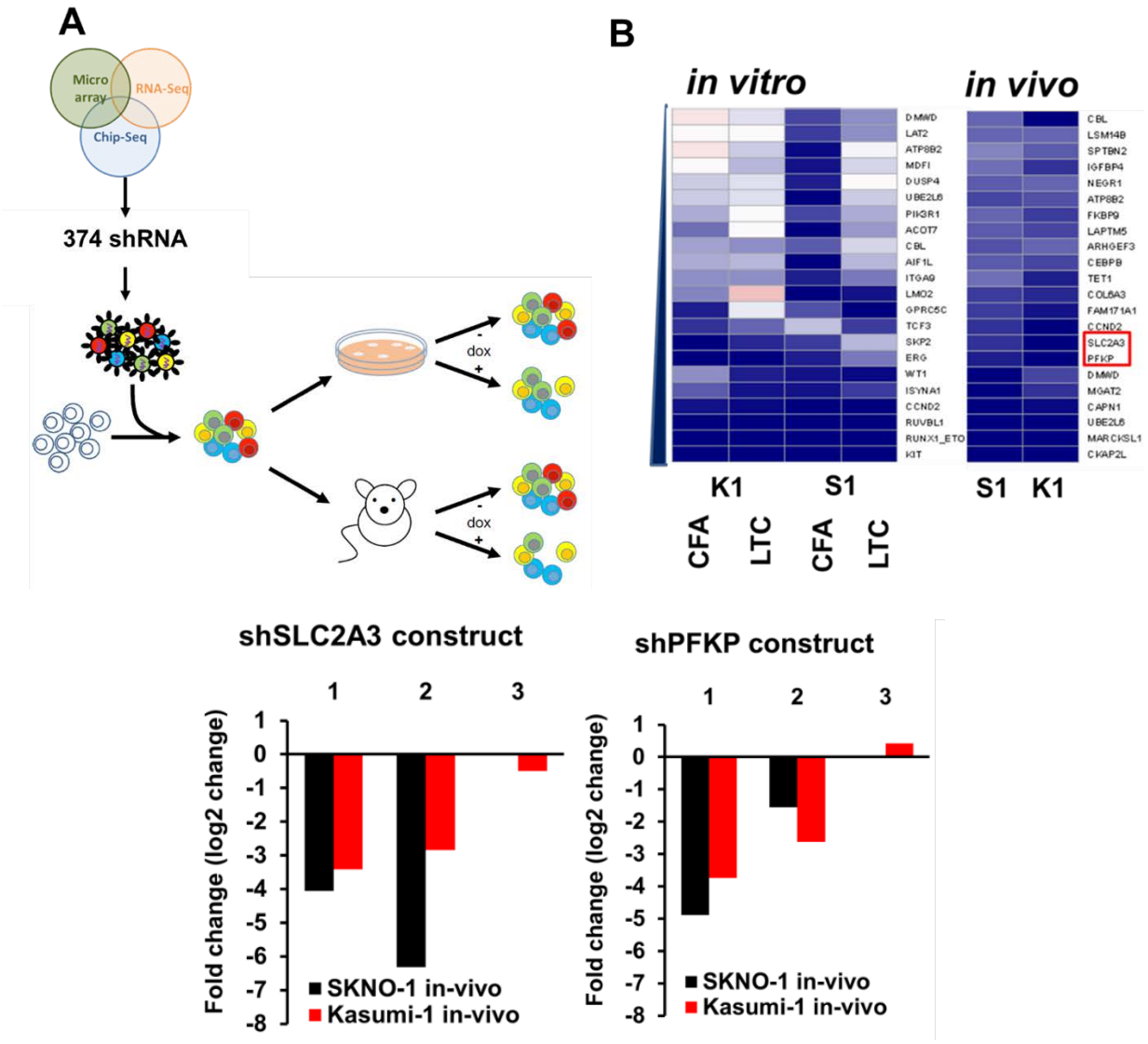

Figure 1-11: shRNA *in vitro* and *in vivo* screen identifies SLC2A3 and PFKP as potential partner genes for RUNX1/ETO. A) Scheme of RNAi screen targeting 374 shRNA constructs conducted with dox-induced and no-dox arms for both *in vitro* and *in vivo* arms. B) Heatmap showing top hits of potential partner genes of RUNX1/ETO displayed as fold changes calculated based on collapsed changes of shRNAs using the RRA approach of MAGeCK. SLC2A3 and PFKP were depleted only in *vivo* but not identified *in vitro* (highlighted in red box). CFA, colony formation assay; LTC, long-term suspension culture; K1, Kasumi-1; S1, SKNO-1. C) Fold change of shSLC2A3 and shPFKP constructs *in vivo*. Two constructs were depleted in both cell lines. Figures were modified from Martinez-Soria et al. (2018).

shRNA	Cell lines	Construct	log2fold change	P-value
shSLC2A3	Kasumi-1	1	-3.41	1.08E-06
		2	-2.84	0.002031
		3	-0.50	0.368761
	SKNO-1	1	-4.05	0.002054
		2	-6.31	2.7E-08
		3	0.03	0.970968
shPFKP	Kasumi-1	1	-3.74	2.13E-07
		2	-2.62	0.010734
		3	0.41	0.492792
	SKNO-1	1	-4.88	5.78E-06
		2	-1.55	0.132151
		3	-0.02	0.974915

Table 1-1: Log2 fold change and p-value for shSLC2A3 and shPFKP depletion *in vitro*. Fold change of all the constructs of SLC2A3 and PFKP *in vitro* in both Kasumi-1 and SKNO-1.

1.13 Hypothesis and aims

Therefore, this thesis describes the functions of glycolysis to promote leukaemogenesis. I hypothesised the oncogenic transcription factor RUNX1/ETO dysregulates *SLC2A3* and *PFKP* to reprogramme metabolic functions for leukaemic propagation.

The aims of this thesis are:

1) To validate *SLC2A3* and *PFKP* as the direct targets of *RUNX1/ETO* and as a potential therapeutic target in both *in vitro* and *in vivo* assays. These will include siRNA- and shRNA-mediated knockdown on RUNX1/ETO-positive cell lines, primary and patient-derived xenograft (PDX) cells.
2) To explore the mechanism of potential metabolic reprogramming through *SLC2A3* and *PFKP* in RUNX1/ETO-driven leukaemia in limited nutrient and oxygen conditions. This will include assessing the proliferation and colony formation in limited nutrient and oxygen conditions. The metabolic reprogramming will also be evaluated by using Seahorse Metabolic Assay.

3) To evaluate the efficacy of small molecule inhibitors in eradicating leukaemic cells. Firstly, by using a glycolysis inhibitor alone and in potential combination with a novel cell cycle inhibitor, palbociclib. Furthermore, investigation of the potential mechanism by which palbociclib-treated cells shunt its metabolic pathway will also be conducted.

Chapter 2 : Materials and Method

2.1 Materials

2.1.1 *Laboratories Equipment and Software*

2.1.1.1 Laboratories Equipment

Equipment	Manufacturer
Flow cytometry	
FACSCanto II	BD Biosciences
FACSCalibur	BD Biosciences
Fortessa X20	BD Biosciences
Attune NxT	ThermoFisher Scientific
FACSAria III	BD Biosciences
Thermal cycler	
ViiA 7 Real-Time PCR System	ThermoFisher Scientific
GeneAmp PCR 2700	AB Applied Biosystem
Centrifuge	
Centrifuge 5804R	Eppendorf
Centrifuge 5804	Eppendorf
Centrifuge 5415 R	Eppendorf
Centrifuge 5424	Eppendorf
Ultracentrifuge	Eppendorf
Incubator	
Hypoxia	Baker Ruskinn
Imaging	
ChemiDoc MP	Bio-Rad
GBox	Syngene
Seahorse Analyser	
Seahorse Analyser	Agilent Technologies
Nanodrop	
Nanodrop-ND100	Nanodrop Technologies

Table 2-1: Equipment used in the study.

2.1.1.2 Software

Software	Manufacturer
FACS Diva	BD Biosciences
FlowJo v10.0.8	FlowJo, LLC
Seahorse Wave Desktop	Agilent Technologies
SnapGene Viewer	GSL Biotech LLC
Primer Express 2.0	Applied Biosystem
QuantStudio Real-Time PCR System	Applied Biosystem
SDS 2.3	Applied Biosystem
Living Image 4.5.5	Perkin Elmer

Table 2-2: Software used for analysis of data.

2.1.2 *Chemicals and Reagents*

2.1.2.1 Kits and chemicals

Name	Manufacturer
RNeasy Mini Kit	Qiagen
RevertAid™ H Minus cDNA Synthesis Kit	Thermo Fisher Scientific
QIAquick Gel Extraction Kit	Qiagen
DNeasy Blood & Tissue Kit	Qiagen
EndoFree Plasmid Maxi Kit	Qiagen
QIAprep Spin Miniprep Kit	Qiagen
QIAshredder	Qiagen
BCA Protein Assay Kit	Bio-Rad
Immobilon Western Chemiluminescent HRP Substrate	Milipore
FITC Annexin V Apoptosis Detection Kit I	BD Bioscience
BV421 Annexin V	BD Bioscience
2-(N-(7-Nitrobenz-2-oxa-1,3-diazol-4-yl)Amino)-2-Deoxyglucose (2-NBDG)	Cayman Chemical
4',6-Diamidino-2-Phenylindole, Dihydrochloride (DAPI)	Sigma
SOB Medium	Sigma
LB Miller	Sigma Aldrich
Platinum® SYBR® Green qPCR SuperMix-UDG	Invitrogen
ATP Detection Assay	Abcam
CellROX Green Flow Cytometry Kit	Life Technoligies
Molecular weight ladder (N3232L)	New England Biolabs
DNA gel loading dye (B7024S)	New England Biolabs

Table 2-3: Kits and chemicals.

2.1.2.2 Tissue culture media and supplements

Reagents	Manufacturer
RPMI 1640, R8758	Sigma
RPMI 1640, R5886	Sigma
DMEM, D5671	Sigma

RPMI 1640, no glucose	Gibco
L-Glutamine	Sigma
GM-CSF	Stemcell Tech.
D-Glucose	Sigma
Sodium Pyruvate (S8636-100ml)	Sigma
Penicillin/Streptomycin	Sigma
StemSpan™ Myeloid Expansion Supplement (SFEM II)	Stemcell Tech.
StemSpan™ Myeloid Expansion Supplement II (100X)	Stemcell Tech.
Seahorse XF Base Media	Agilent
Fetal Calf Serum (FCS)	Gibco

Table 2-4: Tissue culture media and supplements.

2.1.3 *Media Composition and Buffers*

2.1.3.1 Cell culture media

Cells (Condition)	Media	Supplements
Kasumi-1 (Standard Culture)	RPMI 1640, R8758	10% (v/v) FCS
Kasumi-1 (2.5 mM Glucose)	RPMI 1640, no glucose	10% (v/v) FCS 2.5 mM Glucose
Kasumi-1 (1 mM Glutamine)	RPMI 1640, R5886	10% (v/v) FCS 1 mM Glutamine (Sigma)
SKNO-1 (Standard Culture)	RPMI 1640, R8758	20% (v/v) FCS 7 ng/µl GM-CSF
SKNO-1 (2.5 mM Glucose)	RPMI 1640, no glucose	20% (v/v) FCS 7 ng/µl GM-CSF 2.5 mM Glucose
SKNO-1 (1 mM Glutamine)	RPMI 1640, R5886	20% (v/v) FCS 8 ng/µl GM-CSF 1 mM Glutamine (Sigma)
THP-1	RPMI 1640, R8758	10% (v/v) FCS
MV4-11	RPMI 1640, R8758	20% (v/v) FCS
HL-60	RPMI 1640, R8758	20% (v/v) FCS
293T	DMEM, D5671	10% (v/v) FCS 1% (v/v) Sodium Pyruvate 1% (v/v) L-glutamine
BM-iPSC-MSC	SFEM II	Unpublished
Patients-derived xenograft (PDX) and primary cells	SFEM II	StemSpan™ Myeloid Expansion Supplement II (100X) 20% (v/v) FCS

Table 2-5: Cell culture media and composition.

2.1.3.2 Bacterial culture

Inoculation buffer	55 mM MnCl2
	15 mM CaCl2
	250 mM KCl
	10 mM PIPES (pH 6.7)
	Up to 1 l of H_2O
Lysogeny Broth (LB)	25 g LB Miller
medium	Up to 1 l of H_2O
LB agar	6 g Bacto agar
	12.5 g of LB Miller
	Up to 500 ml of H_2O

2.1.3.3 Transfection buffer

$CaCl_2$ solution	36.75 g $CaCl_2$
	Up to 500 ml of H_2O
HeBS, 2X, pH 7.00	16.36 g NaCl
	11.9 g HEPES
	0.213 g Na_2HPO_4
	Up to 1l of dH_2O
Special water	125 µl of 1M HEPES (pH 7.3)
	50 ml of dH_2O

2.1.3.4 Flow cytometry

Flow cytometry staining buffer	2% FCS
	0.02% sodium azide
	PBS
Flow cytometry sort buffer	0.5% (w/v) bovine serum albumin
	PBS

2.1.3.5 Clonogenic assay

Methylcellulose medium	0.56 g methylcellulose
	5 ml PBS
	85 ml corresponding growth medium
	10 ml FCS

2.1.3.6 DNA electrophoresis buffer

5X DNA loading dye	
10X TAE buffer	48.4 g Tris
	11.4 ml glacial acetic acid (17.4 M)
	3.7 f ETA, disodium salt
	Up to 1 l of H_2O

2.1.3.7 Western blotting

Urea buffer	9M Urea
	4% (w/v) CHAPS
	1% (w/v) EDTA
	1% (w/v) DTT
10% SDS:	100 g SDS
	1 l H_2O
10% APS	1 g Ammonium persulfate
	10 ml H_2O
4x Separating Gel Buffer	1.5 M Tris
	0.4% (w/v) SDS
	pH 8.8 with HCl
4x Stacking Gel Buffer	500 mM Tris
	0.4% (w/v) SDS
	pH 6.8 with HCl
10x Tris-Glycine Buffer	250 mM Tris
	1.92 M Glycine
Electrophoresis Buffer	1x Tris-Glycine Buffer
	0.1% (w/v) SDS
Blotting Buffer	1x Tris-Glycine Buffer

	10% (v/v) Methanol
2x SPAG Loading Buffer	50% (v/v) 4x Stacking gel buffer
	20% (v/v) Glycerol
	4% (w/v) SDS
	5% (v/v) β-Mercaptoethanol
	0.1% (v/v) Bromophenol Blue
10x TBS	100 mM Tris-Cl pH 8.0
	1.5 M NaCl
	1 l H_2O
1XTBS-T	10 mM Tris-Cl pH 8.0
	0.15 M NaCl
	0.1% (v/v) Tween
10% Milk	5 g dry milk
	50 ml 1XTBS-T
Ponceau-S red Solution	0.5% (v/w) Ponceau-S red
	1 % (v/v) Acetic acid
	50 ml H_2O

2.1.3.8 Cell cycle

Staining buffer	1 µg/ml DAPI
	0.25% (v/v) Triton-100

2.1.3.9 Enzyme and buffer

Name	Manufacturer
BsmBI	Thermo Scientific
T4 Polynucleotide Kinase	Thermo Scientific
T4 DNA Ligase	Thermo Scientific

Table 2-6: Enzyme and buffer for cloning methods.

2.2 Cell Culture Methods

2.2.1 *Cell Culture*

2.2.1.1 Cell lines

Each cell lines were cultured in standard culture conditions in every experiment unless otherwise stated. Positive acute myeloid leukaemia cell lines (Kasumi-1 and SKNO-1) were used in this study and cultured at 37°C, 5% CO_2. Cells were counted using the trypan blue exclusion method and split to 5.0 x 10^5 cell/ml with fresh, pre-warmed media. Cells are generally passaged 3 times a week.

2.2.1.2 Patients derived xenograft (PDX) materials

Patients' derived xenograft (PDX) materials were obtained from frozen stock in our lab. The PDX materials were prepared by Dr Helen Blair. The frozen vials were thawed in a warmed water bath, cleaned with 75% ethanol and quickly transferred into 10 ml pre-warmed media in 20 ml universal tube. The tube was spun down at 300 g for 5 minutes and the supernatant was removed. A volume of 10 ml fresh warmed media was added into the tube and cells were counted by trypan blue exclusion method (Section 2.2.1.3). The cells were cultured in SFEM II media containing 1X myeloid expansion media and 20% FCS at a concentration of 1.0 x 10^6 cells/ml.

2.2.1.3 Cell Counting

Haemocytometer (Hawksley) with a chamber depth of 1.0 mm was used for counting the cells. The haemocytometer was cleaned with 70% ethanol prior to counting and allowed to dry. A glass coverslip was then fixed in place. Cell suspension and trypan blue were mixed with the ratio 1:1 and 10 µl of the mixture was added to the chamber. Cells in four corner squares were counted (each square was 1 mm^2 equal to 0.1 µl). Cells touching top and left line of each grid were counted and those touching bottom and right line of each grid were not counted. The average number of cells per square was calculated, multiplied by 2 (dilution factor) and 10^4 to obtain the number of cells per ml.

2.2.1.4 Cell Thawing

Frozen cells were thawed rapidly in 37ºC water bath, quickly transferred to 20 ml universal tube and diluted with 10 ml warmed culture media. The cells were then spun down at 300 g for 5 minutes. Supernatant was removed and cells were resuspended in corresponding culture medium and concentration.

2.2.1.5 Cell Freezing

Cells were counted and pelleted at 300 g for 5 minutes. A volume of corresponding freezing media was added to make the concentration 5 x 10^6 cell/ml and transferred a maximum of a ml to a pre-labelled cryovial tube. The tubes were placed in an insulated freezer box or immediately transferred to the -80^{o}C freezer.

2.2.1.6 Cell Lysis

Lysis buffer was prepared by adding 10 µl of β-merchaptoethanol (β –ME) into 1 ml of RLT buffer (Qiagen) and it is stable for a month at room temperature.

Cells were counted and pelleted in a universal tube at 300 g for 5 minutes. The supernatant was removed and 10 ml of PBS was added and spun down at 300 g for 5 minutes. The supernatant was removed and 1 ml of PBS was added into the cells pellet, pipetted up and down and then transferred into a 1.5 ml Eppendorf tube. The tube was centrifuged at 300 g for 5 minutes and PBS was removed. Lysis buffer was added according to the cell number as described in table below. The lysed cells were extracted immediately or stored in -20^{o}C.

Number of cells (x10^6 cell)	Volume lysis buffer (µl)
5.0 – 10	600
0.5 – 5.0	350

Table 2-7: Volume of lysis buffer used to lyse cells according to the number of cells.

2.2.2 *Electroporation*

Small interfering RNA (siRNA) was used as a tool to down-regulate target genes. siRNA is a double-stranded RNA consist of 19-22 nucleotides that can be introduced into the cells by applying electricity, called electroporation. This procedure was first performed to deliver DNA in fibroblasts and then generalised to other cell types including lymphocytes and embryonic stem cells (Wong and Neumann, 1982, Potter et al., 1984, Potter and Heller, 2003). The principle involves electric pulse delivered between two electrodes to increase permeability of cell membrane by forming pores and therefore siRNA may pass through the membrane.

Inside the cytosol, siRNA binds to RNA induced silencing complex (RISC) which separates the more stable antisense dsRNA and remove sense strand. The antisense strand remains attached to the RISC complex and binds to the target

sequence of messenger RNA (mRNA). The target mRNA is then cleaved by RISC complex, degraded and therefore cannot be translated into protein, effectively silencing the gene.

The siRNAs were resuspended in nuclease-free H_2O to produce stock siRNA of 100 µM which was then aliquoted and stored in -20^oC. Prior to the electroporation, cells were counted and pelleted at 300 g for 5 minutes. The pellets were then resuspended in fresh media to make the concentration of 1.0 x 10^7 cell/ml and transferred into an electroporation cuvette. siRNA was added into the electroporation cuvette to the final concentration of 200 nM and gently mixed before placing it in electroporator. The voltage and duration for each cell lines are listed in Table 2-8. As to confirm electricity has been applied, foamy bubbles should be observed in the cells suspension media in cuvette. The cells were then allowed to recover for 15 minutes at room temperature before transferred into culture flask to the final concentration of 0.5 x 10^6 cell/ml and kept at 37^oC in CO_2 incubator.

Cell line	Voltage (V)	Time (ms)
Kasumi-1	330	10
SKNO-1	350	10
PDX and primary cells	350 (twice)	10

Table 2-8: Electroporation voltage and time used to do electroporation for each type of cells.

siRNA	Sequence	Target site location
siRE	5′-CCUCGAAAUCGUACUGAGAAG-3′	2102-2122
	3′-UUGGAGCUUUAGCAUGACUCU-5′	
siMM	5′-CCUCGAAUUCGUUCUGAGAAG-3′	2102-2122
	3′-UUGGAGCUUAAGCAAGACUCU-5′	
siSLC2A	5’-AAGTACGTTATTGTTGACTTA-3’	3254-3274
	3’-UUCGCCAACUGCUUCUCAGGCUGCC-5’	
siPFKP	5’-CAGGAUCAUCGAGGUCGUCGA-3’	592-672
	3’-UCGACGACCUCGAUGAUCCUG-5’	

Table 2-9: siRNA sequences and the target genes.

2.3 Lentivirus production

Lentivirus was produced in 293T cells using calcium phosphate precipitation method consisted of lentiviral envelope (pMD2.G), packaging (pCMVdR8.91) and expression plasmids.

2.3.1 *293T sub-culture*

The 293T cells were cultured in a T175 cm^2 tissue culture flask and split when it reached 70-80% confluency. The medium was aspirated from the flask and gently washed with pre-warmed PBS to remove excess medium and serum. A volume of 2 ml of pre-warmed trypsin/EDTA was added to the cells monolayer and incubated 10-15 minutes at 37^{o}C in CO_2 incubator. EDTA acts as a chelator for calcium and magnesium that are essential for cell to cell attachment, while trypsin breaks focal adhesion of cells to culture vessel and disaggregates adherent cells into single suspension. The cells were checked under the microscope to confirm all the cells were detached from culture flask.

Once all the cells were confirmed to detach, an 8 ml of medium was added to inhibit trypsin activity and mixed by pipetting. The total cell count was determined by trypan blue exclusion method (2.2.1.3) and seeded in a new flask with the concentration of 1-3 x 10^5 cell/ml in 20 ml medium.

2.3.2 *Co-transfection*

A day before co-transfection, the 293T cells were seeded in 100 mm tissue culture dishes at the concentration of 2 x 10^5 cells/ml in 10 ml medium. On the next day, when the cells had reached 30-60% confluency, 5 μg of lentiviral envelope (pMD2.G), 15 μg of packaging (pCMVdR8.91) and 20 μg of expression plasmids were mixed in a sterile microfuge tube. The volume of the mixture was adjusted with HEPES buffer solution to a total volume of 250 μl, followed by addition of 250 μl of 0.5 M calcium chloride solution and mixed well. The solution was then added slowly droplet by droplet into pre-prepared 500 μl of 2X HeBS solution (pH 7.00) in a 5 ml vial and mixed by vortexing. The mixture was left at room temperature for 30-40 minutes to allow the formation of calcium phosphate precipitate. This suspension was then added dropwise onto the 293T cell monolayer and cultured at 37^{o}C in a CO_2 incubator for 12-16 hours. Afterwards, the medium was removed, the cells were

washed with pre-warmed PBS, a 30 ml of fresh growth medium was added and cultured in standard culture condition for three days.

2.3.3 *Lentiviral harvesting and concentrating*

Approximately 90 hours after the co-transfection, the lentivirus supernatant was collected in 50 ml collection tube. It was centrifuged at 600 g for 15 minutes at 4^{o}C, and the supernatant was further filtered using 0.45 μm PVDF membrane filter to remove any residual debris. The lentivirus was concentrated using a Beckman Optima L-100 XP Ultracentrifuge at 120,000 g, 4^{o}C for 2 hours in a swinging bucket rotor. Once completed, the supernatant was removed carefully by decanting, and the viruses were resuspended in 1 ml of corresponding target cells growth media, aliquoted into several tubes and stored in -80^{o}C freezer.

2.3.4 *Lentiviral Transduction*

Lentiviral transduction was performed using spinoculation method. The target cells were pelleted and adjusted to the concentration of 1.0 x 10^{6} cell/ml with standard growth medium. Polybrene was added to the cells to a final concentration of 8 μg/ml to help neutralises charge repulsion between virions and sialic acid of the cells. A total of 500 μl cells were then plated in a 48-well plate and different volume of viruses was added. The plate was centrifuged at 900 g at 34^{o}C for 50 minutes and incubated in a 37^{o}C CO_2 incubator for the next three days.

2.3.5 *Colony Formation Assay*

Colony formation assay was carried out in semi-solid medium to check the ability of a single cell to grow into a colony. Cells were counted and 5000 cells were pipetted into a sterile 20 ml tissue culture tube. A total of 500 μl pre-filtered methylcellulose media was added into the tube and mixed slowly to reduce formation of bubbles. The mixture was then added into a 24-well plate an incubated at 37^{o}C in a CO_2 incubator. After approximately 7-10 days, a colony with at least 30 cells were counted.

2.3.6 *Cell Viability Analysis*

2.3.6.1 Cell cycle

Cell cycle was carried out using nuclear and chromosome counterstain, 4',6-Diamidino-2-Phenylindole, Dihydrochloride (DAPI). DAPI emits blue fluorescence upon binding to AT regions of DNA and is useful for flow cytometry quantification. A total of 1.0 x 10^6 cells was pelleted and washed twice with PBS. The cells were fixed 4% paraformaldehyde (PFA) for 15 minutes and washed twice with PBS. The fixed cells were either directly stained or resuspended in PBS and kept in 4^{o}C for later analysis. A volume of 200 µl staining buffer that contained 0.25%-Triton 100 was added and incubated for 10 minutes in the dark before analyses with flow cytometer. Triton-100 permeabilises the cell membrane and allows DAPI to stain the chromosomes. Flow cytometry data was then analysed using FlowJo software.

2.3.6.2 G0 separation

A total of 1 x 10^6 cells was resuspended in a 1 ml culture media containing 10 µg/ml Hoechst33342 to make the final concentration of 1.0 x 10^6 cell/ml. The cells were incubated at 37^{o}C for 45 minutes in the dark to allow binding of Hoechst33342 to DNA. Next, the cells were stained with pyronin Y at the concentration of 100 µg/ml, further incubated for 15 minutes at 37^{o}C in CO_2 incubator, transferred on ice and measured with flow cytometer. The flow cytometry data was then analysed with FlowJo software.

2.3.6.3 Apoptosis Assay

Apoptosis assay was carried out using either FITC Annexin V apoptosis Detection Kit I or BV421 Annexin V. The FITC Annexin V kit contained two dyes; Annexin V conjugated to FITC that stained early apoptotic cells and propidium iodide (PI) that stained late stages of cell death. Annexin V has higher affinity to the membrane phospholipid phosphatidylserine (PS) in the presence of Ca2+. Cells undergoing apoptosis have its PS exposed to the extracellular environment, bound to Annexin V and can be detected with flow cytometry.

A total of 1.0 x 10^6 cells was washed twice with cold PBS in 5 ml flow cytometry tube and resuspended in 100 µl of 1X Binding Buffer. This buffer contained 100 mM Ca2+ that formed phospholipid-calcium complexes to mediate Annexin V binding to PS. A volume of 5 µl Annexin V was added for one colour analysis or together with 5 µl PI for two colour analyses. The cells were incubated for 15 minutes in the dark at room

temperature and measured immediately by flow cytometry. The flow cytometry data was then analysed with FlowJo software.

2.3.6.4 Reactive Oxygen Species Assay

A total of 5.0 x 10^5 cells was spun down and resuspended in 1 ml fresh media. A positive control was stained with tert-butyl hydrogen proxide (TBHP) at the final concentration of 200 µM and incubated at 37^{o}C for 45 minutes. Following that, cells were then stained with CellROX green at the final concentration of 500 nM and incubated at 37^{o}C for 45 minutes protected from light. CellROX green reagents are cell-permeable and do not fluorescent while in the reduced state. Upon entry into the cells, CellROX is oxidised by reactive oxygen species (ROS) and emits bright green fluorescent. Data was captured with Facs Canto II and analysed using FlowJo software.

2.3.7 *Small molecule inhibitor assay*

Cells were seeded at 5 x 10^5 cell/ml and drugged on day 0. Subsequent analyses was carried out on day 3. Table 2-10 shows small molecule inhibitor used in this study.

Name	Supplier
2-deoxyglucose	Sigma
palbociclib	DC Chemicals

Table 2-10: Small molecule inhibitors used in this study.

Drug combinations study was performed based on Chao-Talalay method. This method used several concentrations for each compound and mixed at a constant ratio as the third drug. Effective concentration that caused 50% of inhibition (EC50) of single treatment was compared to the median effect achieved by the combination of the two drugs to derive a combination index (CI) value. CI was calculated based on the following equation:

$$Combination\ index\ (CI) = \frac{IC50 combo\ of\ D1}{IC50 single\ of\ D1} + \frac{IC50 combo\ of\ D2}{IC50 single\ of\ D2}$$

$$Where; D1 = Drug\ 1\ and\ D2 = Drug\ 2$$

The description of CI values is listed below.

Symbol	Description	
<0.1	+++++	Very strong synergism
0.1-0.3	++++	Strong synergism
0.3-0.7	+++	Synergism
0.7-0.85	++	Moderate synergism
0.85-0.90	+	Slight synergism
0.90-1.10	±	Nearly additive
1.10-1.20	–	Slight antagonism
1.20-1.45	– –	Moderate antagonism
1.45-3.3	– – –	Antagonism
3.3-10	– – – –	Strong antagonism
>10	– – – – –	Very strong antagonism

Table 2-11*:* The combination index values and its description**.** CI values indicate synergism, additive and antagonism effects as outlined in Chao-Talalay method (Cubitt et al., 2013).

2.4 Flow Cytometry and Sorting

2.4.1 *Flow cytometry*

Flow cytometry analyses were carried out to measure endogenous fluorescent protein and immunophenotypes of cells. The analyses were carried out using Facs Calibur, Facs Canto II or Fortessa X20.

2.4.1.1 Endogenous fluorescent protein/marker

Some cells were transduced to express endogenous fluorescent proteins or incubated with a fluorescent marker and therefore cells can be detected by flow cytometry. For endogenous expression of fluorescent protein, a small number of cells were added into FACS tube, pelleted at 300 g for 5 minutes and resuspended with 200 – 500 µl of PBS and analysed according to the appropriate channel. In some cases, the fluorescent colour of the cells in single tube overlapped onto each other, thus compensation setting was required. In this case, a single positive fluorescent colour was prepared, and compensation setting was done according to the machine protocol.

2.4.1.2 Immunophenotyping

A total of 1.0 x 10^6 cells were pelleted in a FACS tube at 300 g for 5 minutes. The cells were washed 2 times with PBS and further blocked by flow cytometry staining buffer for 15 minutes at room temperature. Afterwards, the primary antibody (Table 2-12) was added and incubated at room temperature for 30 minutes in the dark. The cells were washed twice with flow cytometry staining buffer to remove unbound antibody. Cells were resuspended in 200 µl of flow cytometry staining buffer and immediately captured with Flow Cytometry.

Antibody-species raised in	Supplier	Catalogue number
Human Glut3	R&D System	FAB1415G
Mouse IgG2B-Isotype Control	R&D System	IC0041G
Mouse CD45	Biolegend	103109
Human CD45	Biolegend	368521
Human CD34	Biolegend	343613
Human CD33	Biolegend	366605
Human CD15	Biolegend	301903
Human CD14	BD Pharmigen	506180

Table 2-12: Antibody used in the flow cytometry analysis.

2.4.1.3 Sorting

Cells sorting technique was used to isolate cells population from a mixed population. The technique utilises the identification of endogenous fluorescent protein or pre-stained specific immunophenotype to differentiate each population. Cells were sorted using FACs Aria III that is located in Herschel Building and sorting was carried out by Flow Cytometry Core Facility support staffs. Cells labelling with specific immunophenotype was assisted by Dr Helen Blair. Cells for sorting were counted and pelleted at 300 g for 5 minutes. It was then washed twice with PBS at the same speed and time. Cells were then resuspended in sort buffer and proceed with the sorting. The sorted cells were collected in the flow cytometry staining buffer, washed and continued with further application.

2.5 Molecular Biology Methods

2.5.1 *Cloning*

The cloning procedure involved insertion of shRNA sequences into digested vector. Briefly, synthesised oligonucleotides were phosphorylated to create overhang templates before being ligated into a linearised vector.

2.5.1.1 Oligo phosphorylation

The sense and antisense oligonucleotides were synthesised from Sigma-Aldrich (Table 2-13). In the reaction that contains ATP, the complementary oligonucleotides were hybridised and phosphorylated on the 5' terminus to create oligo duplex, thus able to ligate into the desired vector.

shRNA	Primers	
shPFKP1	Fwd	**AGCG**ACGTGTTTGACTGCAGGAAGAA**TAGTGAAG CCACAGATGTA**TTCTTCCTGCAGTCAAACACGC
	Rv	**GGCA**GCGTGTTTGACTGCAGGAAGAAT**ACATCTG TGGCTTCACTA**TTCTTCCTGCAGTCAAACACGT
shPFKP2	Fwd	**AGCG**CGCATATGAGCAGAATTAATTA**TAGTGAAGC CACAGATGTA**TAATTAATTCTGCTCATATGCA
	Rv	**GGCA**TGCATATGAGCAGAATTAATTAT**ACATCTGT GGCTTCACTA**TAATTAATTCTGCTCATATGCG
shPFKP3	Fwd	**AGCG**CTCCCGCTACTGTGTCCAACAA**TAGTGAAG CCACAGATGTA**TTGTTGGACACAGTAGCGGGAA
	Rv	**GGCA**TTCCCGCTACTGTGTCCAACAAT**ACATCTGT GGCTTCACTA**TTGTTGGACACAGTAGCGGGAG
shSLC2A3#1	Fwd	**AGCG**CGCTCCTGGAGCCTTTGAATA**TAGTGAAGC CACAGATGTA**TATTCAAAGGCTCCAGGAGCA
	Rv	**GGCA**TGCTCCTGGAGCCTTTGAATA**TACATCTGTG GCTTCACTA**TATTCAAAGGCTCCAGGAGCG
shSLC2A3#2	Fwd	**AGCG**CGGGAGAAATGTTGTTCATTA**TAGTGAAGC CACAGATGTA**TAATGAACAACATTTCTCCCA
	Rv	**GGCA**TGGGAGAAATGTTGTTCATTA**TACATCTGTG GCTTCACTA**TAATGAACAACATTTCTCCCG
shSLC2A3#3	Fwd	**AGCG**CGACCAAAGAATGTTTATAGCAAA**TAGTGAA GCCACAGATGTA**TTTGCTATAAACATTCTTTGGG
	Rv	**GGCA**CCCAAAGAATGTTTATAGCAAAT**ACATCTGT GGCTTCACTA**TTTGCTATAAACATTCTTTGGTCG
shRUNX1/ETO	Fwd	**AGCG**AAACCTCGAAATCGTACTGAGA**TAGTGAAG CCACAGATGTA**TCTCAGTACGATTTCGAGGTTC
	Rv	**GGCA**GAACCTCGAAATCGTACTGAGAT**ACATCTGT GGCTTCACTA**TCTCAGTACGATTTCGAGGTTT
shNTC	Fwd	**AGCG**ATCTCGCTTGGGCGAGAGTAAG**TAGTGAAG CCACAGATGTA**CTTACTCTCGCCCAAGCGAGAG
	Rv	**GGCA**CTCTCGCTTGGGCGAGAGTAAGT**ACATCTG TGGCTTCACTA**CTTACTCTCGCCCAAGCGAGAT

Table 2-13: shRNA sequences used in this study.

Thermal cyclers were pre-heated to 37ºC and 95ºC. The components of the reactions (Table 2-14) were mixed in a clean 1.5 ml tube.

Components	**Volume (µl)**
Sense oligo (100 µM)	1.0
Antisense oligo (100 µM)	1.0
T4 DNA ligase buffer (Fermentas)	1.0
T4 Polynucleotide kinase (Fermentas)	0.5
H_2O	6.5
Total volume	**10.0**

Table 2-14: Hybridisation and phosphorylation reaction of oligonucleotides.

The tube was incubated at 37ºC for 30 minutes to allow the phosphorylation reaction. It was then transferred to 95ºC thermal block and incubated for 4 minutes to denature the DNA and inactivate the kinase activity. Next, the hybridisation process was carried out by setting the thermal cycler to 70ºC, and the temperature decreases at about 5ºC per minute. Once the thermal block reached 70ºC, the reaction was left for 10 minutes and continued to cool down to 22ºC using the same thermal block. The reaction was left at room temperature for 4 hours or overnight to achieve complete hybridisation. The annealed oligo duplex was diluted 1:200 with H_2O for further application.

2.5.1.2 Vector digest

Vector digest was performed to cleave plasmid DNA using specific restriction endonucleases (Thermo Fisher Scientific) and provide template for shRNA oligonucleotides. In 1.5 ml clean tube, an amount of 1 μg plasmid DNA was mixed with the component as listed in Table 2-15 below.

Components	Volume (μl)
Restriction enzyme	0.5
10X restriction buffer	1.0
H_2O	Up to 20

Table 2-15: Restriction digestion reaction.

The reaction was incubated at the appropriate temperature of the enzymes (mostly 37^{o}C; referred to the datasheet of the enzyme) for one hour.

2.5.1.3 Gel electrophoresis

Electrophoresis was performed to separate the DNA by size for visualisation and purification of the digested plasmid. The electrophoresis gel was prepared by mixing 0.5 g agarose in 50 ml 1X TAE buffer and heated in microwave until the agarose was completely dissolved. The mixture was let to cool down for 5 minutes and GelRed Nucleic Acid Stain was added in a ratio of 1:10000. The solution was poured into a gel tray with a comb in place and left to solidify at room temperature. Once it has solidified, the gel was loaded into electrophoresis unit and covered with 1X TAE buffer. Molecular weight ladder (New England Biolabs, N3232L) was loaded into the first well. DNA gel loading dye (New England Biolabs, B7024S) was mixed with plasmid DNA in a ratio of 1:10 and loaded into the next wells. The electrophoresis was set at 100 V until the dye line reached approximately 75% way down of the gel and visualised with BioRad Imaging.

2.5.1.4 Gel purification

Electrophoresed gel was visualised on UV box with proper safety equipment were in place. The digested vector was cut off from the gel by using a clean razor blade and placed in a clean 1.5 ml microfuge tube. The tube filled with the cut vector was weighed after zeroing the scale with an empty tube. The weight of the gel was used to determine how much of buffer required to liquefy the gel in the DNA isolation step.

DNA purification was carried out using QIAquick Gel Extraction Kit (Qiagen, 28704). The excised gel was lysed in high-salt conditions buffer and precipitated by adding

isopropanol. This mixture allows nucleic acid to adsorb to the silica membrane. The DNA was washed with 750 µl PE that contained 70% ethanol to dissolve remaining salt in the silica membrane and finally eluted with an appropriate volume of elution buffer.

2.5.1.5 Ligation

Ligation reaction was carried out to ligate oligo duplex (2.5.1.1) into its appropriate digested vector. In this reaction, DNA ligase mediates ligation of the 3'-hydroxyl end (acceptor) to 5'-phosphoryl end (donor) with the presence of ATP to create new phosphodiester bond. The mixture of the reaction is described in the table below:

Components	Proportion
Vector	30 ng
Insert	1 µl
10X T4 DNA ligase buffer	1 µl
T4 DNA ligase	2.5 U
H_2O	Up to 10 µl

Table 2-16: Ligation reaction mix preparation.

The reaction was carried out at room temperature for longer than 3 hours or overnight. The products were either stored at -20^{o}C or directly transformed into bacteria.

2.5.2 *Bacterial transformation*

Bacterial transformation is a technique to introduce exogenous DNA into a bacteria cell. In our lab, we used Stbl3 competent bacteria derived from HB101 *Escherichia Coli* (*E. Coli*) as a tool to store and amplify plasmids. It was first purchased from Life Technologies and thereafter were amplified in our lab.

2.5.2.1 Production of competent bacteria Stbl3

Stbl3 was prepared from competent *E. Coli* based on Inoue et al. (1990 #226). All of the containers, buffers and solutions were prepared sterile and aseptic technique was practised during this protocol. The cells were treated without antibiotics unless otherwise stated.

Stbl3 was grown overnight on LB agar plate without antibiotics at 37^{o}C. Colonies were picked and cultured in 25 ml LB broth in 250 ml flask for 6-8 hours at 37^{o}C with

vigorous shaking (250-300 rpm). This culture was then used to inoculate three different 500 ml flasks containing 250 ml LB media. Each flask received 2 ml, 4 ml and 10 ml, respectively and incubated overnight at 18-22^{o}C with moderate shaking (200 rpm).

The next morning, OD_{600} was monitored using spectrophotometer at every 45 minutes. Once the OD_{600} reading reached between 0.4 and 0.6, the culture vessel was transferred onto ice for 10 minutes. The cells were then harvested in 50 ml tubes by centrifugation at 2500 g for 10 minutes at 4^{o}C. The medium supernatant was removed and the tubes were placed upside down on a tissue paper for 2 minutes to completely remove the media. The cells were resuspended in a 40 ml ice-cold Inoue transformation buffer by swirling gently on ice and harvested by centrifugation at 2500 g for 10 minutes at 4^{o}C. The supernatant was removed as described previously, and the cells were then resuspended in 10 ml ice-cold Inoue transformation buffer. DMSO was added to the final concentration of 7% and the bacterial suspension was mixed gently on ice by swirling and left on ice for 10 minutes. The bacterial mix was then quickly aliquoted into a sterile microfuge tubes and snapped-freeze by immersing in liquid nitrogen before storing in -80^{o}C for long-term storage.

The efficiency of the competent bacteria was tested by transforming either ligation products (section 2.5.2.2) and/or supercoiled plasmid (section 2.5.2.3) on LB agar plate containing different antibiotics.

2.5.2.2 Ligation product

Plasmids from ligation (section 2.5.1.5) were transformed in a ratio of 1:3 vector:insert ratio. Stbl3 competent bacteria were thawed on ice approximately about 20-30 minutes before transformation starts. As much as 4 µl of plasmid from ligation was used to transform 50 µl Stbl3 competent bacteria in 1.5 ml microfuge tube. The tube was mixed by flicking and incubated on ice for 30 minutes. It was then incubated in thermal block at 42^{o}C for 42 seconds to create pores on bacterial membrane in the presence of $CaCl_2$ in the Inoue transformation buffer. The tube was incubated on ice for 2 minutes before 250 µl of SOC media was added, mixed and incubated in 37^{o}C bacterial incubator with moderate shaking for 1 hour. At this stage, there were no antibiotics added to allow production of antibiotic resistance proteins encoded by the plasmid backbone. After an hour, 50 µl and 200 µl of transformed bacteria were plated on LB agar plate containing plasmid specific antibiotic and incubated in 37^{o}C bacterial incubator for 12-16 hour. The bacterial colonies were either processed or kept in 4^{o}C for up to a week and a half.

2.5.2.3 Supercoiled plasmid

A total of 1 - 2 µl supercoiled plasmid that contained 300 ng-1000 ng of DNA was transformed in 25 µl Stbl3 competent bacteria. The mixture was directly plated on LB agar plate containing plasmid specific antibiotic and incubated in 37^{o}C bacterial incubator for 12-16 hour. The bacterial colonies were either processed or kept in 4^{o}C for up to a week and a half.

2.5.2.4 Mini prep plasmid isolation

Mini prep plasmid isolation was carried out using Qiagen QIAprep Miniprep Kit to separate small amount of plasmid ranging from 5 – 25 µg. In general, the procedure consists of alkaline lysis of bacteria with the presence of RNAse A, neutralisation and binding of plasmid to the silica column, washing for removing endonucleases and salts and elution of DNA. All centrifugation steps in this procedure were carried out at 17,900 g at room temperature.

A single colony from transformation from section 2.5.2.2 was picked using pipette tip and transferred into a 5 ml LB medium containing appropriate antibiotics. The culture was incubated for 12-18 hours in a 37^{o}C bacterial incubator with vigorous shaking (200-250 rpm). The bacteria cells were harvested by centrifugation at 6,800 g for 3 minutes at room temperature. They were resuspended in 250 µl of buffer P1

containing LyseBlue (0.1% v/v) and RNAse A (100 μg/ml). LyseBlue is used to indicate inefficient cell lysis and incomplete precipitation of SDS, cell debris and genomic DNA in the following steps. The cells were lysed in 250 μl alkaline lysis buffer, buffer P2 and the solution turned blue in the presence of LyseBlue. The cells suspension was mixed gently by inverting the tube 5-6 times until homogenously coloured solution was achieved. The lysis mixture was incubated at room temperature for 5 minutes and terminated by adding 350 μl neutralisation buffer (buffer N3). At this stage, the solution was immediately mixed until it became colourless. Buffer N3 contained high-salt conditions that precipitated denatured proteins, chromosomal DNA, cellular debris and SDS; however, it allowed the plasmid DNA to stay soluble. To separate the plasmid DNA and precipitates, the sample was centrifuged for 10 minutes in a tabletop microcentrifuge. The supernatant was applied to QIAprep 2.0 spin column and centrifuged for 1 minute to allow plasmid DNA binding to the column. The column was washed twice; firstly with 500 μl buffer PB to remove endonuclease and, secondly, with 750 μl buffer PE that contained 70% ethanol to remove remaining salts. These washing steps were carried out by centrifugation for 1 minute. Additional centrifugation was carried out for 1 minute to remove residual wash buffer. Finally, plasmid DNA was eluted into a clean 1.5 ml microfuge tube by adding 50 μl buffer EB, incubated for 1 minute and centrifuged for 1 minute. Plasmid DNA was stored at -20^{o}C until further application been carried out.

Sequence verification of whether there is successful integration of the shRNA sequences was performed by sending the plasmid DNA sample for sequencing. The primer used to confirm the sequence is listed in Table 2-17 below.

Vector	Sequence (5' to 3')
pLKO.5d.miRNA30	GCCTGCTTCTCGCTTCTGTTC

Table 2-17: Primer sequence used for plasmid DNA sequencing.

2.5.2.5 Maxi prep

To isolate larger plasmid quantity which is up to 500 µg, Qiagen EndoFree Plasmid Maxi kit was used. The procedures consist of alkaline lysis (NaOH/SDS), neutralisation, endotoxin removal, binding of the plasmid DNA to the QIAGEN resin, removing the impurities, plasmid elution with high-salt buffer, and concentrated and desalted of the plasmid.

A single colony from transformation from section 2.5.2.2 was picked using pipette tip and transferred into a 5 ml LB medium containing appropriate antibiotics. The culture was grown as a starter culture by incubating at 37°C for approximately 8 h with vigorous shaking (225 – 300 rpm).

After 8 hours incubation, a 500 µl of the culture was transferred into 250 ml LB media with the appropriate selection antibiotic and grown at 37°C for 12 – 16 h with vigorous shaking. The bacterial cells were pelleted by centrifugation at 4,000 g for 15 min at 4°C and were resuspended in 10 ml Buffer P1. Buffer P1 was supplemented with 1% LyseBlue and 100 µg/ml RNAse A. The bacteria was then lysed by adding 10 ml of Buffer P2 that contains alkaline lysis buffer. The tube was mixed by gentle inverting for six times or until the mixture turned homogeneously blue. The mixture was then incubated for 5 min at room temperature. The lysis reaction was terminated by adding 10 ml chilled Buffer P3. The tube was gently inverted six times or until the suspension became completely colourless. It was immediately transferred into QIAfilter Cartridge and incubated for 10 min at room temperature to float the precipitates. These precipitates contained proteins, plasmid DNA and detergent. The lysate was then filtered through the cartridge and 2.5 ml of endotoxin removal reagent (Buffer ER) was added. The solution was mixed by inverting the tubes for ten times and incubated on ice for 30 min.

A 10 ml Buffer QBT was added into QIAGEN-tip 500 and left to drain completely by gravity flow. The lysate was then applied to the QIAGEN-tip and allowed to empty by gravity flow. The Qiagen-tip was washed twice with 30 ml Buffer QC to remove the contaminants. The plasmid was then eluted with 15 ml high-salt buffer (Buffer QN), followed by the addition of 10.5 ml room-temperature isopropanol to precipitate DNA during the centrifugation step. The centrifugation was performed at 16,000 g for 30 min at 4°C. The supernatant was carefully discarded and the DNA pellet was washed with endotoxin-free 70% ethanol at 16,000 g for 10 min at 4°C to remove remaining

salt. The supernatant was discarded and the DNA pellet was dissolved in 400 – 500 µl endotoxin-free Buffer TE.

2.5.3 *RNA Extraction*

Extraction of RNA was done using Qiagen RNeasy kit which is based on silica membrane spin column nucleic acid purification. The negatively charged DNA backbone binds to the negatively charged silica membrane through the positively charged salts bridge.

Lysed cells in RLT buffer were added into Qiashredder Mini Spin Column to homogenise high molecular weight genomic DNA and other high-molecular weight cellular components.

A volume of 70% ethanol was then added to the homogenised lysate and mixed by pipetting. This mixture precipitates nucleic acids out of solution. The homogenised lysate was transferred into Qiagen Mini Spin column and centrifuge at 13,000 rpm for 2 minutes. The flow-through was transferred into a fresh 2 ml centrifuge tube and isopropanol at 2 times volumes of the sample was added and kept in -20^{o}C for protein precipitation (section 2.5.5).

Spin column containing RNA was washed three times; once with salt-containing buffer RW1 and twice with ethanol-containing buffer RPE. A total of 700 µl buffer RW1 was added into the spin column tube and centrifuge at 8,000 g for 30 seconds to wash out the impurities.

Then, 700 µl of buffer RPE that contained 80% ethanol was added to mini spin column and centrifuged at 8,000 g for 30 seconds to wash out impurities, followed by a second wash with 500 µl buffer RPE and centrifuged at 8,000 g for two minutes. The spin column was centrifuged again at 13,000 rpm for one minute to completely remove any carryover of buffer RPE.

Finally, the spin column was placed in a clean microfuge tube and 30-50 µl of RNase free water was added to the centre of mini spin column. The tube was centrifuged at 8,000 g for one minute to collect RNA and stored in -20^{o}C.

2.5.4 *Densitometry Analysis*

DNA and RNA was quantified using Nanodrop, ND-1000 that can measure as low as 2 ng/µl up to 3000 ng/µl of nucleic acid. The samples were thawed completely, vortexed and spun briefly. The pedestal of Nanodrop was clean with dH_2O using Kimwipes. Upon opening the Nanodrop program on the computer, 1 µl of dH_2O was loaded onto the pedestal to initialise the instrument. An appropriate buffer that was used to elute the RNA was then pipetted onto the pedestal to blank the measurement. In case of RNA, it was RNAse-free water; however, it might be different for DNA samples. An amount of 1 to 2 µl of the samples was pipetted onto the pedestal to measure the nucleic acid concentration. The purity of nucleic acids was assessed based on the 260/280 nm ratio, where a pure RNA is generally between 1.8-2.0 ratio and 1.7-2.0 for DNA.

2.5.4.1 cDNA Synthesis

Synthesis of complementary DNA (cDNA) from RNA was carried out using RevertAid First Strand cDNA Synthesis Kit. The reaction includes binding of random primers to RNA and synthesis of hybrid DNA by reverse transcriptase in the presence of deoxynucleotide triphosphates.

This protocol was carried out on ice throughout the procedures unless otherwise stated. A total of 500-1000 ng RNA was used as template to make cDNA and mixed with 1 µl random primer in a 0.2 ml PCR tube. Then, nuclease-free H_2O was added to make the total volume of 12 µl. The reaction was incubated in thermal cycler at 70^{o}C for 5 minutes and cooled down to 4^{o}C to let random primers anneal to the single-stranded RNA.

A master mix of one sample reaction was prepared based on the following components:

Components	**Volume (µl)**
5X reaction buffer	4
dNTP	2
RevertAid H Minus	1
RiboLock RNase Inhibitor	1
Total	**8**

Table 2-18: Master mix components for cDNA synthesis for one sample.

A volume of 8 µl master mix was then added to the tube, incubated at 25^{o}C for 10 minutes to extend the random hexamer primers and continued with reverse transcriptase by incubating at 42^{o}C for 60 minutes. The enzyme was then heat-

inactivated at 70ºC for 10 minutes. The product was diluted with H_2O to a final concentration of 4-10 ng/µl, stored in -20ºC for longer storage or continued for further application.

2.5.4.2 Quantitative Real-Time Polymerase Chain Reaction

Quantitative real-time polymerase chain reaction (RT-PCR) is a technique to amplify gene of interest in real-time by the use of fluorescent reporter that binds to the DNA. In our lab, we use Platinum® SYBR® Green qPCR SuperMix-UDG as a reporter, that intercalates with double-stranded DNA and emits high fluorescence upon excitation.

Primers targeting each gene of interest were synthesised from Sigma (Table 2-21). Forward and reverse primers were designed using Primer Express 2.0 by covering two different exons and have a melting temperature between 50-60ºC. The length of the primers was generally between 18-22 bp with consideration of 40-60% GC content. Forward and reverse primers were synthesised in individual tubes and lyophilised in H_2O to make a final concentration of 100 µM. Each of forward and reverse primers was mixed in a tube to make the final concentration of 10 µM.

A master mix of a single reaction was prepared based on the following components:

Components	**Volume (µl)**
2X SyBr Green	5.0
Primer mix (10 µM)	0.3
H_2O	2.7
Total	**8.0**

Table 2-19: Master mix components for RT-PCR.

For each target gene, a triplicate was prepared and a volume of 8 µl master mix was pipetted into the bottom of 384-well plate and 2 µl of cDNA (2.5.4.1) was added later. The 384-well plate was sealed using heat-resistant adhesive film (MicroAmp® Optical Adhesive Film, Applied Biosystems), centrifuged for 1 minute at 1,000 g and loaded into the Real-time PCR Machine (Applied Biosystem).

Table 2-20 listed the thermal profile of PCR reaction:

Temperature (°C)	**Time**	**Cycles**
50	2 min	1
95	10 min	
95	15 s	40

60	1 min	
95	15 s	1
60	15 s	
95	15 s	

Table 2-20: Temperature profile for RT-PCR reaction.

Data were analysed using SDS 2.3 System Software or QuantStudio Real-Time PCR System. Comparative Ct method was used in most of the analysis by first normalising Ct values of each gene to the internal control gene i.e.: housekeeping gene to produce ΔCt values. Next, the ΔCt values were compared to the control ΔCt value of particular experiment, yielding ΔΔCt. Relative RNA expression was finally linearised using antilog to the base of 2 since Ct value was represented in two-fold expression change.

Genes		**Sequence**
GAPDH	Fwd	GAAGGTGAAGGTCGGAGTC
	Rv	GAAGATGGTGATGGGATTTC
CYCLO	Fwd	CAGGTCCTGGCATCTTGTCC
	Rv	TTGCTGGTCTTGCCATTCCT
TUBULIN	Fwd	AGGAGCTGGCAAGCATGTG
	Rv	CGGTGCGAACTTCATCGAT
PFKP	Fwd	TGAAGGAGCAATTGATACCCAAA
	Rv	CCAGCTGCGTGACGACAA
SLC2A3	Fwd	GCGCGGGTGTGGTTAATACT
	Rv	TCCTTCTTCCTGCCCTTTCC
SLC2A1	Fwd	GCCCCCCAGAAGGTGATC
	Rv	GCAGGATGCTCTCCCCATAG
SLC2A5	Fwd	GGGAGGCTGACGCTTGTG
	Rv	GTTGTACCCATACTGGAAGGATGAC
TBP	Fwd	CCTAAAGACCATTGCACTT
	Rv	GTTCGTGGCTCTCTTATCCT
RUNX1/ETO	Fwd	AATCACAGTGGATGGGCCC
	Rv	TGCGTCTTCACATCCACAGG
CCND2	Fwd	CTGTGTGCCACCGACTTTAAGTT
	Rv	TGCTCCCACACTTCCAGTTG
CCND1	Fwd	GCCCTCTGTGCCACAGATGT
	Rv	GAAGCGTGTGAGGCGGTAGT
CCND3	Fwd	CAGGCCTTGGTCAAAAAGCA
	Rv	GCGGGTACATGGCAAAGGTA
HK3	Fwd	GGACAGGAGCACCCTCATTTC
	Rv	CCTCCGAATGGCATCTCTCAG
HK2	Fwd	GAGCCACCACTCACCCTACT
	Rv	CCAGGCATTCGGCAATGTG

HK1	Fwd	GCTCTCCGATGAAACTCTCATAG
	Rv	GGACCTTACGAATGTTGGCAA
GPI	Fwd	CAAGGACCGCTTCAACCACTT
	Rv	CCAGGATGGGTGTGTTTGACC
ALDOC	Fwd	ATGCCTCACTCGTACCCAG
	Rv	TTTCCACCCCAATTTGGCTCA
PFKP	Fwd	GCATGGGTATCTACGTGGGG
	Rv	CTCTGCGATGTTTGAGCCTC
TPI1	Fwd	CTCATCGGCACTCTGAACG
	Rv	GCGAAGTCGATATAGGCAGTAGG
PGK1	Fwd	GAACAAGGTTAAAGCCGAGCC
	Rv	GTGGCAGATTGACTCCTACCA
PKM2	Fwd	ATGTCGAAGCCCCATAGTGAA
	Rv	TGGGTGGTGAATCAATGTCCA
ENO1	Fwd	GCCGTGAACGAGAAGTCCTG
	Rv	ACGCCTGAAGAGACTCGGT
ALDOA	Fwd	ATGCCCTACCAATATCCAGCA
	Rv	GCTCCCAGTGGACTCATCTG
G6PD	Fwd	CGAGGCCGTCACCAAGAAC
	Rv	GTAGTGGTCGATGCGGTAGA
PGLS	Fwd	GGAGCCTCGTCTCGATGCTA
	Rv	GAGAGAAGATGCGTCCGGT
PDG	Fwd	ATGGCCCAAGCTGACATCG
	Rv	AAAGCCGTGGTCATTCATGTT
TKT	Fwd	TCCACACCATGCGCTACAAG
	Rv	CAAGTCGGAGCTGATCTTCCT
TALDO1	Fwd	CTCACCCGTGAAGCGTCAG
	Rv	GTTGGTGGTAGCATCCTGGG
PISD	Fwd	CCACCGACTGGACTGTGTC
	Rv	CCGCTCGTTATGGCAGAAGA
ACAD9	Fwd	AGTTCTTGGGACCCGTGGAA
	Rv	GTCTTGAGTACATGGTGTTGGAG
BAX	Fwd	CTGCAGAGGATGATTGCCGC
	Rv	ATCAGTTCCGGCACCTTGGT
BCL2	Fwd	GCCTTCTTTGAGTTCGGTGG
	Rv	GAAATCAAACAGAGGCCGCA
NOXA	Fwd	CAGAGCTGGAAGTCGAGTGTGC
	Rv	GGAGTCCCCTCATGCAAGTTTTT
P21	Fwd	GACACCACTGGAGGGTGACT
	Rv	CAGGTCCACATGGTCTTCCT
CDK4	Fwd	TGCAGAGATGTTTCGTCGAAA
	Rv	CCCAACTGGTCGGCTTCA
CDK6	Fwd	CTTCGAGCACCCCAACGT
	Rv	GGTTTCTCTGTCTGTTCGTGACACT

Table 2-21: Forward and reverse primer sequence for RT-PCR analysis.

2.5.5 *Protein Analysis*

Protein analysis was performed to determine protein expression level by separating the protein based on the molecular weight. Briefly, purified protein samples were run through electrophoresis system and immunoblotted with a specific antibody, hence the expression of the protein can be detected.

2.5.5.1 Protein purification and quantification

Protein quantification was done using Bradford Assay (Bio-Rad) that utilises Coomassie Brilliant Blue G-205 which changes colour in different physiological conditions. In acidic condition, Coomassie Blue is cationic, mainly doubly protonated and is red in colour. In the presence of protein, the first electron is donated to the charged groups of the protein, disrupts the structure and exposes the hydrophobic pocket of the protein. The dye then binds to these pockets with sulfonic acid groups binding to positive amines and stably bound Coomassie Blue emits blue fluorescence, unprotonated form and can be measured spectroscopically.

Protein precipitate from section 2.5.3 was spun down at 13,000 g for 15 minutes at 4^{o}C. The supernatant was removed, a 50-70 µl of urea buffer was added to the tube and mixed by pipetting. The tube was left on the roller mixer for 15 minutes at room temperature to completely dissolve the proteins. The protein samples were diluted with urea buffer in a ratio of 1:10. Besides that, standard was prepared by making a stock of bovine serum albumin (10 mg/ml) in H_2O. The standard was diluted in urea buffer ranging from 0 mg/ml to 2.0 mg/ml. Both protein samples and standards (5 µl) were pipetted into 96-well plate in triplicate. Bradford dye concentrate was diluted 1:5 in H_2O and a volume of 195 µl was pipetted into each sample and standard well. The plate was quickly measured in FLUOstar Omega Microplate Reader (BMG Labtech) at A595 nm. The protein quantity was calculated by constructing a standard curve of the standards against its absorbance values. The absorbance value of the triplicates was averaged and relatively calculated according to the standard curve.

2.5.5.2 SDS-PAGE electrophoresis

Sodium dodecyl sulfate polyacrylamide gel electrophoresis (SDS-PAGE) was used to separate proteins according to molecular weight. Firstly, linear protein chains were prepared by adding reducing agent (β-mercapthoethanol) that cleaves disulphide bonds and produces linear polypeptide chains. Hence, SDS that is present in both gel and running buffer provides uniform negative charge to the proteins during electrophoresis.

The SDS-PAGE gels consisted of two layers; the top layer was stacking gel usually prepared at 4% acrylamide. The less concentrated gel provides bigger pores and allows all the proteins to stack before migrating to the bottom layer. The bottom layer was separating gel which the percentage of acrylamide varies based on the molecular weight of protein of interest (7-20%). Higher percentage of acrylamide is useful to detect low molecular weight as it travels slowly in dense acrylamide pores, while, higher molecular weight protein can be detected in lower acrylamide percentage.

The SDS-PAGE separating gels were cast with the components of 30% acrylamide diluted with deionised water to the desired percentage, 0.1% (w/v) ammonium persulphate (APS) and 0.01% (w/v) Tetramethylethylenediamine (TEMED). The solution was quickly mixed and poured into 2.0 mm or 1.5 mm gel casting chamber followed by addition of 200 μl of isopropanol. In the mixture, TEMED induces APS decay to release free SO4- ions, which react with acrylamide molecules and start polymerisation. The overlay of alcohol on top of the gel prevents oxygen molecules from reacting with SO4- ions and inhibit the polymerisation reaction. After 15 minutes, isopropanol was removed and the stacking gel mixture was prepared at 4% acrylamide and poured on top of the separating gel. Desired comb was inserted onto the chamber and left to solidify for approximately 15 minutes. The gel was used directly or stored in 4^{o}C up to a week.

Before running the electrophoresis, the protein samples were prepared in 1X loading buffer containing 20% (v/v) glycerol, 4% (w/v) SDS, 5% (v/v) β-Mercaptoethanol and 0.1% (v/v) Bromophenol Blue. As described previously, SDS gives uniform charge of unfolded protein catalysed by β-Mercaptoethanol, while glycerol and bromophenol blue give weigh to the sample volume and track the protein movement.

The gels were placed in electrophoresis tank containing electrophoresis buffer. Samples and protein ladder were carefully loaded into the wells and the electrophoresis was started at 80V until the proteins (indicated by bromophenol blue) reached separating gel. The voltage was increased to 100-150V until all the protein samples reached the bottom of the gel.

2.5.5.3 Immunoblotting

Immunoblotting was used to detect the separated proteins by immobilising the protein onto activated membrane, probing with specific antibodies and detecting it with a developer.

Gel was removed from the electrophoresis unit and placed onto a methanol activated PVDF membrane (0.4 μm) and blotting sandwich was assembled using wet sponges and filter papers. The blotting process was performed in blotting buffer at 100 V for one hour. The transfer was assessed by staining the membrane with Ponceau-S red staining for few minutes. The stain was removed by washing the membrane with water followed by blocking the membrane with 10% TBST-milk for one hour. The membrane was then incubated with the primary antibody (Table 2-22) in 4^{o}C overnight or at room temperature for one hour.

After primary antibody incubation, membrane was washed with TBST solution for three times, 5 minutes each to remove unbound primary antibody. It was then incubated in secondary antibody prepared in 10% TBST milk for one hour at room temperature. The washing step was repeated to remove unbound secondary antibody following by detection by chemiluminescence.

Enhanced chemiluminescence (ECL) was used to detect the protein of interest. ECL substrates A and B was mixed freshly at 1:1 ratio and pipetted onto the membrane for one minute. The activated HRP conjugate was then captured using Chemi Doc imaging instrument.

Antibody-species raised in	Supplier	Catalogue number
RUNX1 - Rabbit	Cell Signalling Technology	CST14334
PFKP – Rabbit	Cell Signalling Technology	D2E5
ATG7 – Rabbit	Cell Signalling Technology	D12B11
Actin – Mouse	Abcam	AB49900
GAPDH – Mouse	HyTest Ltd	564 Mab 6C5

Table 2-22: Antibodies for detection of proteins using western blotting technique.

2.6 Metabolic Assay Methods

2.6.1 *Glucose Uptake Assay*

Glucose uptake was done by incubating the cells with fluorescent glucose, 2-(N-(7-Nitrobenz-2-oxa-1,3-diazol-4-yl)Amino)-2-Deoxyglucose (2-NBDG). The glucose molecule was modified at C-2 position with NBDG fluorescent molecule. Upon entry into the cells, the molecule is phosphorylated by hexokinase, trapped within the cells and can be analysed by flow cytometry. Cells were incubated in glucose-free media for 12-16 hours. 2-NBDG was added into the culture at the final concentration of 200 μM and incubated for another 3 hours at 37°C in CO_2 incubator. Cells were washed twice with cold PBS to slow down metabolic activity, resuspended in 300-400 μl cold PBS, transferred into facs tube and quickly analysed with flow cytometer. The data was analysed using FlowJo software.

2.6.2 *ATP Assay*

Luminescent ATP Detection Assay Kit was purchased from Abcam (Ab113849). This assay detects total levels of cellular ATP based on the production of light caused by the reaction of ATP with added firefly's luciferase and luciferin. The emitted light is proportional to the ATP concentration inside the cells. The reaction can be summarised as follows:

$$ATP + D - luciferin + O2 \rightarrow Oxyluciferin + AMP + PPi + CO2 + Light$$

A total of 5 x 10^4 cells was seeded in a 500 µl in a 96-well plate. 50 µl of detergent was added into each well to disrupt the cell membrane. Plate was shaken for 5 minutes in an orbital shaker at 600-700 rpm to lyse and stabilise the ATP molecule. A total of 50 µl of luciferin substrate solution was added to each well and shaken again on orbital shaker at 600-700 rpm for 5 minutes. The plate was covered with aluminium foil for 10 minutes at room temperature. Luminescence readings were

captured using Omega plate reader. Each luminescence readings were subtracted from background well before taking the average. ATP level was calculated as relative to the experimental control.

2.6.3 *Seahorse Glycolysis Stress Test*

Seahorse assay is a real-time measurement of extracellular acidification and oxygen consumption that reflects the changes of glycolysis flux. Cells were plated in Seahorse 96-well plate in non-buffered medium and followed by sequential injection of glycolysis inhibitors using Seahorse XFe96 Analyzer machine. In all steps of this experiment, the media used was Seahorse XF Base media.

2.6.3.1 Plate preparation and hydration of sensor cartridge

Seahorse 96-well plate was coated with Corning Cell-Tak prior to experiment. Cell-Tak adhesive is a formulation of polyphenolic proteins extracted from marine mussel, *Mytilus edulis.* In higher pH, Cell-Tak adhesive comes out from solution and adsorbs to the first surface it contacts. The optimal Cell-Tak concentration for Seahorse XF96 plate is 22.4 µg/ml. A total of 1245 µl of neutral buffer, NaOHCO3 1M was added to Cell-Tak solution and 25 µl was quickly applied into each well and left for 20 minutes at room temperature. Each well was washed twice with 200 µl of sterile water and stored in 4^{o}C.

The XFe96 sensor cartridge that came with the plate was hydrated on the day prior to the experiment. A total of 200 µl of PBS was added into each well of utility plate and sensor cartridge was lowered to submerge the sensors in the PBS solution. The plate was placed in 37^{o}C supplemented without CO_2.

2.6.3.2 Seahorse media preparation

The media was supplemented with 1 mM glutamine and 3% FBS and warmed to 37^{o}C. NaOH 1M and HCl 1M were used to adjust the pH value to 7.4.

2.6.3.3 Sample preparation

On the morning of the experiment, 2.0 x 10^5 cells for each well were pelleted at 300 g for 5 minutes, washed with phosphate buffered saline (PBS) and resuspended in 25 µl of warm media. The 25 µl of cells was pipetted slowly along the side of each well to form a monolayer except for background wells. For each well, a minimum of triplicate was prepared. To the background wells (highlighted in black colour in Figure 2-1) 25 µl of assay medium was added. The plate was then centrifuged at 200 g for 1

minute with zero braking. The plate was transferred to 37°C incubator not supplemented with CO_2 for 30 minutes to ensure the cells have completely attached. After the cells were confirmed to stably attach to the culture surface by microscope, a 125 µl of warm assay media was pipetted along the side of all wells to make a total volume of 175 µl and returned to the incubator for 15 minutes. The confirmation of the health of the cell included cell morphology, seeding uniformity and no cells in background wells.

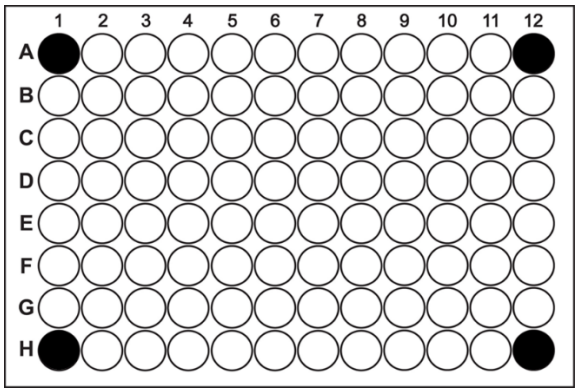

Figure 2-1: Seahorse Analyzer 96-well plate. Background wells highlighted in black.

2.6.3.4 Compound preparation

The compounds used in the glycolysis stress assay were glucose, oligomycin and 2-deoxyglucose (2DG) with a final concentration of 100 mM, 2.5 µM and 50 mM, respectively. The concentration of stock compounds loaded in each port were prepared based on the volume in the wells after every injection. The details of the concentration prepared are illustrated in Table 2-23 below.

Port - Compound	Volume in culture well after every injection; starting volume = 175 µl (µl)	Final concentration in each well	Volume injected (µl)	Stock concentration to prepare	
A – Glucose	200	100 mM	25	800 mM	8X
B – Oligomycin	225	2.5 µM	25	22.5 µM	9X
C – 2-DG	250	50 mM	25	500 mM	10X

Table 2-23: The stock concentration prepared and port of injection for glycolysis stress assay.

2.6.3.5 Seahorse glycolysis stress test normalisation

Seahorse plate was loaded into Seahorse XFe96 Analyzer located in Flow Cytometry Facs Facility. After running the plate, the cells were lysed with lysis buffer and protein

assessment were performed according to the protein assessment method (section 2.5.5.1). Next, extracellular acidification rate were analysed using Wave 2.0 software.

2.7 In-vivo studies

2.7.1 *Mice strain*

Animal work was carried out in accordance to Home Office regulations with project license number PPL60/4522. Two immunodeficient mice strains were used in this study and the characteristic of each strain is listed below.

Abbreviation	Strain name	Source
NSG	*NOD.Cg-Prkdcscid Il2rgtm1Wjl/SzJ*	Jackson Laboratory
Rag2$^{-/-}$ ɣC$^{-/-}$ (RG)	*Rag2−/−Il2rg−/−129×Balb/c*	Jackson Laboratory

Table 2-24: Mouse strain used in the study.

Mice weighing and checking were carried out at least once per week. Checking of mice general health included movement, signs of anaemia, coat quality, piloerection, and the colour of the eyes, paws, feet and ears. The mice were humanly killed when they reached the endpoints listed below:

1. Body weight loss of 20% or more, (30% if mouse under treatment).
2. Body weight loss of 10% – 20 % and maintained low for three days.
3. Tumour size is 1 cm in any dimension, (1.5 cm if mouse under treatment).
4. Tumours are affecting the mice movement.
5. Any sign of sickness that is severely affecting the health of the mouse.

2.7.2 *Xenotransplantation models of t(8;21) AML*

2.7.2.1 Intrahepatic transplantation

Intrahepatic injection was used to transplant Kasumi-1 cells based on the method established by our lab before (Soria et al., 2008). Briefly, injection was performed using a fine flexible Hamilton needle. Newborn mouse was held firmly by the end of the thumb and the index finger then the needle was inserted in the top of the chest under the skin. When the needle reached the end of the ribs, the needle was pushed toward the mouse chest in 45° towards the right of the mouse where it was bent and reached the liver. The cells then released slowly and the needle was withdrawn smoothly. After the injection, the mouse was placed back to the nest and monitored closely for any sign of health deterioration.

2.7.2.2 Intrafemoral transplantation

Cells were injected with interfemoral (IF) route in NSG female mice. The injections were performed under a sterile environment in a category II hood. Mice were anaesthetised with 5% isoflurane then anaesthesia was marinated with 2-3% isoflurane. Before transplantation, mice were weighed and injected with 5 mg/kg Carprofen for analgesia. The injected leg was shaved and sterilised with skin disinfection spray. A hole was made in the injected femur by inserting 29G insulin needle in the kneecap and through the femur then the needle was removed and new needle with the sample was inserted and 20 µl of cell suspension was injected. Mice were placed back into the cage and monitored for anaesthesia recovery.

2.7.2.3 Intravenous

Intravenous (IV) injection route was used to inject the 2FDG. Mice were held tightly in a restraint tube under category II hood. If the tail vain was not clear then the tail is either massaged or placed in warm water to reveal the vain. The tail was stretched straight tightly and the needle inserted at around 180° and the drug released steadily. Once the injection was completed, the pressure was applied on the injection site for 10-30 seconds to prevent any bleeding then the mouse placed back into the cage and monitored.

2.7.3 *In vivo imaging*

Bioluminescence was measured by *in vivo* imaging system (IVIS). Mice were intraperitoneal (IP) injected with 5 mg/kg luciferin. After 5 minutes from luciferin injection, mice placed in the anaesthesia induction box and anaesthetised with 5% isoflurane followed by maintaining the anaesthesia at 2-3% isoflurane. Mice were moved to the IVIS machine, the head was placed into a face mask and the body temperature was maintained at 37°C via heat mat. After 10 minutes of the luciferin injection, imaging was performed. Once imaging was completed, mice were placed back into the cage and monitored for recovery.

2.7.4 *Mice dissection and cells isolation*

The mice where dissected for isolation of leukaemic cells depending on the engraftment patterns. Tumours, spleen, bone marrow were regularly harvested. The spleen and tumours were weighed first then homogenised and the cells passed through a cell strainer using PBS under sterile conditions. For a collection of the bone marrow, femur, tibia, desk, and spine were regularly collected and cleaned from any muscles and tissues.

Harvested cells washed with PBS at least once and counted using trypan blue and also methylene blue to eliminate the mouse blood cells count.

Chapter 3 : Validation of *SLC2A3* and *PFKP* as potential partner in RUNX1/ETO in maintaining leukaemic survival

3.1 Introduction

RUNX1/ETO is an oncogenic transcription factor classically known as transcription repressor in AML (Gelmetti et al., 1998). We showed that RUNX1/ETO can also activate target genes to drive leukaemic propagation and survival (Martinez-Soria et al., 2018). The associated shRNA screen suggested two putative RUNX1/ETO target genes, *SLC2A3* and *PFKP* as crucial components of the RUNX1ETO programme. For each of the genes, two shRNAs were depleted significantly *in vivo;* however, there were no changes in *in vitro* assays. Both of the genes are the key genes involved in glycolysis.

SLC2A3 is also known as GLUT3 and facilitates the transport of glucose across the plasma membrane. It has the highest affinity to glucose (Km approximately 1.4 mM) compared to the other members in the family (Arbuckle et al., 1996, Ian et al., 2008). SLC2A3 was the third of 14 members of SLC2 family that was cloned from mouse brain and was originally thought to be a neuronal transporter (Nagamatsu et al., 1992, Ian et al., 2008). However, SLC2A3 is also expressed in both vascular and intravascular in human lymphocytes, monocytes/macrophages, neutrophils and platelets (Mantych et al., 1992). High expression of SLC2A3 is predominantly seen in advanced tumours such as squamous cell laryngeal cancer and is associated with poor survival in glioblastoma (GBM) patients (Starska et al., 2015, Cosset et al., 2017). Some studies have suggested that SLC2A3 is associated with cancer stem cells properties (Flavahan et al., 2013, Cosset et al., 2017).

The expression pattern of *SLC2A3* was cross-examined on the BloodSpot website (Bagger et al., 2016). This database provides expression plot of genes in healthy and cancerous haematopoietic cells at different maturation stages. In normal cells, *SLC2A3* shows a low expression in stem cells with further increasing expression as the cells differentiate (Figure 3-1-A&B). The expression of *SLC2A3* is elevated in normal myeloid differentiated stages, to support the substantial increase in energy need associated with cell activation. For instance, in the case of the maturation of monocytes to macrophages, energy is required to undergo changes in shape and size to facilitate phagocytosis. In RUNX1/ETO-leukaemia, *SLC2A3* expressions were shown to be significantly ($p<0.01$) upregulated when compared to stem cells populations (Figure 3-1-A). High expression was also observed in other AML subtypes and is thought to support high rate of glucose uptake to meet energy demand and promote leukaemic cells expansion in the immature myeloid population.

Another target that also scored in the *in vivo* shRNA screen was *PFKP,* a gene that encodes the platelet isoform of phosphofructokinase (PFK), a gatekeeper in glycolysis. Other isoforms of PFK are PFKL and PFKM; however, only *PFKP* is shown to be dysregulated in cancer (Thakkar et al., 2010). From BloodSpot database, *PFKP* is shown to be highly expressed in both normal haematopoietic stem cells and other AML subtypes including RUNX1/ETO-leukaemia and gradually decreases in differentiated stage. The fact that stem cells rely heavily on anaerobic glycolysis to maintain dormant and quiescent state (Ito and Suda, 2014) might explain the high expression of *PFKP* in these populations.

3.2 Aims

This chapter aims to validate *SLC2A3* and *PFKP* as direct targets of RUNX1/ETO by using RNAi approach in both *in vitro* and *in vivo*. The strategy that will be used to achieve this aim is individual knockdown to evaluate the effect of each gene as well as double knockdown on both genes in targeting the axis of glycolysis.

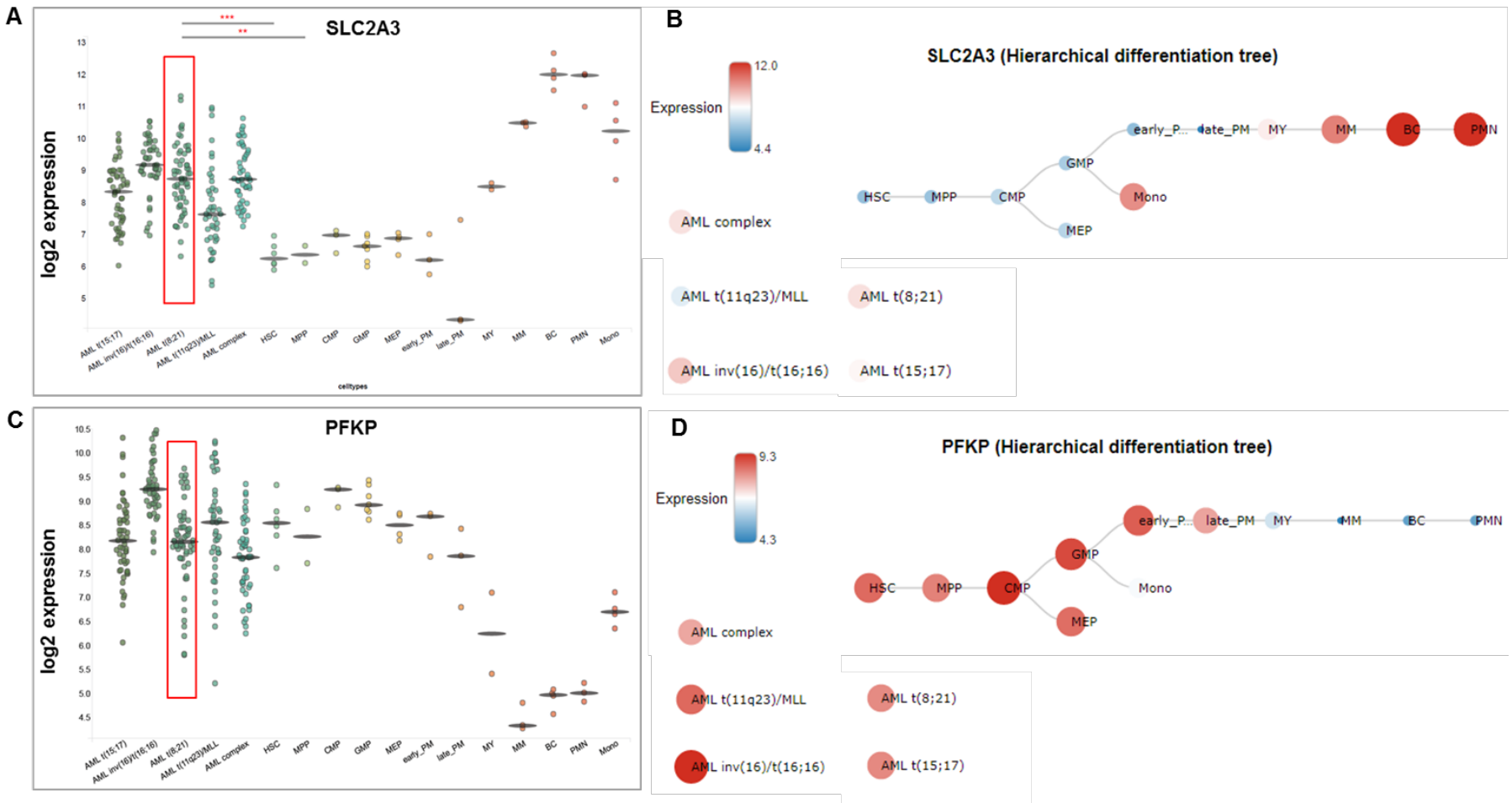

Figure 3-1: Snapshots of *SLC2A3* and *PFKP* expression data from BloodSpot. A, C) Strip charts show *SLC2A3* and *PFKP* expression relative to normal counterparts in haematopoietic system and different AML subtypes. Each dot represents one sample and grey eclipse indicates median. Significance was evaluated using students t-test **p<0.01), ***p<0.001. (B, D) Hierarchical tree showing the relationship between different cell types in database. The colour represents the expression level of the genes, and node size indicates median gene expression. HSC, haematopoietic stem cells; MPP, multipotent progenitors; CMP, common myeloid progenitors; GMP, granulocyte monocyte progenitors; MEP, megakaryocyte-erythroid progenitor cell; PM, promyelocyte; MY, myelocyte; MM, metamyelocytes; BC, band cells; PMN, polymorph nuclear cells; Mono, monocytes.

3.3 Results

3.3.1 *Knockdown of RUNX1/ETO abolished its binding in close proximities region based on Chip-sequencing data*

Firstly, I sought to examine RUNX1/ETO binding location on *SLC2A3* and *PFKP* genes by cross-inspection of Chip-sequencing and RNA-sequencing data (Ptasinska et al., 2012, Ptasinska et al., 2014). Ptasinska (2012) has identified RUNX1/ETO target sites by chromatin immunoprecipitation (ChIP) followed by high-throughput sequencing (ChIP-sequencing) on Kasumi-1 cell line 48 hours post-RUNX1/ETO knockdown by siRNA. The antibody used in the experiments targeted specific ETO protein, and the genome-wide cell line ChIP-sequencing data was validated by comparing primary, patient-derived t(8;21) AML cells. High-confidence of RUNX1/ETO target regions was identified based on ETO ChIP peaks that were shared between mock-transfected and mismatch control-transfected cells and finally, cross-inspected with peak disappearances upon RUNX1/ETO knockdown. RNA-sequencing data set was derived from a four-day siRUNX1/ETO knockdown in Kasumi-1 cell line consisted of three independent biological replicates (Ptasinska et al., 2012).

As depicted in Figure 3-2-A, RUNX1/ETO occupied an open chromatin region located 20 kb upstream of *SLC2A3* in both mock and mismatch-transfected cells. Knockdown of RUNX1/ETO diminished its binding to this element and further reduced the RNA expression of this gene. Figure 3-2-B shows an RUNX1/ETO binding peak at 150 kb upstream of the transcriptional start site of the *PFKP* gene in both mock and mismatch-transfected cells, and the peak disappeared upon RUNX1/ETO knockdown. However, the expression of *PFKP* was barely reduced in RUNX1/ETO knockdown cells.

I next examined whether RUNX1/ETO depletion affected the expressions of other family members of these two genes. Figure 3-2-A bottom panel shows other SLC2 family members that were detected in Kasumi-1 cell line, which were *SLC2A1* and *SLC2A5*. Depletion of RUNX1/ETO did not lead to reduction of *SLC2A1;* however, *SLC2A5* increased upon knockdown of RUNX1/ETO.

For *PFKP,* depletion of RUNX1/ETO led to a 30% reduction of *PFKP* expression. Furthermore, only *PFKL* was highly expressed but the expression was barely

reduced upon *RUNX1/ETO* knockdown. Another isoform, *PFKM* was not detected in the RNA-sequencing data.

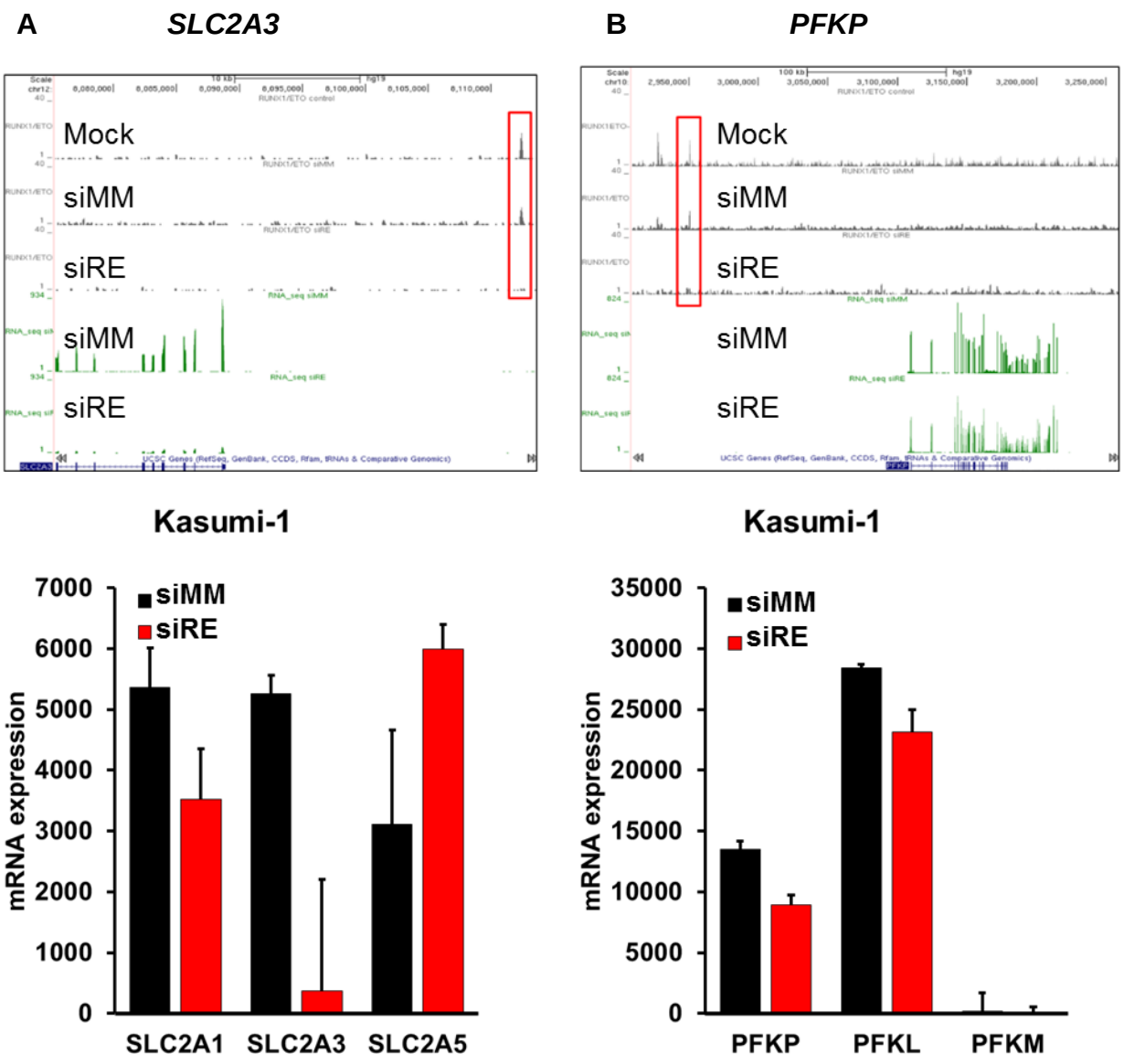

Figure 3-2: Identification of *SLC2A3* and *PFKP* as partner genes in Kasumi-1 cells. A&B) Top: UCSC genome data aligned Chip-sequencing and RNA-sequencing of *RUNX1/ETO* knockdown and mismatch control siRNA 48 hours after knockdown. A&B) Bottom: Expression level of different transporters of *SLC2A3* and isoforms of *PFK* with and without *RUNX1/ETO* knockdown after 48 hours (n=3 independent experiments).

3.3.2 *In vitro validation of SLC2A3 and PFKP as RUNX1/ETO partner genes*

RNA sequencing, ChIP-sequencing and shRNA screening data indicated that *SLC2A3* exhibit potential partner genes bound by RUNX1/ETO. However, *PFKP* was determined to be affected in longer exposure of RUNX1/ETO knockdown based on bead array time course data (Figure 3-3). Therefore, to validate whether RUNX1/ETO directly regulates *SLC2A3* and *PFKP,* I employed two well-studied cell lines in t(8;21) AML: Kasumi-1 and SKNO-1. Small interfering RNA (siRNA) targeting *RUNX1/ETO* (siRE), mismatch-control transfected (Pui et al.), mock-transfected as well as siRNA targeting *SLC2A3* (siSLC2A3) and *PFKP* (siPFKP) were used in the experiments. siRE was designed to target against the fusion site of RUNX1/ETO mRNA and, thus, does not interfere with wild type RUNX1 or ETO mRNA (Heidenreich et al., 2003). Mismatch control, siMM contained two centrally located A-to-U transversions in comparison to siRE. siRNAs targeting *SLC2A3* and *PFKP* mRNA were purchased from Qiagen, and the sequences are listed in Table 2.1. The siRNAs were delivered to the cells by electroporation with an electroporator on day 0, 4 and 7. Cells were collected on day 2, 4, 7 or 10 for RNA analysis.

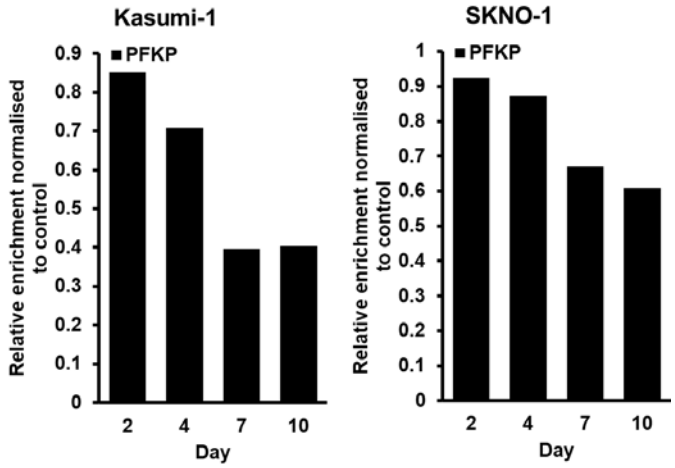

Figure 3-3: Long-term knockdown of RUNX1/ETO leads to greater reduction of PFKP. Bead array analyses on day 2, 4, 7 and 10 were performed on the cell lines treated with siRNA targeting RUNX1/ETO. The relative enrichments were normalised to the control (siMM).

As shown in Figure 3-4-A, *SLC2A3* expression levels diminished by almost 60% in siRE-treated Kasumi-1 cell lines 48 hours post-transfection and almost completely disappeared on day 10 when compared to mock treated control, indicating that

SLC2A3 is a transcriptional target of RUNX1/ETO. In contrast, *PFKP* expression only slightly reduced by 20% in Kasumi-1 cells on day 2 post-transfection, and gradually reduced to ~50% with serial electroporation on day 7 and 10. In SKNO-1 cell line, 50-80% *RUNX1/ETO* knockdown caused *SLC2A3* mRNA to reduce to 40% after a prolong siRNA treatment and had an only negligible impact on *PFKP* mRNA levels.

Taken together, *SLC2A3* is directly affected by RUNX1/ETO in both Kasumi-1 and SKNO-1 cell lines. Depletion of *RUNX1/ETO* led to a massive reduction of *SLC2A3* especially in Kasumi-1, while a modest reduction was observed in SKNO-1. *PFKP*; however, requires a potent and longer knockdown of *RUNX1/ETO* before loss of expression could be observed in Kasumi-1 cell line. However, no substantial *PFKP* changes observed in SKNO-1 cell line.

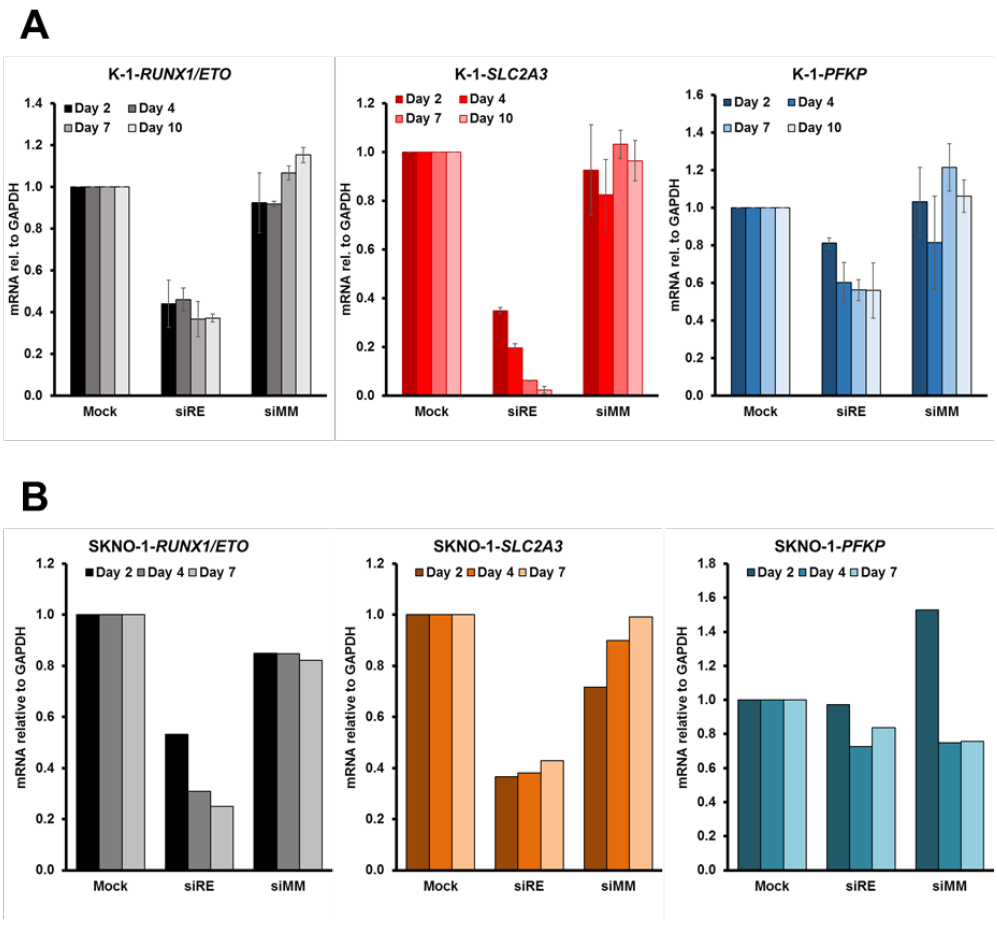

Figure 3-4: Knockdown of *RUNX1/ETO* in t(8;21) positive cell lines reduces *SLC2A3* mRNA but takes longer to inhibit *PFKP* expression in Kasumi-1 cell line. A) Kasumi-1 cells were transfected with either 200 nM corresponding siRNA or mock treated by electroporation on day 0, 4 and 7. Cells were harvested on day 2, 4, 7 and 10 and checked for RNA expressions (n=3, non-independent experiments). B) SKNO-1 cells were transiently transfected with corresponding siRNA or mock treated by electroporation on day 0, 4 and 7. Cells were harvested on day 2, 4, 7 and 10 and checked for RNA expressions (n=1).

3.3.2.1 Single knockdown of SLC2A3 and PFKP by siRNA did not reduce leukaemia burden; however double knockdown strategy led to loss of populations

RUNX1/ETO knockdown substantially reduced *SLC2A3* transcript level and modestly impaired *PFKP* transcript in Kasumi-1 cells. So, I next sought to investigate if depletion of individual gene or double knockdown targeting *SLC2A3* and *PFKP* would affect the leukaemic propagation. I reasoned that a double knockdown strategy targeting these genes would completely impairs glycolytic functions, as shown in GSEA analysis (Figure 5-1). Cells were serially transfected with siRNA on day 0, 3 and 6, with 200 µM of corresponding siRNA and cultured at 5 x 10^5 cells/ml. Since this experiment included double knockdown of *SLC2A3* and *PFKP*, each individual siRNA was treated in combination with siMM, making up 400 µM total final concentration of siRNA. Cells were counted on day 3, 6, 9 and 12. RNA analyses were done on day 3, 6 and 9.

Figure 3-4 shows the mRNA level of *RUNX1/ETO, SLC2A3* and *PFKP* on day 3, 6 and 9 in Kasumi-1 cell line. As expected, depletion of *RUNX1/ETO* led to 70% reduction of *SLC2A3* mRNA on day 3 and almost depleted to 0.5% on day 9. *PFKP* transcript level gradually decrease over the period of transfection with a reduction of 10% on day 3 and 40% on day 9. In siSLC2A3 treated cells, *SLC2A3* mRNA level reduced by 60% on day 3, 6 and 9, and the depletion had no effect on *RUNX1/ETO* and *PFKP* mRNA levels. Furthermore, siPFKP treatment caused a 60-70% reduction of *PFKP* mRNA on day 3 and 9. Similarly, double knockdown of both *SLC2A3* and *PFKP* reduced expression of both genes by 60-70% between day 3 and 9.

Figure 3-5 shows the corresponding proliferation curve for each of the knockdown cells. Mismatch treated control had a doubling time of 72 hours on day 12. There were no changes observed in *SLC2A3* and *PFKP* knockdown as both of them had 74 and 73 hours doubling time respectively on day 12. However, double knockdown of *SLC2A3* and *PFKP* caused the cells to increase the doubling time to 98 hours which was similar to the doubling time observed in siRUNX1/ETO treated cells.

Collectively, Kasumi-1 cells were not affected by even a substantial knockdown of either *SLC2A3* or *PFKP*. However, the double knockdown approach targeting *SLC2A3* and *PFKP* led to a slower proliferation mimicking *RUNX1/ETO* knockdown cells.

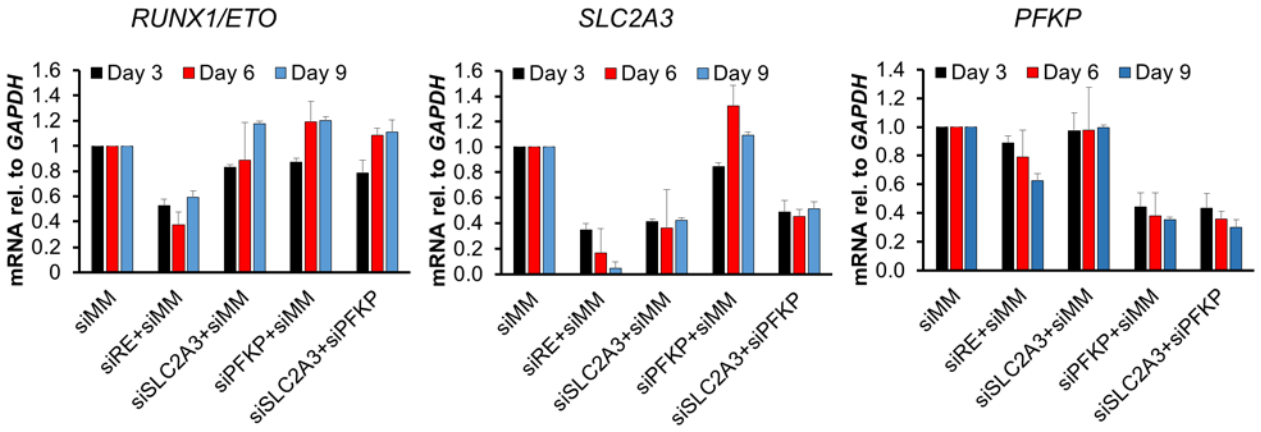

Figure 3-5: mRNA expression level of *RUNX1/ETO, SLC2A3* and *PFKP* after series of electroporation in double knockdown approach in Kasumi-1 cells. Kasumi-1 cell were transfected with siRNA on day 0, 3, and 6 and cells were harvested on day 3, 6 and 9 for RNA analyses (n=3, non-independent experiments).

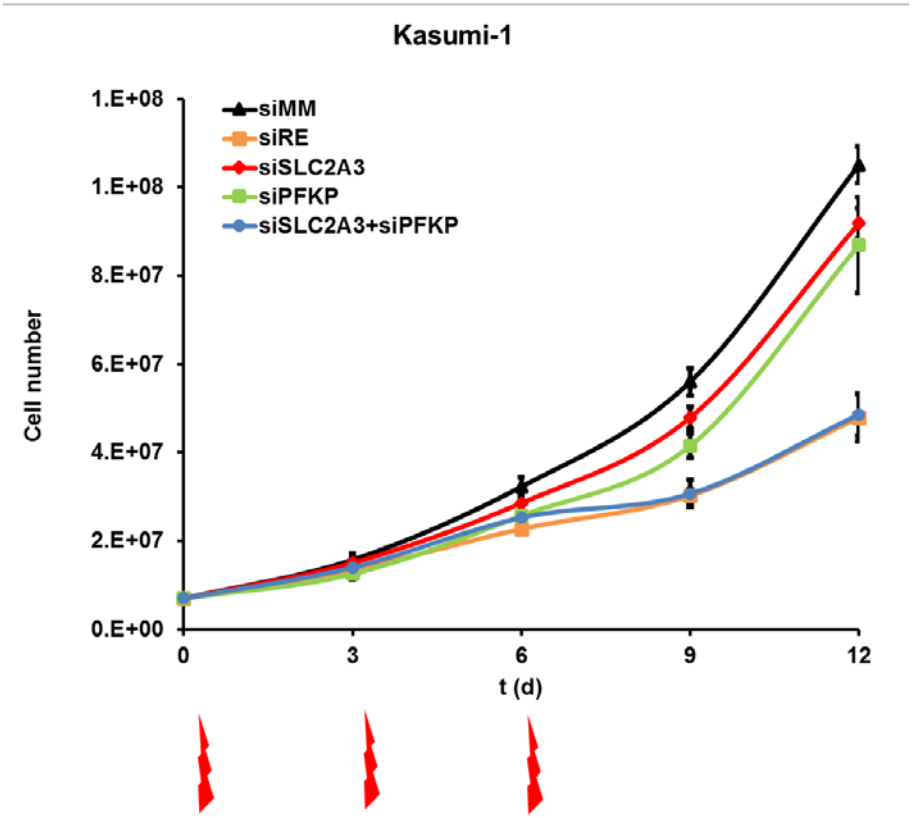

Figure 3-6: siRNA treated Kasumi-1 cell line reduces proliferation in double knockdown strategy. Cells were transfected with 200 µM of corresponding siRNA in combination with 200 µM siMM at day 0, day 3 and day 6. Cells were counted on day 3, 6, 9 and 12; and re-cultured at 0.5 x 10^6 cell/ml after counting. Number of cells were calculated based on accumulation of cells at every timepoint divided by the dilution factor (n=3, non-independent experiments).

3.3.2.2 Loss of SLC2A3 did not affect expression of other glucose transporters

Since *SLC2A3* knockdown did not affect the leukaemic proliferation *in vitro*, I wondered about the possibility of increased expression of other glucose transporters in order to compensate for loss of *SLC2A3*. Based on the RNA sequencing data (Figure 3-2), there were two other transporters, *SLC2A1* and *SLC2A5,* that were highly expressed in Kasumi-1 cells. SLC2A1 is another glucose transporter that is predominantly overexpressed in cancer (Yan et al., 2015), whereas SLC2A5 functions to transport both glucose and fructose into the cells.

Figure 3-6 shows the transcript levels for both *SLC2A1* and *SLC2A5* after 3 electroporations in Kasumi-1 cell. Neither individual nor double knockdown of *SLC2A3* and *PFKP* caused changes in the expression of *SLC2A1* and *SLC2A5.* An increment was only observed for *SLC2A5* in *RUNX1/ETO* knockdown cells, which it increased 2-fold on day 9. This result indicates that there were no changes in other transporters to potentially compensate loss of *SLC2A3* in Kasumi-1 cells.

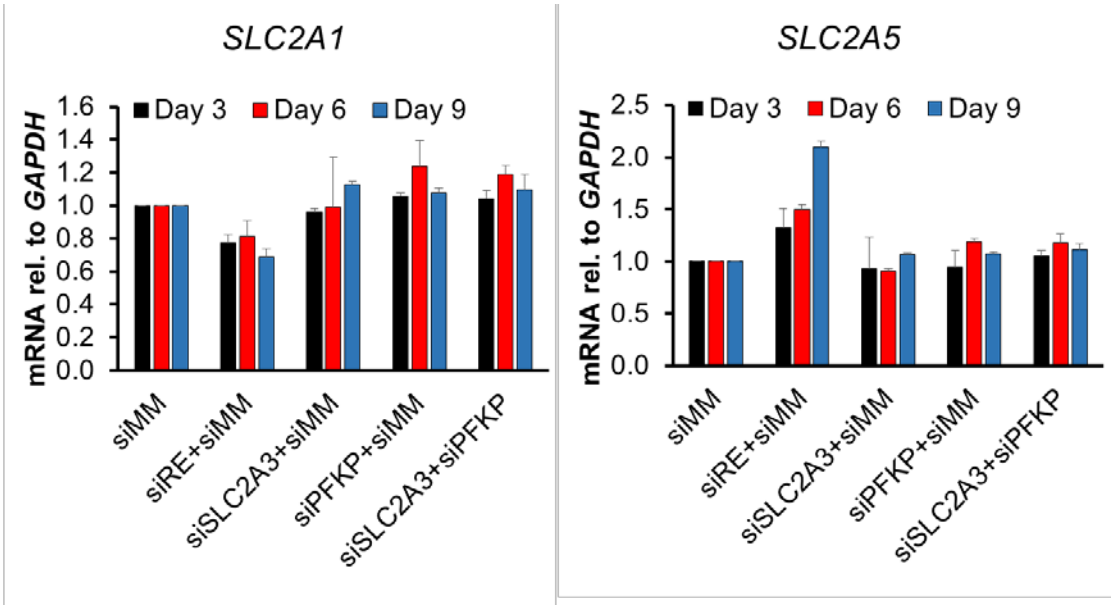

Figure 3-7: mRNA expression level of *SLC2A1* and *SLC2A5* after series of electroporations in Kasumi-1 cell line. Kasumi-1 cell were transfected with siRNA on day 0, 3, and 6 and cells were harvested on day 3, 6 and 9 for RNA analyses. RNA expression was measured against shNTC-treated cells and GAPDH served as a housekeeping gene (n=3, non-independent experiments).

3.3.3 *In vivo validation of SLC2A3 and PFKP as potential therapeutic target for leukaemic expansion and survival*

Depletion of *SLC2A3* and *PFKP* did not reduce leukaemic burden in Kasumi-1 cell line. However, this finding is expected as the genes were not scored *in vitro* in the shRNA screen. I next sought to explore the functional role of these genes *in vivo* by shRNA-mediated knockdown. A constitutive shRNA expression vector, pLKO.5d.miRNA30 was used in this study (Figure 3-7-C). This vector incorporates shRNA sequences into endogenous human micro-RNA backbones, miR-30a, that is processed through complete RNAi biogenesis pathway and leads to a stable shRNA system in both *in vitro* and *in vivo* (Martinez-Soria et al., 2018). The system utilises polymerase II promoters to generate micro-RNA30a-based shRNA, allowing constitutive and potent gene knockdown (Stegmeier et al., 2005, Dickins et al., 2005). Dickins (2005), demonstrated a single copy of shRNA expressed from Polymerase II 5' LTR drove extremely efficient knockdowns in comparison with conventional shRNA-expressing vector containing Polymerase III U6 promoter. Although several studies have shown that U6 promoter drives efficient shRNA expression in haematopoietic cells (An et al., 2006, Banerjea et al., 2003); however, it is often associated with high toxicities (An et al., 2006, McBride et al., 2008) through possible interference with endogenous miRNAs (An et al., 2006). In contrast to that, miR30-based shRNA system has been reported to overcome this issue (McBride et al., 2008).

3.3.3.1 Production of cells stably expressing shRNA targeting SLC2A3 and PFKP using human miRNA30 shRNA vector

Cells stably expressing shRNA targeting *SLC2A3* and *PFKP* mRNA were produced using second generation lentiviral vectors as described in Materials and Method section 2.4. Three shRNAs for each *SLC2A3* and *PFKP* were designed and oligonucleotides were cloned into this vector. Plasmid DNAs were extracted and sent for Sanger sequencing for sequence validation. Sequencing primer was designed 110 bp upstream of shRNA insert which enabled the sequences to be confirmed as

illustrated in Figure 3-7-D. The left side of the figure shows part of vector sequence, and the right side proves successful insertion of shRNA sequence.

Lentivirus containing these shRNAs was produced by co-transfecting 293T cells with the packaging vector pCMVdeltaR8.91, the envelope vector pMD2.G and transfer vectors with the pLKO.5d.miRNA30 backbone (Figure 3-7-A-C).

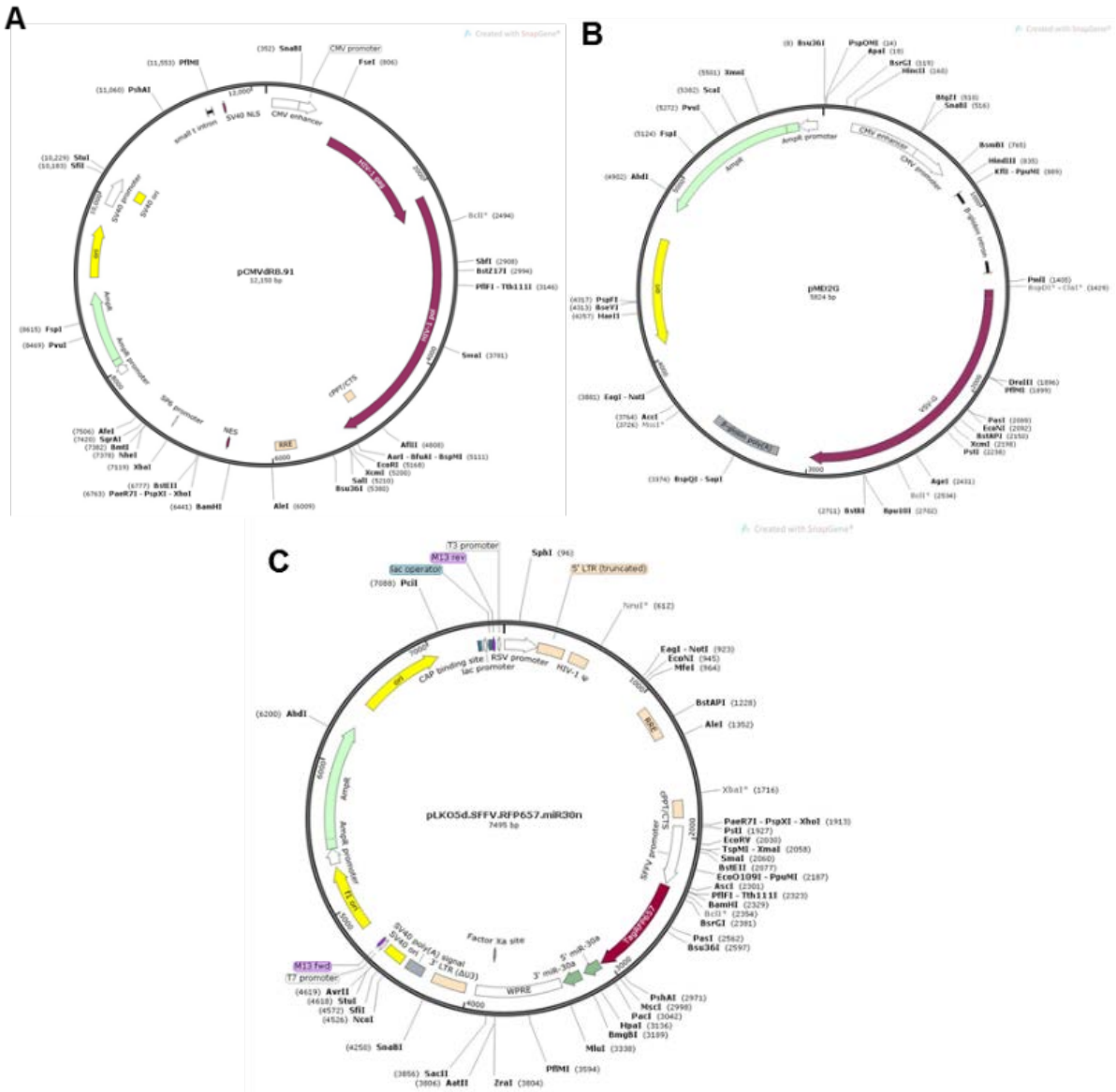

Figure 3-8: Maps of packaging, envelope and transfer vectors used to produce cells stably expressing shRNA. A) Map of packaging vector, pCMVdeltaR.8.91. B) Map of envelope vector, pMD2.G. C) Map of transfer vector (pLKO5d.SFFV.miRNA30. Representative of RFP657 expressing vector. D) Electropherogram showing confirmation of the pLKO5d.miRNA30 vector sequence by Sanger sequencing. The left panel showed nucleotide sequence associated with the vector and right panel showed shRNA sequences confirming the insertion of shRNA.

To produce shRNA virus particles, 293T cells were transfected by calcium phosphate precipitation method. The precipitates were added onto 293T cells cultured at 30-40% confluency seeded a day before. I employed three different variants of pLKO.5d.miRNA30 harbouring either RFP657, dTomato or eGFP as fluorescent marker, thus enable the cells to be viewed under a microscope equipped with different filters (Figure 3-8). To view the cells, I used an inverted microscope that was equipped with three filters which were Dapi, GFP and Texas Red; but only two filters can be used to visualise the cells which were, GFP and Texas Red for the expression of eGFP and dTomato fluorescent proteins respectively.

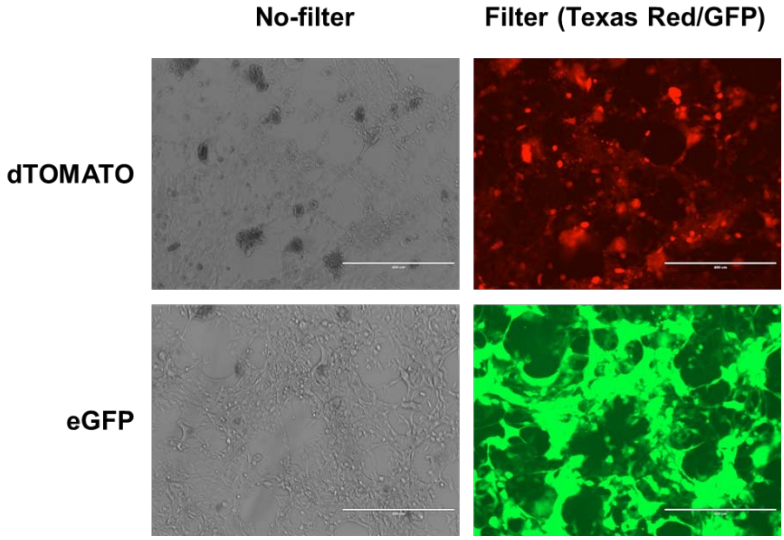

Figure 3-9: Transfection of 293T cells with pLKO5d.miRNA30 expressing colours associated with the transfer vector. 293T cells were seeded at a density of 2 x 10^5 cells/ml in a 10 cm tissue culture dish a day before lentiviral co-transfection. A total of 15 µg DNA of packaging plasmid, pCMVdeltaR8.91, 5 µg DNA of envelope plasmid, pMD2G and 20 µg DNA of transfer plasmid, pLKO5d.miRNA30 were mixed to produce precipitates using calcium phosphate method. Images were captured 72 hours post-transfection using an inverted microscope equipped with Texas Red and GFP filters. Images were captured at 100X magnification using phase contrast microscope.

Due to high virus titre produced by this transfer vector, concentrating the viruses was not required. This step was considered crucial as high speed centrifugation might led to loss of virus particles. To determine virus efficiency, a series of virus supernatant volume was used to transduce target cell. Briefly, in 48-well plate, cells were prepared in a density of 1.0 x 10^6 cell/ml in 500 µl media volume and supplemented with 8 µg/ml polybrene. Virus supernatant was added to the cells and plate was centrifuged at 900 g, 50 minutes at 34^{o}C. Cells were collected on day 3-post transduction and gene transfer efficiency was determined by checking the level of endogenous fluorescent protein expression using flow cytometry. Based on the vector map, shRNA is placed adjacent to the fluorescent marker (Figure 3-7-C); therefore the fluorescent percentage indicates successful integration coupled with expression of shRNA. FlowJo analyses of cytometry data showed a high transduction efficiency with non-concentrated virus as showed in Figure 3-9 and Table 3-1.

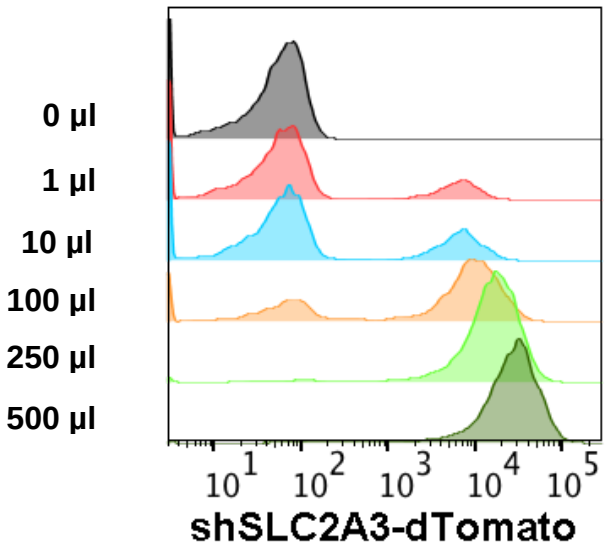

Figure 3-10: High transduction efficiency was achieved using pLKO5d.miRNA30 vector. Cells were lentivirally transduced with a series of virus supernatant according to the transduction method. Transduction efficiency was captured on day 4 post-transduction by flow cytometry. Flow cytometry data were processed using FlowJo software and image is representative of an analysis from a virus supernatant.

Volume of virus (µl)	Percentage of transduction (shSLC2A3-dTomato/PE)
0	0.0
1	17.1
10	26.0
100	72.6
250	96.5
500	98.2

Table 3-1: High virus transduction efficiency was achieved using pLKO5d.miRNA30 vector. Cells were lentivirally transduced with a series of virus supernatant according to the transduction method. Transduction efficiency was captured on day 4 post-transduction by flow cytometry. Flow cytometry data were processed using FlowJo software and image is representative of an analysis from a virus supernatant.

To determine if shRNA expression leads to silencing of target genes, mRNA level was analysed according to RT-PCR method as described in Materials and Method section. Cells were harvested on day 4-post transduction, washed and protein assessment was carried out as described below.

For *SLC2A3,* only two from four constructs were shown to have reduced transcript level; shSCL2A3#1 construct reduced the expression up to 50%, while shSLC2A3#2 led to 90% knockdown of *SLC2A3* in Kasumi-1 cell line (Figure 3-10-A). For *PFKP*, while shRNA construct #1 (shPFKP#1) caused a 50% reduction at RNA level, the other two shRNA; shPFKP#2 and shPFKP#3 led to 65% reduction when compared with the control (Figure 3-10-B).

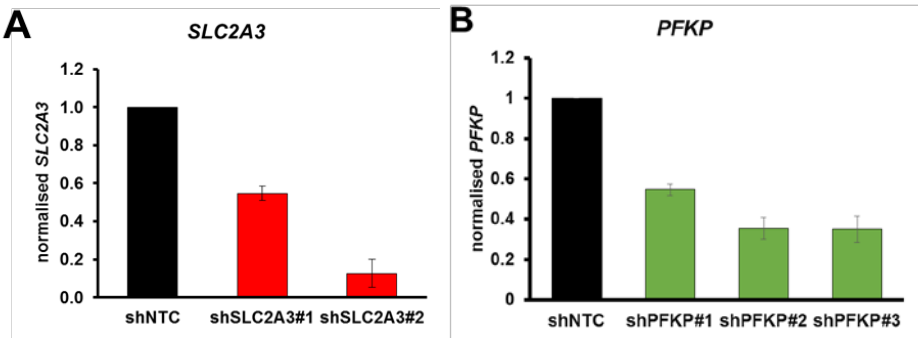

Figure 3-11: mRNA analyses for shRNA constructs selected to be used in this study. Cells were lentivirally transduced with vector expressing shRNA targeting *SLC2A3* and *PFKP* and harvested 72-hours post transduction. RNA expression was

measured against shNTC treated cells and *GAPDH* served as a housekeeping gene. A) Two shRNA constructs targeting *SLC2A3* with construct number 2 had 90% reduction of SLC2A3 mRNA (n=3). B) Three *PFKP* shRNA with shPFKP#2 and shPFKP#3 had 65% knockdown at mRNA level and shPFKP#3 was chosen to be used in this study. Error bars represents SD of three non-independent experiments (n=3).

These genes were further validated in double knockdown approach as similar as in siRNA-mediated knockdown. I then selected shSLC2A3#2 and shPFKP#3 constructs to be used in subsequent experiments. From this point onward, both constructs are referred as shSLC2A3 and shPFKP respectively; unless otherwise stated. Cells were lentivirally transduced with pLKO5d vector expressing shRNA targeting non-targeting control (shNTC), *SLC2A3* (shSLC2A3)*, PKFP* (shPFKP), *SLC2A3+PFKP* (shSLC2A3+shPFKP) and *RUNX1/ETO* (shRUNX1/ETO). Each shRNA targeting each gene associated with different colour as listed in Table 3-2 for useful manipulation in the subsequent experiments. After 72-hours post transduction, the transduction efficiency was analysed with flow cytometry and cells were either harvested for mRNA analyses and protein quantification or fixed with 2% paraformaldehyde for flow cytometry analysis.

Target shRNA	Associated colour
shNTC	RFP657
shSLC2A3	dTOMATO
shPFKP	eGFP/dTOMATO
shRE	dTOMATO

Table 3-2: Each shRNA associates with different colour expression. Each colour has different excitation and emission spectrum, thus serves as useful tool to be manipulated during flow cytometry analyses.

Figure 3-11 indicates level of mRNA after shRNA knockdown on *SLC2A3, PKFP* and *RUNX1/ETO*. An 80% depletion of *RUNX1/ETO* led to a statistically significant 80% loss of *SLC2A3* transcript level ($p<0.01$), but caused a non-significant 20% reduction in *PFKP* mRNA. Knockdown of *SLC2A3* and *SLC2A3+PFKP* led to significant 70-80% loss of *SLC2A3* transcript ($p<0.01$). Both *PFKP* and *SLC2A3+PFKP* knockdowns caused *PFKP* mRNA level to reduce significantly to 15% remaining mRNA levels ($p<0.01$). However, *SLC2A3* knockdown did not have any impact on *PFKP* and vice versa showing that both genes do not regulate each other. Furthermore, depletion of *SLC2A3* and/or *PFKP* seemed to have no impact in

RUNX1/ETO expression level. These data showed that, constitutive expression of shRNA using miRNA30 backbone drives a strong gene knockdown at mRNA level.

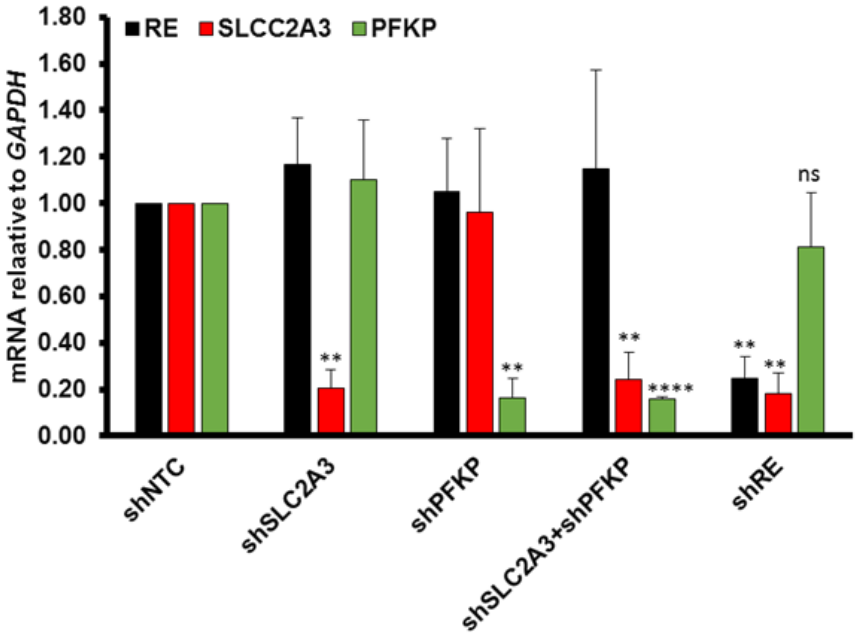

Figure 3-12: mRNA level of *SLC2A3* and *PFKP* upon knockdown with shRNA in double knockdown approach. Cells were lentivirally transduced with vector expressing shRNA targeting *SLC2A3* and *PFKP* and harvested 72-hours post transduction for RNA analyses. RNA expression was measured against shNTC treated cells and *GAPDH* served as a housekeeping gene. Error bars represents standard deviations of three independent experiments. Significance was evaluated using students t-test, ns: not significant, **p<0.01, ***p<0.001, p****<0.0001 (n=3).

SLC2A3 protein knockdown was assessed using flow cytometry. Cells on day 4 post-transduction were fixed and permeabilised before incubating with FITC-conjugated SLC2A3 antibody. Cells were analysed using flow cytometry at FITC-channel and Isotype IgG2B control was used as a negative control. Protein level by western blot was not accomplished after three antibodies did not give any conclusive results. Flow cytometry data showed a significant two-fold protein reduction in *RUNX1/ETO* knockdown sample compared to experimental control, shNTC (Figure 3-12-B and Table 3-3) confirming the mRNA transcript data described previously. In addition to that, *SLC2A3* knockdown cells reduced 2.5-fold of protein in comparison to shNTC. Whereas, double knockdown of *SLC2A3* and *PFKP* caused more potent reduction of SLC2A3, which was 3.3-fold in comparison with the control.

For PFKP protein assessment, protein lysate was co-extracted during RNA extraction during ethanol precipitation method as described in Materials and Method section. Protein containing flow-through was collected, precipitated with acetone and continued with western blotting. *PFKP* and double knockdown led to a reduction of PFKP protein level in Kasumi-1. However, RUNX1/ETO knockdown and shSLC2A3 knockdown did not led to reduction of PFKP protein level. This observation is in line with mRNA level data as shown previously.

Taken together, the shRNA constructs selected in this study drove a potent knockdown in both mRNA and protein level. *RUNX1/ETO* knockdown in Kasumi-1 cell line did not show any effect on *PFKP* mRNA and protein level; however, this could be due to early timepoint when the cells were harvested.

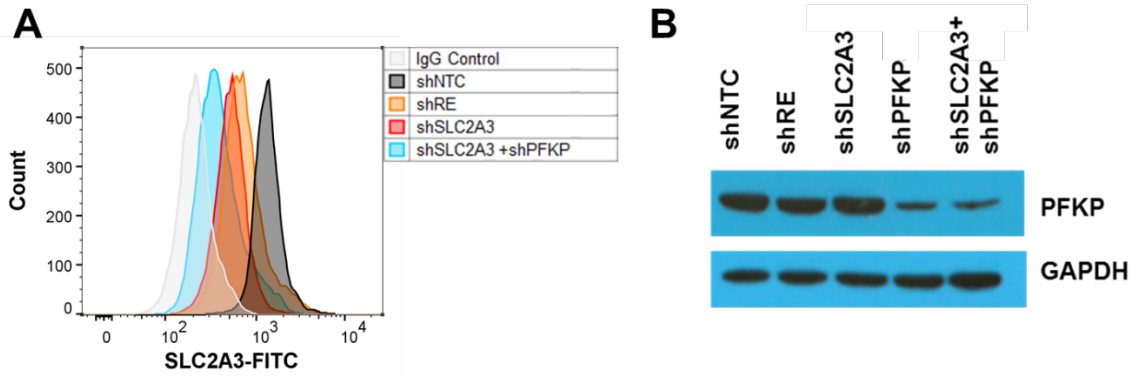

Figure 3-13: Protein level of SLC2A3 and PFKP upon knockdown with shRNA in double knockdown approach. Cells were lentivirally transduced with vector expressing shRNA targeting SLC2A3 and PFKP and harvested 72-hours post transduction for protein quantification. A) Cells were fixed with 4% paraformaldehyde, permeabilised with 0.25% Triton-X 100 and stained with mouse anti-human Glut3 Alexa Fluor 488-conjugated antibody. Cells were analysed with flow cytometry at

FITC-channel (n=3). B) Membrane was blotted against α-RHD antibody and α-GAPDH loading control.

Sample	SLC2A3-FITC (Geo Mean)
IgG Control	213
shNTC	1328
shRE	711*
shSLC2A3	513**
shSLC2A3+shPFKP	394**

Table 3-3: Geometric mean of SLC2A3 protein measured by flow cytometry. Cells were fixed with 4% paraformaldehyde, permeabilised with 0.25% Triton-X 100 and stained with mouse anti-human Glut3 Alexa Fluor 488-conjugated antibody. Cells were analysed with flow cytometry at FITC-channel. Error bars represent standard deviation of the mean (n=3). Significance was evaluated using students t-test *p<0.05), **p<0.01.

3.3.3.2 RUNX1/ETO moderately regulates PFKP expression

Based on the mRNA levels of *PFKP* in siRNA treated cells in Kasumi-1 cells, RUNX1/ETO was suggested to moderately regulate *PFKP* expression, therefore a potent knockdown is required to confirm the direct regulation of RUNX1/ETO on *PFKP*. Three independent experiments using shRNA-mediated knockdown resulted in two *RUNX1/ETO* expression pattern. As indicated in Figure 3-13, in shRE-A cell pool, RUNX1*/ETO* knockdown led to 90% reduction of *RUNX1/ETO* mRNA and caused 50% reduction of *PFKP* mRNA. In the other two experiments, where *RUNX1/ETO* mRNA reduced to 70% (higher than shRE-A cell pool), *PFKP* expression level reduced by maximally 10%. These observations were in line with the prolong treatments with siRUNX1/ETO data, that potent *RUNX1/ETO* knockdown is required to impact *PFKP* transcript levels.

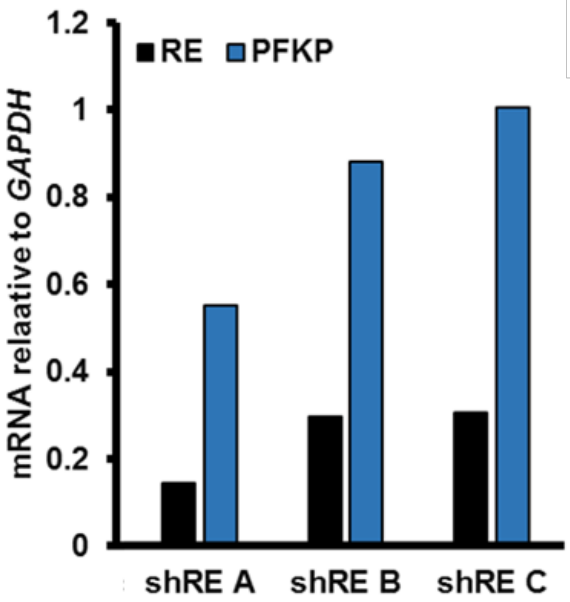

Figure 3-14: Potent knockdown of *RUNX1/ETO* led to greater loss of *PFKP* in Kasumi-1 cells. Cells were lentivirally transduced with shRNA targeting *RUNX1/ETO* in three independent experiment. Cells were harvested on day 4 post-transduction for RNA analyses. *RUNX1/ETO* and *PFKP* expressions levels were normalised to shNTC (n=1).

3.3.3.3 Neither individual knockdown on SLC2A3 or PFKP nor double knockdown induce compensation of other transporters

I then sought to determine if potent constitutive shRNA-mediated knockdown leads to differential expression of other transporters as described previously in section 3.3.2.2. Figure 3-14 showing the expression level of *SLC2A1* and *SLC2A5* after individual and double knockdown of *SLC2A3* and *PFKP*. *SLC2A3* knockdown caused insignificant reductions of both *SLC2A1* and *SLC2A5* mRNA level. Depletion of *PFKP* led to a minimal 30% but significant reduction of *SLC2A1* and insignificant 20% reduction of *SLC2A5* mRNA level. Double knockdown of *SLC2A3* and *PFKP;* however, caused no changes in *SLC2A1* transcript level and insignificant 30% reduction of *SLC2A5.* Whilst, *RUNX1/ETO* knockdown led to 40% reduction of *SLC2A1* but no change was observed in *SLC2A5* transcript level.

Taken together, potent and constitutive shRNA knockdown on *SLC2A3* and *PFKP* did not contribute to any changes of *SLC2A1* and *SLC2A5* expressions. However,

this mRNA was measured at 72 hours timepoint post-transduction, perhaps it is still too early to see the downstream effect of the knockdown on these genes.

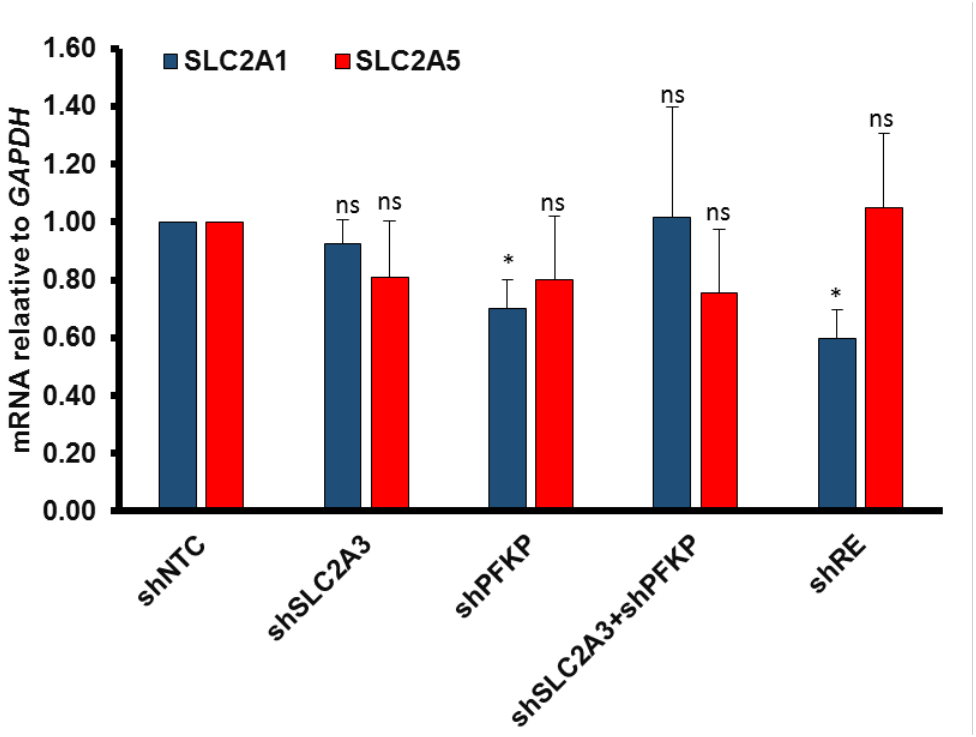

Figure 3-15: Neither individual nor double SLC2A3 and PFKP knockdown induced *SLC2A1* and *SLC2A5* at mRNA level. Cells were lentivirally transduced with vector expressing shRNA targeting *SLC2A3* and *PFKP* and harvested 72-hours post transduction for RNA analyses. RNA expression was measured against shNTC treated cells and *GAPDH* served as a housekeeping gene. Error bars represents standard deviations of three independent experiments. Significance was evaluated using students t-test, *p<0.05 (n=3, independent experiments).

3.3.3.4 Reduced glucose uptake in both normoxia and hypoxia

Before continuing *in vivo,* I next asked if *SLC2A3* knockdown impairs its primary physiological function, which is passaging glucose molecule into the cells. To answer that, glucose uptake assay was performed in Kasumi-1 cell line in standard culture condition in normoxia and hypoxia. The reasoning behind hypoxia culture condition was to determine if limited oxygen on *SLC2A3* knockdown have greater effects on its physiological functions as low oxygen content showed to increase expression of glucose transporters, and promote higher glycolysis (Yu et al., 2012, Christensen et al., 2015). Figure 3-15 shows the expressions of *SLC2A3* in normoxia and hypoxia with and without *SLC2A3* knockdown. The samples were normalised to shNTC in

normoxia condition as I wanted to show the differential expression of *SLC2A3* in each condition. In hypoxia condition, *SLC2A3* mRNA level increased 2-fold higher in shNTC sample when compared to the control shRNA in normoxia. Furthermore, in normoxic condition, *SLC2A3* knockdown caused 70% mRNA reduction in comparison to the shNTC. While *SLC2A3* knockdown in hypoxia condition led to only 30% mRNA reduction when compared to shNTC in normoxia; however, the actual reduction was 60% as it compared to its own shNTC in hypoxic condition. Therefore, I postulated, in hypoxia condition, leukaemic cells exhibit higher dependency on *SLC2A3* expression and thus its knockdown will give greater impact in its primary function.

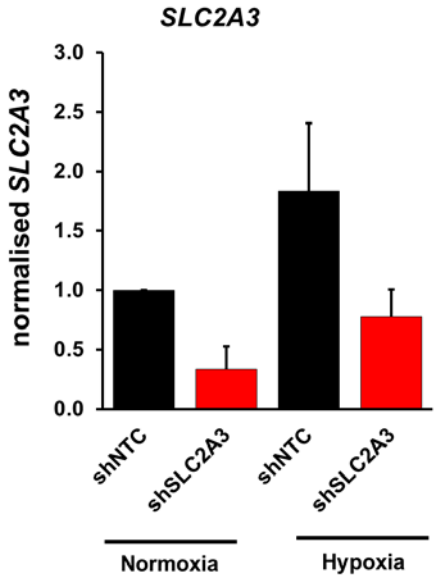

Figure 3-16: *SLC2A3* expression level in shNTC-expressing Kasumi-1 cell line. Cells were lentivirally transduced with shRNA expressing RFP657 or dTOMATO and incubated in both normoxic and hypoxic conditions for 72 hours. mRNA analyses were measured against shNTC treated cells and *CYCLO* served as a housekeeping gene. Error bars represent standard deviation (n=3).

I next performed glucose uptake assay utilising green fluorescent labelled glucose, 2-NBDG, which was used primarily to monitor glucose uptake in cells. Studies have shown that 2-NBDG competes with the naturally occurring D-glucose to enter the cell (Lloyd et al., 1999, O'Neil, 2005), indicates that this molecule has the same kinetics as glucose and provides as useful quantitative marker for glucose uptake. 2-NBDG has the same structure of glucose except that on C-2 position of glucose was replaced by fluorescence molecule, NBDG. Upon uptake into the cells, hexokinase phosphorylated on C-6 position and trapped the molecule within the cells. As the C-2 was replaced by NBDG, the phosphorylated molecules incapable to undergo further

reaction in glycolysis pathway and accumulate in the cells. The green fluorescents emitted by NBDG can be detected by flow cytometry and that represents direct measurement of glucose uptake into cells.

To determine this, Kasumi-1 cells were lentivirally transduced with either RFP657 or dTOMATO and collected after 72 hour post-transduction. Briefly, a total of 0.1 – 0.2 x 10^6 cells were cultured in 200 – 400 µl of glucose-free media for 12-18 hours as per manufacturer's recommendation in standard 20% oxygen content and limited 1% oxygen content. On the next morning, 2-NBDG was added to a final concentration of 200 µM and incubated for 180 minutes in standard tissue culture incubation. The cells were washed once with PBS and cytometry analysis was performed immediately with proper compensation setting applied for each sample due to overlapped spectrum of green and dTOMATO.

Overall, 2-NBDG glucose uptake was lower in all samples in hypoxia condition. Knockdown of *RUNX1/ETO* significantly diminished its glucose uptake capacity in both normoxia and hypoxia which recorded 30% and 20% reduced fluorescence intensity when compared to their own wild type in each condition (p-value<0.05 for both). Interestingly, *SLC2A3* knockdown significantly decreased 20% of 2-NBDG uptake in normoxia (p-value<0.05), but more potent effect was observed in hypoxic condition which recorded significant 30% reduction in comparison to wild type in hypoxia (p-value<0.05). The observation was also consistent in double knockdown in higher oxygen condition which recorded 25% reduction of 2-NBDG uptake which is significant in comparison to the wild type cells (p-value<0.01). In hypoxic condition, although double knockdown caused the cells to reduce glucose uptake by 15% when compared to its wild type control; however, it was not significant. Interestingly, while there was no changes of 2-NBDG fluorescence intensity observed in *PFKP* knockdown cells in normoxic condition, *PFKP* knockdown in hypoxia significantly reduced glucose uptake by 20% when compared to its wild type Kasumi-1 (p-value<0.05).

Taken together, RUNX1/ETO illustrates addiction to glucose through *SLC2A3* and that depletion of *SLC2A3* led to a significant reduction of glucose uptake in both conditions, with a greater loss observed in the limited oxygen content. Although *SLC2A3* showed to have higher expression in hypoxic condition; however, this was not necessarily associated with higher glucose uptake.

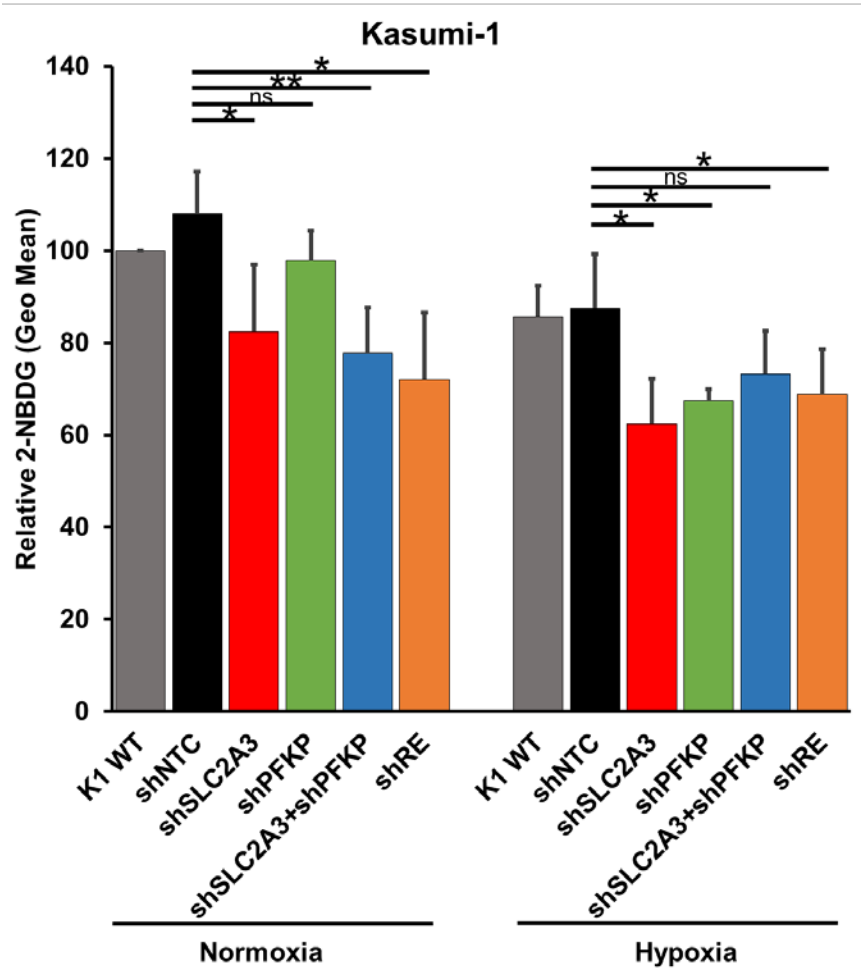

Figure 3-17: Knockdown of *SLC2A3* reduced glucose uptake in Kasumi-1 cell line. Cells were lentivirally transduced with shRNA expressing RFP657 or dTOMATO and incubated in glucose-free media for 12-18 hours. The next day, 2-NBDG was added to the final concentration of 200 µM, incubated for 3 hours and analysed with cytometry on FITC channel (n=3, independent experiments).

3.3.3.5 PFKP knockdown cells loss to shNTC in vivo in newborn Rag2$^{-/-}$Il2rg$^{-/-}$129 ×Balb/c mice

To further validate if *SLC2A3* and *PFKP* are important in leukaemia propagation *in vivo* competitive transplantation was performed in newborn *Rag2*$^{-/-}$*Il2rg*$^{-/-}$129 ×Balb/c (RG) mouse strain as depicted in Figure 3-17. Cells were lentivirally transduced with either shNTC- or shSLC2A3+shPFKP-expressing vector at approximately 30% transduction efficiency on the day of mice were born. The reason behind this transduction percentage was to ensure only one particle of virus integration per cells. Four days later, cells were sorted and mixed with approximately 25% of each population. A total of 2.5x10^5 cells in 25 µl was intrahepatically injected

into the mice. Liver serves as the main organ for perinatal haematopoiesis and the development is most rapid in the first few weeks of life. Thus, transplantation of human haematopoietic cells into the liver of immunodeficient newborn mice is thought to have better engraftment and expansion, as well as reconstitute a human immune system. Our team has previously established intrahepatic injection of t(8;21) cell line shown to have better engraftment compared to other animal model and method (Soria et al., 2008). Moreover, a study showed that intrahepatic transplantation of CD34+ human cord blood cells into newborn RG mice led to adaptive immune system and provide a useful tool for *in vivo* therapeutic study (Traggiai et al., 2004). Mice were humanely killed when they showed the endpoints as detailed in the licenses. Tumours from the mice were harvested and processed for further downstream analyses.

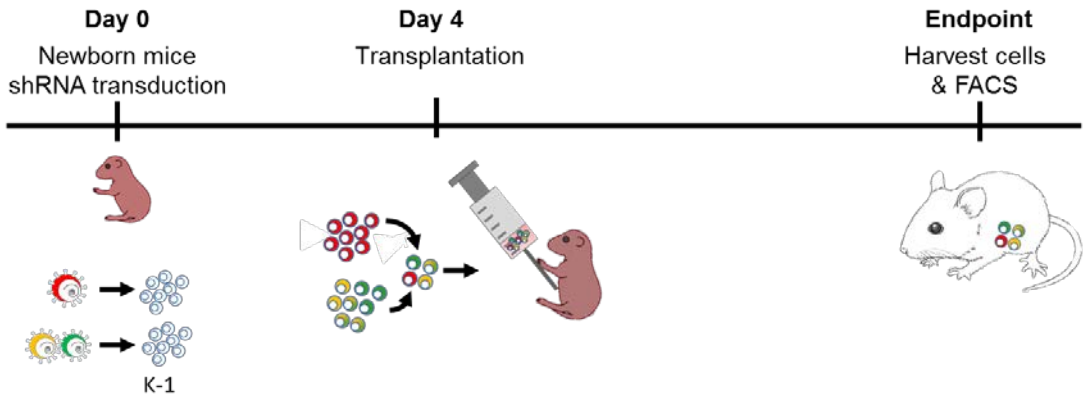

Figure 3-18: Scheme of competitive intrahepatic transplantation in Rag2$^{-/-}$Il2rg$^{-/-}$129×Balb/c. Kasumi-1 cells were lentivirally transduced with either shNTC- or shSLC2A3+shPFKP-expressing vector on the day the mice were born. Cells were sorted with FACS Aria sorter on day 4 and 25% of each population were mixed in a single mixture. A total of 2.5x10^5 cells in 25 µl media were intrahepatically transplanted in newborn RG mouse. Mice were killed when it reached endpoint and tumours were harvested for further analyses.

The proportion of cells at baseline (pre-transplantation) were shown in Figure 3-18-A and knockdown level of each population was determined by mRNA analysis (Figure 3-18-B). *SLC2A3* and *PFKP* individual knockdown caused 70% reduction in mRNA transcript level after 72-hour transduction. Whereas, double knockdown of the two genes led to 70% reduction of *SLC2A3* transcript and 80% in *PFKP* transcript level. The same pool of cells was cultured *in vitro* in standard culture condition. The percentage of shRNA-expressing cells was measured every couple of days by flow

cytometry. Figure 3-20 summarises the proportion of cells at baseline, *in vitro* endpoint and from tumours harvested from two mice out of six mice that have been transplanted with Kasumi-1 cell line. Cells from tumours were sorted using FACS Aria Sorter for mRNA analysis.

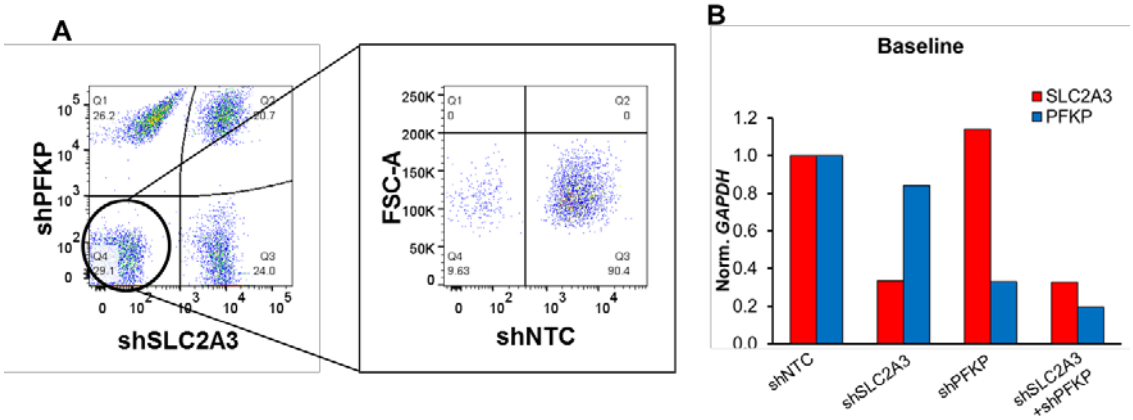

Figure 3-19: Proportion of cells before transplantation and RNA transcript level at baseline. A) Lentivirally transduced Kasumi-1 were sorted and 25% of each population was mixed before being transplanted newborn Rag2$^{-/-}$Il2rg$^{-/-}$129×Balb/c mice. B) Graph showing mRNA level of sorted cells before transplantation (n=1).

In vitro endpoint showed that shNTC outcompeted all other populations in the long-term suspension culture as it increased from 25% to 44% at the end of experiment (Figure 3-19 and Figure 3-20). Double knockdown of *SLC2A3* and *PFKP* led to the greatest loss among all other shRNA, which recorded 5% remaining population at the end of experiment while *SLC2A3* knockdown caused the cells to increase to 34% on day 35-post mixing. Apart from that, *PFKP* knockdown led to 17% remaining cells at the endpoint of the culture.

On the contrary, *in vivo* assay showed that shNTC cells competitively loss to *SLC2A3* knockdown cells in two mice harvested. FACS analyses recorded 5% and 2% of shNTC-expressing cells in mice 1 and 2 respectively. Surprisingly, *SLC2A3* knockdown cells outgrew all other population to make up 86% and 93% of cells in both mice 1 and 2 respectively. While *PFKP* knockdown caused the cells to reduce to 2% in mice 1 and completely diminished leukaemic cells in mice 2; however, double knockdown of *SLC2A3* and *PFKP* led to higher cell proportion when compared to shNTC-expressing cells. For instance, in mice 1, 7% of double knockdown cells remained in the tumour which was higher than the control (5%). RT-PCR analyses of

these cells showed that transcript levels of *SLC2A3* were reduced to 50% in both *SLC2A3* knockdown and double knockdown cells (Figure 3-20). While, there was a 50% reduction of *PFKP* mRNA in *PFKP* knockdown cells; however, in double knockdown it was only 30% depletion observed. In mice 2, double knockdown led to remaining 5% of cells which was greater than 2% of shNTC-expressing cells. RT-PCR analyses of these cells revealed a greater knockdown compared to mice 1. There was 80% knockdown of *SLC2A3* mRNA level in *SLC2A3* knockdown cells and 70% knockdown in double knockdown population. Whereas, *PFKP* transcript showed to have 70% reduction in the double knockdown cells. No RT-PCR analyses could be done on *PFKP* knockdown cells as the number of cells in the pool were very low. The other four mice did not develop any tumour and no sign of sickness was observed throughout the period of study.

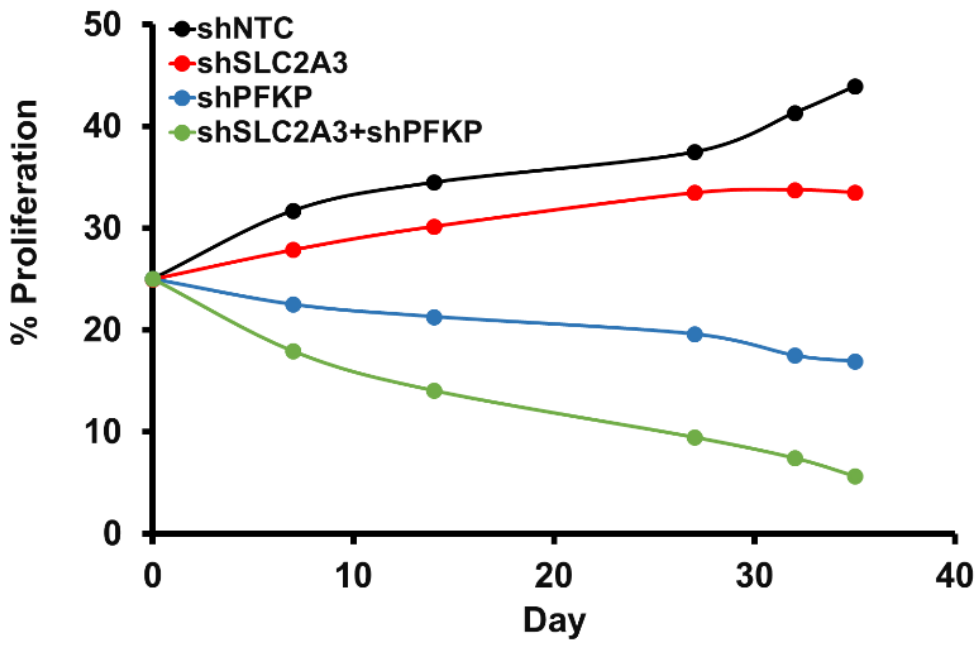

Figure 3-20: Graph showing competitive loss of shSLC2A3-,shPFKP- and shSLC2A3+shPFKP-transduced Kasumi-1 cells *in vitro* from the same pool of cells transplanted *in vivo*. Cells were cultured in standard culture condition and fluorescence changes were monitored using flow cytometry. The change in the fluorescence percentages of each timepoint were normalised to the baseline of each construct (n=1).

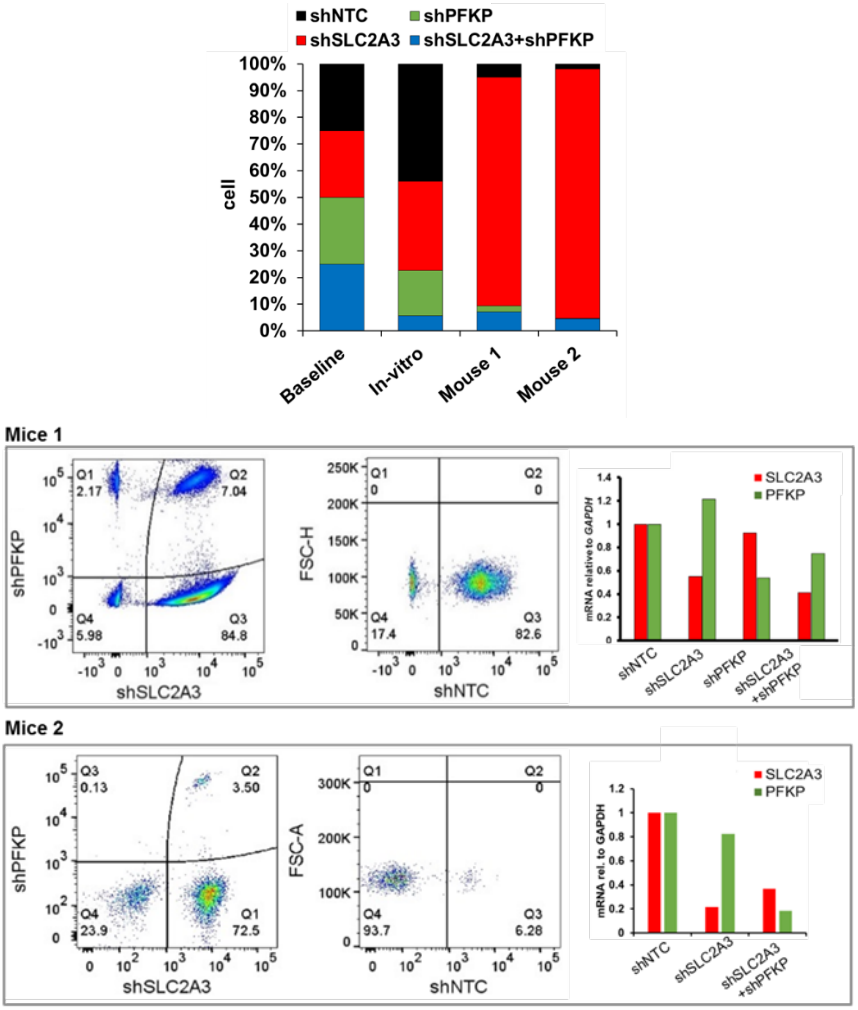

Figure 3-21: Graph summarises competitive assay *in vivo* in Rag2$^{-/-}$Il2rg$^{-/-}$129×Balb/c mouse model. Cells were mixed with a 25% proportion of each shRNA knockdown cells and intrahepatically transplanted in RG newborn mice. The same pool of cells were cultured in standard culture condition *in vitro* and monitored every couple of days by flow cytometry. Mice were killed when it reached endpoint and tumours were harvested for analyses.

3.3.3.6 PFKP is essential in leukaemia survival in vivo, but not SLC2A3 in NSG mouse model

As described in 3.3.3.5, *PFKP* depletion impaired RUNX1/ETO-leukaemic propagation and survival *in vivo*. However, that was not the case for *SLC2A3* as the knockdown led to the expansion of cells in RG mouse model. Previously, in shRNA screen we relied on intrafemoral transplantation in NOD.Cg-Prkdc^{scid} Il2rg^{tm1Wjl}/SzJ (NSG) mouse model. I reasoned it may be due to different animal model used previously and the place where the leukaemic cells transplanted could led to this unlikely findings. I next sought to find the answer if it's due to animal model and place

of transplantation in this section. Figure 3-21 showing the scheme utilised in this experiment. Cells were lentivirally transduced with either shNTC- or shSLC2A3+shPFKP-expressing vector at MOI of 0.3, sorted on day 4 and mixed. The cells mixture was injected into the intrafemoral space in adult NSG mice as described in Materials and Method section. The engraftments were monitored for physical signs of leg tumours or abnormal lesion in all parts of the body, and humanely killed when it reached the endpoints as described in the license.

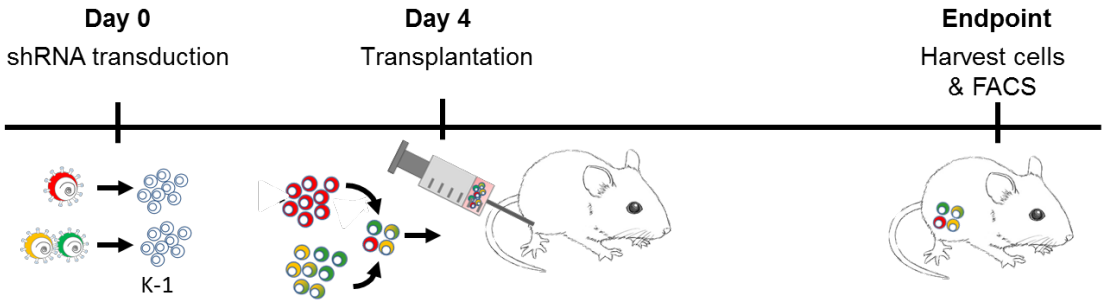

Figure 3-22: Scheme of competitive intrafemoral transplantation in NOD.Cg-Prkdc^{scid} Il2rg^{tm1Wjl}/SzJ. Kasumi-1 cells were lentivirally transduced with either shNTC- and shSLC2A3+shPFKP-expressing vector and mixed on day 4 with 25% of each population. A total of 1.0x10^5 cells in 20 µl of media were intrafemorally injected in adult NSG mice. Mice were killed when it reached endpoint and tumours were harvested for further analyses.

Figure 3-22 showing the proportion of cells mixture before transplantation (baseline) constituted of 24% of shNTC-, 23% of shSLC2A3-, 18% shPFKP-expressing cells and 35% double knockdown cells. mRNA analysis showed 60% reduction of *SLC2A3* transcript derived from *SLC2A3* knockdown sorted cells. However, there were not enough cells for *PFKP* knockdown and double knockdown cells to perform RT-PCR analysis.

The summary of this experiment is shown in Figure 3-23. To distinguish between human and mouse cells, the samples were stained with human CD45 (hCD45) and mouse CD45 (mCD45) markers. Additional surface marker, human CD33 (hCD33) was also added to confirm the population of myeloid lineage which is expressed in Kasumi-1 cell line. Mouse 1 formed tumour in left ovary and the size was approximately 40 times bigger than normal ovary (Figure 3-23-A&B). Cells from this tumour exhibited 97% positive for hCD33 from 41% hCD45 marker. In this sample, shNTC-expressing cells recorded 100% of cells and outcompeted all other

populations. Mouse 2 developed leg tumour and unexpectedly double knockdown cells outcompeted all other populations from 81% of hCD45 positive population (Figure 3-23-A&C). By meticulously observing the dot plot in flow cytometry analyses, the fluorescents of shNTC-positive cells in Mouse 1 were homogenously scattered in the detection channel and looked alike to the shNTC in the baseline. From my experience, this is what I would see if the cells homogenously engraft and form tumours. Interestingly, in Mouse 2, a tight fluorescents formed in a distinct area when compared to the double positive for *SLC2A3*+*PFKP* knockdown cells in the baseline. It is thought that these cells originated from single cell and that selectively promote clonal leukaemic growth. However, this need to be further validated by downstream experiment, such as ligation-mediated PCR. There was no tumour detected in the other four mice. This experiment took 138 days until I got to detect some abnormal lesions in two of the six mice transplanted. The period was much longer than usual time it took to detect the tumours in our previous study which were about 6-8 weeks.

As a summary, transplantation of leukaemic cell line targeting *SLC2A3* and *PFKP* in the bone marrow resulted in variable results. Together with previous experiments from section 3.3.3.5, I summarised that there was an issue with engraftment when working with these two genes. Nevertheless, *PFKP* knockdown cells competitively loss in these two experiments, hence validated the shRNA screen result. Whereas, in the case of *SLC2A3,* the niche of where the cells engraft and proliferate could also pivotal in determining the fate of the leukaemic cells.

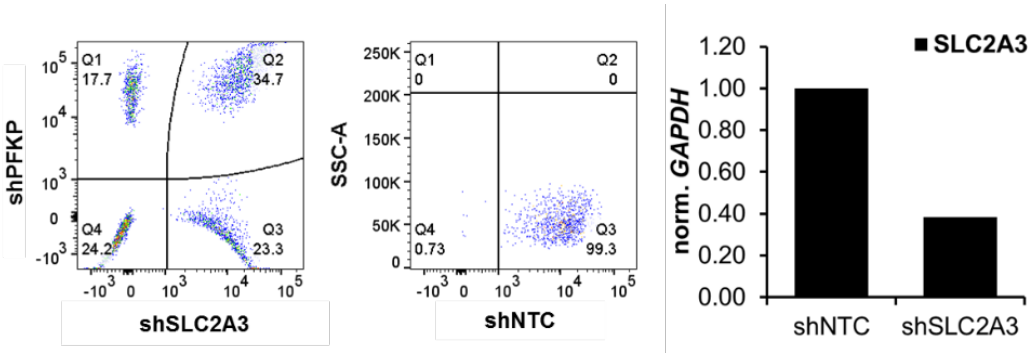

Figure 3-23: Proportion of cells before transplantation and RNA transcript level at baseline. Lentivirally transduced Kasumi-1 were sorted and 25% of each population was mixed before being intrafemorally transplanted in NSG NOD.Cg-Prkdc^{scid} Il2rg^{tm1Wjl}/SzJ. Graph on the left showing mRNA analysis of sorted cells before transplantation. GAPDH serves as housekeeping gene (n=1).

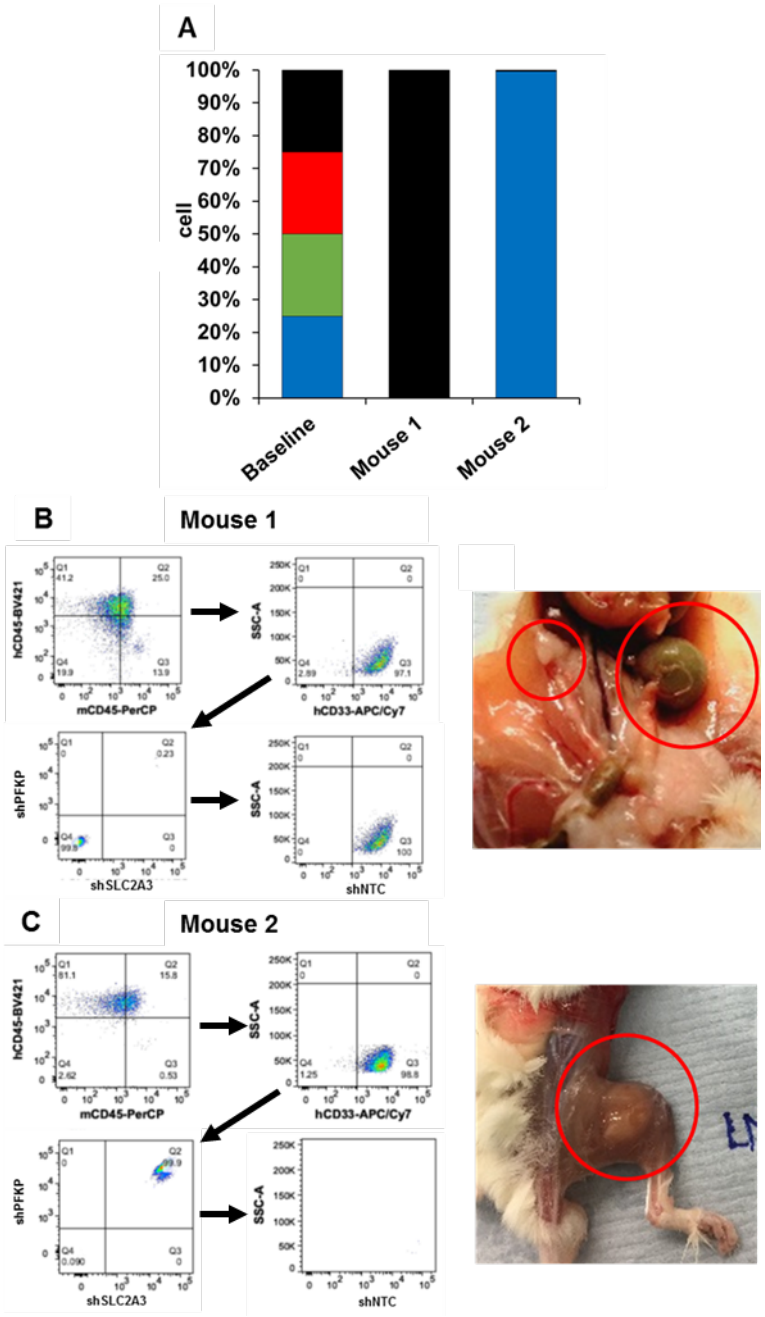

Figure 3-24: Graph summarises competitive assay *in vivo* in NSG mouse model. Cells were mixed before intrafemorally transplanted into NSG mice A) Proportion of cells at baseline before transplantation and endpoints from two engrafted mice. B&C) Cells from tumours were stained with human CD45, mouse CD45 and human CD33 to distinguish between human and mouse cells. B) In mouse 1, tumour formed in left ovary (big red circle) and the ovary was approximately 40 times bigger than normal ovary (smaller red circle). C) In mouse 2, tumour was detected on right leg.

3.3.3.7 SLC2A3 potentially as tumour suppressor in vivo

Collectively from previous two *in vivo* experiments, I summarised that there were hardly engraftments in both mouse models. However, decent data and study involving Kasumi-1 cells particularly in RG strain mice had been established in our lab (Soria et al., 2008, Martinez-Soria et al., 2018). I then proceed the next experiment focusing only on RG mouse. As detailed in section 3.3.3.5, knockdown of *SLC2A3* drives leukaemic expansion in RG mouse model*,* therefore, next investigation focused on *SLC2A3* only. I then thought the number of virus infection per cell was not enough to drive *SLC2A3* response *in vivo.* In this experiment, highest transduction efficiency was chosen as it was successfully tested in our recent publication (Martinez-Soria et al., 2018).

Single shRNA knockdown was performed following the scheme depicted in Figure 3-17 except that only one shRNA lentivirus targeting *SLC2A3* was used to transduce the cells. shNTC- and shSLC2A3-expressing cells were mixed with a proportion of 50% each and intrahepatically injected in *RG* newborn mice. Mice were monitored if there was any physical sign of abdominal tumours, and humanely killed when it reached the endpoints as described in the license. Cells from tumours were harvested, analysed by flow cytometry and sorted for RNA analyses. Figure 3-24 depicted the proportion of cells before transplantation in newborn mice analysed using FACS Calibur and transcript level for both shNTC- and shSLC2A3-expressing cells (baseline). Further RT-PCR analysis showed 90% reduced transcript level of *SLC2A3* expression in *SLC2A3* knockdown cells compared with the control.

As depicted in Figure 3-25, *in vivo* single knockdown of *SLC2A3* competitively gained its population over shNTC-expressing cells in all five transplanted mice. *SLC2A3* knockdown cells grew from 50% of cells on baseline to 77% of cells in mice 1 represented in Figure 3-25. The greatest increase was observed in mice 4 as the shSLC2A3-expressing cells gained 98% of cells in the tumour (Figure 3-25). mRNA analyses of sorted *SLC2A3* knockdown cells showed reduced transcripts in all five mice as shown in Figure 3-26. There were slight increase of mRNA levels in all five mice when compared to the baseline; however, the increments were within the ranges observed with this shRNA construct *in vitro*.

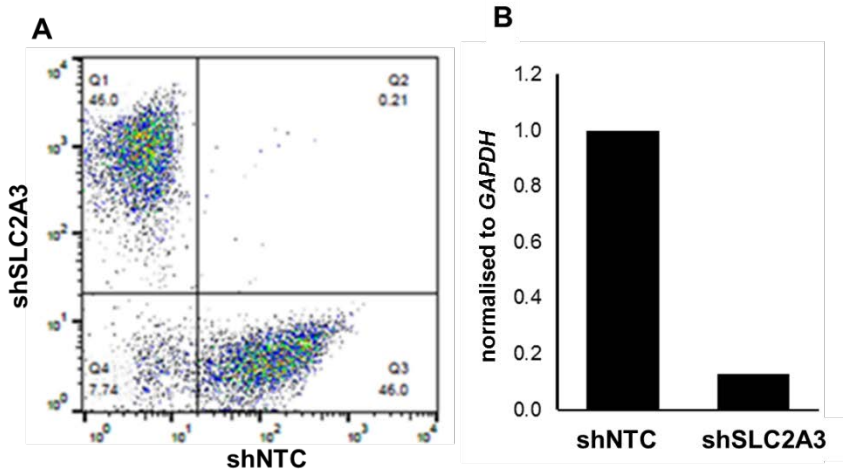

Figure 3-25: The proportion of cells and RNA transcript level before intrahepatic transplantation in Rag2$^{-/-}$Il2rg$^{-/-}$129×Balb/c newborn mice. A: cells were transduced with shNTC- and shSLC2A3-expressing cells on the day the mice were born. Cells were analysed with flow cytometry on day-4 post transduction, mixed in single tube with 50% proportion of each population and re-analysed with flow cytometry before intrahepatically injected in newborn Rag2$^{-/-}$Il2rg$^{-/-}$129×Balb/c mice. Flow cytometry data was analysed by FlowJo software. B: Remaining cells were extracted and checked for RNA transcript (n=1).

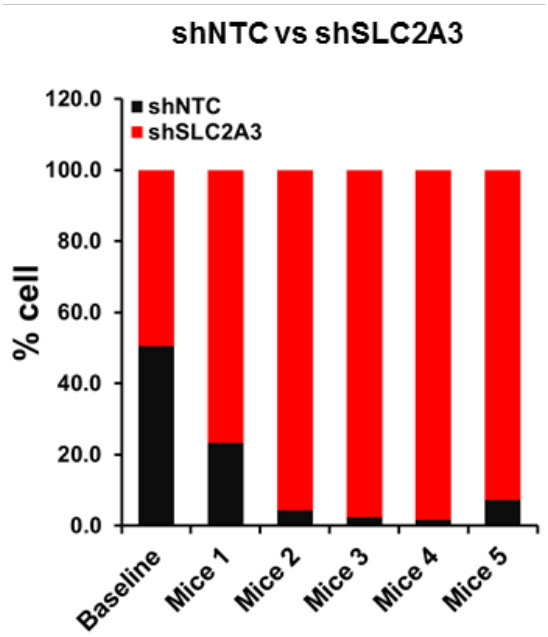

Figure 3-26: Kasumi-1 cell line competitive loss of shNTC to shSLC2A3-expressing cells *in vivo*. A 50% mixture of shNTC- and shSLC2A3-expressing cells was intrahepatically transplanted into five newborn Rag2$^{-/-}$Il2rg$^{-/-}$129×Balb/c mice. Mice that reached endpoint were killed and cells from the tumours were harvested. Cells were analysed with flow cytometry and its fluorescence intensities were calculated accordingly.

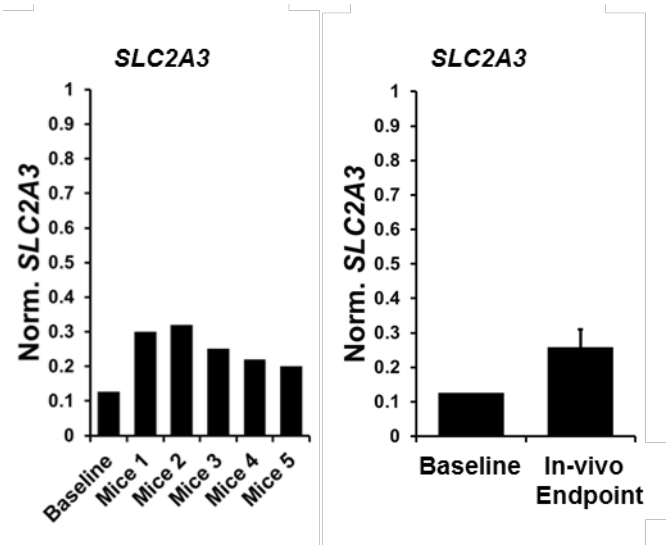

Figure 3-27: mRNA level of SLC2A3 from SLC2A3 knockdown cells harvested from baseline and *in vivo* tumours. Cells expressing shSLC2A3 from both baseline and tumours were harvested, sorted and extracted for mRNA level. Left: mRNA level from baseline and shSLC2A3-expressing cells of individual mouse. Right: Average mRNA level of shSLC2A3-expressing cells from five mice compared to the baseline.

3.3.3.8 SLC2A3 knockdown reduces glucose uptake and possible longer survival

Previous *in vivo* experiments on RG mice (3.3.3.5 & 3.3.3.7) indicated *SLC2A3* knockdown cells outcompeted other populations, including control. Upon completing the studies, there was an unusual observation I noticed from the mice that developed tumours. The tumours felt not as solid as normal Kasumi-1 cell tumour experienced by Dr Helen Blair or Mr Hasan Issa, whom have performed many *in vivo* experiments using the same cell line and mouse model. Apart from that, the tumour size did not grow as quickly as it usually grew. So, I thought possibly *SLC2A3* knockdown alone will independently lead to a slower progression of leukaemic cells *in vivo* and therefore increase in the survival. In this experiment lentiviral transduction was performed with either shNTC- or shSLC2A3-expressing vector on Kasumi-1 cell line associated with pSLIEW vector (K-1.pSLIEW). This cell line expresses firefly luciferase and enabled us to monitor cells engraftment by *in vivo* imaging system (IVIS) (Bomken et al., 2013). After 72 hours-post transduction, the cells either shNTC- or shSLC2A3-expressing cells were intrahepatically transplantated into two groups of 4-days old newborn RG mice. IVIS imaging were performed on day 30, 44

and 57 following luciferin injection. Mice were humanely killed when it reached the endpoint as listed in the study licence (Figure 3-27).

Apart from that, *in vivo* glucose uptake assay was also performed in this group of animals by utilising 2-deoxy-2-[^{18}F]fluoro-d-glucose (2FDG), a glucose analogue with a positron-emitting ^{18}F substitution of the 2-hydroxy group which is transported into the cells by glucose transporters. It was developed subsequently from 2-Deoxy-D-glucose (described in chapter 5) for brain glucose mapping in human (Fowler and Ido, 2002), and further characterised as glucose uptake marker in both *in vitro* and *in vivo* studies (Leung, 2004, Kung, 2012, Kuwert, 2003). In a 2002 study, FDG uptake was shown to be significantly associated with higher expression of glucose transporter-1 (SLC2A1) in tumour section from untreated breast cancer patients and correlated with disease severity (Brown et al., 2002). In line with this, I postulated that *SLC2A3* knockdown will lead to reduce glucose uptake *in vivo* measured by 2FDG. 2FDG administration was performed by Mr Saimir Luli and Ms Julian Hunter.

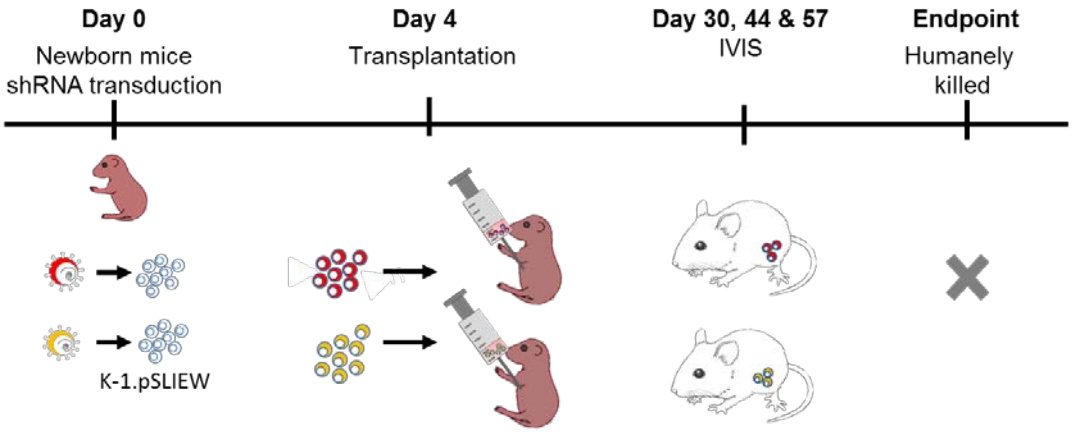

Figure 3-28: Scheme of survival analysis study using shRNA- and shSLC2A3-expressing cells in Kasumi-1.pSLIEW cell line. Kasumi-1.pSLIEW cells were lentivirally transduced with either shNTC- or shSLC2A3- expressing vector and intrahepatically transplanted in 4-days old RG mice. Bioluminescent imaging was performed on day 30, 44 and 57 to monitor the engraftment. Mice were humanely killed when it reached the endpoint described in the license.

Figure 3-28-A shows the bioluminescent images using IVIS which demonstrated development of localised abdominal engraftment of Kasumi-1.pSLIEW cell line. Total flux of the signals for both shNTC and shSLC2A3 transplanted mice is indicated in Figure 3-28-B. Bioluminescent signals of shNTC transplanted mice developed a rapid spread of signal once it was initiated as seen between day 44 and 57 (Figure 3-28-

B). Mouse 2 had low bioluminescent signal on day 57; however, the tumour grew rapidly and killed by day 65. Although shSLC2A3 transplanted mice 7 and 10 showed a spread signal on day 44 via IVIS; and mouse 9 on day 57, I barely could feel the tumour, an observation noticed in line with the previous experiment and therefore were left for longer period. By day 52, mouse 10 showed sign of sickness and was humanely killed. It had enlarged gallbladder approximately 30 times bigger than normal size, while the tumour weighed only 0.62 gram. Mouse 7 developed physically viable tumour and killed on day 52.

Overall, shNTC transplanted mice survived a median of 61 days post-transplantation while shSLC2A3 mouse delayed tumorigenesis for 70 days; however, the result was not significant as there were not enough animals (p-value=0.12) (Figure 3-29). A larger animal study would give a clear and affirmative result for this experiment.

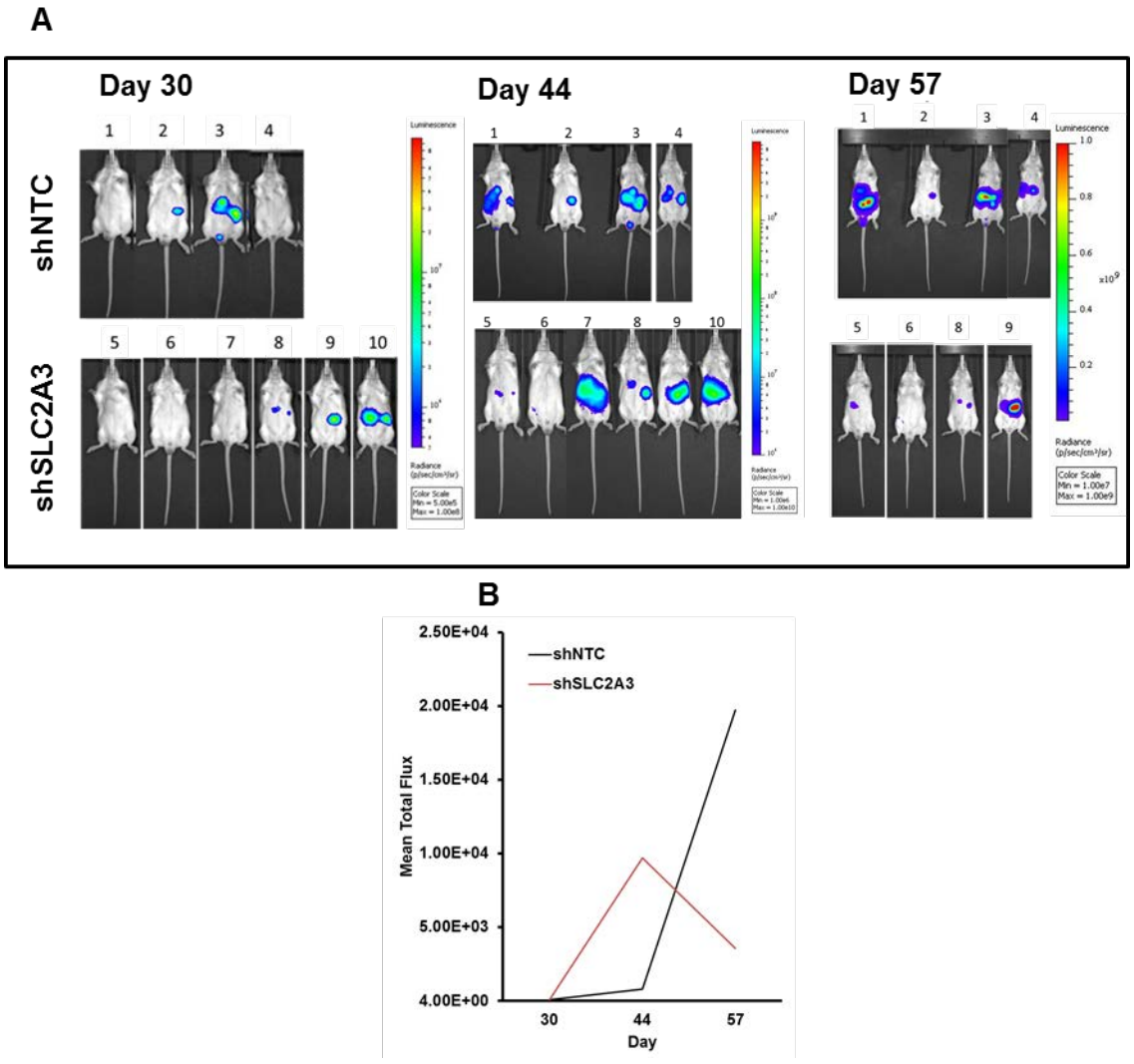

Figure 3-29: Bioluminescent images of shNTC and shSLC2A3 transplanted RG mice. A) Bioluminescent image of shNTC and shSLC2A3 transplanted mice on day 30, 44 and 57. Mice were injected with luciferin 10 minutes prior to imaging and

images were captured using IVIS system. B) Mean bioluminescent total flux of both shNTC and shSLC2A3 transplanted mice for day 30, 44 and 57.

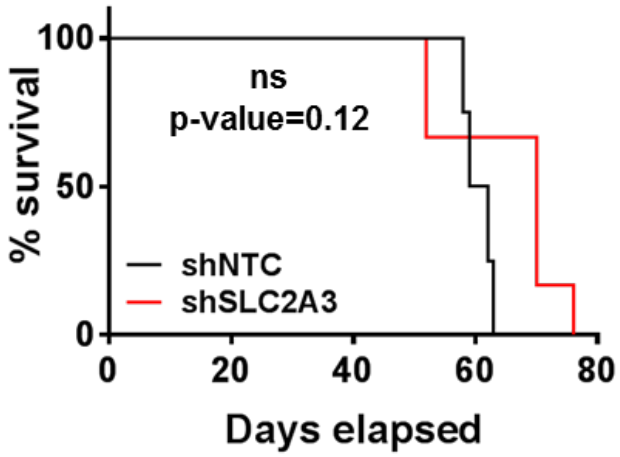

Figure 3-30: Survival analysis of shSLC2A3-expressing Kasumi-1.pSLIEW cell lines promotes insignificant delayed tumorigenesis *in vivo* (p-value=0.12). Kasumi-1.pSLIEW cells were lentivirally transduced with shSLC2A3-expressing vector and intrahepatically transplanted into newborn mice (n=4 for control and n=6 for shSLC2A3).

Figure 3-30 showing bioluminescent and 2FDG fluorescent images of control and *SLC2A3* knockdown mice analysed on the same range of intensity. Two shNTC-expressing mice demonstrated high signals of tumour bioluminescent and associated with localisation of 2FDG fluorescent. In *SLC2A3* knockdown, only one mouse is associated with high intensity of tumour bioluminescent and no signal of 2FDG detected.

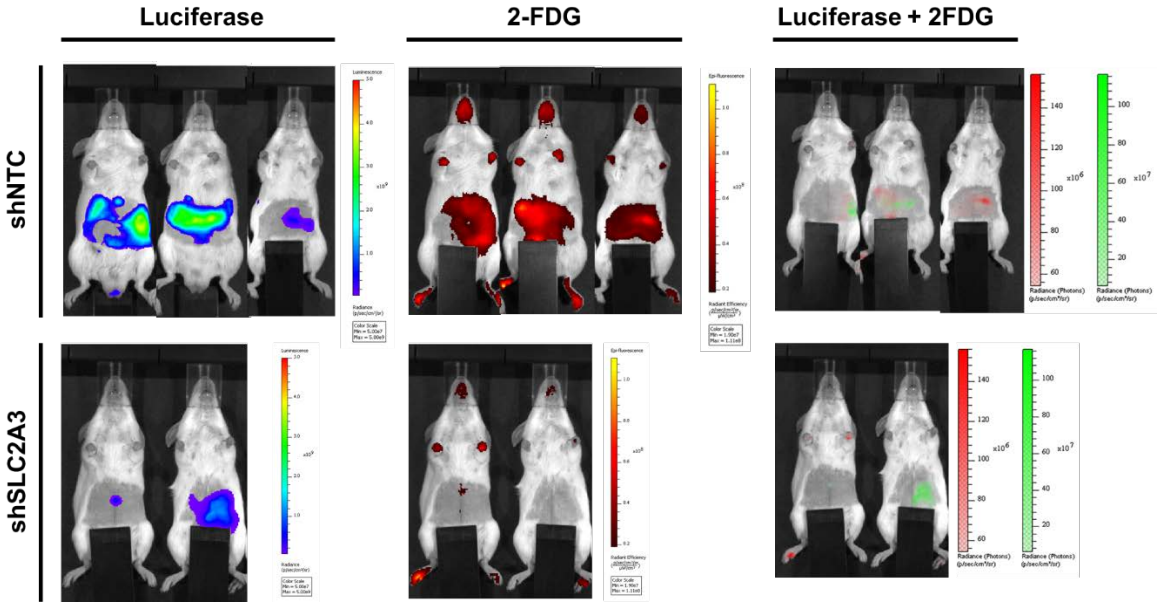

Figure 3-31: SLC2A3 knockdown reduces glucose uptake *in vivo*. Kasumi-1.pSLIEW cells were lentivirally transduced with shSLC2A3-expressing vector and intrahepatically transplanted into newborn mice (n=3 for control and n=2 for shSLC2A3). Mice were injected with 2FDG prior to imaging. Fluorescence and bioluminescent images were overlapped using Living Image software.

3.4 Summary

The major focus of this chapter was to determine if *SLC2A3* and *PFKP* are potential therapeutic targets for RUNX1/ETO-leukaemia survival and propagation. The outcomes of this study showed irresponsive roles of *SLC2A3* in disease progression *in vivo* and contradicted the shRNA screen result. Although glucose uptake was compromised both *in vitro* and *in vivo*; however, the *in vivo* survival result was not significant to conclude if *SLC2A3* is indeed required for leukaemic propagation. On the other hand, *PFKP* was shown to be a crucial partner gene required by RUNX1/ETO leukaemia. *In vitro* analysis showed that RUNX1/ETO moderately regulates the expression of *PFKP;* however, *in vivo* experiments demonstrated the leukaemic propagation relies heavily on this gene.

Chapter 4 : RUNX1/ETO alters leukaemic metabolism through *SLC2A3* and *PFKP in vitro*

4.1 Introduction

The subject of cancer and metabolism has grown over the past few years. Accumulated evidences have shown that cancer cells rewire their metabolic programme to promote survival and proliferation (Noble et al., 2017, Choi and Park, 2018, Hou et al., 2017). Alterations in cancer metabolic programming demands an increase in the import of nutrients from the extracellular environment such as glucose, glutamine and amino acids (Choi and Park, 2018, Jones et al., 2018, Hou et al., 2017).

As described in the previous chapter, *SLC2A3* and *PFKP* are highly expressed in cancers to promote glucose uptake and glycolysis. Higher glucose uptake selectively progresses the cancer cells towards the glycolytic pathway and secretion of lactate to the extracellular fluid, even under aerobic condition (Warburg, 1956b). This pathway, called aerobic glycolysis or the Warburg effect, produces acidic environment surrounding the tumour and is thought to be the microenvironment required for tumour progression (Nagarajan et al., 2016). Glutamine is also required in parallel with glucose to maintain pools of carbon and nitrogen sources which serve as building blocks for the assembly of various macromolecules. Higher uptake of these two molecules also gives the advantage in obtaining reducing power in the form of NADH and $FADH_2$, these either function to fuel ATP generation or maintain cellular redox capacity (Pavlova and Thompson, 2016).

Low oxygen content is another critical component for tumour progression and is well established in solid tumours such as breast cancer (Sgarbi et al., 2018, Semenza, 2017). In blood cancer, it could also be assumed that high blast cell proliferation requires high oxygen consumption and this would eventually reduce the oxygen availability in the blood vessel. Leukaemic initiating cells (LICs) originate from haematopoietic stem/progenitor cells and reside in the most hypoxic areas within normal HSC niche. Oxygen content in the bone marrow varies from 6%, in close proximity to the vessels, to anoxia in the most distant regions (Deynoux et al., 2016). Additionally, low oxygen condition triggers upregulation of many metabolic genes including *SLC2A3* (Mimura et al., 2012) and *PFKP* (Singh et al., 2017). In leukaemia, these two genes are not well studied; hence this chapter characterises the dependency of these two genes in RUNX1/ETO-leukaemia *in vitro*.

4.2 Aims

The aims of this chapter are:

i- to study competitiveness of *SLC2A3* and *PFKP* in restriction of nutrients and oxygen upon shRNA-mediated knockdown.

ii- to assess the metabolic phenotype changes upon depletion of *SLC2A3* and *PFKP* through Seahorse metabolic assay.

4.3 Results

4.3.1 *Role of SLC2A3 and PFKP in RE-leukaemia assessed by in vitro constitutive expression of shRNA*

In section 3.3.2, I have shown that transient knockdown of *SLC2A3* and *PFKP* with siRNA did not affect the proliferation when compared to the experimental control. This result was predicted as demonstrated by the previous shRNA screen, where we have observed that these two genes only scored *in vivo* but not *in vitro* (chapter 3). To further study the role of these genes *in vitro*, I have used constitutively expressed vector pLKO.5d.miRNA30 targeting these two genes and characterised the impact on survival and metabolic potential which will be described in the following sections.

4.3.2 *Constitutive expression of shSLC2A3 lead to loss of RUNX1/ETO-leukaemic populations in competitive assay setting under nutrient and oxygen deprivation conditions*

Competitive assay comprising at least two different populations in a single pool of cells is designed to measure the ability of one population to outcompete one another. A gene that is crucial for cell survival and propagation will be lost in long-term culture in comparison to the experimental control.

As illustrated in Figure 4-1, cells were set-up in a competitive assay setting by mixing the experimental control cells and shRNA knockdown cells into a single pool. Before mixing, each cells population was transduced with shRNA lentivirus expressing

different endogenous fluorophore at MOI 0.3 and the changes in cell pool was monitored by flow cytometry. The gain and loss of fluorescence fractions over time represent the ability of each population to populate and outcompete each other. Cells were transduced with shRNA lentiviral vectors targeting *RUNX1/ETO* (tagged with dTomato), *SLC2A3* (tagged with dTomato), *PFKP* (tagged with eGFP) and *SLC2A3+shPFKP* (tagged with dTomato+eGFP). For the control, shNTC-expressing cells were tagged with RFP657 fluorophore. On day 4 post-transduction, knockdown cells were analysed by flow cytometry, washed and mixed with shNTC. In RUNX1/ETO competitive assay setting, there were only two populations involved, which were *RUNX1/ETO* knockdown cells (shRE) and shNTC-expressing cells (shNTC). Each of the populations was mixed at 50% of transduced cells. For competitive assay targeting *SLC2A3* and *PFKP*, there were four populations in a single pool. Each *SLC2A3*- (shSLC2A3), *PFKP*- (shPFKP), *SLC2A3+PFKP*-expressing cells (shSLC2A3+shPFKP) and shNTC was mixed at approximately 25% of cells. Flow cytometry analysis was carried out after mixing to establish a baseline at day 0 and changes of the fluorescence were monitored every three to four days.

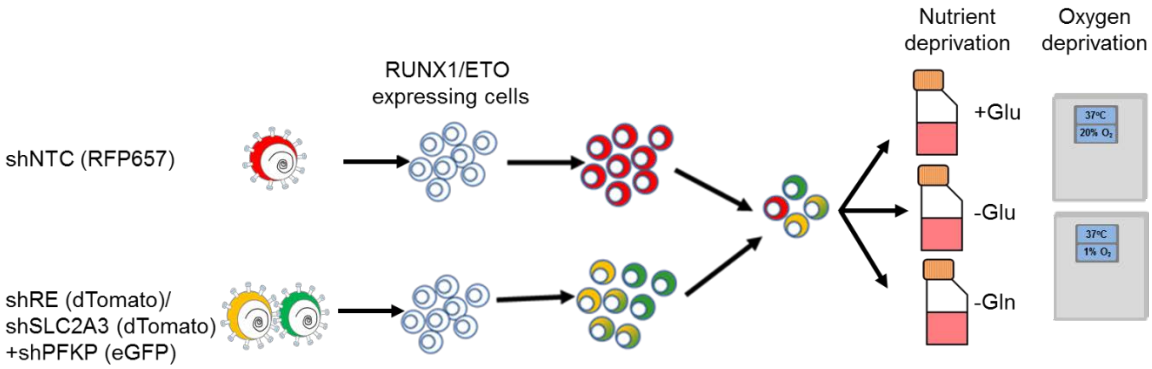

Figure 4-1: Scheme of competitive assay setting utilising constitutive shRNA expression. RUNX1/ETO-positive cells were lentivirally transduced with shRNA vector expressing different colour targeting NTC, *SLC2A3, PFKP* or double knockdown (*SLC2A3* and *PFKP*). Cells were analysed by flow cytometry on day 4 and mixed with approximately 25% of each population. *In vitro* experiment conditions included incubation of cells under oxygen, glucose and glutamine suppressed condition. O_2: oxygen, -Glu: low glucose, -Gln: low glutamine.

Glucose limitation was included in the assay after considering two aspects; Firstly, glucose is the primary substrate of glycolysis; hence, overall energy production would be affected by limiting this substrate. Secondly, SLC2A3 exhibits the highest affinity towards glucose (Ian et al., 2008, Arbuckle et al., 1996) and if the gene is depleted, it will demonstrate the dependency of cells to glucose through *SLC2A3.* Standard

medium used in current leukaemia cell lines (Kasumi-1 and SKNO-1) culture contains 11 mM glucose (+glu), and the concentration was reduced four-fold lower to 2.5 mM in low glucose condition (-glu). The 2.5 mM glucose level was in between normal physiological glucose level in blood (4-8 mM) and Km of SLC2A3 (1.4 mM).

As described earlier, glutamine provides nitrogenous compounds for cellular biosynthesis of amino acids and lipids. Therefore, glutamine deprivation in the media would reduce both carbon and nitrogen sources. The glutamine content was reduced ten times lower to 0.2 mM in culture media (-gln).

Another part of the assay was the limitation of oxygen content. I reasoned oxygen might play a role in the behaviour of the genes as they were shown to be responsive *in vivo* in the shRNA screen. I postulated, low oxygen content leads to higher dependency of *SLC2A3* and *PFKP* to support increase in glycolysis. While the standard incubation (normoxia) was set at 20% oxygen, the hypoxia incubation was set to 1% of oxygen. The experiments involving hypoxia were conducted inside the hypoxia station at all times.

4.3.3 *Limitation of nutrient and oxygen significantly impact the cell proliferation of Kasumi-1 cells*

Firstly, I sought to determine whether limitation of nutrient and oxygen results in slower growth of the cells. Kasumi-1 cells were seeded at 5.0 x 10^5 cell/ml in +glu, -glu and –gln condition media and placed in normoxia and hypoxia incubator. Cells were counted at 24-, 48- and 72-hour timepoint using standard trypan blue counting method.

Figure 4-2-A indicates growth curve of Kasumi-1 cells in different culture media in both normoxia and hypoxia incubation conditions. Cells cultured in normoxia +glu doubled at 65-hour post-seeding and significantly proliferated at higher rate than cells cultured in hypoxia and nutrient deprivation conditions (p-value<0.05) (Figure 4-2-B). Furthermore, hypoxia had no impact on nutrient deprivation cultured as indicated in the Figure 4-2-B.

Collectively, low oxygen and nutrient deprivation caused lower cells number of Kasumi-1 cells, but, combination of both factors did not have any impact on the proliferation.

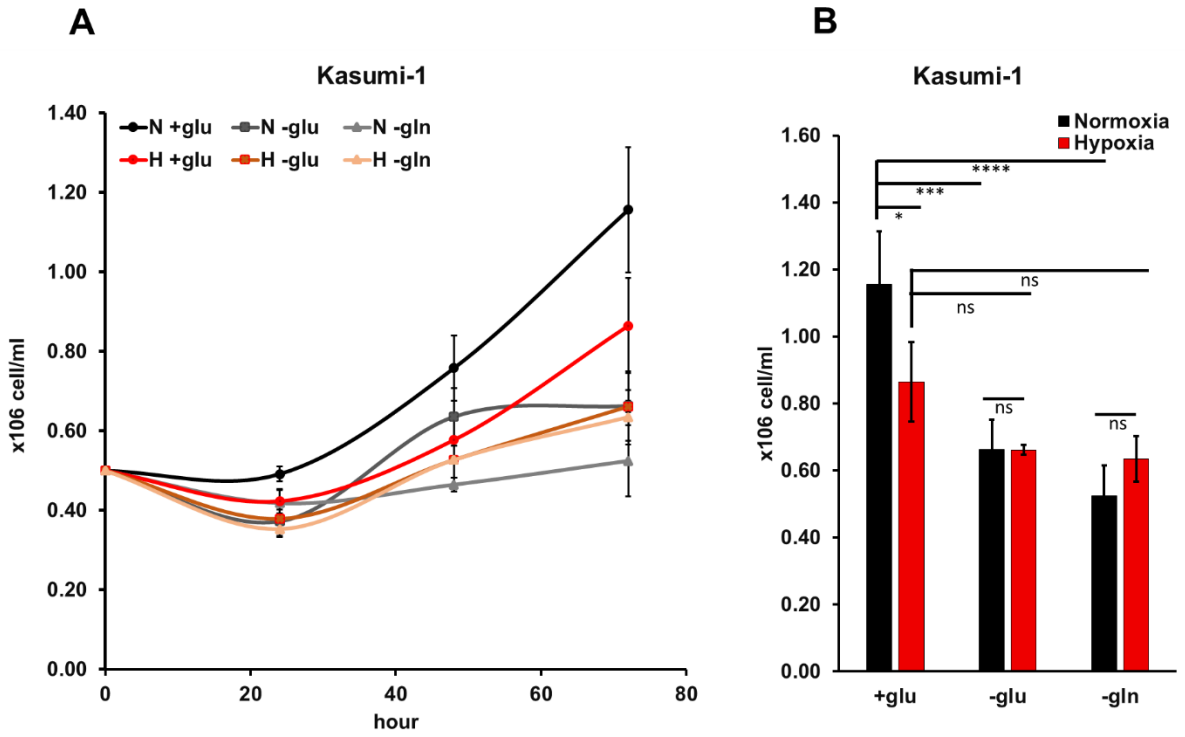

Figure 4-2: Proliferation curve for Kasumi-1 cells in oxygen and nutrient limitation condition. Cells were seeded at 5.0 x 10^5 cell/ml at day 0 and counted at the timepoint indicated on the x-axis. A) The growth of Kasumi-1 cells at different timepoint. B) Comparison of cells number at 72-hour timepoint. Significance was evaluated using 2-way Anova using PRISM software. p*≤0.05, **p<0.01, ***p<0.001, p****<0.0001. Error bars indicate standard deviation (n=3, independent experiments). N: Normoxia, H: hypoxia, +glu: high glucose, -glu: low glucose, -gln: low glutamine.

4.3.4 *RUNX1/ETO as master regulator in t(8;21) leukaemia*

Figure 4-3 to Figure 4-7 show changes of the fluorescence of shRNA knockdown cells in long-term competitive assay. In general, cells transduced with shNTC outcompeted shRE populations in all culture conditions in both normoxia and hypoxia conditions, for both Kasumi-1 and SKNO-1 cell lines (Figure 4-3 and Figure 4-5). In Kasumi-1 cell line, shRE cells started to loss as early as on day 3 observed in normoxia conditions. However, in hypoxic conditions, loss of shRE cells did not occur as rapid as in normoxia. These results indicate that RUNX1/ETO is indeed the master regulator of t(8;21) leukaemia. *RUNX1/ETO* knockdown in Kasumi-1 cells showed trends of resistance in hypoxia condition (Figure 4-5); but, consequently, the cells were outcompeted by shNTC cells at the end of the experiments (Figure 4-3).

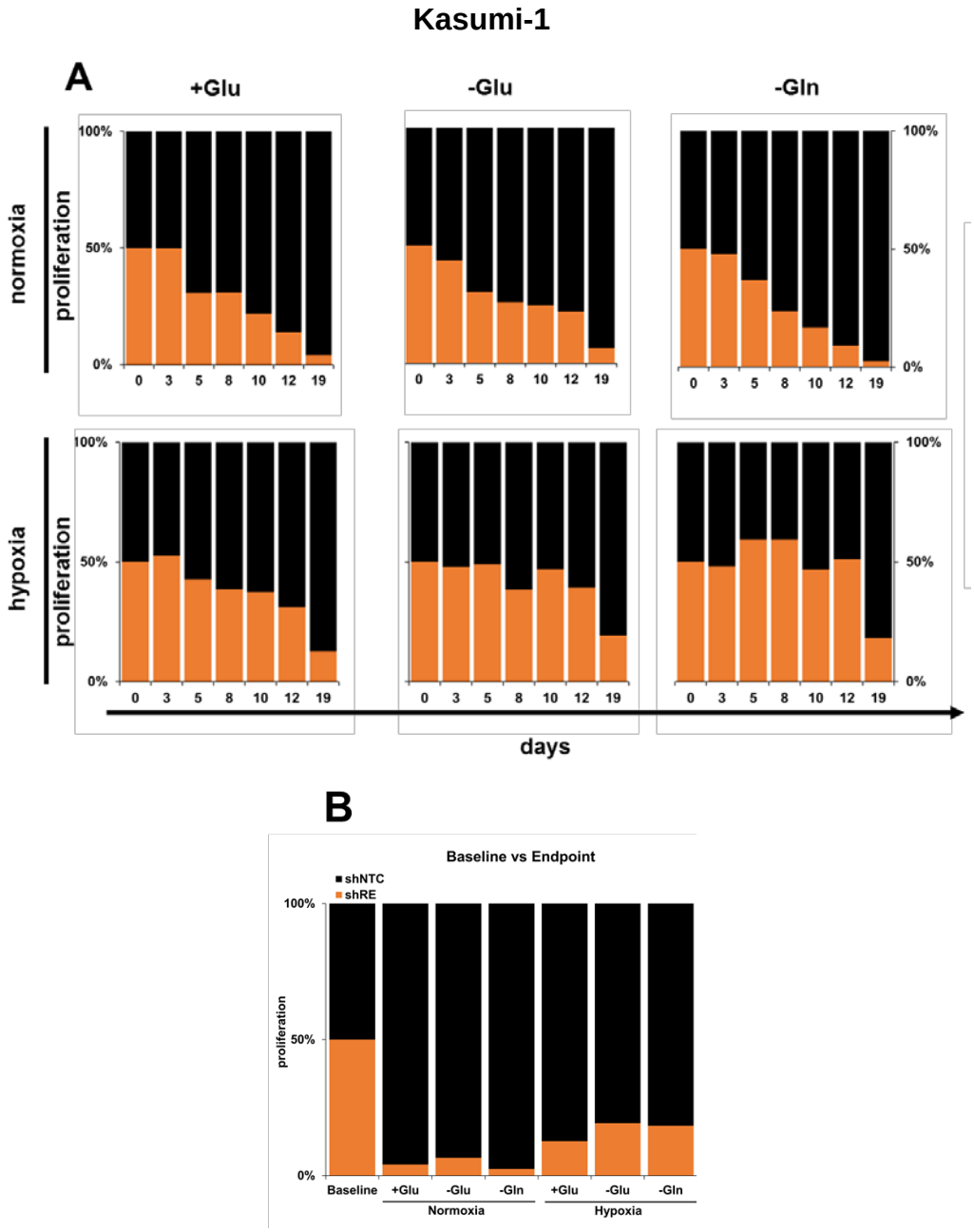

Figure 4-3: Stacked column showing competitive loss of shRE to shNTC in all culture conditions in Kasumi-1 cells. A) shNTC and shRE cells were mixed on day 0 in standard media (+glu), glucose or glutamine deprived media (-glu and –gln respectively) and cultured in normoxic or hypoxic conditions. Fluorescence percentages were monitored by flow cytometry at least once a week. Briefly, the percentage of fluorescence was calculated by excluding non-transduced cells and every timepoint was normalised to day 0 as well as fractionised to an amount of 25% to get a matrix of 100%. B) Summary of fluorescence percentages between baseline and endpoint in different culture conditions. Populations of shRE loss compared to shNTC in all culture conditions (n=1).

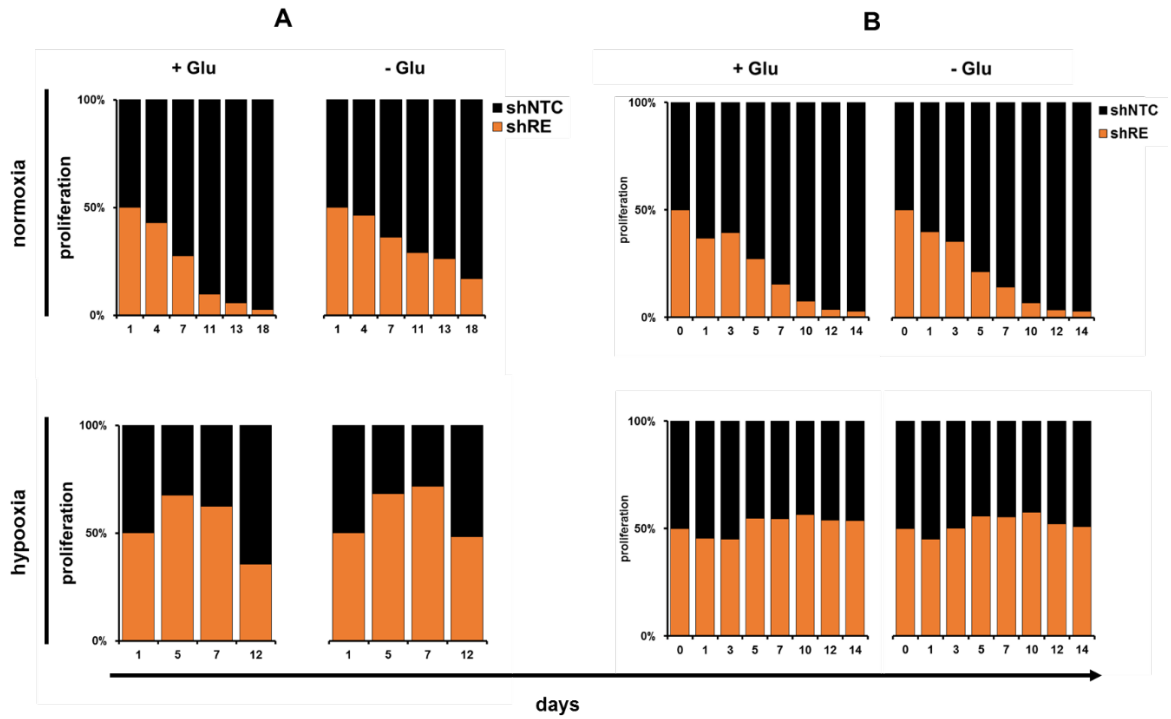

Figure 4-4: Different experiments show trends of resistance of shRE cells in hypoxia conditions in Kasumi-1 cells. A&B) shNTC and shRE cells were mixed on day 0 in standard media (+glu), glucose or glutamine deprived media (+glu and –gln respectively), and cultured in normoxic or hypoxic conditions. Fluorescence percentages were monitored by flow cytometry at least once a week. Briefly, the percentage of fluorescence was calculated by excluding non-transduced cells and every timepoint was normalised to day 0 as well as fractionised to an amount of 25% to get a matrix of 100%. B) Summary of fluorescence percentages between baseline and endpoint in different culture conditions. Populations of shRE loss compared to shNTC in all culture conditions (n=1).

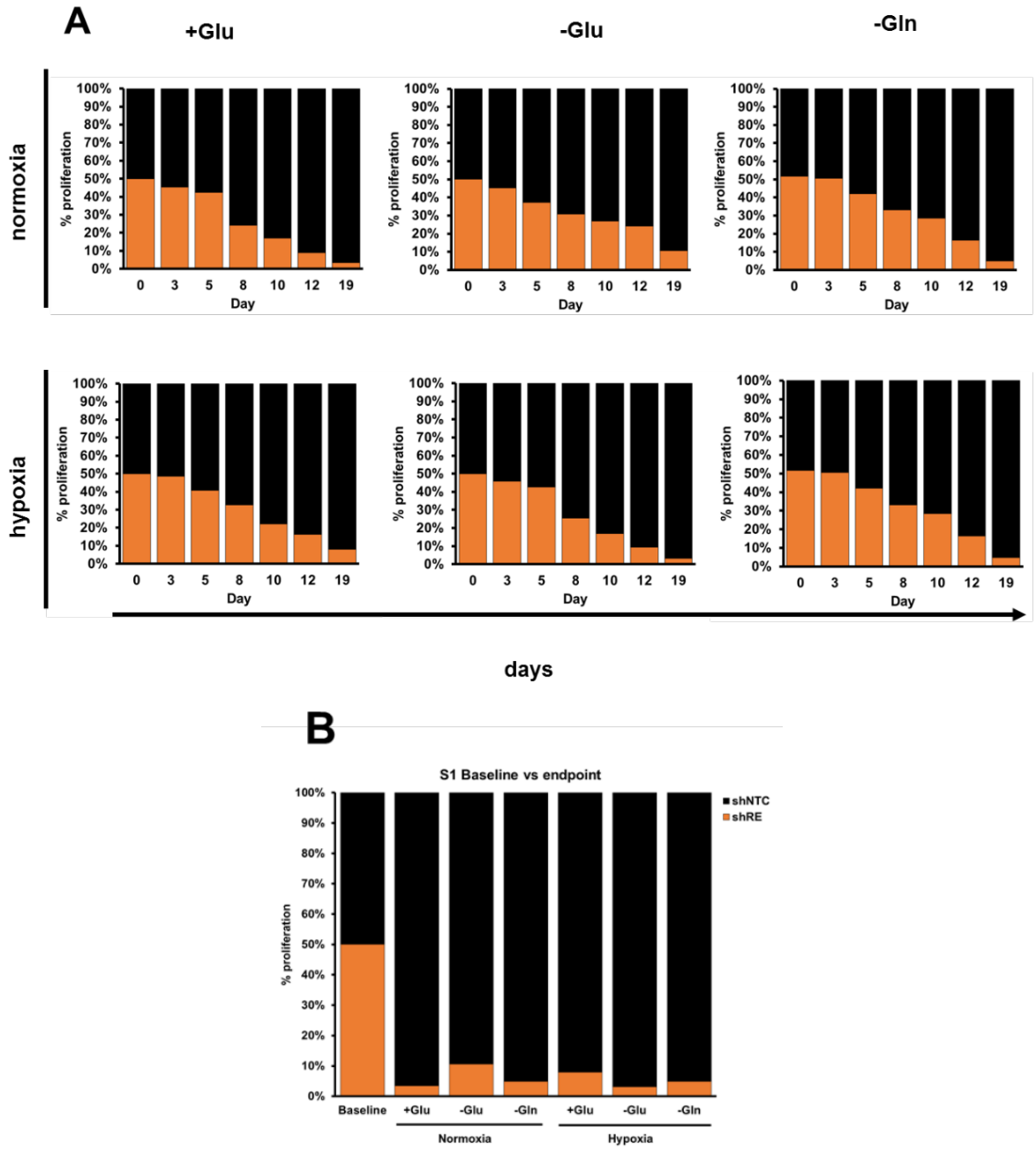

Figure 4-5: Stacked column showing competitive loss of shRE to shNTC in all culture conditions in SKNO-1 cell line. A) shNTC and shRE cells were mixed on day 0 in standard media (+glu), glucose or glutamine deprived media (-glu and –gln respectively), and cultured in normoxic or hypoxic conditions. Fluorescence percentages were monitored by flow cytometry at least once a week. Briefly, the percentage of fluorescence was calculated by excluding non-transduced cells and every timepoint was normalised to day 0 as well as fractionised to an amount of 25% to get a matrix of 100%. B) Summary of fluorescence percentages between baseline and endpoint in different culture conditions. Populations of shRE loss compared to shNTC in all culture conditions (n=1).

4.3.5 *Glucose addiction via SLC2A3 in RUNX1/ETO-leukaemia in Kasumi-1, but not in SKNO-1*

Overall, in Kasumi-1 cells the percentage of shNTC cells increased in all culture conditions (Figure 4-6). In normoxia +glu condition, there was no significant reduction of the shSLC2A3 population. Whereas, in normoxia –glu condition, a statistically significant shSLC2A3 cells were outcompeted by shNTC ($p<0.01$). The same observation was also seen in hypoxia –glu condition. *SLC2A3* knockdown cells were significantly outcompeted by shNTC at the end of the experiment ($p<0.05$). Moreover, neither normoxia nor hypoxia conditions had substantially affected *SLC2A3* knockdown cells cultured in glutamine deprivation media.

shNTC cells significantly outcompeted *PFKP* knockdown cells in all culture conditions ($p<0.05$), with the smallest fraction of cells observed in normoxia –gln condition ($p<0.001$). Double knockdown of *SLC2A3* and *PFKP* significantly caused the cells to competitively loss to shNTC in all culture conditions ($p<0.05$) with *SLC2A3* knockdown cells significantly contributed towards the effect (p-value<0.05). *PFKP* knockdown; however, insignificantly caused the loss in double knockdown populations observed in hypoxia +glu and –gln conditions.

On the contrary, knockdown of *SLC2A3* and *PFKP* in SKNO-1 resulted in unexpected and inconclusive outcomes as indicated Appendix 4-1.

Taken together, at MOI of 0.3, *SLC2A3* shown to be responsive in limited glucose and oxygen conditions in Kasumi-1 cells, but not in SKNO-1 cells. In Kasumi-1 cells, *PFKP* knockdown showed to be an important regulator in glycolysis, whereby the knockdown led to loss of cell populations in all culture conditions. Furthermore, targeting both *SLC2A3* and *PFKP* led to a significant depletion of leukaemic population in Kasumi-1 cells (p-value<0.05).

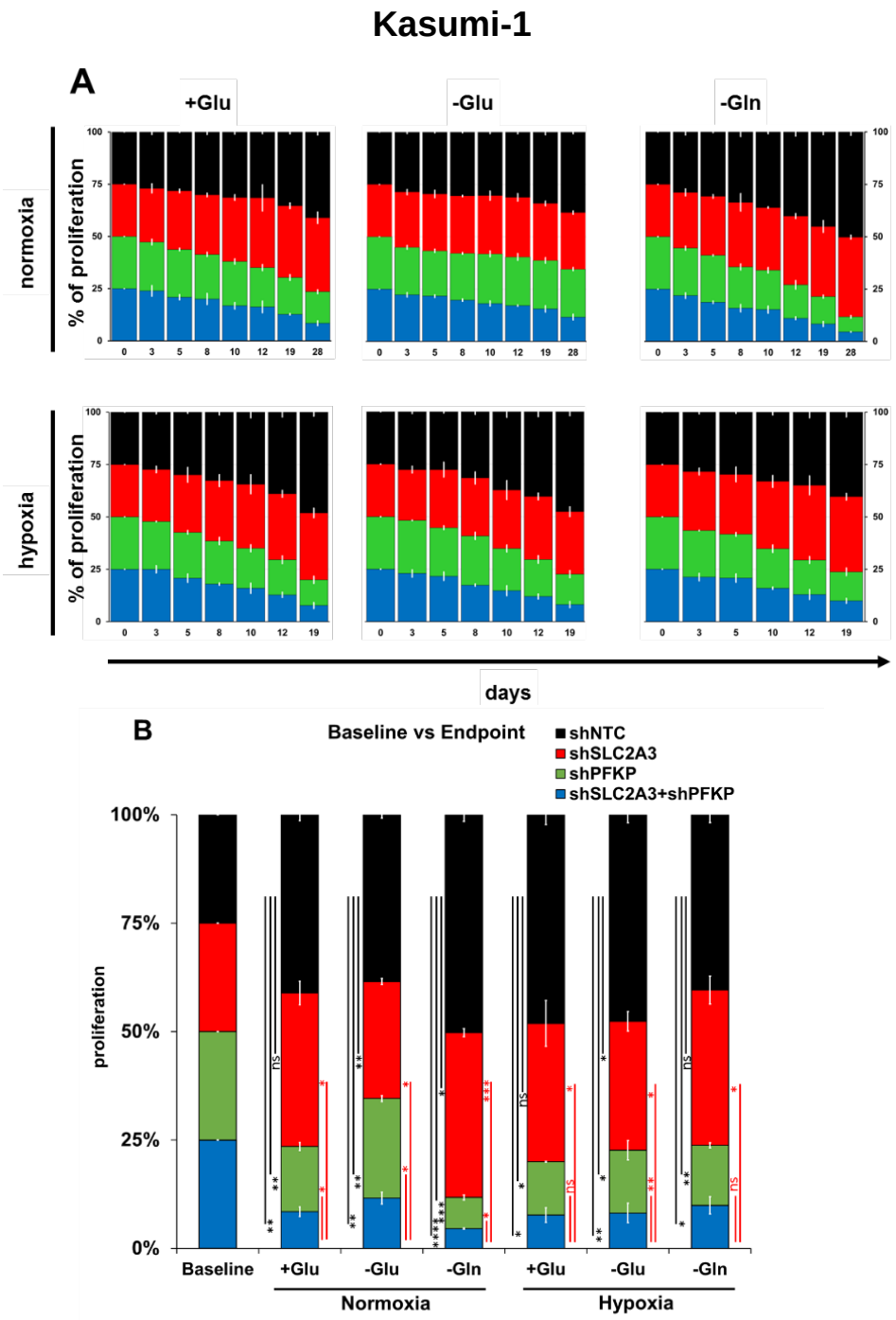

Figure 4-6: Stacked column showing competitive loss of shSLC2A3 in the absence of glucose, glutamine and oxygen in Kasumi-1 cell line at MOI 0.3. A) shNTC, shSLC2A3, shPFKP and shSLC2A3+shPFKP cells were mixed on day 0 in standard media (+glu), glucose or glutamine deprived media (+glu and –gln respectively), and cultured in normoxic or hypoxic conditions. Fluorescence percentages were monitored by flow cytometry at least once a week. Briefly, the percentage of fluorescence was calculated by excluding non-transduced cells and at every timepoint was normalised to day 0 as well as fractionised it to an amount of 25% to get a matrix of 100% for all the populations. B) Summary of fluorescence percentages between baseline and endpoint in different culture conditions. Significance was evaluated using one-way Anova for each culture condition using PRISM software. p*≤0.05, **p<0.01, ***p<0.001, p****<0.0001. Error bars indicate standard deviation (n=3, independent experiments).

4.3.6 *SLC2A3 knockdown cells exhibit more profound loss with higher virus particles per cell*

As mentioned in chapter 3 (section 3.3.6), I wondered if the amount of virus particle per cell have a different impact on cell survival especially on *SLC2A3* knockdown cells. The assays were then repeated at higher transduction rate to see the differences in both Kasumi-1 and SKNO-1. Both Kasumi-1 and SKNO-1 cells were lentivirally transduced at more than 90% efficiency. However, due to limitations in virus production at this stage (will be described in the chapter conclusion), only Kasumi-1 cells were continued to culture in standard and limited glucose in both normoxia and hypoxia conditions with double knockdown approach following the scheme in Figure 4-1.

Whereas, SKNO-1 cells were transduced with either shNTC- or shSLC2A3-expressing lentivirus and mixed on day 4-post-transduction. SKNO-1 cells were cultured in either +glu media and placed in normoxia or in -glu media in hypoxia condition. Due to a very low number of cells during this assay, the fluorescence was captured only once, at day 7-post mixing.

Figure 4-7 shows the changes of shRNA-expressing cells in each culture condition. In Kasumi-1 cells, the shNTC-expressing cells significantly outcompeted other populations in all culture conditions ($p<0.05$). Confirming the previous experiments, hypoxia –glu significantly caused the biggest loss of *SLC2A3* knockdown cells (p-value<0.001). Furthermore, *PFKP* knockdown caused the cells to significantly loss to shNTC cells in all culture conditions (p-value<0.001). Finally, double knockdown of *SLC2A3* and *PFKP* significantly loss to shNTC-expressing cells.

In contrast to the findings with MOI 0.3, SKNO-1 cell line showed a more potent reduction of *SLC2A3* knockdown cells in both normoxia +glu and hypoxia -glu. In these two conditions, shNTC cells grew from 50% of cells at day 0 to 82% of cells on day 7 and successfully outcompeted *SLC2A3* knockdown cells (Figure 4-7-C).

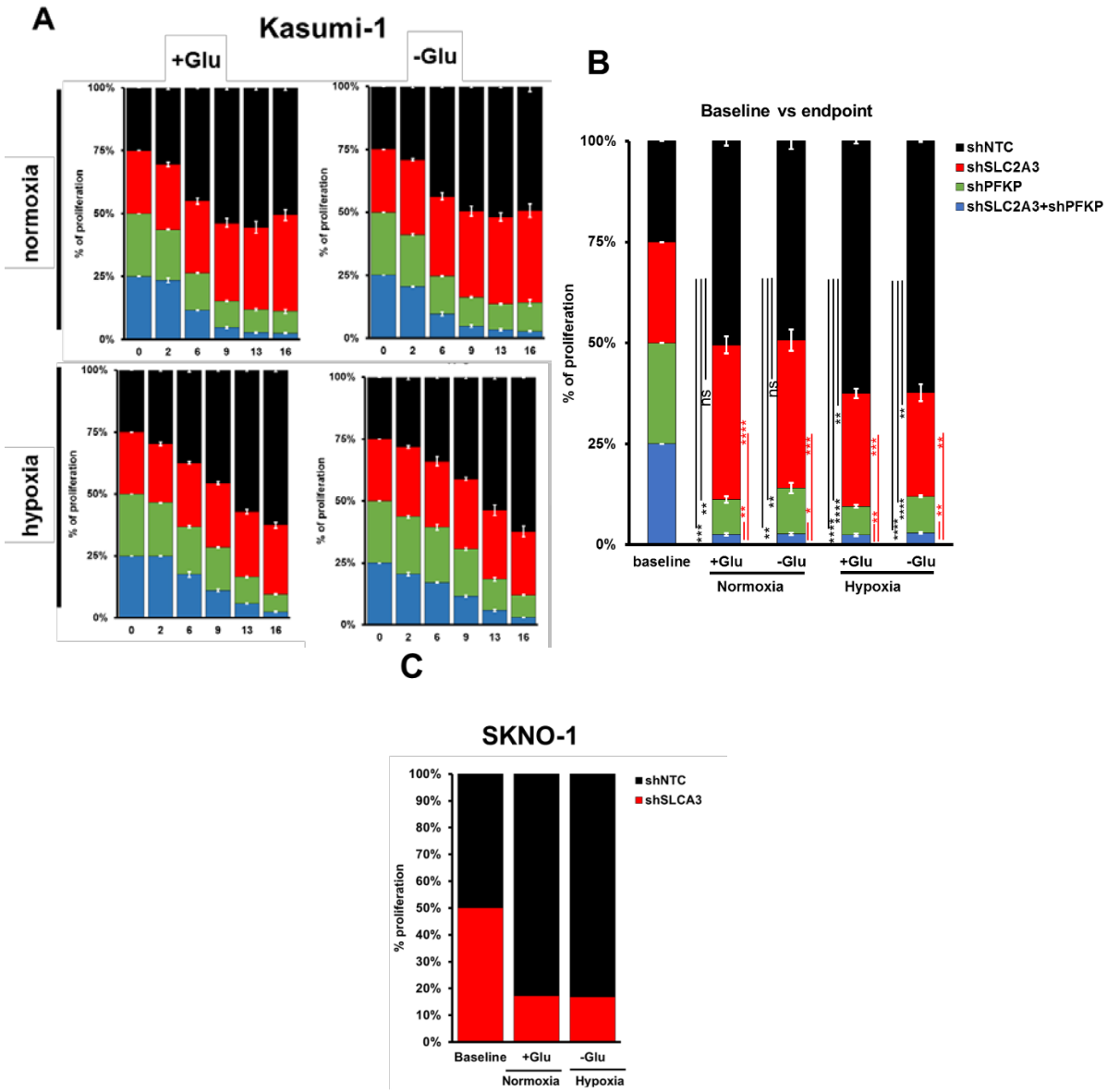

Figure 4-7: Stacked column showing competitive loss of shSLC2A3-expressing cells in the absence of glucose and oxygen at higher transduction efficiency in both Kasumi-1 and SKNO-1 cell lines. A) Kasumi-1 cells; shNTC, shSLC2A3, shPFKP and shSLC2A3+shPFKP cells were mixed on day 0 in standard media (+glu) and glucose deprived media (-glu) and cultured in normoxic and hypoxic conditions. B) Summary of percentages between baseline and endpoint in different culture conditions (n=3). C) SKNO-1 cells; shNTC- and shSLC2A3-expressing cells were mixed on day 0 in either standard media (+glu) or glucose deprived media (-glu). Cells in the standard media were incubated in normoxic conditions, whereas cells in limited glucose were cultured in hypoxic condition (n=1). Fluorescence percentages were monitored by flow cytometry at least once a week. Briefly, the percentage of fluorescence was calculated by excluding non-transduced cells and at every timepoint it was normalised to day 0 as well as fractionised to an amount of 25% to get a matrix of 100% for all populations. Significance was evaluated using one-way Anova for each culture condition using PRISM software. p*≤0.05, **p<0.01, ***p<0.001, p****<0.0001. Error bars indicate standard deviation (n=3 independent experiments).

Based on these observations, higher transduction efficiency drove more potent effect, particularly on *SLC2A3* knockdown cells in both Kasumi-1 and SKNO-1 cells. In Kasumi-1 cells, both *PFKP* and double knockdown robustly diminished leukaemic propagation and survival. However, I wondered which condition would give the most substantial effect especially on *SLC2A3* knockdown cells in terms of reducing the leukaemic burden?

I further explored the outcomes from these two experiments in Kasumi-1 cells. Comparison was performed between shNTC-expressing cells and shRNA-knockdown cells at the endpoints to find out which condition gave the most substantial effect (Figure 4-8). With MOI 0.3 transduction (Figure 4-8-A), hypoxic –glu condition contributed to the most prominent effect, where I observed a statistically significant 40% loss of shSLC2A3 cells (p-value <0.01) when compared to the normalised shNTC cells. Whereas, *PFKP* and double knockdowns showed to be significantly loss in all culture conditions (p-value <0.001).

With higher transduction efficiency (Figure 4-8-B), *SLC2A3* knockdown cells were significantly lost in all culture conditions. The biggest loss was recorded in hypoxia –glu condition, in which 41% of cells remained at the end of the experiment (p-value<0.001). In normoxia +glu content, *SLC2A3* knockdown minimally reduced to 76% (p-value<0.01).

Additionally, both *PFKP* and double knockdown significantly loss in all culture conditions (p-value<0.001).

In summary, culturing the Kasumi-1 cells in limited glucose and oxygen have shown more substantial effect particularly on *SLC2A3* knockdown cells. Therefore, this culture condition was carried forward for further characterisations. In parallel, culturing cells in normoxia with +glu content was also performed to see the difference of glucose and oxygen would impact on *SLC2A3* and *PFKP*.

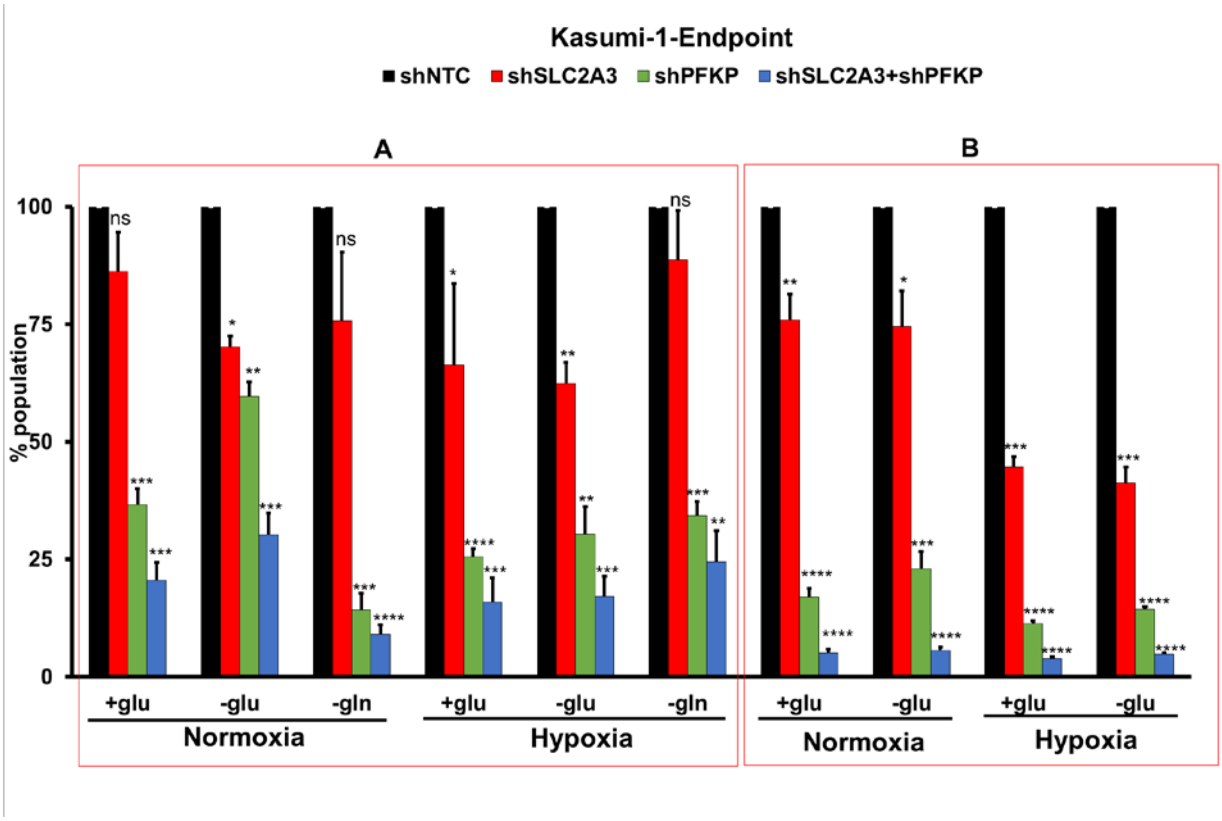

Figure 4-8: Percentage of remaining cells of each shRNA knockdown at endpoints. Percentage of shRNA-expressing cells was calculated by normalising to shNTC-cells at endpoints. Percentages were compared between lower transduction efficiency (A) and higher transduction efficiency (B). Significance was evaluated using Student's t-test for each group. ns: not significant, p*≤0.05, **p<0.01, ***p<0.001, p****<0.0001. (n=3, independent experiments).

4.3.7 *Glucose diminished clonal capability in SLC2A3 knockdown in Kasumi-1 cell line*

To further characterise *SLC2A3* and *PFKP* in self-renewal capacity of t(8;21) leukaemia, colony formation assays were performed in both Kasumi-1 and SKNO-1 cell lines. The assays were performed by including nutrient deprivation media as well as oxygen limited conditions. Cells were transduced with shRNA at high transduction efficiency of more than 90% and collected on day 4. Cells were seeded in 24-well tissue culture plate on semi-solid medium at the density of 0.5 x 10^4 cells/ml. On day 10 post-seeding, colonies that contained more than 50 were counted and images were captured.

In general, shNTC cells formed the highest number of colonies in all culture conditions when compared to all shRNA knockdown cells (Figure 4-9). *RUNX1/ETO* knockdown substantially abrogated the colony forming ability in all culture conditions indicating that it is indeed the master for self-renewal capacity in t(8;21) leukaemia.

Furthermore, in +glu condition, *SLC2A3* knockdown did not have any substantial effect on the colony formation. Moreover, the size of the colonies between shNTC and shSLC2A3 cells were almost similar as shown in Figure 4-9-B. However, in –glu condition, *SLC2A3* knockdown cells reduced the colonies by one-half and associated with much smaller colonies when compared against shNTC. In hypoxia, culturing the *SLC2A3* knockdown cells in standard methylcellulose media caused the colony forming to reduce by 30% when compared to shNTC. Limitation of glucose in hypoxia did not further impact the self-renewal capacity in the *SLC2A3* knockdown cells. Furthermore, the size and shape of the colonies were identical in both of these two conditions.

On the other hand, *PFKP* knockdown reduced the number of colonies by half in +glu condition in both normoxia and hypoxia. Limitation of glucose further reduced the number of colonies by almost 75% in both of the oxygen conditions. Interestingly, double knockdown of *SLC2A3* and *PFKP* seemed to have no additive impact as the colonies recovery were almost similar to *PFKP* knockdown.

Furthermore, plating the knockdown cells in glutamine deprivation semi-solid media completely abrogated clonogenicity in all shRNA treated cells as pictured in Figure 4-9-B. Moreover, by comparing shNTC cells between standard culture and -gln, limitation of glutamine caused 50% reduction in the number of colonies.

Taken together, targeting *SLC2A3* alone modestly impaired self-renewal capacity of Kasumi-1 cells. However, reducing glucose in culture media gave a better reduction in self-renewal capacity in *SLC2A3* knockdown. This observation was also similar in *PFKP* knockdown and in double knockdown.

Kasumi-1

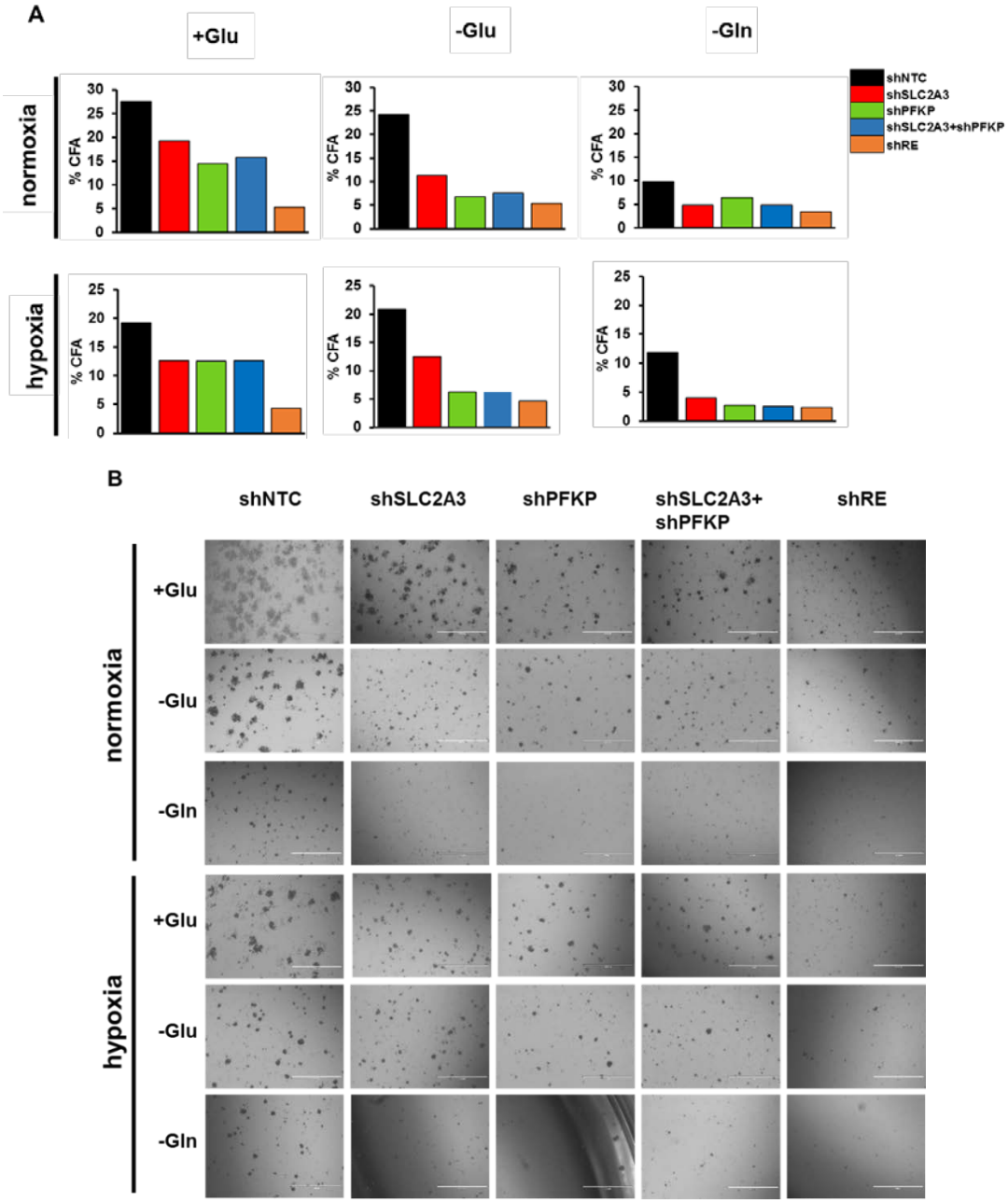

Figure 4-9: Colony forming ability of SLC2A3 knockdown was affected in reduced glucose condition. Cells were lentivirally transduced with shRNA targeting SLC2A3, PFKP and RUNX1/ETO and plated in semi-solid methylcellulose media. Colonies were counted on day 10 when the colonies in control sample contained at least 50 cells. A) Percentage of colonies were calculated against the initial number of cells seeded on day 0. B) Phase contrast pictures of colonies captured on day 10. Data were average of n=2 independent experiments. For each experiment, 2 wells of colonies were prepared for every sample. For shPFKP in hypoxia –gln, there were only pictures on the edge of the plate as no colonies/cells observed in the middle of the plate.

4.3.8 *Glucose and oxygen limitations corrupt cell cycle in SLC2A3 knockdown cells*

Knockdown of *SLC2A3* and *PFKP* in different culture condition caused RUNX1/ETO leukaemic cells to behave differently. Kuang et al. (2017) has demonstrated that low glucose renders accumulation of cells in G1/G0 phase. I wondered if the losses of cell populations were associated with cell cycle mechanism, and more interestingly if limitation of glucose caused different cell cycle profile particularly for *SLC2A3* knockdown cells. To answer this question, analysis of cell cycle was performed by flow cytometry. Briefly, 1 x 10^6 shRNA knockdown cells were collected on day 12 post-transfection, fixed with 4% paraformaldehyde (PFA) and stained with DAPI. Data were captured using FACS Canto II and analysed with FlowJo software.

As indicated in Figure 4-10, consistence with our previous findings (Martinez-Soria et al., 2018, Martinez et al., 2004), *RUNX1/ETO* knockdown caused a significant block in G0/G1 phase in all culture conditions compared with the control (p-value<0.01)

In normoxia +glu condition, the number of shNTC cells in G0/G1 phase was recorded to be 77% of cells. *SLC2A3* knockdown cells slightly increase the number of cells in the G0/G1 phase which was 78%. However, a statistically significant increase of cells in G0/G1 were observed in *PFKP* knockdown (p<0.01, 82.5%) and double knockdown (p<0.01, 83.7%). While shNTC cells recorded 17% of cells entering S phase, *SLC2A3* knockdown caused an insignificant reduction of 16% of cells in S phase. A significant decrease in the number of cells that enter S phase was observed in both shPFKP (p-value<0.01, 13%) and double knockdown cells (p-value<0.01, 12.3%).

Greater effects on the cell cycle phases were observed in hypoxic conditions. In general, oxygen-limited condition led to a higher G0/G1 phase as well as smaller G2/M phase in shNTC-expressing cells when compared with its counterpart in normoxia. In the G0/G1 phase, shNTC cells recorded 85% of cells, whereas *SLC2A3* knockdown cells significantly increased the cells in this phase to 90% (p-value<0.05). Higher G0/G1 phase was also observed in *PFKP* and double knockdown cells. *PFKP*

knockdown recorded 91% of cells (p-value<0.01), whereas 93.8% of cells recorded in double knockdown (p-value<0.001).

More interestingly, *SLC2A3* knockdown cells showed to behave differently in the suppression of glucose and oxygen conditions. By comparing against normoxic +glu condition, culturing shSLC2A3 cells in hypoxia –glu halved the percentage of cells entering S phase (p-value<0.01). Suppression of glucose and oxygen also caused a significant 90% of *SLC2A3* knockdown cells in G0/G1 phase, whereas 77% of cells were recorded in normoxia +glu condition.

Taken together, *SLC2A3* knockdown caused significantly higher accumulation of G0/G1 cells only in limited oxygen and glucose condition caused, but not in standard condition. However, *PFKP* and double knockdown increased the proportion of cells in G0/G1 phase in all culture conditions. Nevertheless, depletion of *RUNX1/ETO* diminished the proliferative capacity of the cells indicating that it is indeed the master regulator of cell cycle in t(8;21) leukaemia.

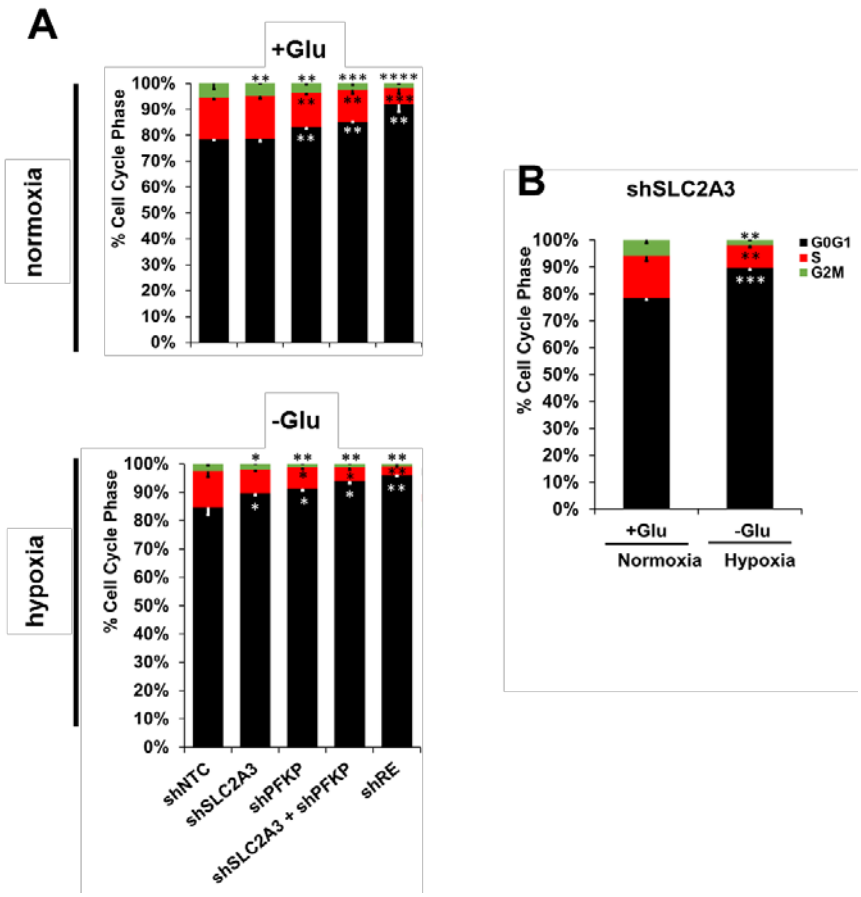

Figure 4-10: Cell cycle profile of SLC2A3, PFKP and RUNX1/ETO knockdown cells in different culture conditions. Transduced cells with shNTC, shSLC2A3, shPFKP and shSLC2A3+shPFKP were cultured in either standard (+glu) and glucose deprived media (-glu) and incubated in normoxic and hypoxic conditions. Cells were harvested, fixed in 4% PFA, stained with DAPI and analysed with flow cytometry. A) Cell cycle profiles for shNTC, shSLC2A3, shPFKP and shSLC2A3+shPFKP in normoxia +glu and hypoxia -glu conditions. B) Cell cycle profile comparing shSLC2A3 cells in normoxia +glu and hypoxia –glu condition. Significance was evaluated using Student's t-test, ns: not significant, p*≤0.05, **p<0.01, ***p<0.001, p****<0.0001 (n=3, independent experiments).

4.3.9 *Hypoxia induced cell death of SLC2A3 knockdown cells*

To pursue the reason for increased of G0/G1 phase in the knockdown cells, I looked into a potential association with cell death. To address this, I used Annexin V apoptosis assay. In apoptotic cell, the membrane phospholipid phosphatidylserine (PS) is translocated from the inner membrane to the outer layer of the plasma membrane, hence exposing PS to the external cellular environment. Annexin V is a 35-36 kDa Ca2+ dependent phospholipid-binding protein that has high affinity to PS and binds to cells with exposed PS. Annexin V antibody can be conjugated to fluorophore, in this case BV421 and can be detected by flow cytometry. This assay did not discriminate between early and late apoptosis cells as it was not used in conjunction with dead cells staining. Kasumi-1 cells were lentivirally transduced and cultured in normoxia high glucose (+glu) and hypoxia low glucose (-glu). Apoptosis analysis was performed on day 4 and day 9. Briefly, cells were harvested and incubated in Annexin V-BV421 in Ca2+ containing buffer. The fluorescence was captured using FACS Canto II and analysed using FlowJo software.

Figure 4-11-A shows the percentage of Kasumi-1 cells positive for Annexin V for shRNA cells in both normoxia and hypoxia with high and low glucose. Knockdown of *RUNX1/ETO* led to minimal changes of apoptotic body in standard culture condition.

In normoxia +glu condition, shNTC-expressing cells recorded 19.4% of apoptosis cells on day 4 and increased 1.5-fold on day 9. Longer incubation in hypoxia –glu condition caused Annexin V positive cells to increase 2.6-fold.

Percentage of Annexin V positive cells in *SLC2A3* knockdown increased slightly on day 9 in normoxia +glu condition. Interestingly, in hypoxia –glu culture, the percentage of apoptotic cells was two-fold higher on day 4 when compared with its counterpart in normoxia +glu condition. Annexin V positive cells continued to increase 3-fold on day 9.

On the other hand, knockdown of *PFKP* increased two-fold of cells in apoptosis cells from 22% on day 4 to 46% on day 9 in normoxia +glu. Culturing the *PFKP*

knockdown cells in hypoxia –glu resulted in a massive 76% increase of Annexin V positive cells on day 9, which was nearly two-fold higher than on day 4 (35%).

Moreover, double knockdown caused the highest induction of apoptosis in all conditions. In normal culture condition, the percentage of dying cells increase 2-fold from day 4 to day 9. More prominent effect was observed in limited oxygen and glucose condition, where it recorded 52% and 84% of apoptotic cells on day 4 and day 9, respectively.

In agreement with the Annexin V staining, examination of cell cycle distribution also revealed increase of subG1 population in *SLC2A3* and *PFKP* knockdowns with hypoxia showed to have greater effects (Figure 4-11-B). Hypoxia caused a significant 5-fold increase of subG1 of shNTC cells (p-value<0.01). The same observation was also observed in *SLC2A3* knockdown cells, in which subG1 cells significantly increased 4-fold in the low oxygen condition (p-value<0.05). Moreover, *PFKP* and double knockdown in standard condition caused higher subG1 phase in comparison to the shNTC. Furthermore, culturing the cells in hypoxia minimally increased the subG1 cells to 1.7- and 1.6-fold in both *PFKP* and double knockdown respectively. Despite the high induction of Annexin V positive cells in shRE cells in hypoxia –glu condition; however, subG1 analyses did not revealed any increase of subG1 population. This could be due to the cells undergo apoptosis at G2/M or late S phase and result in indistinguishable G1 or early S phase peaks (Wlodkowic et al., 2009).

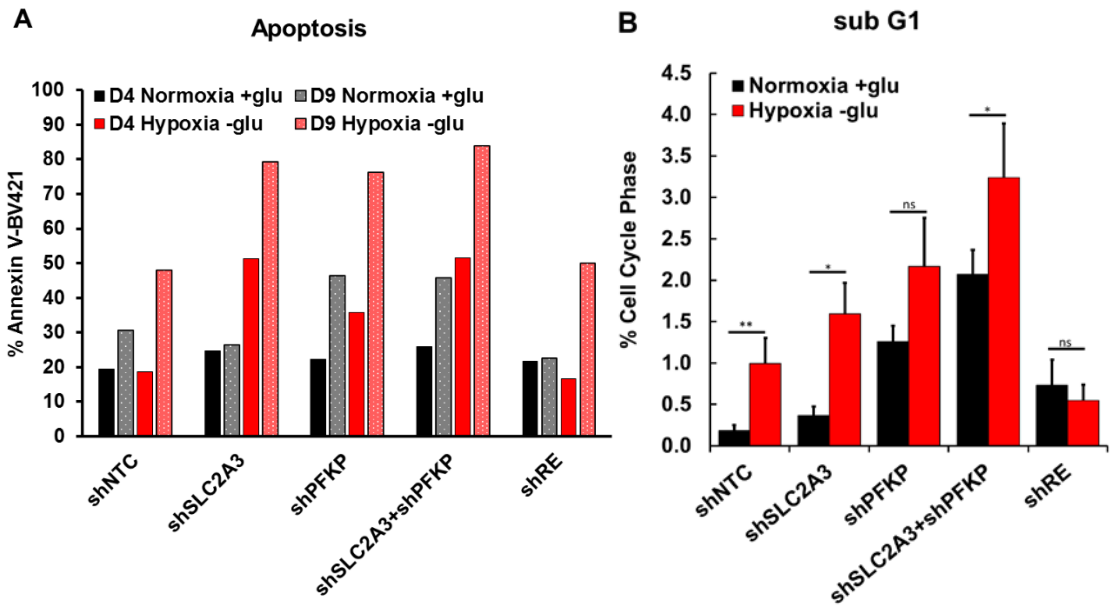

Figure 4-11: Fractions of Annexin V positive cells in Kasumi-1 cells treated with shRNA. Cells were lentivirally transduced with shRNA targeting *SLC2A3, PFKP* and *RUNX1/ETO* and cultured in limited oxygen and glucose content. A) Cells were stained with Annexin V for detection of apoptosis body (n=1). B) Cells were fixed in 4% PFA, stained with DAPI and analysed with flow cytometry. Significance was evaluated using students t-test, ns: not significant, p*≤0.05, **p<0.01. Error bar represents standard deviation (n=3, independent experiments).

4.3.10 *CCND1 and CCND2 genes were affected in SLC2A3 knockdown cells*

Knockdown of *SLC3A3* and *PFKP* in limited glucose and oxygen condition resulted in a lower proportion of cells in G2/M phase. As shown in the previous chapter (Figure 3-17), knockdown of *SLC2A3* reduced glucose uptake in both normoxia and hypoxia conditions. Further, studies have shown that glucose and hypoxia are inter-related with expressions of some cell cycle genes. For instance, Stamateris et al. (2016) demonstrated that low glucose rendered the expression of *CCND2. CCND2* was also downregulated in hypoxia in MYC-dependent manner (Keith et al., 2011). This gene was shown to be a crucial transmitter in RUNX1/ETO-leukaemia propagation (Martinez-Soria et al., 2018). Based on the abovementioned evidences, I wondered if downregulations of *SLC2A3* and *PFKP* have any effects on the expressions of this

gene. RNA analyses were performed on shRNA-transduced cells harvested on day 10 post-transduction.

Figure 4-12 showed the expression level of cell cycle-related genes in Kasumi-1 cells in normoxia standard condition (N +glu) and hypoxia limited glucose condition (H -glu). In line with our previous findings (Martinez-Soria et al., 2018), *RUNX1/ETO*-knockdown caused 60% and 80% reductions in both *CCND2* and *CCND1* transcript levels in both normoxia +glu and hypoxia –glu conditions, with hypoxia – glu condition had a slightly greater effect. However, *CCND3* levels increased upon depletion of *RUNX1/ETO. RUNX1/ETO* knockdown caused the *CCND3* expression level to increase by two-fold in normoxia +glu and 3.5-fold in hypoxia –glu condition.

In *SLC2A3* knockdown cells, *CCND2* mRNA levels reduced to approximately 60% in both normoxia +glu and hypoxia -glu respectively. While *PFKP* knockdown has greater effect on the survival of the cells (Figure 4-6 & Figure 4-7), it caused only 30% reductions in *CCND2* mRNA levels in both conditions. *CCND1* mRNA expression level was down to 60% in normoxia +glu condition; however, it was slightly lower in hypoxia –glu condition. In the case of *SLC2A3* and *PFKP* double knockdown, transcript levels of *CCND2* and *CCND1* were down to 40% and 20% respectively, mimicking the expression levels in *RUNX1/ETO* knockdown cells. Furthermore, neither single nor double knockdowns of *SLC2A3* and *PFKP* reduced the expression levels of *CCND3* mRNA.

Taken together, knockdown of *SLC2A3* and *PFKP* reduced the mRNA levels of *CCND1* and *CCND2*. However, hypoxia and limitation of glucose did not cause any differential expressions on the three cyclin-D genes. Hypoxia and glucose limitation only showed to have an impact on *CCND3* expression in *RUNX1/ETO* knockdown cells.

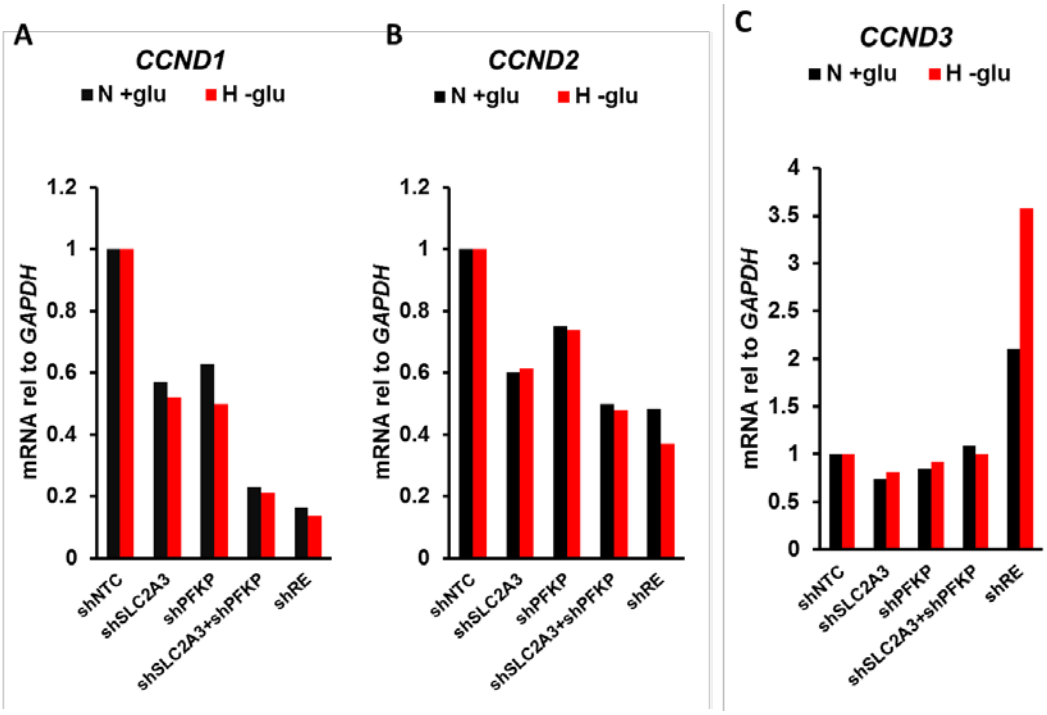

Figure 4-12: Cell cycle-related gene upon shRNA-mediated knockdown.
Kasumi-1 cells were lentivirally transduced with shRNA targeting *SLC2A3, PFKP* and *RUNX1/ETO* and cultured in limited oxygen and glucose content. Cells were harvested on day 8 post-transduction and extracted for RNA analysis. N +glu: Normoxia high glucose, H -glu: Hypoxia low glucose (n=1).

4.3.11 *SLC2A3 and PFKP as the determinant factor in RUNX1/ETO glycolytic function in vitro*

As previously shown, RUNX1/ETO-leukaemia cells increased glucose uptake through *SLC2A3* (section 3.3.3.4). I questioned if it also regulates cell glycolytic functions through a *SLC2A3*-dependent manner. I next performed Seahorse Glycolytic Stress Assay to measure changes in extracellular acidification as an indicator of glycolytic flux. The basis of this assay is the conversion of glucose to lactate in glycolysis pathway that is transported out from the cell and resulted in increased acidity in the extracellular medium. The instrument directly measures the acidification rate and reports this as extracellular acidification rate (ECAR). Figure 4-13 illustrates the sequential compound injections resulting in changes in glycolytic profiles. In this assay, glucose-induced response is reported as rate of glycolysis. The second injection is oligomycin, an ATP synthase inhibitor. This compound inhibits mitochondrial ATP production, shifts the energy production to glycolysis and increases ECAR as maximum glycolytic capacity. The final injection is acute injection of 2-deoxyglucose (2DG), a glucose analogue that inhibits glycolysis pathway resulting in decrease of ECAR. Kasumi-1 cells were lentivirally transduced and harvested on day 4 post-transduction. A total of 2.0 x 10^5 cells was prepared in glucose-free Seahorse XF Base media and plated on pre-coated Seahorse 96-well plate with CellTak Adhesive. Seahorse XF Base media is free of bicarbonate to prevent changes of pH in the media due to cells respiration during plate preparation. The plate was placed in Seahorse XFe96 Analyzer located in Flow Cytometry Core Facility in Medical School. Results were captured and analysed with Seahorse Wave Software.

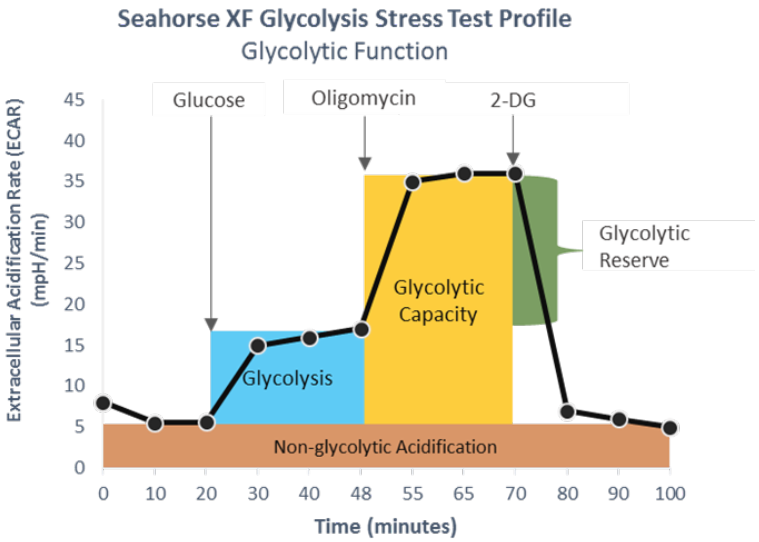

Figure 4-13: Seahorse Glycolysis Stress Test. Sequential injections of glucose, oligomycin and 2DG results in changes in glycolytic profiles. Modified from Agilent Technologies.

Figure 4-14-A revealed glycolytic functions of t(8;21) leukaemia were impaired upon shRNA knockdown on the target genes when compared to the control. Control cells (shNTC) increased glycolysis function after injection of glucose and the rate rose minimally upon inhibition of the oxidative phosphorylation (OXPHOS) pathway leaving 30% of glycolytic reserve after 2DG injection. This indicates glucose is indeed metabolised mainly through glycolysis pathway rather than OXPHOS confirming that this cell line relied more on the least efficient energy production. Besides that, knockdown of RUNX1/ETO completely diminished the glycolytic phenotypes showing that it is undoubtedly the master regulator of glycolysis in t(8;21) leukaemia.

Next, knockdown of *SLC2A3, PFKP* and both genes reduced glycolytic function to nearly 30% lower than shNTC-expressing cells (Figure 4-14-B). Interestingly, oligomycin injection caused glycolytic capacity to reduce by half in both *SLC2A3* and *PFKP* knockdown cells when compared to the control (Figure 4-14-C). Whereas, double knockdown reduced ECAR rate to 30% when compared to the control. Notably, inhibition of OXPHOS neither induced major surge in glycolysis nor glycolytic capacity in these knockdown samples indicating that *SLC2A3* and *PFKP* are undeniably crucial in regulating glycolysis in these cells (Figure 4-14-B/C/D).

Collectively, RUNX1/ETO leukaemia controls glycolysis through *SLC2A3* as well as *PFKP.* Knockdown on these genes impaired glycolytic functions mimicking *RUNX1/ETO* knockdown indicating the roles of *SLC2A3* and *PFKP* in maintaining glycolysis in this subtype of leukaemia.

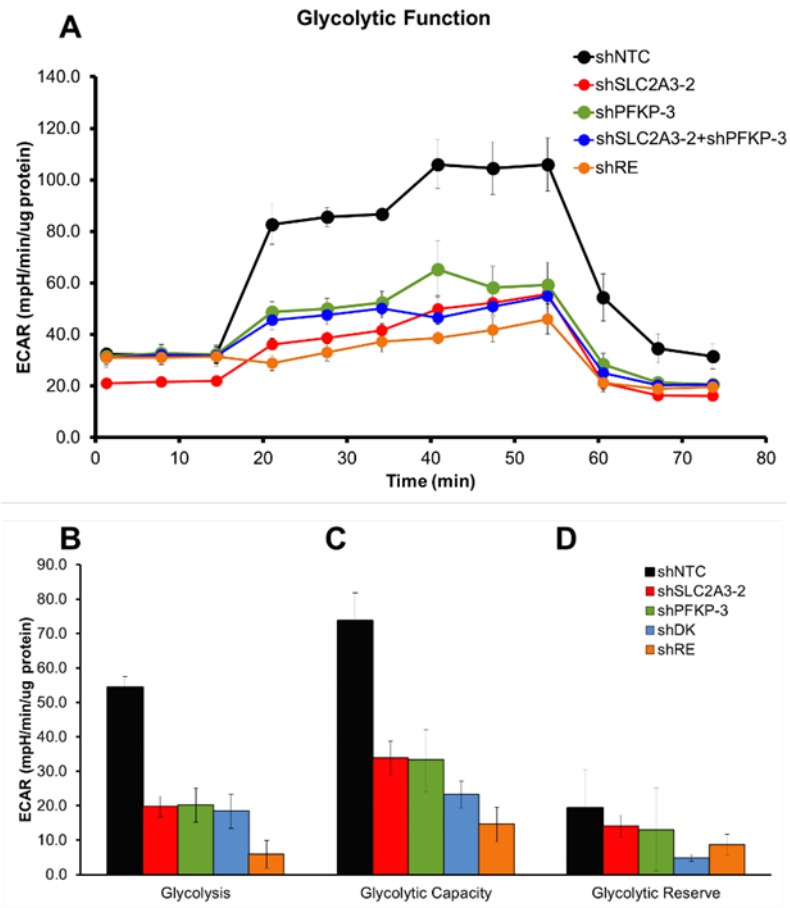

Figure 4-14: Extracellular acidification of *SLC2A3, PFKP* and *RUNX1/ETO*. Cells were lentivirally transduced with shRNA targeting *SLC2A3, PFKP* and *RUNX1/ETO* and plated in Seahorse 96-well plate. Glucose, oligomycin and 2DG were used for acute injection and ECAR readings were normalised to protein concentration (n=3).

4.4 Summary

This chapter characterised the *in vitro* functions of *SLC2A3* and *PFKP* as required partner genes of RUNX1/ETO, as well as the controller of glycolysis in this subtype of leukaemia. Firstly, nutrient deprivation conditions had the biggest impact on Kasumi-1 cells proliferation. Hypoxia was observed to significantly reduce the cell number in standard condition media, but did not have any influence when in combination with nutrient deprivation conditions.

Depletion of *RUNX1/ETO* completely diminished the propagation and survival of leukaemic cells regardless of nutrient and oxygen limitations in both of the cell lines. The deflated populations associated with an increase in cell cycle arrests, lower expression of cell cycle-related genes and reduced self-renewal capacity. However, an interesting finding was observed in higher proportion of apoptotic cells in restricted glucose and oxygen condition, whereas this was not observed in standard condition. Nonetheless, knockdown of RUNX1/ETO completely diminished glycolytic phenotypes proving that it is indeed the master regulator of glycolysis.

SLC2A3 required glucose for proliferation and self-renewal ability and limitation of oxygen increased the dependency. Depletion of *SLC2A3* alone is not enough to cause cell cycle arrest; but, glucose and oxygen restriction led to a higher G0/G1 phase. Even though *CCND2* and *CCND1* expressions were reduced in the knockdown cells, interestingly, there were no differences in both of the settings. Instead, the reduced propagation of *SLC2A3* knockdown cells in restricted glucose condition was more related to the increase in apoptosis induction and associated with the increased of sub G1 populations. *PFKP;* however, showed to be crucial in all culture conditions. Loss of *PFKP* caused cell cycle arrests and increase of apoptotic cells. Besides, depletion of both *SLC2A3* and *PFKP* abrogated leukaemic cells in all culture conditions, which was associated with higher number of cells in G0/G1, increased number of apoptotic cells as well as reduced levels of mRNA expression of cell cycle-related genes. In Seahorse glycolytic stress assay, knockdown of *SLC2A3, PFKP* or double knockdown of both genes simultaneously abrogated glycolytic functions showing that these genes are indeed required to drive glycolysis in RUNX1/ETO-leukaemia.

Chapter 5 : Efficacy of small molecule inhibitor in RUNX1/ETO-positive leukaemia

5.1 Introduction

Chromosomal rearrangement leading to t(8;21) leukaemia fuses *RUNX1* to *ETO* and generates the aberrant transcriptional regulator, RUNX1/ETO. Current treatments involve intensive and genotoxic chemotherapy, which can reduce patients' quality of life and long-term remissions (de Rooij et al., 2015). Previous work has identified pathways that were affected by this oncogenic transcription factor such as cell cycle, MTOR and MYC-signalling (Martinez-Soria et al., 2018).

Gene signatures associated with glycolysis were identified as enriched in RUNX1/ETO-positive cells (Martinez-Soria et al., 2018). *RUNX1/ETO* knockdown led to the dysregulation of genes within the glycolysis pathway, as shown in GSEA analysis (Figure 5-1). Studies have shown that cancer cells rely heavily on glycolysis even in the presence of oxygen (Warburg, 1956a). Consequently, the extracellular lactate level increases making the environment more acidic and favourable for cancer growth (Sonveaux et al., 2008). For instance, higher extracellular acidification levels was shown in Burkitt lymphoma cell line that promotes cell growth (Noble et al., 2017).

Furthermore, it has been demonstrated that RUNX1/ETO promotes disease progression through direct regulation of *CCND2*, a gene involved in the cell cycle progression (Martinez-Soria et al., 2018). Inhibition of the cell cycle machinery by palbociclib (Fidler et al.) leads to a promising therapeutic intervention in AML cells with the t(8;21) fusion (Martinez-Soria et al., 2018). Palbociclib inhibits CDK4/6 binding to CCND2, thus reducing phosphorylation of Rb1. This prevents progression of cells from G1 to S phase, and results in the cell cycle arrest (Finn et al., 2009). Palbociclib has been successfully combined with the hormonal therapy letrozole in estrogen-receptor (ER)-positive human advanced breast cancer, and significantly increased progression-free survival by nearly two-fold (24.8 months in palbociclib+letrozole vs 14.5 months in placebo-letrozole group; both with 95% confidence interval) (Finn et al., 2016, Finn et al., 2009). This makes this drug a compelling candidate as a potential curative strategy in RUNX1/ETO- positive AML.

5.2 Aims

The aims of this chapter are:

i- to evaluate the efficacy of small molecule inhibitors targeting the glycolysis pathway, and potential combination with a cell cycle inhibitor.

ii- to investigate the potential mechanism by which palbociclib-treated cells shunt its metabolic pathway.

5.3 Results

5.3.1 *Glycolysis pathway is severely affected in the absence of RUNX1/ETO*

Gene set enrichment analysis (GSEA, Broad Institute) was used to analyse changes in the glycolysis pathway, by comparing experimental gene sets against hallmark gene-set signatures (Subramanian et al., 2005). In this analysis, two sets of RNA sequencing data were used; *RUNX1/ETO* knockdown in Kasumi-1 cells by siRNA (siRE) and mismatch-control (Pui et al.) (Figure 5-1). The x-axis ranks the most up-regulated genes (left end) to the most down-regulated genes (right end). The y-axis indicates enrichment score (ES), which increases when genes are encountered in the pathway and decreases vice-versa leading to an assessment of the distribution within the set of all genes in a particular pathway. The enrichment score indicates to what degree a gene set is over-represented at either the top or bottom of the list. Genes with higher expression in siMM-cells have higher ES and are ranked on the left side of the graph, whereas the lower expression in siRE treated cells have lower ES and are plotted on the right section of the graph. The bottom part of the plot indicates the value of the ranking metric moving down the list of ranked genes. In the Kasumi-1 cell line, GSEA analysis suggests that the glycolysis pathway is significantly affected in siRE-treated cells (FDR $q=<10^{-3}$).

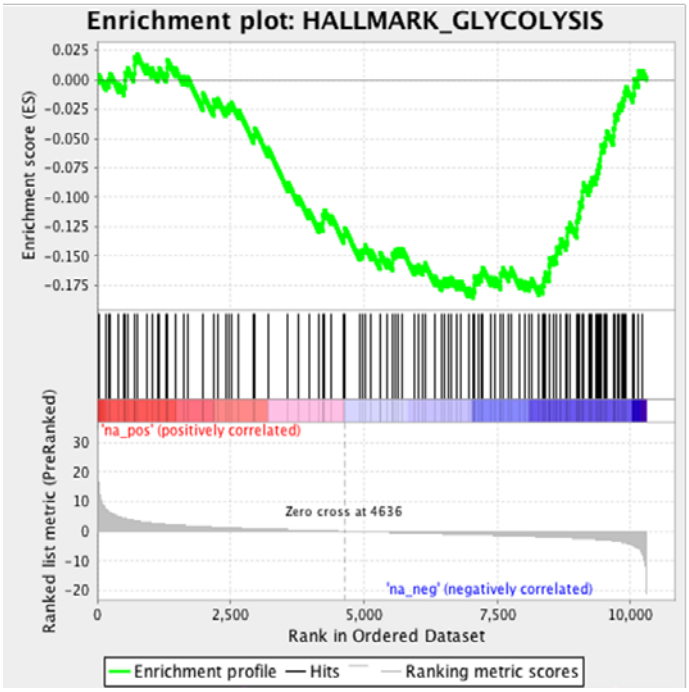

FDR q value		0.0006270	
Normalised ES score		-2.5382364	
GENE SYMBOL	RANK IN GENE LIST	RANK METRIC	RUNNING ES
PAM	9217	-2.5409	-0.0906
NASP	9257	-2.5848	-0.0872
TPI1	9291	-2.6222	-0.0832
GNE	9352	-2.7075	-0.0818
PGAM1	9377	-2.7454	-0.0769
HMMR	9407	-2.7943	-0.0725
CD44	9429	-2.8181	-0.0674
CYB5A	9446	-2.8453	-0.0617
null	9452	-2.8521	-0.0549
IDH1	9521	-2.9598	-0.0544
HS2ST1	9547	-2.9904	-0.0496
ME2	9557	-3.0048	-0.0432
null	9679	-3.2064	-0.0479
ALDOA	9685	-3.2185	-0.0411
ENO1	9703	-3.2480	-0.0355
HK2	9715	-3.2818	-0.0294
HOMER1	9763	-3.3885	-0.0267
DDIT4	9785	-3.4341	-0.0216
PGK1	9835	-3.6312	-0.0191
PFKP	9875	-3.7808	-0.0157
null	9893	-3.8610	-0.0101
DEPDC1	9927	-4.0069	-0.0061
LDHA	10059	-4.7997	-0.0118
null	10077	-4.9890	-0.0062
PYGB	10082	-5.0277	0.0007
STC2	10150	-5.6923	0.0013
ENO2	10162	-5.7968	0.0075
PLOD2	10235	-7.6797	0.0077

Figure 5-1: GSEA plot of hallmark glycolysis pathway in siMM versus siRE. Genes in hallmark glycolysis pathway showed significant impairment in siRE versus siMM (FDR Q value = 0.0006). Top section of the figure plots the enrichment score for each gene, and the bottom section indicates the value of the ranking metric moving down the list of ranked genes. Analysis was carried out using Broad Institute software by comparing the experimental gene sets against hallmark gene signature. FDR, false discovery rate; ES, enrichment score.

As described in chapter 3 and 4, shRNA-mediated knockdown targeting *SLC2A3* and *PFKP* showed variable effects in Kasumi-1 progression *in vitro* and *in vivo,* particularly in *SLC2A3* knockdown cells. However, the GSEA analyses clearly indicate the glycolysis pathway was affected upon loss of *RUNX1/ETO*. *In vivo* experiments showed that depletion of *SLC2A3* alone may not be sufficient for leukaemia propagation (chapter 3). Furthermore, targeting the axis of glycolysis via *PFKP* could be pursued as a novel approach to tackling RUNX1/ETO-leukaemia. Based on sections 3.4.5, although the experiment has to be repeated due to the issue with engraftment, *PFKP* knockdown completely diminished leukaemic burden in both mouse models (chapter 3).

Thus, the question arises as to whether there is value to targeting the whole glycolysis pathway using glycolysis antagonist. Of the many glucose analogues which have been studied, 2-deoxyglucose (2DG) has best been demonstrated to

effectively inhibit glucose metabolism and cancer propagation (Aft et al., 2002, Zhong et al., 2009, Goldberg et al., 2012). This molecule is a structural derivative of glucose ($C_6H_{12}O_6$) which has hydrogen replaces for hydroxyl at the second carbon atom ($C_6H_{12}O_5$) (Figure 5-2-A). Upon intake into the cells, 2DG can be phosphorylated by hexokinase at 6-carbon to become 2-deoxyglucose-phosphate (2DG-P). 2DG-P is unable to undergo further reactions as the hydrogen at 2-carbon blocks isomerase from converting 2DG-P to fructose-6-phosphate (Figure 5-2) (Nelson et al., 1996, Aft et al., 2002). This cause a halt in the glycolysis pathway just before the PFKP enzyme (Aft et al., 2002); thereby reducing the intracellular ATP levels (Cheng et al., 2012). Consequently, cancer cells cease growth (Jeon et al., 2015) and 2DG mediates the cells to undergo apoptosis (Aft et al., 2002, Saleem et al., 2012, Luo et al., 2018).

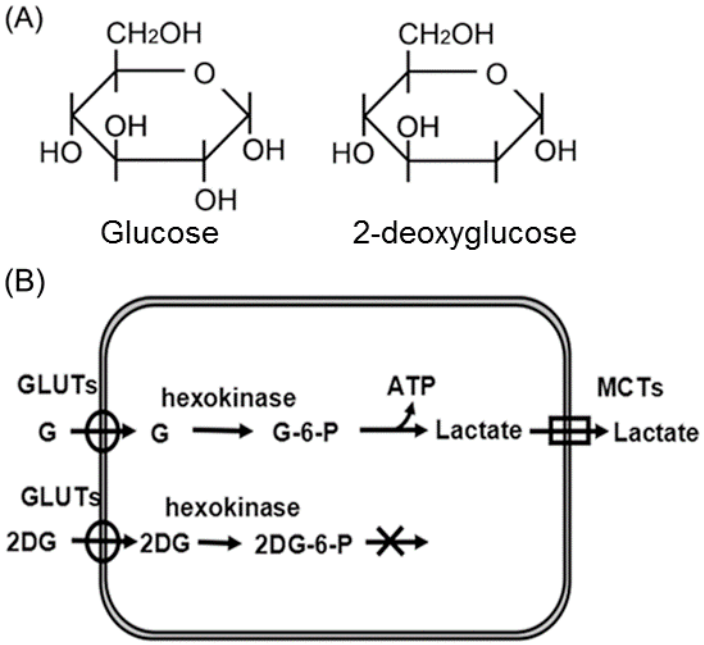

Figure 5-2: 2DG structure and mechanism of action. A) Structural comparison between naturally occurring glucose and 2DG. 2DG replaces hydroxyl with hydrogen at the second carbon. Empty lines indicate hydrogen molecule. B) 2DG mechanism of action. 2DG enters the cell through the glucose transporter and is phosphorylated by hexokinase. Due to low levels of intracellular phosphatase, 2-DG-PO_4 is trapped in the cell. 2-DG-PO_4 is unable to undergo further metabolism. High intracellular levels of 2-DG-6-PO_4 cause allosteric and competitive inhibition of hexokinase. This results in the inhibition of glucose metabolism. Adapted and modified from Zhang et al. (2016).

5.3.2 *RUNX1/ETO-positive cells exhibit increased dependency on glycolysis compared with other AML cell lines*

To assess 2DG efficacy on the proliferation of RUNX1/ETO cells, a panel of AML cell lines including RUNX1/ETO-positive cells were treated with a concentration ranging from 1 µM to 10 mM. Although, these concentrations were considered pretty high for a small molecule inhibitor, 2DG has been classically used at even higher concentrations (Jeon et al., 2015, Yamaguchi et al., 2011, Zagorodna et al., 2011). Another reason for this was to mimic the physiological concentration of glucose in the culture media which was 11 mM.

Briefly, the cells were seeded at $5x10^5$/ml and treated with 2DG in triplicate in 96-well plates. The viability of the cells was assessed using WST-1 assay and the absorbance reading was captured at 450 nm in FLUOstar Omega plate reader. WST-1 assay involves cleavage of stable tetrazolium salt WST-1 to a soluble coloured formazan which is released into the media. The absorbance readings were analysed using GraphPad PRISM to produce a dose-response curve and determine the GI50 of 2DG for each cell line. The curve was presented as log [inhibitor] vs response that fit a non-linear regression model, assuming a Hill slope of -1.0.

Figure 5-3 indicates 2DG inhibited the growth of all AML cell lines in a dose-dependent manner. Notably, both RUNX1/ETO positive cell lines (SKNO-1 and Kasumi-1) displayed greater sensitivity to the inhibitor when compared to other AML cell lines. The dose that caused 50% inhibition of proliferation (GI_{50})was 60 µM and 200 µM for SKNO-1 and Kasumi-1 respectively. Further, the maximum inhibitory concentrations for both RUNX1/ETO positive cells were three-fold lower than other AML cell lines (Table 5-1).

The dose for Kasumi-1 is relatively high; however, it is still below the maximum concentration (C_{max}) of 700 µM of the highest dose level used in clinical trials focusing on advanced and drug-resistant adult tumours (Stein et al., 2010, Raez et al., 2013). The finding of Kasumi-1 as being more sensitive to 2DG compared with other AML cell lines was also described previously (Miwa et al., 2008). Although the

concentration reported in their study was 5-fold higher than our finding, it was due to the earlier timepoint they captured in their assay. Notably, Miwa et al. (2008) also showed that Kasumi-1 cell line is resistant to oxidative phosphorylation inhibition by oligomycin, a potent inhibitor for mitochondria activity.

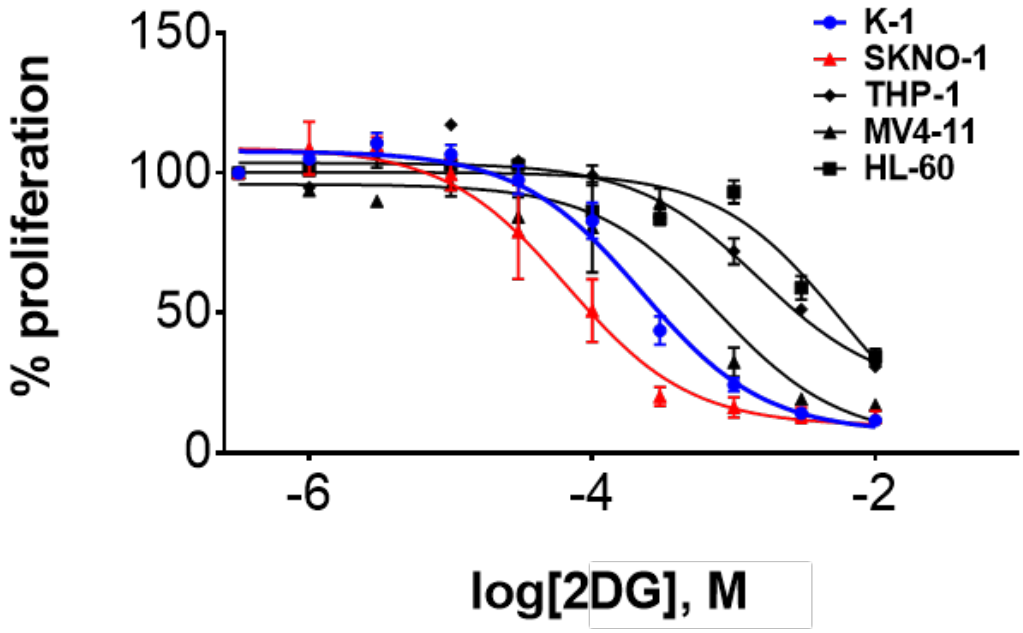

Figure 5-3: Dose-response curve of 2-deoxyglucose across a panel of AML cell lines. GI_{50} of 2DG across AML cell lines was determined using the WST-1 assay at 72-hours post-treatment. Absorbance readings were captured using FLUOstar Omega plate reader at 450 nm and analysed using PRISM to generate log (concentration) vs response curve (n=4).

Cell line	Maximum effect (mM)
SKNO-1	3
Kasumi-1	3
THP-1	10
MV4-11	Not determined
HL-60	Not determined

Table 5-1: 2DG maximum effect on AML cell lines. Maximum inhibitory effect was determined at the highest concentration that caused the maximum inhibition.

To further investigate the effect of 2DG on cell proliferation, three drug concentrations of 0.5, 1 and 2 times of GI_{50} were administered to both RUNX1/ETO positive cell lines. Kasumi-1 cell line was treated with 100 µM ($0.5XGI_{50}$), 200 µM ($1XGI_{50}$) and 400 µM ($2XGI_{50}$), while SKNO-1 was treated with 30 µM ($0.5XGI_{50}$), 60 µM ($1XGI_{50}$) and 120 µM ($2XGI_{50}$). The cells were counted 72 hours after treatment using the standard trypan blue exclusion method. As indicated in Figure 5-4, 2DG treatment reduced Kasumi-1 cell count as compared to the vehicle control. At $1XGI_{50}$ and $2XGI_{50}$ dose, the proliferation of Kasumi-1 cells was severely impaired by almost half. A sub-lethal dose ($0.5XGI_{50}$) of 2DG however, caused only a slight reduction of the cell numbers compared to the vehicle control at the 72 hour timepoint. For SKNO-1, $1XGI_{50}$ dose halved the number of cells when compared to the control, while $2XGI_{50}$ caused a massive 10-fold reduction of viable cells as shown in Figure 5-4.

Taken together, RUNX1/ETO-positive cell lines showed to be more sensitive to 2DG as compared to other AML cell lines and that resulted in reduced cell number in both of the cell lines.

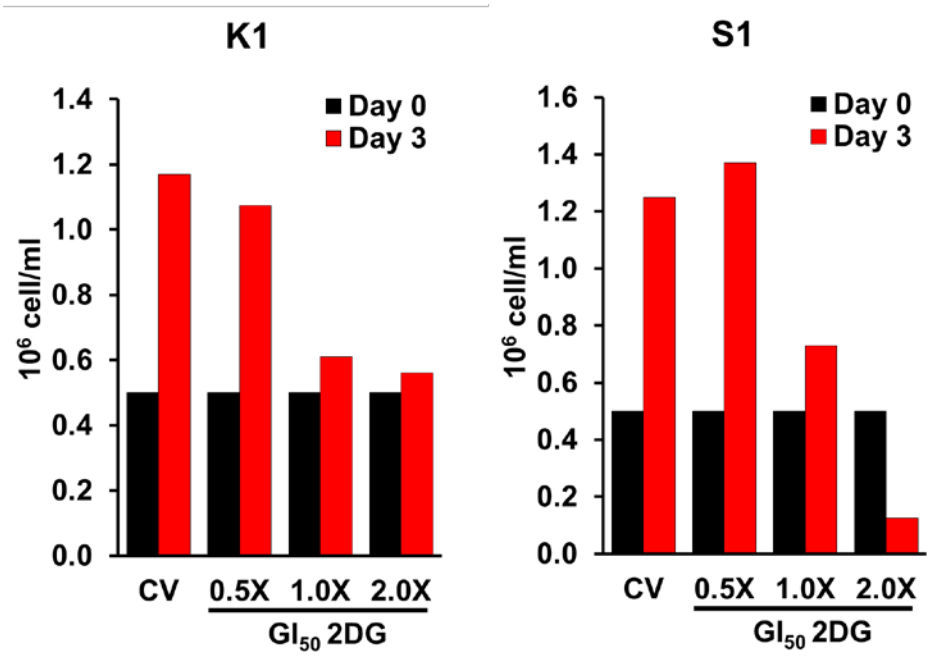

Figure 5-4:2DG treatment inhibited cell proliferation in Kasumi-1 and SKNO-1 cell lines. Cells were treated with 0.5, 1 and 2 times of 2DG GI_{50} for 72 hours and counted according to trypan blue cell count method. Bar graph showing decreased cell number of viable cells in 2DG treated cells compared to the vehicle control. (Kasumi-1, n=2; SKNO-1, n=1).

5.3.2.1 Combination of 2DG with novel cell cycle inhibitor additively impairs leukaemia propagation

Although reports have shown that 2DG is an effective agent to hamper cancer cell proliferation *in vitro*, *in vivo* studies using 2DG as a single agent have been disappointing. For instance, 2DG treatment alone did not reduce tumour burden in a xenograft of a pancreatic tumour model (Goldberg et al., 2012). However, when it is combined with another inhibitor (Ras inhibitor S-*trans-trans* farnesylthiosalicylic acid), 2DG synergistically inhibited *in vivo* tumour growth with no toxic side effects observed in the animals (Goldberg et al., 2012). Furthermore, the combination treatment exhibited strong and significant apoptotic cell death when compared with single agents used in the study.

A recent *in vitro* study has shown that 2DG and palbociclib combination synergistically inhibits acute lymphoblastic leukaemia cell line after 48-hour treatment and a more pronounced effect was observed after 72-hour treatment (Zhelev et al., 2015). This has led to the question whether the combination of 2DG and palbociclib would lead to the same observation in RUNX1/ETO-leukaemia. I then sought to answer this question by testing it on RUNX1/ETO cell line *in vitro*. The GI_{50} dose of palbociclib for both Kasumi-1 and SKNO-1 was established between 20-100 nM respectively (Figure 5-5) (Martinez-Soria et al., 2018).

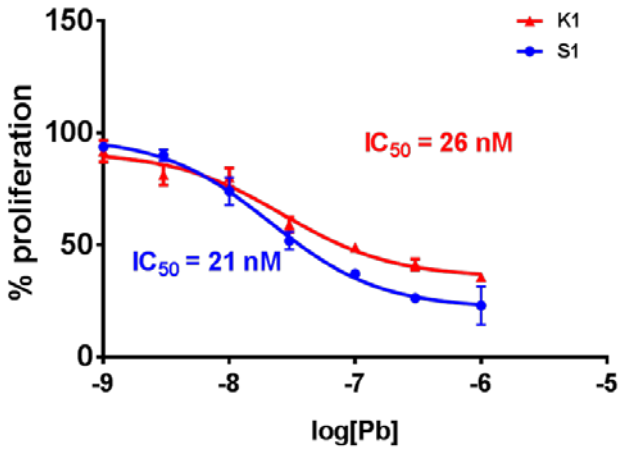

Figure 5-5: Dose-response curve of palbociclib in RUNX1/ETO-positive cell lines. 1XGI_{50} of palbociclib in RUNX1/ETO-positive cell lines was determined using luciferase assay at 72-hour time point. Luminescence was captured using FLUOstar

Omega plate reader and analysed using PRISM to generate log (concentration) vs response curve (n=3).

I then selected a range between GI_{50} concentrations for Kasumi-1 cells for drug combination study which were 100 µM and 60 nM for 2DG and palbociclib respectively. Kasumi-1 cells expressing the luciferin gene were treated with a fixed 1:2 molar ratio of the GI_{50} value of each drug and combination (Chou, 2010, Chou and Talalay, 1984).

Figure 5-6 depicts the curve shift for each drug combinations analysed in PRISM Software. Due to different molarity of 2DG and palbociclib concentrations, graphs were transformed to two dose-response curves. Reading values for untreated and lowest effect were normalised to 100% and 0% respectively, and non-linear regression was applied to fit the curve. Chou-Talalay addresses the concentration that cause inhibition as effective concentration (EC), instead of GI.

2DG combination with palbociclib resulted in lower EC_{50} values when compared with single drug treatment. Single 2DG and combination with palbociclib treatment in Kasumi-1 recorded as 187 µM and 100 µM EC_{50} value. While combination of palbociclib with 2DG halved the palbociclib EC_{50} value from 68 nM to 35 nM. Combination of 2DG and palbociclib at ED_{50} resulted in a 1.04 CI value, indicating an additive value of these two drugs.

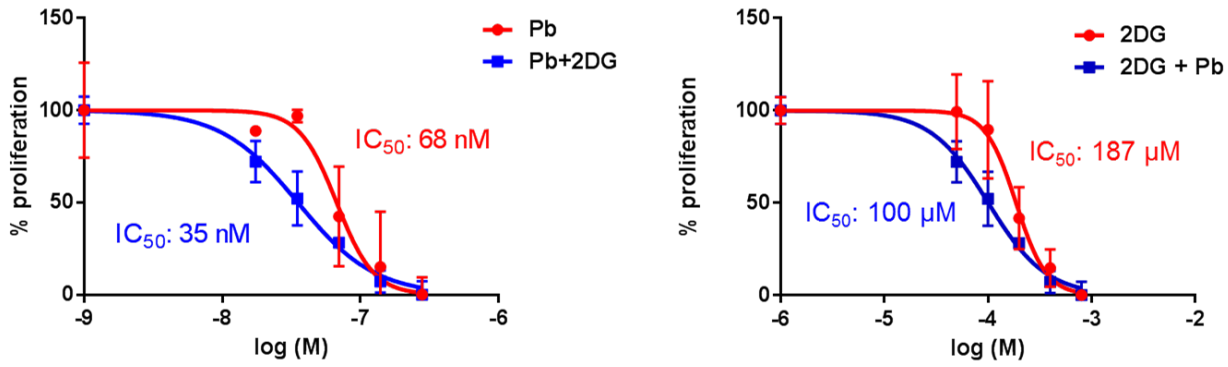

Figure 5-6: Dose-response curve for 2DG and palbociclib combinations in Kasumi-1 cell line. Kasumi-1 cells were treated with a fixed range of concentrations of 2DG and palbociclib for 72-hours. Viability was assessed by luciferase assay using FLUOstar Omega plate reader. Reading values were analysed using PRISM to generate log (concentration) vs response curve. Error bar represents SD (n=3).

5.3.2.2 Apoptosis predominantly caused by hindrance in glycolysis pathway but minimally related with cell cycle inhibition in Kasumi-1 cells

Treatment of Kasumi-1 cell line with 2DG impaired cell proliferation as depicted by low cell counts after 72 hours 2DG treatment (Figure 5-4). However, the counts did not discriminate dead cells as the indication for cytotoxicity. Next, I pursued to check the effect of 2DG treatment on the induction of apoptosis process with the application of FITC-Annexin V-propidium iodide (PI) apoptosis assay. As described earlier, Annexin V binds to the cells with exposed PS, whereas PI is the nuclear and chromosomal staining agent, thus, enables the identification of different phase of the cell death. Cells were harvested 72 hours after treatment with 2DG and incubated with FITC Annexin V and PI solution in Ca2+-containing buffer. The fluorescents were captured using FACS Canto and analysed using FlowJo software.

Figure 5-7 shows quadrants plots that represents phases of cell death. Quadrant Q4 represents viable cells (-FITC Annexin V/-PI), while quadrant Q3 represents early apoptosis (+FITC Annexin V/-PI). Quadrant Q2 and Q1 indicate late apoptosis (+FITC Annexin V/+PI) and already dead/necrotic cells (-FITC Annexin V/+PI) respectively. The percentage of cells present in both, early and late phase of apoptosis, in response to the vehicle control was set to 100%, and percentage obtained for treated cells were normalised to these control values.

A sub-lethal dose of 2DG (100 µM) did not cause any significant increase of early or late apoptosis in the Kasumi-1 cell line (Figure 5-8). However, a 1XGI_{50} dose of 2DG caused a statistically significant two-fold increase of both early apoptosis and late apoptosis stages of cell death when compared to the vehicle control. A slightly more potent effect was observed in 2XGI_{50} of 2DG, where number of cells in both early and late apoptosis increased 2.3-fold. On the contrary, palbociclib single treatment hardly affected cell death with Annexin V staining indicating 10-30% reductions at different GI_{50} ratios. Cells treated with a sub-lethal dose of 2DG and palbociclib recorded 1.3-fold higher apoptosis in the Kasumi-1 cells. Finally, combination of palbociclib with 2DG showed similar rates of apoptosis as 2DG alone.

Taken together, 2DG treatment induced a significant increase in the apoptotic bodies in Kasumi-1 cells. On the contrary, palbociclib as cell cycle inhibitor, did not induce apoptosis. Its combination with 2DG slightly increase the percentage of cells in late phase apoptosis; however, this was mainly induced by 2DG.

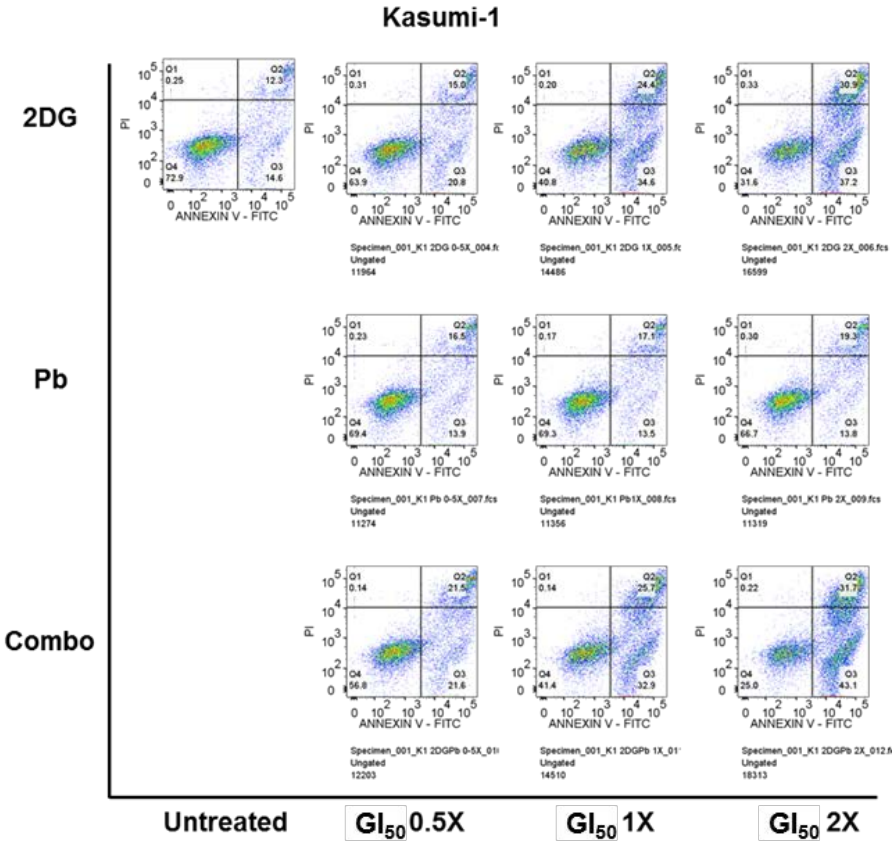

Figure 5-7: Representative of apoptosis assay for Kasumi-1. Upper panel refers to 2DG treated cells, middle panel refers to palbociclib treated cells and bottom panel represents combination treatment. Annexin V and Annexin V+PI percentages of each sample was set normalised to vehicle control that was set to 100%.

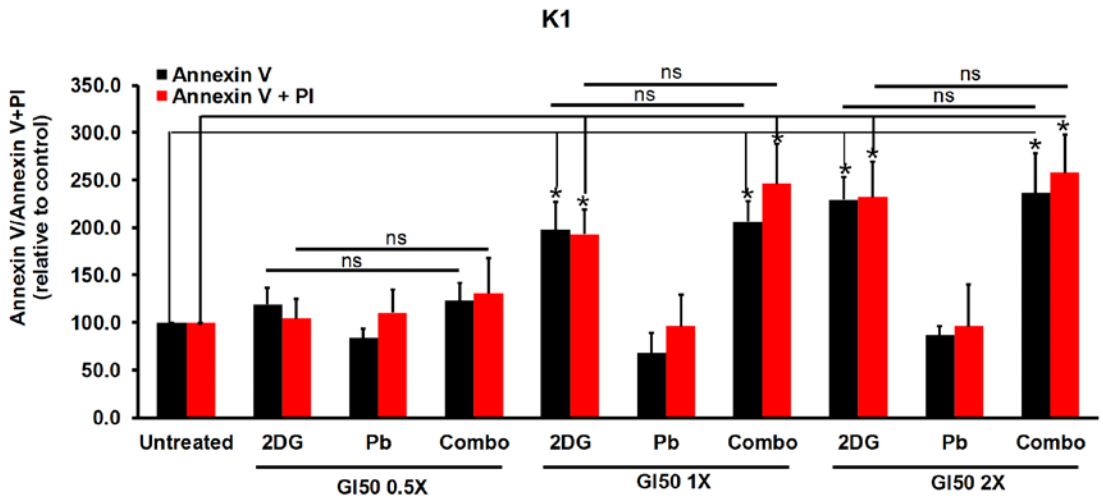

Figure 5-8: 2DG inhibition of glycolysis on the induction of apoptosis in Kasumi-1 after 72 hours treatment. Cells treated with 2DG and vehicle control were incubated with FITC Annexin V and PI to determine the proportion of apoptotic cells. Significance was evaluated using students t-test, ns: not significant, p*≤0.05, **p<0.01. Error bar represents standard deviation (n=3).

5.3.2.3 2DG induces subG1 cells, while palbociclib halts cycling cells; however, both do not contribute to quiescent cells

To investigate whether the increase in apoptosis in Kasumi-1 cells is associated with a cell cycle mechanism, I performed cell-cycle analysis with cells treated with these compounds. Cells were treated with 2DG, Palbociclib or combination at their respective GI_{50} dose for 72 hours and fixed with 2% PFA for DAPI staining. Fluorescence was captured using FACS Canto II and analysed with FlowJo software.

Figure 5-9 (left) shows the cell cycle profile of Kasumi-1 cells treated with 2DG and Palbociclib. 2DG treatment significantly halved the cells entering G2/M phase when compared with 6.2% of untreated control and slightly reduced the percentage of cells in S phase. Both Palbociclib alone and in combination with 2DG significantly reduced the fraction of cells in the S and the G2M phase by three-fold. The concurrent pattern was also observed in G0/G1 phase. While 2DG treatment slightly, but significantly increased the number of cells present in G0/G1 phase, Palbociclib alone and in combination with DG significantly increased the fraction of G0/G1 cells from 80% to 90%.

In agreement with the Annexin V staining, examination of cell cycle distribution also revealed a 2.4-fold increase of subG1 in response to 2DG treatment, while Palbociclib did not cause a substantial change in this cell fraction. However, combination treatment caused a significant 4-fold increase of cells in this phase.

Both 2DG and Palbociclib caused accumulation of cells in G0/G1 phase and I wondered if the cells in this phase have a higher proportion of quiescent cells, which might affect chemosensitivity. To answer this question, I performed live Hoechst 33342/Pyronin Y staining on the treated cells. Hoechst 33342 stains only DNA and Pyronin Y stains both DNA and RNA, thus this method enables the discrimination of RNA content. Briefly, after 72 hours incubation with 2DG and Palbociclib, Kasumi-1 cells were stained with 10 µg/ml Hoechst 33342 for 45 minutes and followed by 100 µg/ml of Pyronin Y for 15 minutes. Cells were immediately analysed with FACS Canto and further analyses were done using FlowJo software.

Figure 5-10 showing Hoechst 33342 and Pyronin Y staining profile for the treated Kasumi-1 cells. The untreated control recorded 14% of cells in the G0 phase, the highest among all other samples. Both 2DG and Palbociclib single treatments significantly reduced the accumulation of cells in this phase by 40%, whereas combination treatment caused a significant reduction of G0 cells by more than 50%.

Taken together, the increase of apoptotic cells after 2DG treatment is associated with a slight increase in G0/G1 cell cycle arrest, as well as a rise of subG1 phase. Furthermore, Palbociclib treatment predominantly halts cells in G0/G1 phase, with minimal increase of subG1 cells. Remarkably, combination treatment of 2DG and Palbociclib increased the subG1 phase and blocked the cell cycle progression at G0/G1 phase, which led to a decreased proportion of cells in the G2/M phase. Moreover, neither single nor combination treatments caused the cells to be in a quiescent state (Figure 5-10).

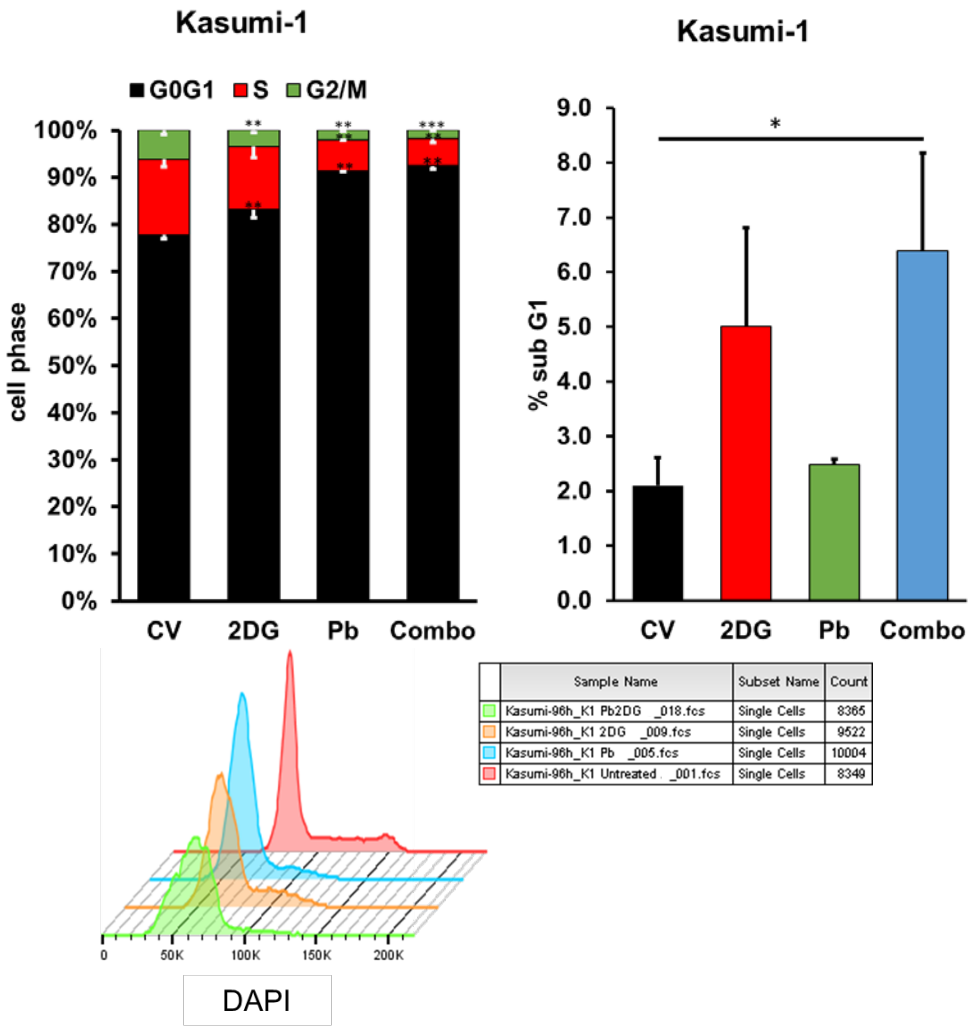

Figure 5-9: Cell cycle profile of Kasumi-1 cells in response to 2DG and Palbociclib treatment. Cells were treated with GI_{50} of 2DG, Palbociclib and combination for 72 hours, fixed with 2% PFA and stained with DAPI. Cells were captured with flow cytometry and analysed with FlowJo software. Significance was evaluated using students t-test, p*≤0.05, **p<0.01. Error bar represents standard deviation (n=3, independent experiments)..

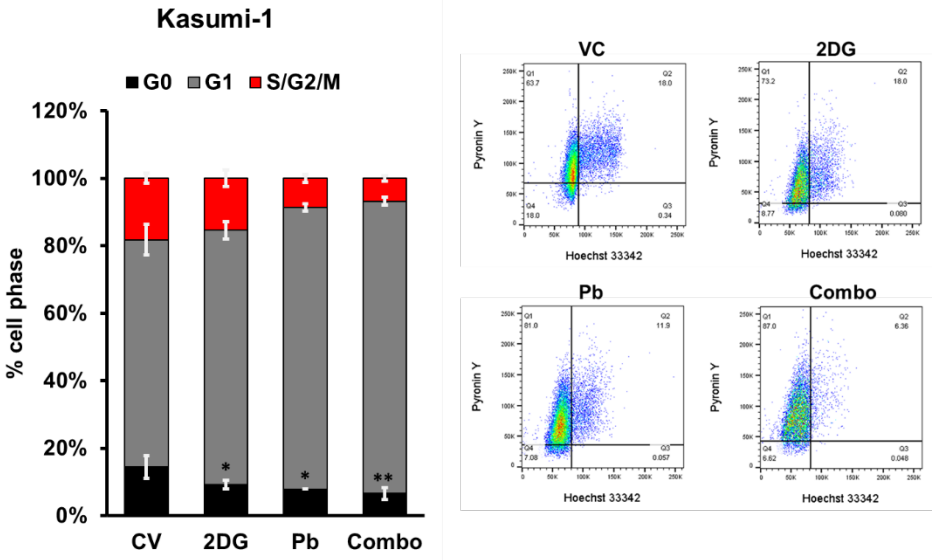

Figure 5-10: Cell cycle distribution indicated by Pyronin Y and Hoechst33342 staining of Kasumi-1 cells. Cells were treated with GI_{50} of 2DG, Palbociclib and combination for 72 hours. Cells were stained with 10 µg/ml Hoechst 33342 and 100 µg/ml Pyronin Y. Cells were captured with flow cytometry and analysed with FlowJo software. Significance was evaluated using students t-test, p*≤0.05, **p<0.01. Error bar represents standard deviation (n=3 independent experiments).

5.3.2.4 Palbociclib treatment impairs glycolysis, but shunts expression of some genes in the pentose phosphate and oxidative phosphorylation pathways

Previous experiments which focusing on combination of 2DG and palbociclib were performed before RNAseq data of palbociclib treated cell was available. RNAseq data showed that there is a substantial overlap of pathways between cells treated with palbociclib and *RUNX1/ETO* knockdown cells. Interestingly, glycolysis pathway was showed to be enriched, as were other pathways such as MTOR and MYC signalling (Figure 5-11) (Martinez-Soria et al., 2018). Further GSEA analysis showed that palbociclib treatment impaired the hallmark set of genes involved in the glycolysis pathway as indicated in Figure 5-12.

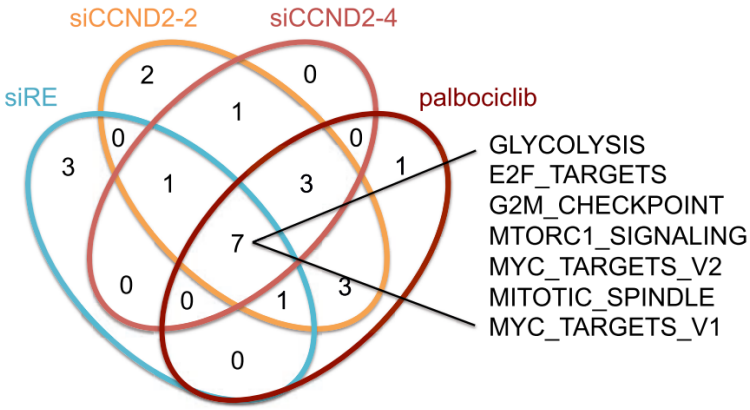

Figure 5-11: Hallmarks of cancer pathways shared between palbociclib treatment, CCND2, and RUNX1/ETO knockdown. Set of pathways that overlapped in RUNX1/ETO knockdown, CCND2 knockdown and palbociclib treatment (Martinez-Soria et al., 2018).

I next sought to check if the glycolysis pathway is affected by palbociclib treatment by performing analysis of mRNA expression levels on set of genes involve in this pathway. This analysis also included Kasumi-1 treated with 2DG and a combination of the two drugs, since these two drugs led to an additive effect as described previously (Figure 5-6); therefore, this combination would lead to a severe impact on the pathway. Kasumi-1 cells were treated with either vehicle control, 200 µM 2DG, 30 nM palbociclib or a combination (combo) of the two drugs for 3 days and harvested for mRNA analysis. Besides genes involved in the glycolysis pathway, this mRNA analysis also included genes in the pentose phosphate pathway (PPP) and oxidative phosphorylation pathway (OXPHOS). Figure 5-13 shows the fold-change of mRNAs involved in these pathways. In general, genes involved in glycolysis were downregulated in 2DG and palbociclib treatments. Combination of 2DG and palbociclib additively reduced the expression of genes in this pathway. There were no apparent changes observed in the PPP pathway except an incremental increase of *PGLS* (1.3-fold) and *PGD* (1.2-fold) levels in palbociclib and combo treated cells respectively. Interestingly, in the OXPHOS pathway, the *PISD* gene was shown to be increased by 1.6-fold in 2DG treated cells, 1.3-fold in palbociclib treated cells and 1.4-fold in the combination treatment.

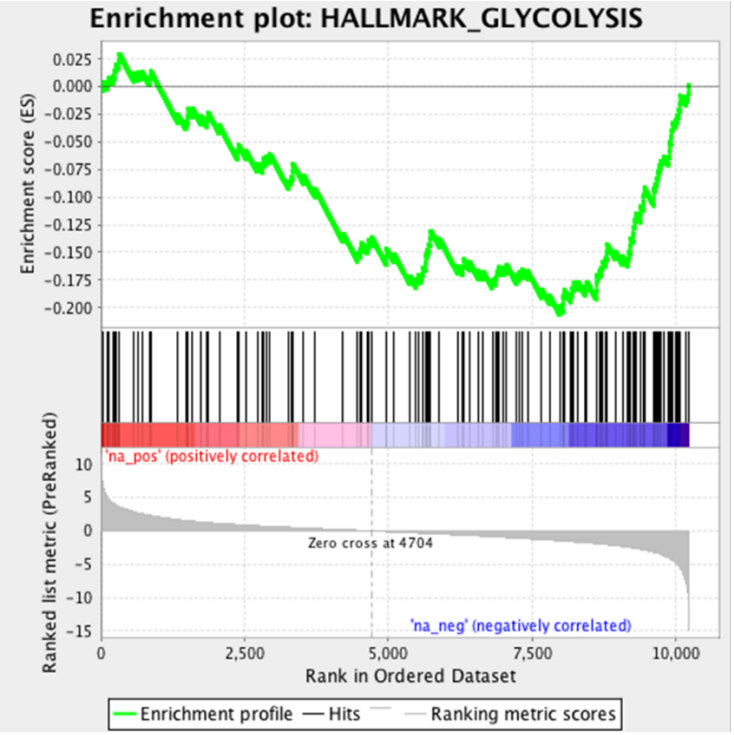

FDR q value	0.0002480
Normalised ES Score	-2.5382364

GENE SYMBOL	RANK IN GENE LIST	RANK METRIC SCORE	RUNNING ES
GALE	9376	-2.742027	-0.114981
GOT2	9387	-2.757779	-0.108396
PSMC4	9425	-2.825943	-0.104484
TPI1	9439	-2.85058	-0.098195
ENO1	9447	-2.860356	-0.091313
PFKP	9614	-3.18491	-0.100174
SAP30	9615	-3.184916	-0.092598
PAXIP1	9644	-3.245778	-0.087795
DEPDC1	9670	-3.313572	-0.082695
GOT1	9685	-3.353539	-0.076505
VLDLR	9741	-3.539011	-0.066701
HAX1	9781	-3.68094	-0.062987
STMN1	9867	-4.006685	-0.063828
PGK1	9879	-4.054762	-0.057341
ALDH7A1	9884	-4.076795	-0.050162
HMMR	9912	-4.201707	-0.04526
STC2	9927	-4.307048	-0.03907
SDC1	9939	-4.38597	-0.032583
PRPS1	9989	-4.736648	-0.02986
LDHA	10024	-4.992755	-0.025651
NASP	10052	-5.275941	-0.020748
AURKA	10072	-5.546384	-0.015054
SLC37A4	10080	-5.686388	-0.008171
CENPA	10166	-7.451145	-0.009012
KIF20A	10209	-9.206566	-0.005595

Figure 5-12: Gene set enrichment analysis of palbociclib-treated cells in the Kasumi-1 cell line. Genes in the hallmark glycolysis pathway showed significant impairment in palbociclib treated cells (FDR Q value = 0.0002). The top section of the figure plots the enrichment score for each gene, and the bottom section indicates the value of the ranking metric moving down the list of ranked genes. Analysis was carried out using Broad Institute software by comparing the experimental gene sets against hallmark gene signature. FDR, false discovery rate; ES, enrichment score.

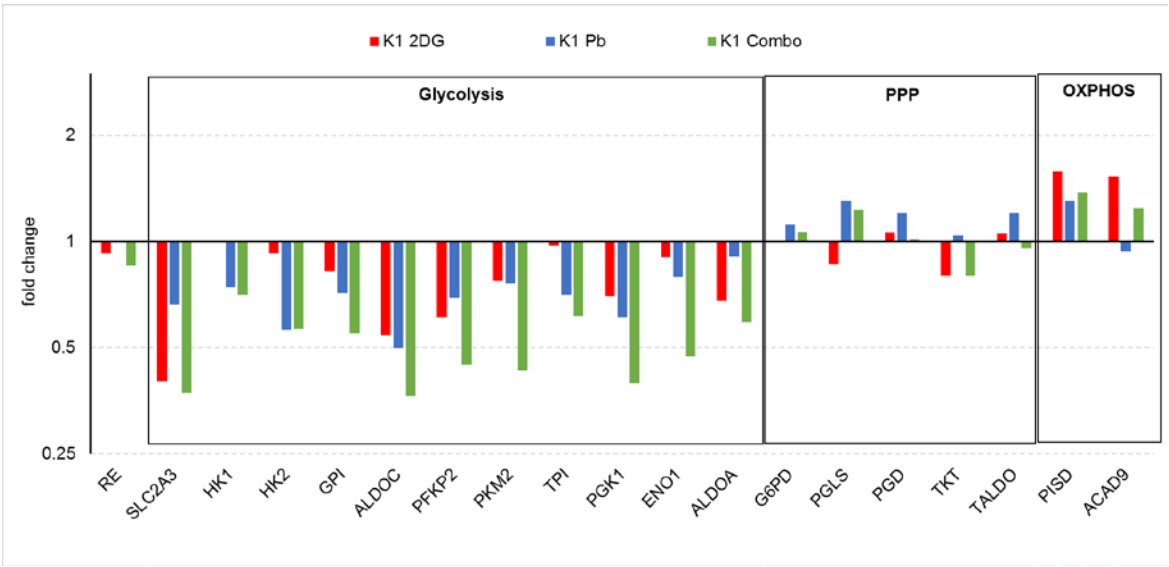

Figure 5-13: mRNA analysis on genes in glycolysis, pentose phosphate pathway and oxidative phosphorylation pathways. Kasumi-1 cells were treated with 200 µM, 30 nM palbociclib and combinations. Cells were harvested after 3 days and analysed for gene expressions. Each gene was normalised to untreated and *CYCLO* serves as housekeeping gene (n=1).

5.3.3 *Palbociclib treatment increase ATP production in the Kasumi-1 cell line*

RT-PCR data showed palbociclib treatment caused upregulation of gene related to OXPHOS. I wondered if that is a result of increased ATP level, as increased ATP production is a predicted consequence of OXPHOS activity. For the next sections, I focused on palbociclib treatment as this drug is currently used in clinical trials (Finn et al., 2016) and there is a potential for repurposing the drug in RUNX1/ETO-leukaemia (Martinez-Soria et al., 2018). Kasumi-1 cells were treated with 30 nM of palbociclib for 72 hours for ATP levels measurement. Fluorescent readings were measured using the Omega Plate Reader at 570 nm. Interestingly, cells treated with palbociclib induced a significant 1.6-fold higher ATP production than untreated control cells, indicating that palbociclib treatment caused the cells to be more dependent on OXPHOS (Figure 5-14).

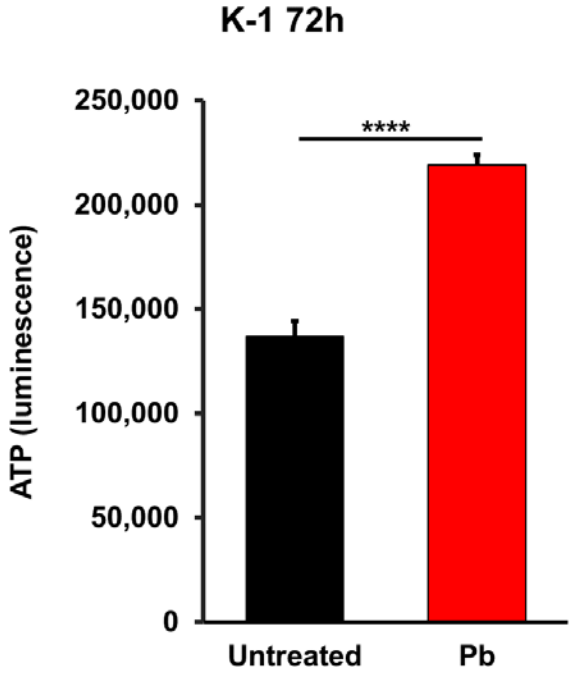

Figure 5-14: Palbociclib treated cells increased ATP production. Kasumi-1 cells were treated with 50 nM palbociclib for 72 hours. ATP was assessed by ATP assay using FLUOstar Omega plate reader at 570 nm. Significance was evaluated using students t-test, ****p<0.0001. Error bar represents standard deviation (n=3, independent experiments).

5.3.4 *Low glutamine induced palbociclib resistance*

Following an increase of *PISD* expression in 2DG and palbociclib treated cells (Figure 5-13), I sought to cross-check the function of this gene. The *PISD* gene codes for phosphatidylserine decarboxylase (PISD) and this protein catalyses the conversion of phosphatidylserine (PS) to phosphatidylethanolamine (PE) in the inner mitochondrial membrane. In the synthesis of PS, serine is the precursor required to form PS and becomes part of membrane phospholipids (Vance and Tasseva, 2013, Hoffmann et al., 2005). Serine is derived from glucose backbone to produce nonessential amino acid and during the synthesis, glutamine is required as nitrogen backbone donor. Therefore I hypothesised, limiting glutamine in palbociclib treated cells would reduce the precursor for phospholipids synthesis and lead to less viable cells.

I then focused on palbociclib treatment in glutamine-suppressed media. Kasumi-1 and SKNO-1 cells were treated with 50 nM, 100 nM palbociclib and 200 nM palbociclib in high/standard glutamine (2 mM) or low glutamine (0.1 mM) media. Cells were incubated for 3 days and viability was assessed by a trypan blue count. The cell counts were normalised to the untreated vehicle control count of each condition. Interestingly, the low glutamine condition resulted in a higher cell number in palbociclib treatment. In Kasumi-1 cells, palbociclib treatment in high glutamine media caused a significant 40% reduction of cell number in 50 nM concentration and a 60% reduction in both 100 and 200 nM concentrations (p-value<0.001) (Figure 5-15-A). Interestingly, in the low glutamine condition, there was no change in 50 nM palbociclib treatment and only a 25% reduction in both 100 and 200 nM concentrations. However, in SKNO-1 cells, a prominent effect was observed with a higher concentration of palbociclib (200 nM), which recorded a 70% loss of cells in high glutamine media (Figure 5-15-B). Remarkably, low glutamine has less effect on cell viability; there was 60% of remaining cells at the end of the experiment. On the other hand, lower concentrations of palbociclib (50 nM and 100 nM) did not have any remarkable changes between high and low glutamine conditions in SKNO-1 cells. Treatment with 50 nM palbociclib reduced 30% of the cells in both high and low

glutamine media. While 100 nM palbociclib treatment reduced the cells to 60% remaining cells in high glutamine media; however, the cell count in 100 nM treatment was slightly higher (80%) in low glutamine media.

The effect of low glutamine on cell viability varies in these two cell lines. In Kasumi-1 cells, there was a clear indication of resistance in low glutamine condition even at low palbociclib concentration. In SKNO-1, although there were no substantial differences observed at lower palbociclib concentrations, the trend of resistance increased as the dose increased. These unexpected findings were also described by Pan et al. (2016). Their study showed low glutamine induced resistance through specific histone hypermethylation, which will be discussed further in chapter 7.

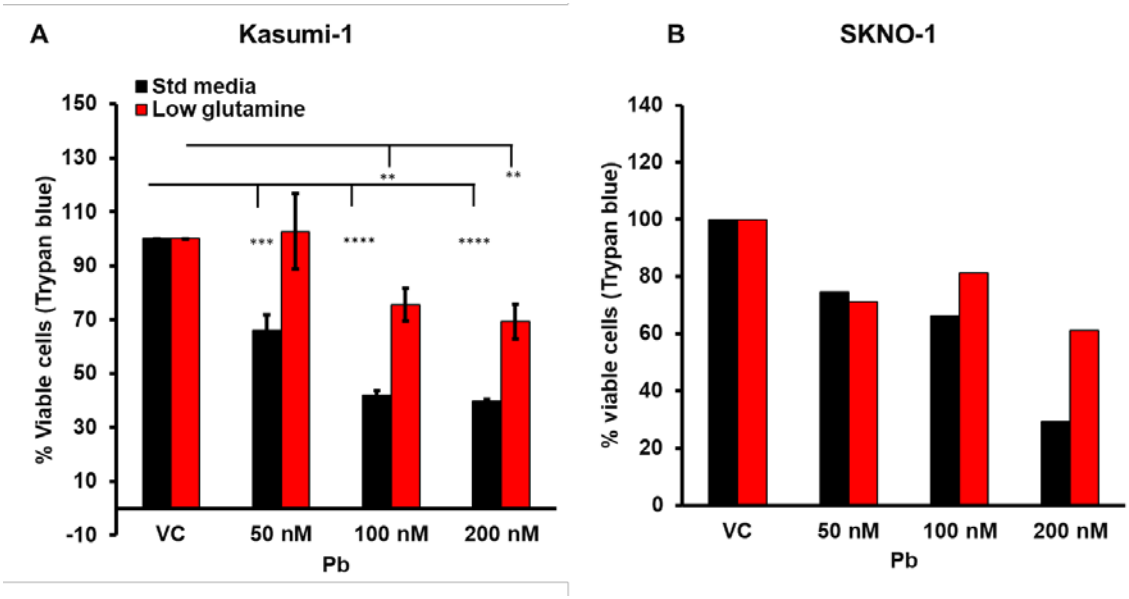

Figure 5-15: Glutamine induced resistance in RUNX1/ETO cells. Cells were treated with 100 nM and 200 nM in high (standard media) and low glutamine (0.1 mM) media for 3 days. Cell viability was assessed by standard trypan blue counting. Data were normalised to the untreated vehicle control for each condition (Kasumi-1, n=3 independent experiments; SKNO-1, n=2). VC: vehicle control. Significance was evaluated using students t-test, **p<0.01, ***p<0.001, ****p<0.0001. Error bar represents standard deviation (n=3, independent experiments).

5.3.4.1 Palbociclib reduces the level of reactive oxygen species to maintain survival

Given that palbociclib treatment increased ATP production in Kasumi-1 cells, I wondered if this leads to oxidative stress in these cells. ATP production is the hallmark of oxidative phosphorylation and several studies have shown that increased ATP production associated with low oxidative stress is suggested as pro-protective mechanism (Lagadinou et al., 2013, Jones et al., 2018); and ultimately leading to slow-cycling and drug resistant cells (Roesch et al., 2013).

To address this question, I performed a flow cytometry ROS detection assay on Kasumi-1 cells treated with palbociclib. I also included a low glutamine parameter in this assay, as low glutamine increased cell viability as described in the previous section. This assay utilised fluorogenic probes that exhibit bright green stable fluorescence upon oxidation by ROS. Kasumi-1 cells were treated with 50 nM palbociclib and 100 nM palbociclib in high/standard glutamine (2 mM) or low glutamine (0.1 mM) media. After 72 hours incubation, 5.0 x 10^5 cells were harvested in 1.0 ml media and stained with CellROX green reagent to a final concentration of 1 µM. A positive control was prepared an hour before the addition of CellROX green reagent by incubating the untreated cells with tert-butyl hydroperoxide (TBHP) at the final concentration of 200 µM. In cells, TBHP inhibits membrane-bound enzymes and causes membrane protein aggregations. In red blood cells, TBHP reacts with haemoglobin and forms free-radicals (L. K. Patterson, 1981, Roy and Sil, 2012). The positive control was incubated at 37^{o}C for 45 minutes before CellROX green reagent was added at the final concentration of 500 nM. Following that, cells were incubated at 37^{o}C for 45 minutes and protected from light. Data was captured at FITC-channel using flow cytometry and analysed using FlowJo software.

Figure 5-16 shows the percentage of ROS-positive cells in both high and low glutamine media. In high glutamine media, while 50 nM palbociclib reduced the number of ROS-positive cells by a third, higher palbociclib treatment halved the percentage of ROS-positive cells when compared to 37% of ROS-positive cells in the untreated. Interestingly, in low glutamine media, the level of ROS-positive cells

reduced by more than a half in comparison to the untreated vehicle control in high glutamine media. Palbociclib treatment at 50 nM and 100 nM in low glutamine condition increased ROS-positive cells by almost half when compared to its control.

Taken together, palbociclib treatment caused low cellular ROS level in Kasumi-1 cells. Interestingly, low glutamine significantly (p-value<0.01) decreased ROS level which is in contrast to the previous findings (Reid et al., 2013, Burgess, 2013). Furthermore, combination of palbociclib and low glutamine did not cause substantial changes on the cellular ROS level.

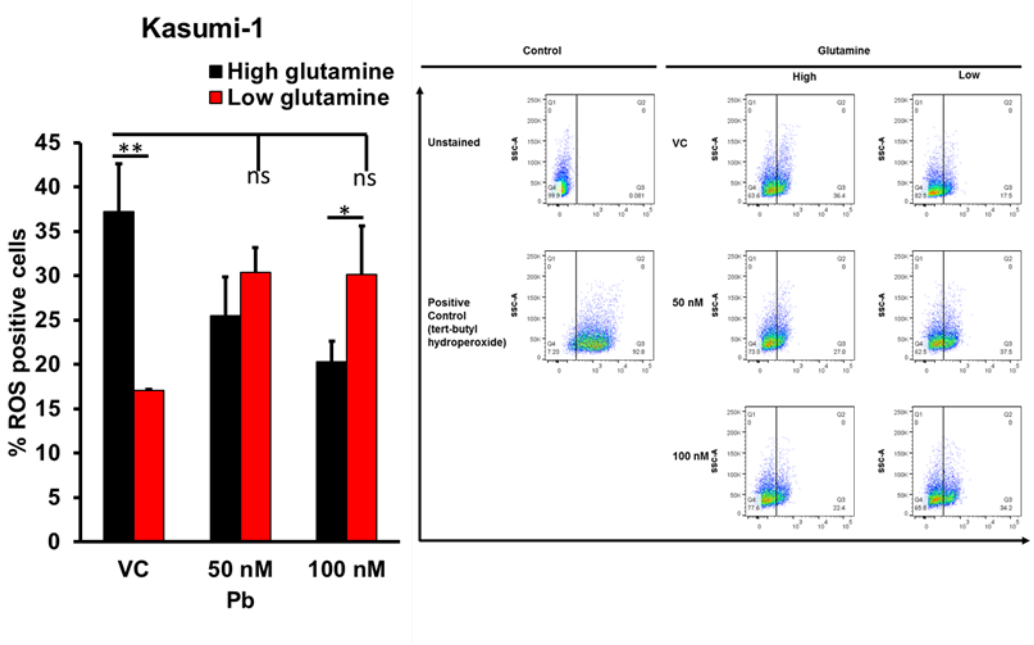

Figure 5-16: Reactive oxygen species (ROS) in palbociclib treated Kasumi-1 cells cultured in high and low glutamine media. Cells were treated with palbociclib with high or low glutamine-containing media. Cells were incubated for 72 hours and stained with CellROX green reagent for 45 minutes at 37ºC protected from light. Stained cells were captured using flow cytometry at FITC-channel. Left panel: Bar chart showing the percentage of ROS-positive cells between vehicle control and palbociclib treated cells in both high and low glutamine media. Right panel: Scatter plot of flow cytometry analyses using FlowJo software. Significance was evaluated using Student's t-test, ns: not significant, *p<0.05, **p<0.01, ns: not significant (n=3 in-dependent experiments).

5.4 Summary

RUNX1/ETO-leukaemia cells are more sensitive to 2DG inhibition than other AML cells. Besides that, palbociclib is particularly effective in targeting actively cycling cells. Combination of 2DG and palbociclib led to a slightly additive effect associated with increased apoptotic cells, mainly induced by 2DG. Both single and combination treatments increased G1 cell cycle arrest and severely impaired expression of genes involved in glycolysis. This combination should be further characterised in terms of its mechanism of action, as well as a potential RUNX1/ETO-leukaemic therapeutic intervention *in vivo.*

Further experiments focused on palbociclib treatment as this drug is currently being used in clinical trial (Finn et al., 2009, Finn et al., 2016). Palbociclib treatment caused G0/G1 cell cycle arrest; however, it is neither associated with apoptosis nor dormancy. mRNA analysis revealed palbociclib treatment caused downregulation of genes involved in glycolysis, and a higher expression of *PISD* which is implicated in glutamine-derived serine biosynthesis in OXPHOS. As a consequence, palbociclib treated cells showed a higher ATP production, suggesting that palbociclib treatment might induce OXPHOS activity. Increased expression of *PISD* indicates a requirement of glutamine; however, limitation of glutamine increased resistance in palbociclib treated cells. GSEA analysis revealed the glutamine synthesis pathway is deprived in palbociclib treatment (Appendix 5-1). Furthermore, palbociclib treatment reduced the level of ROS. Taking this together, palbociclib treatment caused the cells to stop cycling, shift to OXPHOS activity and induce resistance through deprivation of glutamine synthesis.

Appendix 5.1: Palbociclib treatment impairs a set of genes involved in glutamine deprivation identified by Peng et al. (2002).

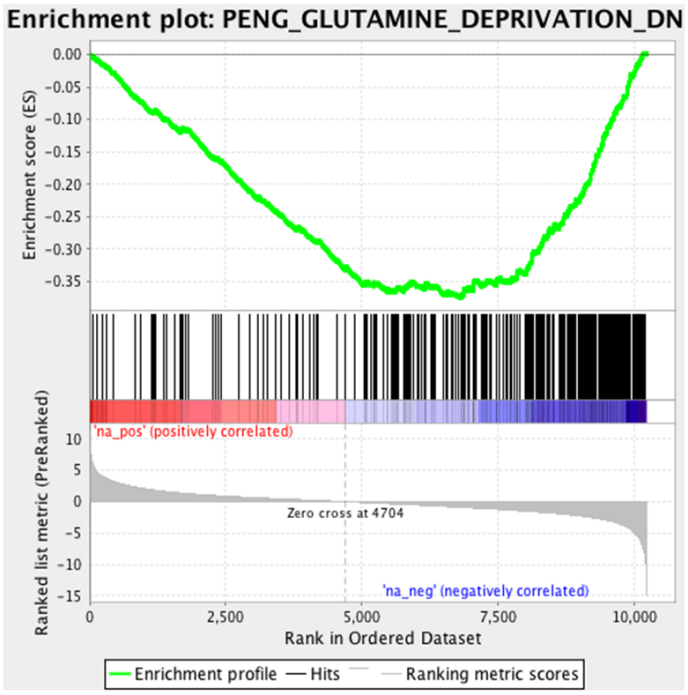

Data set	Palbociclib vs Control
Normalised ES	-7.4462047

Chapter 6 : *In vitro* Functional Analysis of *SLC2A3* and *PFKP* in t(8;21) Patient-derived Xenograft

6.1 Introduction

AML is characterised by clonal and molecular heterogeneity which in turn affects response to treatment (Wang et al., 2017b, Grimwade et al., 2016). Despite the relatively good prognosis observed in the t(8;21) AML disease subtype (Byrd et al., 2002, Grimwade et al., 2010) a substantial number of patients relapse further highlighting the need to address intra-tumour heterogeneity when designing treatment strategies.

Preclinical prioritisation and patient-relevant models are essential in childhood leukaemia. Furthermore, unlike in acute lymphoid leukaemia (ALL) where all blasts are marked by equipotent stem cell properties irrespective of their immunophenotypic stage (Elder et al., 2017), the stemness of AML presents in only a subset of cells (Yassin et al., 2019). Despite recent progress in acute ALL preclinical models (Pal et al., 2016, Bomken et al., 2013) there are no RUNX1/ETO PDX. Currently, most studies and preclinical testing for novel targets and drugs in RUNX1/ETO-leukaemia are performed on two established cell lines, Kasumi-1 and SKNO-1(Soria et al., 2008, Martinez et al., 2004, Martinez-Soria et al., 2018). These models have been derived from relapsed disease and thus do not retain the molecular complexity at disease presentation.

Furthermore, cell lines proliferate in niche-independent suspension cultures and thus fail to capture the plethora of networks regulating leukaemia biology in patients. Over the years, primary t(8;21) blasts culture has been challenging as the cells do not propagate both *in vitro* and *in vivo*. However, primary and PDX preclinical platforms are essential to define the function of RUNX1/ETO partner genes and develop novel “chemo-free” targeted therapies for leukaemogenesis.

Recently, our laboratory has successfully developed and validated PDX material from relapsed t(8;21)-leukaemia in immunocompromised mice. A xenograft mouse model for t(8;21) leukaemia has not been described previously, thereby establishing *in vivo* patient model for this leukaemia subtype. One PDX, namely RL048 harbours a *KIT D816V* activating mutation and has a p53 wild-type status; the primary immunophenotype details for this sample are listed in Appendix 6-1 (Assi et al.,

2019). This t(8;21) PDX model has been instrumental to define the roles of the oncogenic transcription factor, RUNX1/ETO and its partner genes in a clinically relevant setting.

In order to specify niche-mediated regulatory roles of RUNX1/ETO models I have used a human *ex vivo* cancer-niche platform developed by Dr Deepali Pal (Pal et al., 2016). Epigenetic reprogramming of human bone marrow (BM) stroma cells into pluripotent stem cells (BM-iPSC) has enabled a standardised source for BM mesenchymal stem cells (BM-iPSC-MSC). BM-iPSC-MSC support viability and proliferation of both CD45+ haematopoietic and CD19+ patient ALL blasts (unpublished data). Additionally, recent studies showed that mesenchymal stromal cells (MSCs) directly re-programmed from skin fibroblasts through chemical induction reconstitute bone marrow stroma and have similar molecular signatures to bone marrow mesenchymal stem cells (Lai et al., 2017). Based on the previous success of a preclinical model on bone marrow derived mesenchymal stem cells (MSC) ALL co-culture system (Pal et al., 2016), this chapter focusses on the *in vitro* characterisation of the RUNX1/ETO PDX co-culture with BM-iPSC-MSC and its application in the functional study of *SLC2A3* and *PFKP.*

6.2 Aims

The aims of this chapter are;

i. to establish an *in vitro* platform for RUNX1/ETO PDX cells co-culture with BM-iPSC-MSC and to study the characteristics of cells in short-term culture.
ii. to validate the functionality of *SLC2A3* and *PFKP* gene in this PDX material as well as in other primary material.

6.3 Results

6.3.1 *BM-iPSC-MSC supports short-term in vitro proliferation of RUNX1/ETO PDX cells*

To establish *in vitro* culture conditions for RUNX1/ETO PDX cells, BM-iPSC-MSC were utilised as niche-feeder cells. A 30-40% confluent cell culture was BM-iPSC-MSC cells were pre-prepared in a 12-well Matrigel-coated tissue culture dish 4 days prior to the seeding of PDX cells. A total of 5.0 x 10^5 PDX cells were seeded in 1 ml SFEM II myeloid expansion medium. Characterisation of the PDX cells was carried out on day 0 (at thawing) and day 7-post seeding.

As indicated in Figure 6-1-A, trypan blue cell count showed that the number of viable PDX cells increased four-fold from 5.0 x 10^5 cells on day 0 to 1.9 x 10^6 cells on day 7 with BM-iPSC-MSC co-culture. In contrast, the cells cultured without BM-iPSC-MSC minimally increased to 9.5 x 10^5 cell/ml. Figure 6-1-B shows phase-contrast photographs of PDX cells in co-culture with and without BM-iPSC-MSC on day 0 and day 7-post seeding. The density of the cells visibly increased from day 0 to day 7 when co-cultured with BM-iPSC-MSC.

Cell cycle analysis on day 7 revealed that co-culture of PDX cells with BM-iPSC-MSC did not caused substantial changes in the cycling profiles as well as the subG1 fraction (Figure 6-2).

Collectively, BM-iPSC-MSC supported RL048 PDX propagation *in vitro*.

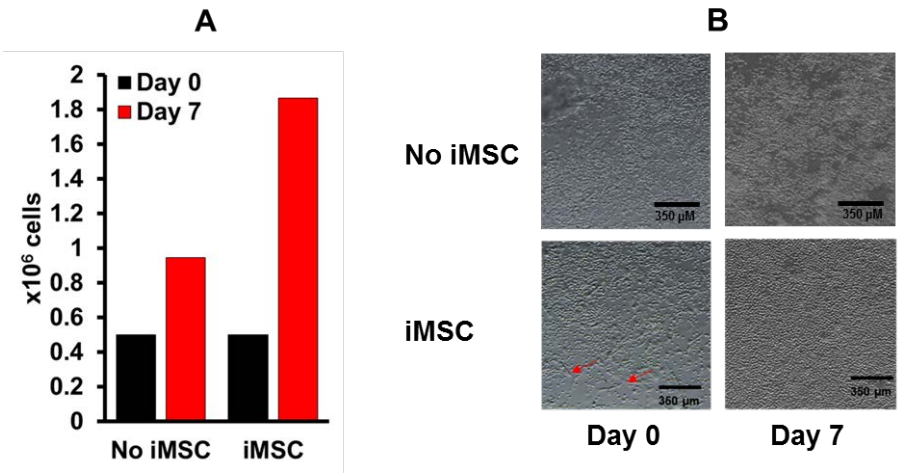

Figure 6-1: BM-iPSC-MSC increases the propagation of RL048 PDX cells *in vitro*. PDX cells were seeded on 30-40% confluent BM-iPSC-MSC at the concentration of 5.0 x 10^6 cells/ml. Readouts were captured on day 0 and day 7-post seeding. A) Cells counts using standard trypan blue method (n=2). B) Phase-contrast photographs of PDX cells co-cultured with BM-iPSC-MSC. Red arrows indicate BM-iPSC-MSC cells (n=1).

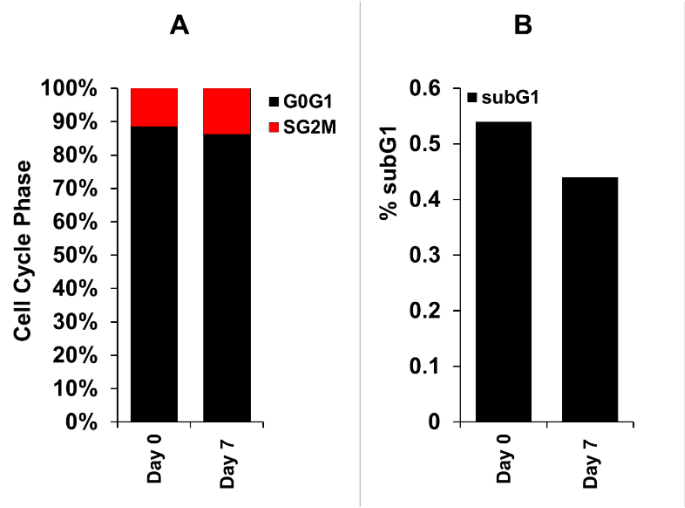

Figure 6-2: Cell cycle profile of RL048 on day 0 and after 7 days cultured on BM-iPSC-MSC. PDX cells were seeded on 30-40% confluent BM-iPSC-MSC at the concentration of 5.0 x 10^5 cells/ml. Cells were incubated with 10 µg/ml Hoechst 33342 staining for 45 minutes and measured by flow cytometry. Analysis was performed using FlowJo software. A) Cell cycle profile of PDX cells on day 0 and day 7. B) SubG1 analysis on PDX cells on day 0 and day 7-post seeding (n=1).

6.3.2 *RL048 differentiate after short-term culture in vitro*

To further characterise the cells differentiation potential in short-term co-culture with BM-iPSC-MSC, immunophenotype profiling was performed by staining the cells with haematopoietic surface markers. The surface markers used in the assay included CD45, CD34, CD33, CD15 and CD14. Human CD45 was used to exclude mouse cells; while CD34 was used to determine stemness property of the cells as well as to differentiate between blasts cells and BM-iPSC-MSC which do not expresses CD34 (Lin et al., 2012). Surface markers CD33, CD15 and CD14 were used to identify potential myeloid specific lineage differentiations. Briefly, cells were washed once and stained with the abovementioned antibodies in flow cytometry staining buffer. Data were captured by flow cytometry and analysed using FlowJo software.

Changes in the immunophenotype of RL048 PDX cells after 7 days in culture were observed with and without BM-iPSC-MSC. (Figure 6-3). A total of 78% of cells were positive for CD34 on day 0; however, after 7 days in culture, the cells lost CD34 expression with 17% CD34+ in culture without BM-iPSC-MSC and 14% CD34+in co-culture with BM-iPSC-MSC. Notably, the cells maintained CD33 expression

throughout the experiments. Gain of CD15 was seen after the short-term culture indicating rise of mature myeloid lineage. The number of CD15-positive cells increased from 14% to 79% in culture without BM-iPSC-MSC and slightly higher in co-culture with BM-iPSC-MSC (87% of cells). Furthermore, CD14 was not expressed at the start of the culture. However, after 7 days in co-culture with BM-iPSC-MSC, 4% of cells were positive for CD14, whereas there was a minimal increase of 1.3% CD14 positive cells in culture without BM-iPSC-MSC.

Taken together, t(8;21) AML cells underwent limited myeloid differentiation in short culture possibly associated with a loss of stemness as indicated by the loss of CD34.

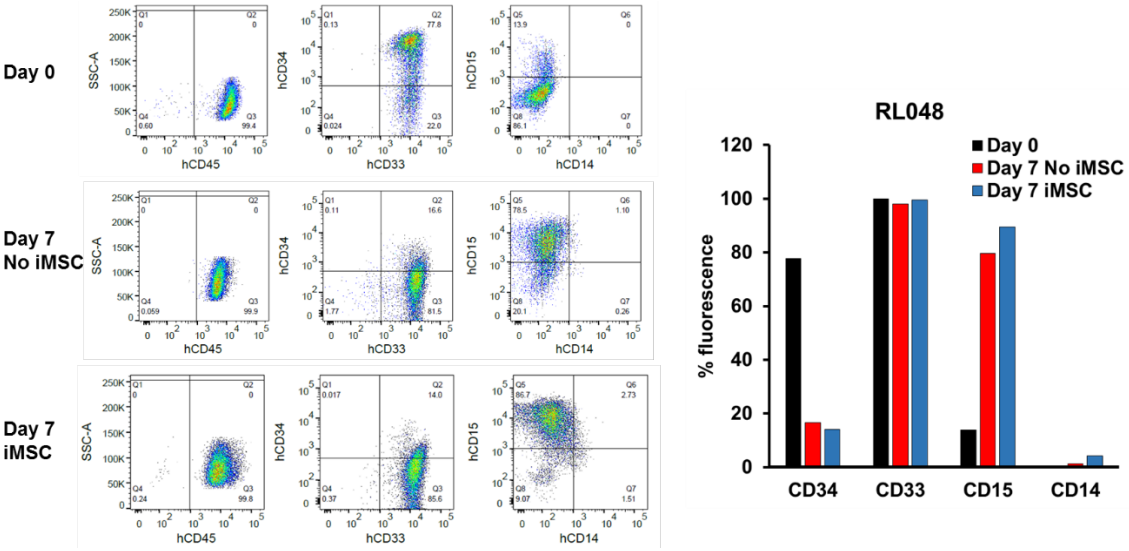

Figure 6-3: Immunophenotype of RL048 cells co-cultured with and without BM-iPSC-MSC. Cells were checked for immunophenotyping on CD34, CD33, CD14 and CD15 on day 0 and day 7 after co-cultured with and without BM-iPSC-MSC. Left: A representative of immunephenotype analysis. Right: Average of immunophenotype analyses (n=2).

6.3.3 *In vitro assessment of SLC2A3 and PFKP in t(8;21) primary and patient-derived xenograft (PDX) materials*

As described in chapter 4, depletion of *SLC2A3* and *PFKP* in Kasumi-1 cells impaired propagation and self-renewal *in vitro* in glucose and oxygen deprivation conditions. The next aim was to validate if *SLC2A3* and *PFKP* are relevant for

propagation of the relapsed t(8;21) leukaemia. To this end, I validated the competitiveness of the cells upon shRNA-mediated knockdown. Cells were transfected with shRNA lentivirus expressing different colours and analysed by flow cytometry after 96 hours. The media used in this experiment was SFEM II media which contained approximately 23 mM of glucose.

The two populations were then mixed, analysed with flow cytometry (day 0) and seeded onto BM-iPSC-MSC plate. Fluorescence of the mixed populations was analysed on day 7-post mixing (Figure 6.4).

The shRNA transduction on the PDX cells resulted in a high efficiency using the same vector used in chapter 3 and 4 (Appendix 6-2). Figure 6-5 shows a line chart of the representation of the four different shRNA populations before and after co-culture. Each population was normalised to 25% on the start of experiment and changes on day 7-post mixing were calculated against the initial percentage. Notably, shNTC recorded 17% increase to reach 42% on day 7 and outcompeted all other populations. *SLC2A3* and *PFKP* knockdown caused the cells to reduce to 19% at the end of experiment. The greatest depletion was observed in double knockdown as it recorded 15% remaining cells on day 7.

I next examined whether this data is reproducible particularly on *SLC2A3* knockdown. Single shRNA knockdown on *SLC2A3* was performed following the same scheme as depicted in Figure 6-4 except that only one shRNA lentivirus targeting *SLC2A3* was used to transduce the cells. Each population was normalised to 50% on day 0 as starting percentage and changes on day 7 was calculated accordingly. Remarkably, shNTC-expressing cells outcompeted *SLC2A3* knockdown cells after 7 days of co-cultured on BM-iPSC-MSC. shNTC expressing cells increased from 50% on day 0 to 61% and 62% on day 7 in both two independent experiments indicated in Figure 6-6. This led to their being 39% and 38% of shSLC2A3-expressing cells at the end of the experiment.

Collectively, these findings highlight the potential roles of *SLC2A3* and *PFKP* in niche-mediate RUNX1/ETO-leukaemia survival and propagation.

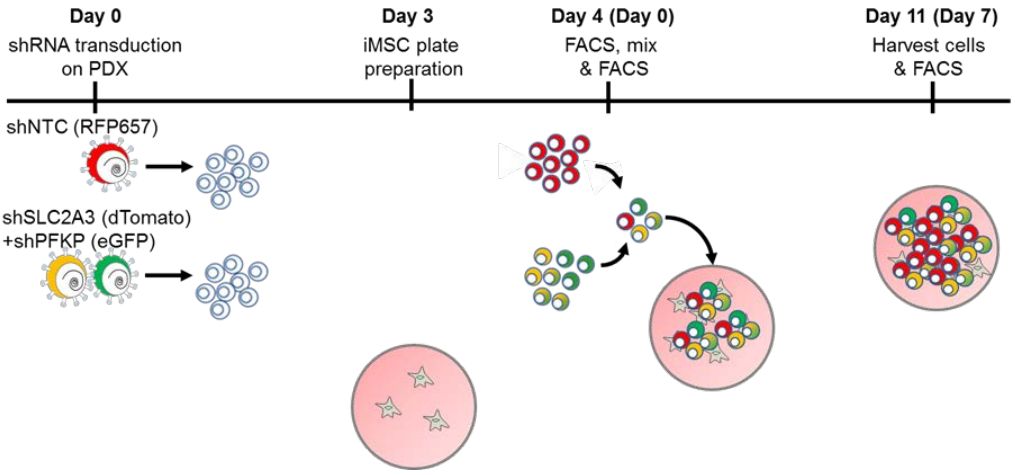

Figure 6-4: Scheme of competitive assay of t(8;21) PDX cells transduced with shRNA and cultured on BM-iPSC-MSC. Cells were transduced with shRNA lentivirus expressing different fluorescent markers. On day 4, transduction efficiencies of the cells were checked by flow cytometry, mixed in single tube and transferred onto BM-iPSC-MSC plate. On day 7-post mixing, cells were collected and checked using flow cytometry.

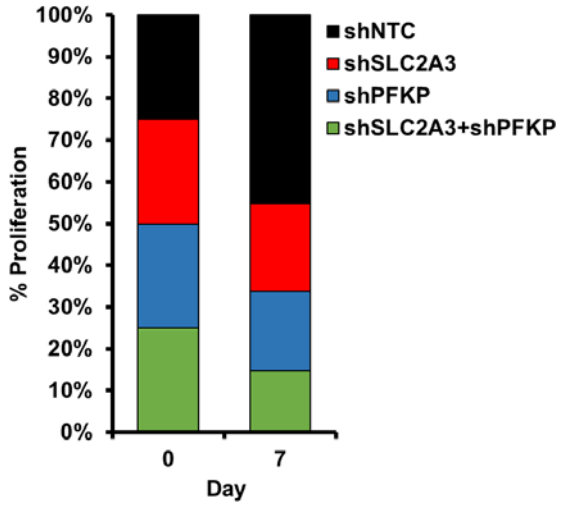

Figure 6-5: Stacked column showing shNTC competitively outcompeted shSLC2A3 and shPFKP populations in t(8;21) PDX cells cultured on BM-iPSC-MSC. shNTC and shSLC2A3/shSLC2A3+shPFKP cells were mixed on day 0 in SFEM media, checked by flow cytometry and cultured on BM-iPSC-MSC cells at standard incubation condition. On day 7, cells were collected and cells fluorescence percentages were monitored by flow cytometry. The percentage were normalised and calculated against day 0 (n=1).

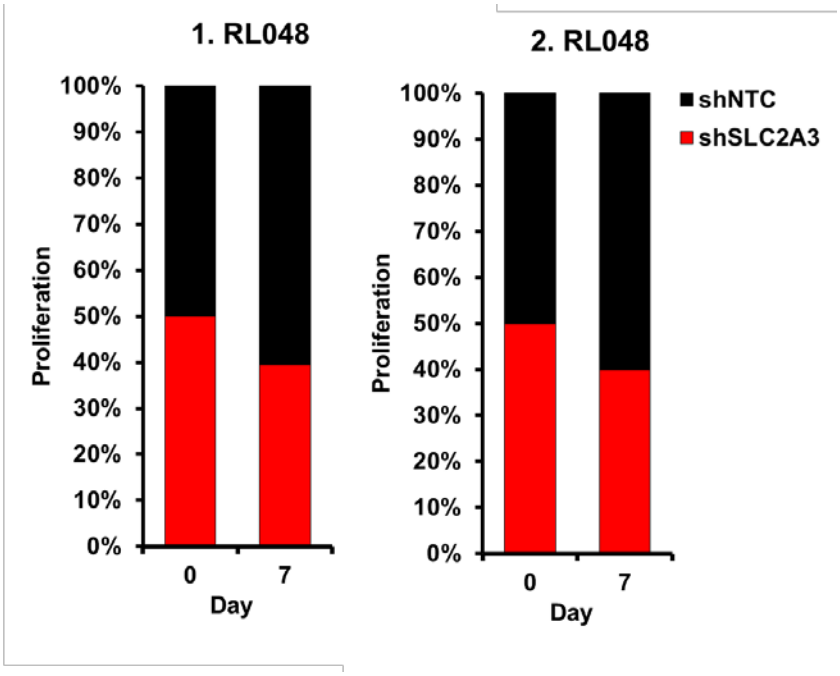

Figure 6-6: shRNA mediated knockdown of SLC2A3 affects competitive fitness of RL048 PDX cells. shNTC and shSLC2A3 cells were mixed on day 0 in SFEM media, checked by flow cytometry and cultured in standard incubator at 37^{O}C. On day 7, cells were collected and fluorescence percentages were monitored by flow cytometry. The percentage were normalised and calculated against day 0. Graphs are two different independent experiments (n=2).

6.3.3.1 RE regulates SLC2A3 and PFKP at transcript level in primary t(8;21)-leukaemia

To address of whether *SLC2A3* and *PFKP* are direct transcriptional target genes of RUNX1/ETO in PDX and primary blasts, siRNA knockdown experiments were performed on two primary t(8;21) samples, LK19 and RL048.

For LK19, a modified siRUNX1/ETO (siRE-fmds) was delivered as a lipid nanoparticle. This experiment was performed by Mr. Hasan Issa who demonstrated the efficacy of modified siRNA in targeting the RUNX1/ETO fusion gene both *in vitro* and *in vivo* (H. Issa PhD thesis 2019). RL048 primary cells were electroporated with siSLC2A3+siPFKP and were harvested for RNA extraction 24-hour post-transfection.

In LK19 cells, knockdown of *RUNX1/ETO* led to a 70% reduction of oncogenic mRNA level itself, and reduced both *SLC2A3* and *PFKP* transcript level to 60% and 70% correspondingly (Figure 6-7-A). Furthermore, double knockdown of *SLC2A3*

and *PFKP* in RL048 blasts cells, led to a reduced 40% of *SLC2A3* and 60% of *PFKP* mRNAs (Figure 6-7-B). Although, the knockdown of both genes were not as potent as in the cell line; however, the knockdown resulted in two distinct morphologies between siMM and siSLC2A3+siPFKP as shown in phase contrast microscopy in Figure 6-7-C. In siMM treatment, many of the cells seen to maintain plasma membrane integrity and smooth granules (red arrows). In contrast, siSLC2A3+siPFKP treatment resulted in irregularities of the cells membrane and coarse intracellular granules as indicated with blue arrow. Furthermore, some of the cells shrunk to smaller sizes after 24-hour treatment with siSLC2A3+siPFKP (green arrow). These cumulative observations suggestive of potential cell death through apoptosis pathway as previously described by Zhang et al. (2017), Bortner and Cidlowski (2002), Sesso et al. (1999).

However, mRNA analyses indicates no induction of apoptotic related genes detected upon depletion of *SLC2A3* and *PFKP* (Figure 6-8-A). Instead, only *CCND1* mRNA level substantially decreased to 40% when compared to the siMM treated control (Figure 6-8-B). This observation was similar to the findings seen in Kasumi-1 cells, where only *CCND1* was substantially reduced (section 4.3.9).

Due to limited availability of PDX cells, no additional experiments were performed on the primary blasts.

In summary, *RUNX1/ETO* regulates *SLC2A3* and *PFKP* expression at mRNA level in primary leukaemic blasts. Knockdown of *SLC2A3* and *PFKP* led to mRNA downregulation and changes in morphology of leukaemic blasts. The double knockdown did not cause inductions of apoptosis genes at mRNA level, but reduced the *CCND1* expression level.

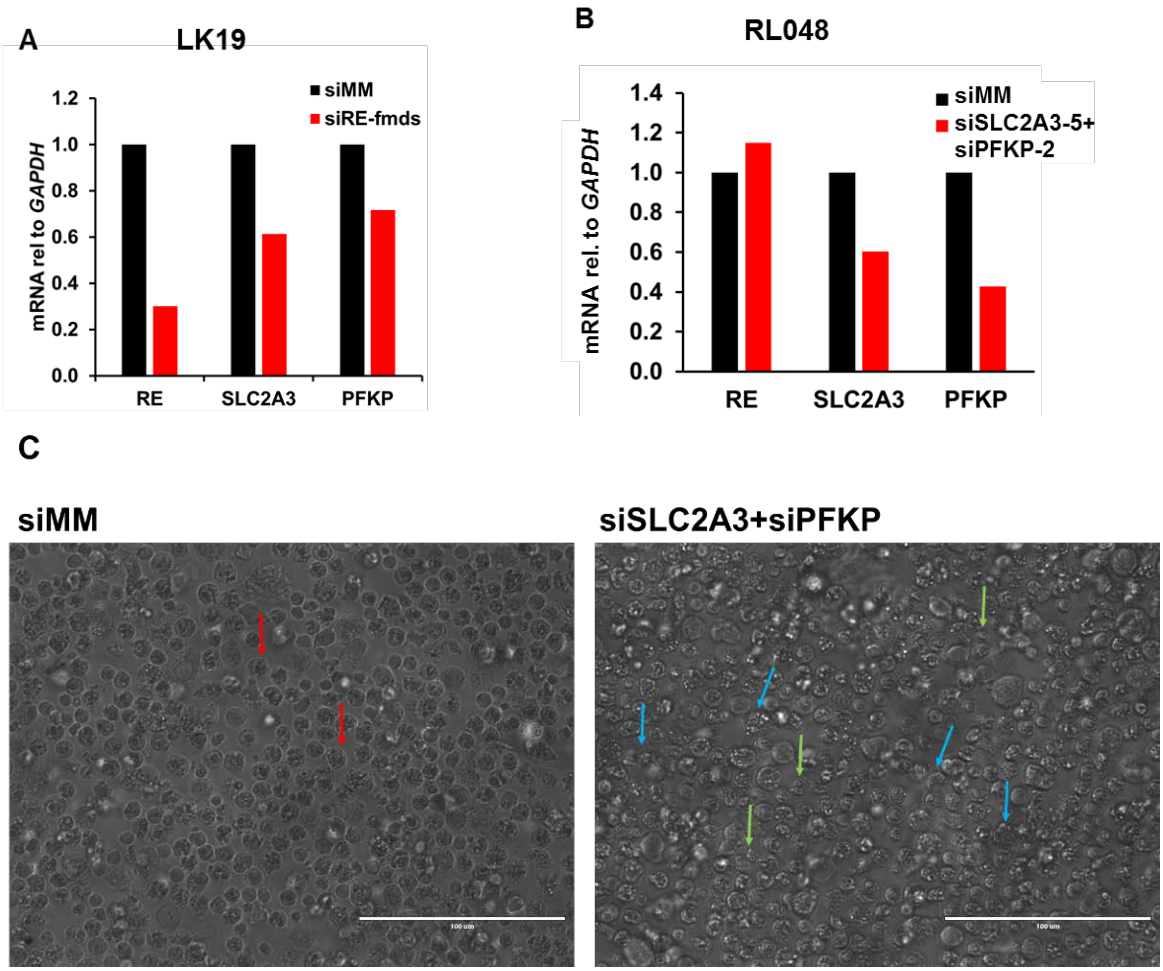

Figure 6-7: Knockdown of *SLC2A3* and *PFKP* changed the cells morphology in primary t(8;21) blasts. A) LK19 blasts cells were treated with a modified siRNA targeting *RUNX1/ETO* in encapsulated liposome and cells were harvested 24-hour post treatment (n=1). B) RL048 blasts cells were transfected with siSLC2A3+siPFKP by electroporation and cells were collected after 24-hours (n=1). C) The morphologies of RL048 cells changed after being transfected with siSLC2A3+PFKP for 24-hour. siSLC2A3+siPFKP caused changes of cell membrane integrity and cytoplasmic granules (blue arrows) and smaller size of cells (green arrows) in comparison to siMM (red arrow), potentially suggestive of apoptosis cell death. Images were captured using phase contrast microscope. Scale bar, 10 μm (n=1).

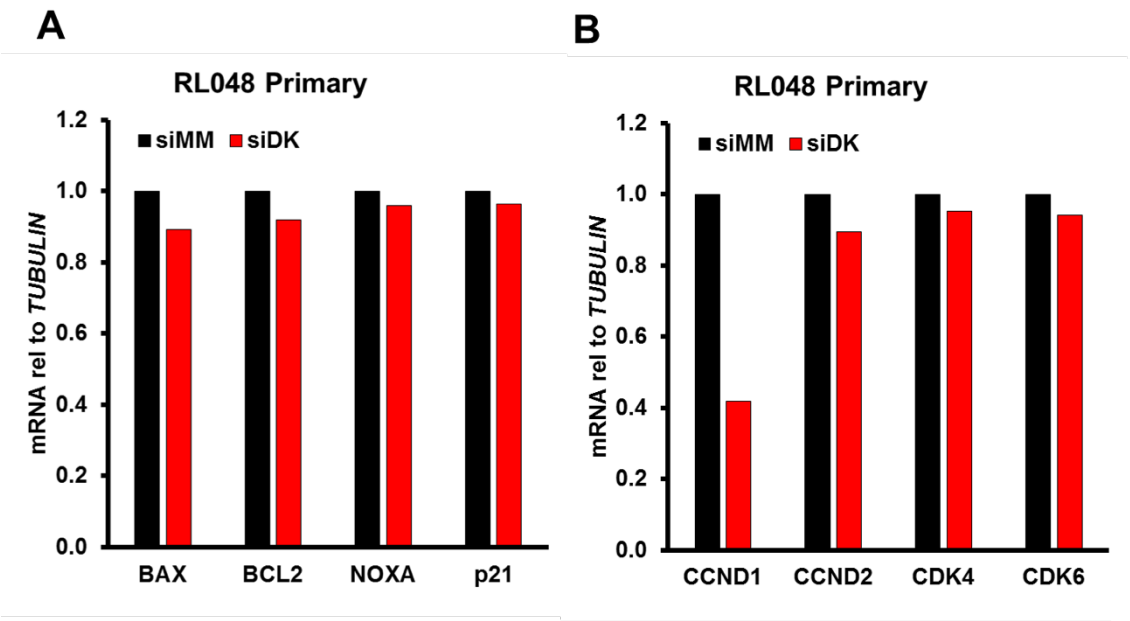

Figure 6-8: Knockdown of *SLC2A3* and *PFKP* led to reduction of *CCND1* mRNA levels in primary t(8;21) blasts. RL048 blasts cells were transfected with siSLC2A3+siPFKP by electroporation and cells were collected after 24-hours. mRNA levels of genes related to apoptosis (A) and cell cycle (B) (n=1).

6.3.3.2 RUNX1/ETO does not regulate TIGAR expressions in wild-type p53

Furthermore, previous study has shown that RUNX1/ETO activates p53 and led to non-ROS associated cell death (Krejci et al., 2008). The p53 protein positively regulates TIGAR which increases the flux to pentose phosphate pathway, thereby producing antioxidant including NADPH and GSH (Lee et al., 2015). Interestingly, *TIGAR* (*C12orf*) located in a close proximity with *CCND2* (Appendix 6-3). *CCND2* has been shown to play a critical role in modulating RUNX1/ETO-leukaemia (Martinez-Soria et al., 2018).

Since the PDX and primary cells used in this study exhibit wild-type p53 (Assi et al., 2019), I wondered if *RUNX1/ETO* controls the expression of *TIGAR*. To answer this question I electroporated siRNA targeting *RUNX1/ETO* in RL048 PDX cells and harvested for mRNA analyses 24-hour post-transfection. mRNA analyses were also performed on the sample from section 6.3.1.1.

The mRNA analyses on siRUNX1/ETO-treated cells revealed that there were no changes detected in *TIGAR* expression levels in both PDX and primary samples (Figure 6-9-A-B). Furthermore, double knockdown on *SLC2A3* and *PFKP* also did not change the *TIGAR* mRNA level (Figure 6-9-C). This data indicates that *RUNX1/ETO* did not regulate the expressions of *TIGAR* gene.

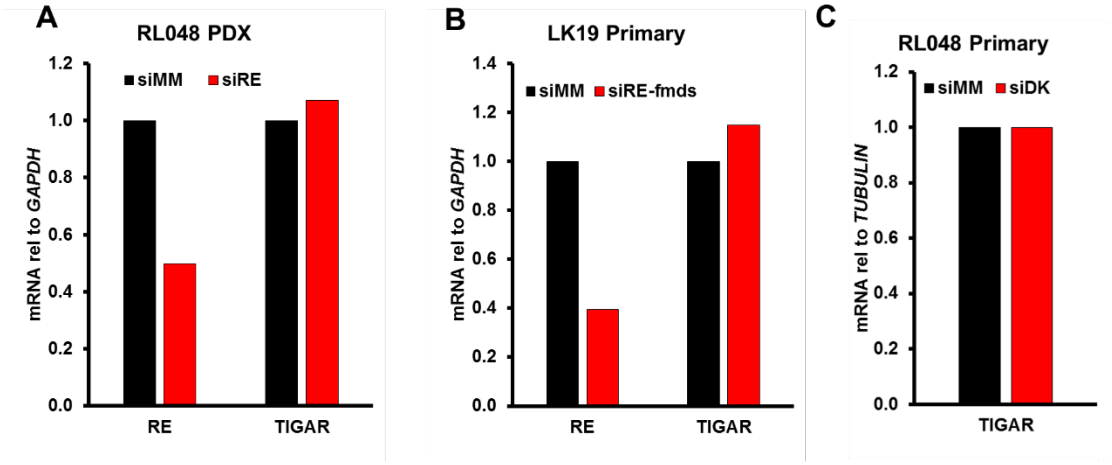

Figure 6-9: *RUNX1/ETO* and *SLC2A3+PFKP* knockdowns did not change the expression of *TIGAR* in wild-type p53 cells. Cells were transfected with siRNA by electroporation and were collected after 24-hours for RNA extraction. mRNA analyses were performed in PDX (A) and primary (B, C) samples (n=1). DK: double knockdown.

6.4 Summary

Collectively, I have characterised the *in vitro* RUNX1/ETO PDX co-culture system with BM-iPSC-MSC and this could be brought forward as pre-clinical platform for other primary or PDX materials of this subtype of leukaemia. BM-iPSC-MSC support improved viability and propagation of RUNX1/ETO PDX cells *ex vivo* as indicated through the cell counts. Following short-term culture, BM-iPSC-MSC directed blast differentiation into specific myeloid specific lineage as indicated by CD33 and CD15 surface markers. However, the culture led the reduction of CD34 surface expression implying a loss of stemness.

Furthermore, knockdown of *SLC2A3* and *PFKP* in PDX cells reduced leukaemic cell proliferation in high glucose media in competitive assay experiments. mRNA levels for both *SLC2A3* and *PFKP* were downregulated upon depletion of *RUNX1/ETO* suggesting that RUNX1/ETO regulates these two genes in primary blasts. Furthermore, transient double knockdown of *SLC2A3* and *PFKP* caused reduction in mRNA levels and resulted in altered cell morphologies; however, no inductions of apoptotic related genes observed in mRNA analyses. *CCND1* expressions were shown to be substantially reduced in the double knockdown strategy. Moreover, neither *RUNX1/ETO* nor double knockdown showed inter-connection on the *TIGAR* expression as shown by the mRNA analyses. This somehow could give an advantage of targeting *SLC2A3* and *PFKP* in p53 intact leukaemia as TIGAR additively can suppress glycolytic activity at PFKP level.

APPENDIX

Appendix 6-1: Immunophenotype profiles of primary blasts RL048.

University's email communication with Dr D. Coleman, Institute for Cancer Studies, University of Birmingham.

RL048 profiles

Relapse with t(8;21) translocation

CD14-

CD15-

CD11b-

89% FLT3+

82% CD34+

86%CD117+

61%CD19+

80%CD33+

5%CD3+

Appendix 6-2: Transduction efficiency of RL048 PDX cells on day 4 after transduction.

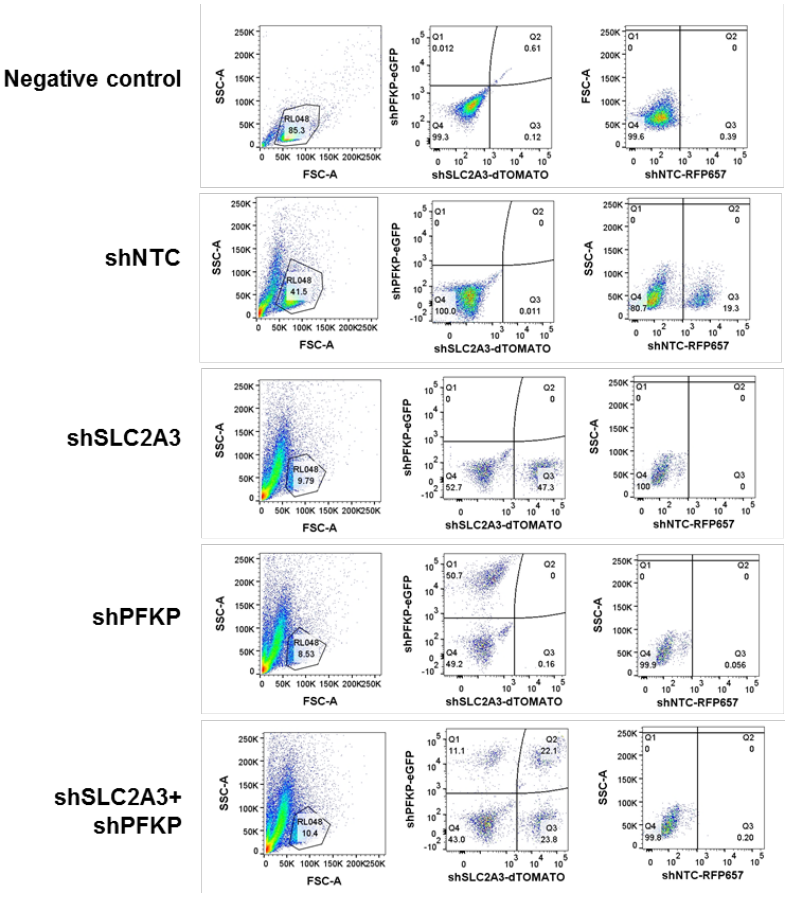

Appendix 6-3: Screenshot of UCSC genome browser indicating close proximity of *TIGAR* (*C12orf5*) to *CCND2* (shown in red box).

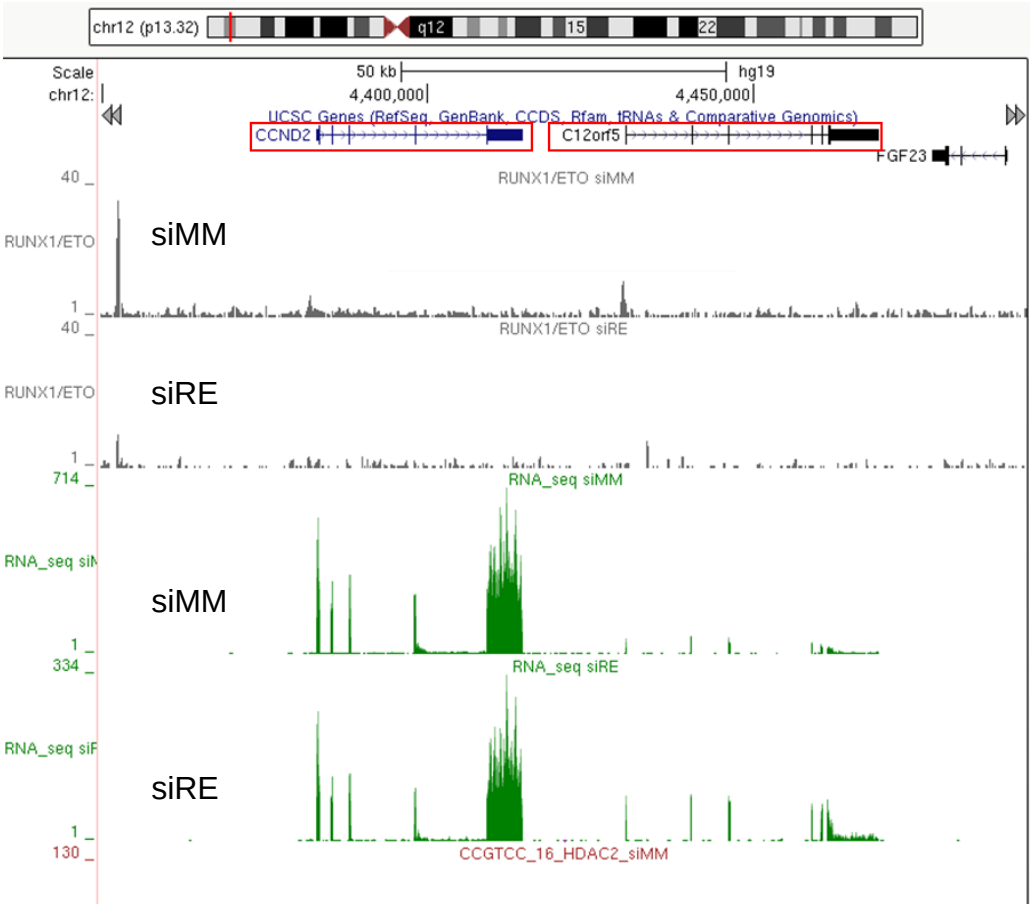

Chapter 7 : Discussion and Conclusion

7.1 RUNX1/ETO is the master regulator in t(8;21) leukaemia

The t(8;21) translocation is the most common genetic alteration in AML and involves rearrangement of the RUNX1 gene on chromosome 21q22 and the ETO gene on 8q22. This rearrangement generates the RUNX1/ETO fusion protein and regarded as the aberrant regulator of the disease.

Loss of RUNX1/ETO knockdown cells in competitive assay experiments confirmed its role in maintaining the leukaemic survival in line with previous findings (Martinez et al., 2004; Soria et al., 2008). The competitive inhibition of wild-type RUNX1 by RUNX1/ETO is considered as the mechanism for leukaemogenesis. RUNX1/ETO competitively shares 60% of the binding peaks with RUNX1 that are enriched with the E-box-binding proteins (Ptasinska et al., 2012). E-box-binding protein forms a stable complex with ETO protein (Zhang et al., 2004b) and interestingly E-box proteins interacts at the RUNX1/ETO locus in both *SLC2A3* and *PFKP* gene (Appendix 7-1). A study demonstrated that deletion of the E-box-like motif within intron 2 of *SLC2A3* substantially abrogated proliferation in 293T cells (Masin et al., 2014).

Furthermore, RUNX1/ETO co-operates with transcription factor AP-1 to maintain expressions of *CCND2* (Martinez-Soria et al., 2018). Loss of RUNX1/ETO leads to reduce expressions of *CCND2* and cell cycles disruption (Martinez-Soria et al., 2018). Additionally, RUNX1/ETO promotes leukaemic clonogenicity by direct binding at the *TERT* promoter and controls CD34 stem cell marker expression (Martinez et al., 2004). These studies corroborate the role of RUNX1/ETO as a master regulator in maintaining leukaemia.

Moreover, the glycolysis stress test showed depletion of RUNX1/ETO severely impairs glycolysis in t(8;21) leukaemia. However, there is a gap of knowledge regarding RUNX1/ETO regulates glycolysis. Recent publications showed putative binding of RUNX1/ETO at the PKM2 gene, a gene that encodes rate-limiting enzyme in the final step of glycolysis (Ptasinska et al., 2012, Yan et al., 2017). One study claimed that RUNX1/ETO directly repressed PKM2 in Kasumi-1 cells and shifted the

cells towards glycolytic phenotype, which is a contrast to its normal biological function (Yan et al., 2017). However, the finding is in contrast with our established data. Firstly, our data shows *PKM* is highly expressed in Kasumi-1 cells and secondly, the depletion of *RUNX1/ETO* do not increased the expression of *PKM* (Appendix 7-2) (Ptasinska et al., 2012). Furthermore, RUNX1/ETO indeed preferentially utilises glycolysis for metabolism, as shown in the glycolysis stress test. In addition, depletion of *SLC2A3* and *PFKP* simulated the glycolytic phenotype caused by RUNX1/ETO knockdown indicating that these two genes are potentially the partner genes of RUNX1/ETO in regulating glycolysis.

7.2 Hypoxia causes decreased proliferation and induces resistance in RUNX1/ETO knockdown cells in Kasumi-1

Hypoxia induced slower Kasumi-1 cell growth when compared with the cells in normoxia conditions (section 4.3.3). Studies have shown that hypoxia induces the cell cycle inhibitor, p27 and blocks the transition of cells from G0 to G1 in the cell cycle phase (Drolle et al., 2015). Hypoxia also decreases the proportion of cells in S phase (Griessinger et al., 2014, Liang et al., 2012, Gardner et al., 2001). In human ovarian cancer cell lines, hypoxia reduces growth rate and acute exposure to hypoxia causes aggressive invasion of cell in an *in vitro* invasion assay (Liang et al., 2012).

Furthermore, *RUNX1/ETO* knockdown in Kasumi-1 cells showed a trend of resistance in hypoxia. This observation could be explained by the accumulation of cells in the G1 phase (section 4.3.8) (Soria et al., 2008, Martinez et al., 2004, Martinez-Soria et al., 2018) seen in both *RUNX1/ETO* knockdown and hypoxia, thus resulted in a delayed effect in the *RUNX1/ETO* knockdown samples.

Several studies have previously shown that low oxygen tension promotes chemoresistance in leukaemia (Griessinger et al., 2014, Hsu et al., 2009, Drolle et al., 2015) and solid tumours (Sullivan et al., 2008, Frederiksen Lisa et al., 2003, Deynoux et al., 2016). For instance, treatment with DNA damaging agent, doxorubicin in AML cell lines in normoxia resulted in apoptosis; however, the amount

of apoptosis was reduced in the hypoxic condition (Hsu et al., 2009). The same findings were also observed in primary AML samples where hypoxia improved the recoverable leukaemia cells after cytarabine treatment when compared to the treated cells in 20% oxygen culture (Griessinger et al., 2014). Notably, both of the chemotherapy agents, especially cytarabine, require cells in the S phase of cell cycle for an effective anti-leukaemic activity (Mills et al., 2018, Farge et al., 2017, Kufe et al., 1980). In line with that, hypoxia induced smaller S phase and G0G1 accumulation hence decreases the sensitivity of this drug (Drolle et al., 2015). The antiapoptosis signalling has been shown to be the protective mechanism in hypoxia-induced chemoresistance (Drolle et al., 2015, Petit et al., 2016). Increased expression of the antiapoptotic proteins was shown to inhibit apoptosis in AML and ALL cells treated with chemotherapy standard treatment agents (Drolle et al., 2015, Petit et al., 2016). Furthermore, in the low oxygen condition, leukaemic cells activate the PI3K pathway and promote cell survival and growth (Drolle et al., 2015).

7.3 Targeting *SLC2A3* and *PFKP* in RUNX1/ETO-leukaemia

7.3.1 *SLC2A3 is not essential for RUNX1/ETO-leukaemia progression in vivo in Kasumi-1 cells but is required in vitro in glucose and oxygen limitation conditions*

Knockdown of *SLC2A3* led to the expansion of the leukaemic population as described in chapter 3. Although *SLC2A3* was shown to be correlated with cancer progression (Cosset et al., 2017, Fei et al., 2012), this was not the case in this study. One possible reason for this is the doxycycline effect. The previous shRNA screen utilised a doxycycline-inducible pTRIPZ vector to induce shRNA expression and gene knockdown. Doxycycline is reported to have an impact on the metabolic gene expression (Ahler et al., 2013). Glycolysis and OXPHOS pathways are enriched in breast cancer cell line, MCF12A, when treated with 1 μg/ml of doxycycline. Ahler et al. (2013) also showed that expression of the *PFK* gene was significantly enriched; however, there was no indication of any glucose transporters being upregulated upon

treatment with the doxycycline. Notably, this finding was conducted *in vitro,* where in our case, there was no indication of *PFKP* and *SLC2A3* as potential candidate genes *in vitro.* Furthermore, both GSEA analysis and RNA sequencing data clearly showed that the glycolysis pathway (Figure 5-1) and *SLC2A3* expression are severely impacted in siRUNX1/ETO treatment (section 3.3.1). Additionally, doxycycline was also reported to impair mitochondrial function in glioma cells, induce glucose consumption in an increasing dose-dependent manner and is associated with decreased cell death (Luger et al., 2018). To confirm a doxycycline effect, a study is being carried out using the inducible vector system which expresses the shRNA targeting *SLC2A3*.

In this study, glucose uptake was compromised in the *SLC2A3* knockdown cells; however, it did not diminish the leukaemic population both *in vivo* (chapter 3) and *in vitro* in standard culture conditions (section 4.3.5). These findings are in agreement with a recent study that demonstrated that low glucose levels did not affect the leukaemic stem cell (LSC) population. Instead, these cells rely more on amino acid metabolism to support proliferation (Jones et al., 2018). A characteristic of LSCs is the presence of low reactive oxygen species (ROS) and their ability to re-established AML *in vivo* re-transplantation (Lagadinou et al., 2013, Jones et al., 2018). Interestingly, only AML blasts with high ROS were affected by glucose starvation (Jones et al., 2018). Furthermore, glucose uptake is not affected in the ROS low LSCs in the absence of amino acids showing that glucose is not essential in this population. This notion was supported by increased production of glycolysis products, pyruvate and lactate in AML high ROS blasts but not in ROS low LSCs (Jones et al., 2018). Jones's study highlighted the metabolic inflexibility of LSCs with regard to glucose metabolism which is in stark contrast to the classic knowledge of high dependence of HSCs on glycolysis (Suda et al., 2011).

Furthermore, the *in vivo* outcomes were also in line with a recent publication that warrants caution when targeting genes related to metabolism. Despite well-established evidence of *HIF* as the main driver for cellular quiescence and chemoresistance (Ishikawa et al., 2007), one study showed that deletion of *HIF-1a* caused unexpected aggressive *in vivo* development of AML after chemotherapy

(Velasco-Hernandez et al., 2018). The transcriptomic analysis of the cells revealed enrichment of mRNA processing, DNA replication and protein folding which support the progression of the disease (Velasco-Hernandez et al., 2018).

Moreover, the *in vitro* competitive assay showed the *SLC2A3* knockdown cells were dependent on glucose and oxygen limitation conditions (section 4.3.5). Limitation of nutrients increases the expressions of the transporters, thereby increasing the dependency of the cells to the transporter. For instance, glutamine starvation increased glutamate transporter (SLC1A3) expression (Tajan et al., 2018). Deletion of *SLC1A3* selectively abrogated cell proliferation in glutamine deprivation condition, but no effect was observed in well-fed glutamine cultures (Tajan et al., 2018). Furthermore, expressions of *SLC2A3* was also shown to be higher in hypoxia environment (section 3.3.3.4), thus, showing that *SLC2A3* is indeed dependent on glucose and oxygen to support the proliferation.

CCND1 and *CCND2* expression was downregulated in the *SLC2A3, PFKP* and double knockdown cells (section 4.3.10). Studies have shown that cell cycle-related protein CCND2 is required for glucose-induced proliferation (Stamateris et al., 2016, Moreno-Asso et al., 2013). Interestingly, glucose controlled the expression of *CCND2* in quiescent β-cells through glucokinase-mediated glycolysis (Salpeter et al., 2011). Glucokinase is the enzyme to mediate phosphorylation of glucose in liver and pancreas. Both low glucose and loss of glucokinase abrogated the CCND2 level in mouse and human β-cells (Salpeter et al., 2011). In addition, in low glucose supply, the cell metabolic sensor, AMPK is activated and stabilises the cell cycle inhibitor, p27 and further increasing cell cycle arrest (El Mjiyad et al., 2010, Jones and Thompson, 2009, Liang et al., 2007).

Moreover, a higher Annexin V positive cells associated with a higher sub G1 fractions were observed in low glucose and oxygen condition in the *SLC2A3* and *PFKP* knockdown cells (section 4.3.9). Hypoxia is shown to mediate glucose-dependent cell death through ATP depletion as shown in a study (Steinbach et al., 2003). Low ATP is a potent activator for AMPK. AMPK could be either tumour-suppressor roles or tumour-supportive roles. Activation of AMPK by metformin attenuates esophageal squamous cell carcinoma and promotes cell death as indicated by increased of

apoptotic cells (Feng et al., 2014). However, in AML, an *in vivo* study demonstrated that activation of AMPK is required for leukaemia initiating cells (LICs) maintenance (Saito et al., 2015). This study also showed that deletion of *AMPK* diminishes LICs located in the bone marrow (Saito et al., 2015).

Furthermore, hypoxia increases intracellular ROS levels in breasts cancer cells (Azimi et al., 2017) and ROS can mediate cell death (Reczek and Chandel, 2017). The notion that hypoxia induced the ROS level is a contrast to the well understanding that the generation of ROS occurs in high oxygen level. The mechanism of which hypoxia induces generation of ROS is not well understood (Murphy, 2012). Recent evidences showed that the mitochondrial ROS (mtROS) is produced at complex III of the electron transport chain in the mitochondria in hypoxia condition and stabilises HIF1-α (Mansfield et al., 2005, Guzy et al., 2005). Consequently, ROS mediates the activation of hypoxia-induced epidermal growth factor receptor and contributes towards breast cancer cells migration (Azimi et al., 2017). ROS is also reported to associate with the increased risk of relapse and poor survival in AML (Johnson et al., 2011). However, current data are lacking on the cause of cell death and further study is required to rule out the mechanistic of the cell death as well as glucose regulation on the cell cycle.

In conclusion, the gain of the *SLC2A3* knockdown cells in the *in vivo* competitive assay setting in this study could be assumed by a scenario. The cells reprogrammed towards more of stem cells-like property to drive leukaemogenesis; thus, they did not rely on glucose for proliferation. Moreover, a study also showed that targeting a gene related to metabolism is not a straightforward approach in eliminating LSCs which was also supported by others (Vukovic et al., 2015, Velasco-Hernandez et al., 2014).

However, this was not the case in the PDX sample where the *SLC2A3* knockdown led to a reduced population in high glucose and oxygen conditions. These cells exhibit a *KIT* activating mutation which confers poor prognosis in the t(8;21) AML (Beghini et al., 2000). The presence of both RUNX1/ETO and KIT mutations resulted in the aggressive leukaemic phenotypes and murine fatality (Nick et al., 2012b). Furthermore, the PDX cells contain wild-type p53 which is in contrast to the Kasumi-1 and SKNO-1 cells used in this study (Banker et al., 1998, Martinez-Soria et al., 2018,

Asou et al., 1991, Matozaki et al., 1995). The roles of p53 in regulating glycolysis will be discussed in section 7.3.3.

7.3.2 *PFKP as a potential therapeutic target in treating RUNX1/ETO-leukaemia*

In vivo and *in vitro* experiments in both cell lines and PDX cells showed that *PFKP* plays an important roles in the RUNX1/ETO leukaemia propagation. *PFKP* is shown to be primarily over-expressed in cancers in comparison to its other isoforms; *PFKL* and *PFKM* (Lee et al., 2017). However, its role and mechanism in tumorigenesis are not well understood. The most comprehensive study to date described the stability of PFKP by AKT to prevent degradation of the protein and promote tumour growth in glioblastoma cell lines (Lee et al., 2017). Notably, activating phosphorylation of AKT exclusively at PFKP Ser386 is shown to be higher in a group of PTEN loss patient samples (Lee et al., 2017). AKT is shown to be activated in many cancer cells (Fang, 2015).

Additionally, although PFKP is considered as the axis in the glycolysis pathway, loss of *PKFP* is not always on the advantage side. Several studies have shown that inhibition of the glycolysis axis redirects glucose flux towards shunt pentose phosphate pathway (PPP) (Yi et al., 2012, Yamamoto et al., 2014, Kim et al., 2017b) and thereby increasing NADPH levels as a protective mechanism from ROS (Kim et al., 2017b). Kim et al. (2017b) also demonstrated knockdown of *PFKP* rescued cancer cells from chemotherapy treatment in breast cancer cells and led to the metastatic potential *in vivo*.

Therefore, *PFKP* could be one of the partner genes required by RUNX1/ETO for the leukaemic program. Future studies should be emphasised on the mechanism and *in vivo* setting in RUNX1/ETO cell lines, primary and PDX leukaemia cells to further validate its therapeutic values. Knockdown of PFKP in normal and leukaemic cells is required to validate the specificity of this gene in leukaemic propagations and survivals.

7.4 RUNX1/ETO and p53 in regulating glycolysis

As described earlier (section 1.5.1), p53 suppression on glycolysis is mediated by the TP53-inducible glycolysis and apoptosis regulator (TIGAR). TIGAR inhibits glycolysis and consequently increases flux through PPP (Bensaad et al., 2006). Previous study has shown that RUNX1/ETO ectopic expression of CD34+ cells causes DNA damage and activates p53 that leads to non-ROS cell death (Krejci et al., 2008). However, in this study, depletion of *RUNX1/ETO* did not change the expression level of *TIGAR*. This could be explained by the presence of functional RUNX1 that acts as the co-activator for p53 transcriptional activities (Wu et al., 2013). Notably, p53 target genes are activated after 5 weeks upon ectopic expression of RUNX1/ETO (Krejci et al., 2008), but the mRNA samples in this study were collected after 24 hour post-siRNA treatment. This notion was also supported that TIGAR is induced in a time-dependent manner after ischemic exposure (Zhou et al., 2016).

Furthermore, p53 modulates expression of glucose transporters (Zhang et al., 2013), such as SLC2A3 (Kawauchi et al., 2008). p53 deficient in Ras-transformed MEF cells upregulated SLC2A3 through activation of IKK/NF-KB pathway in p65 dependent manner and consequently accelerated glycolysis without compromising mitochondrial oxygen consumption (Kawauchi et al., 2008). Notably, SLC2A3 was not the only glycolysis-regulating factor in p53 deficient cells, as p65 knockdown led to a more suppressed Ras-transformation capability. The roles of p53 in suppressing glycolysis was also reported *in vivo* (Zhang et al., 2013). Interestingly, Zhang et al. (2013) showed mutant p53 did not increase expression of any glucose transporters; instead, it promoted translocation of SLC2A1 to the plasma membrane mediated by RhoA/ROCK positive signalling both in mice and breast cancer cell lines. Notably, RhoA pathway is reported to be enriched in RUNX1/ETO (Rodriguez-Perales et al., 2015).

As described in chapter 2, *RUNX1/ETO* strongly regulates *SLC2A3* where the expression was almost depleted in the absence of RUNX1/ETO mRNA. Given that *TIGAR* expression level did not change in the double knockdown approach in the

PDX cells, TIGAR gives an advantage in suppressing glycolysis at the axis of *PFKP.* TIGAR has the function similar to the fructose-2-6-biphosphate, a potent inhibitor for PFKP activity. Therefore, targeting *SLC2A3* and *PFKP* in RUNX1/ETO-leukaemia with wild-type p53 could provide a promising therapeutic strategy (Figure 7-1).

However, given the intra-tumour heterogeneity that presents in either primary or PDX cells, one could target both of the TP53 wild-type and mutated subclones. In order to assess the impact of targeting *SLC2A3* and *PFKP* in TP53 mutated subclones, future experiments should include knockdown of *SLC2A3* and *PFKP* with and without *p53* knockdown in both *in vitro* and *in vivo* settings. This strategy will provide a clear appreciation of how these two genes interact with p53 and further unravel the roles of *SLC2A3* and *PFKP* in this subtype of leukaemia.

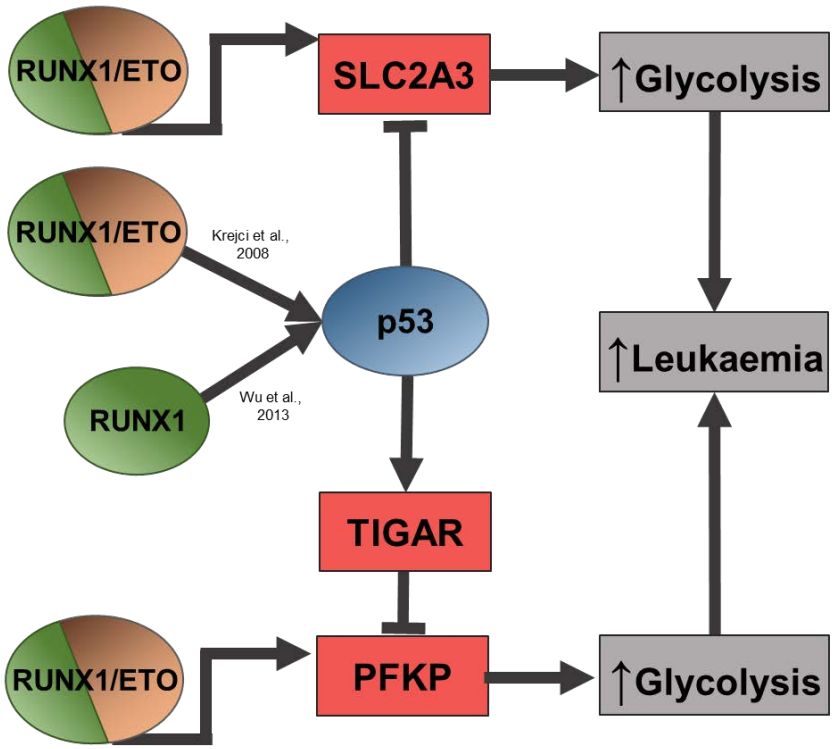

Figure 7-1: Proposed model on RUNX1/ETO cooperation with p53 to mediate glycolysis through SLC2A3 and PFKP. RUNX1/ETO directly targets SLC2A3 and PFKP to promote glycolysis. RUNX1/ETO and RUNX1 competitively regulate p53. P53 controls TIGAR expressions and inhibits glycolysis.

7.5 BM-iPSC-MSC supports RUNX1/ETO PDX cells *in vitro*

Currently, there is a need to establish a pre-clinical model of RUNX1/ETO-leukaemia in order to improve the clinical translation of new targets intervention and drugs strategy. Here I showed, RUNX1/ETO PDX cells can be successfully expanded *ex vivo* with the support of BM-iPSC-MSC niche culture.

Previous studies have shown that mesenchymal stem cells (MSC) culture system supported long-term maintenance of primary AML (Brenner et al., 2017) and primograft ALL blasts *in vitro* (Pal et al., 2016). MSC is easily obtainable; however, its limited lifespan *in vitro* has become a disadvantage for long term application (Baxter et al., 2004) thus a new system is required for the continuous long-term preclinical study. Previous study has shown that induced-MSCs were characterised to exhibit MSC phenotypes and molecular characteristics (Soontararak et al., 2018) making it a suitable platform for a preclinical research.

In this study, leukaemic blasts proliferated at a higher rate with BM-iPSC-MSC support and slightly reduced sub-G1 fractions after 7 days in co-culture. *In vitro* primary AML cell without co-culture support showed stress-induced apoptosis effect associated with low viability (Ryningen et al., 2006). Conversely, co-culture with MSCs shown to have an antiapoptotic effect and support leukaemic growth proliferation through cytokine secretion such as CXCL12 (Brenner et al., 2017). Given that KIT mutation prevalence is high in RUNX1/ETO relapse cases and shorter leukaemia-free survival (Kim et al., 2007), this preclinical model can be a proper model for this subtype of leukaemia. However, more detailed study on the cytokine release by BM-iPSC-MSC and the effect on this PDX should be performed.

Additionally, BM-iPSC-MSC culture reduced the expression of CD34 positive blasts cells and directed the cells toward specific lineage, CD33 and CD15. CD34 is described as the criterium for RUNX1/ETO-leukaemic stemness potential (Mulloy et al., 2003). However, this may not be necessary as the cells are positive for *KIT*+ mutation. Quek et al. (2016) showed that lack of CD34 but the enrichment of *KIT*+ populations have the functional leukaemic stem cells activity. Another study showed

in vivo engraftment success was not linked with the homing capability of CD34+ cells, but mainly correlated with disease behaviour (Pearce et al., 2006). Thus, further experiments are required to determine if the cells are still able to self-renew by either re-transplantation into immunocompromised mice or performing *in vitro* colony formation assay.

Furthermore, expansion of CD15 marks the rise of terminally differentiated myeloid cells which is expressed mainly on mature granulocytes (neutrophils and eosinophils), some monocytes but not on lymphocytes and basophil (Tao et al., 2004). One possible cause of the enrichment is due to IL-3 and G-CSF cytokines that were present in the myeloid expansion media that promote granulocytic differentiation (Mehta et al., 2015, Lachmann et al., 2015).

Consequently, BM-iPSC-MSC supports RUNX1/ETO cells *ex vivo*; however, further optimisation of the myeloid expansion cocktail should be carried out to maintain the leukaemic immunophenotype profiles.

7.6 Palbociclib treated cells reprogrammed metabolic requirement

We have previously shown that palbociclib could provide a novel therapeutic value in treating RUNX1/ETO-leukaemia (Martinez-Soria et al., 2018). Palbociclib treated cells stopped the cells from proliferating by decreasing the cell cycle-related proteins (CDK4/6) and led to senescent (Martinez-Soria et al., 2018). Interestingly, inhibition of the cell cycle machinery by palbociclib at a ten-fold higher concentration than this study caused reactive oxygen species (ROS)-mediated cell death (Wang et al., 2017a, Vijayaraghavan et al., 2017). Wang et al. (2017a) also demonstrated that palbociclib treated cells drive autophagy as a cell-protective mechanism and combination with autophagy inhibitor synergistically induced senescence. Senescence is thought to be an anticancer activity. However, a recent study shows that senescent cells acquired senescence-associated secretory phenotype (SASP) that directly causes transformation of adjacent cells and destruction of the extracellular matrix, a hallmark of cancer growth (Schosserer et al., 2017). SASP

factors include interleukin-1 and -6 that is known to promote tumorigenesis (Kumari et al., 2016), and p-53 loss caused more chemokines than wild-type p53 such as TECK and CXCL5 (Singh et al., 2011, Coppé et al., 2010).

We have also shown that palbociclib treated cells shared a significant signature correlated with the RUNX1/ETO knockdown, making it more attractive for further exploration (Martinez-Soria et al., 2018). In this study, the limitation of glutamine induced resistance in Kasumi-1 cells (section 5.3.2.6) which is in contrast to the well-documented evidence that glutamine deficiency abrogated cell proliferation (Kim et al., 2017a, Tran et al., 2017). Interestingly, a study showed that low glutamine induced BRAF-resistant melanoma cells through histone hypermethylation of H3K27 (Pan et al., 2016). Furthermore, glutamine deficiency caused the depletion of αKG which is the critical factor for histone demethylases. Cross-checked with GSEA analysis showed that genes in glutaminolysis pathway were also impaired in palbociclib treated cells. A question, therefore, arises here. Is the resistance mechanism in G0G1 populations in palbociclib-treated cells are related to the glutamine deficiency?

Furthermore, palbociclib treatment increased ATP production, a consequence of OXPHOS. However, this is in contrast to the low ATP level detected in the G0G1 phase (Du et al., 2017). Furthermore, the ROS levels decreased in palbociclib cells in both standard and glutamine deficiency media. Jones et al., (2018) demonstrated that LSCs are associated with low ROS and not affected by glutamine deprivation. In particular, Farge et al. (2017), have shown high OXPHOS AML cells were exclusively chemo-resistant *in vivo.* The LSCs have been shown to associate with dormancy in G0 population (Al-Asadi et al., 2016), but there was no enrichment of this population in palbociclib treated cells. Nevertheless, Jones et al. study has opened a new perspective in targeting LSCs through metabolic rewiring of the resistance cells. This leads to an open question with current experimental strategy using palbociclib, in which the treatment caused changes in metabolic characteristics and requires further attention. Future study to determine the characteristics of these populations is particularly pertinent for selective combination to eliminate these cells.

7.7 Glycolysis and cell cycle inhibitors as a possible therapeutic combination

Current leukaemia treatments involve intensive and genotoxic chemotherapy, which can severely affect patients' quality of life; hence low-risk treatment regiments are required to address this issue.

The RUNX1/ETO cells showed to be more sensitive to 2DG inhibition in comparison to other AML cells (chapter 5). This observation is in agreement with the previous study that RUNX1/ETO cells are more sensitive to 2DG inhibition but show resistant towards OXPHOS inhibition (Miwa et al., 2008). Furthermore, lower glucose uptake was observed in the hypoxia than in normoxia condition in wild-type cells (section 3.3.3.4). This finding further corroborates that 2DG is more effective in hypoxic condition as the low oxygen induces more glycolytic phenotype. For instance, in Burkitt lymphoma cells, the sensitivity of 2DG is four times lower in hypoxia than in normoxia condition (Pang et al., 2015). Nevertheless, 2DG is also shown to modulate cancer cells in normoxia successfully. A low dose of 2DG is not only effective to eradicate ALL cells in normoxia (Gu et al., 2017) but also sensitise glucocorticoid-resistant cells to chemotherapy drugs (Gu et al., 2017, Hulleman et al., 2009).

Furthermore, as hypoxia is described as common feature of the tumour microenvironment (Hohenberger et al., 1998, Rundqvist and Johnson, 2013), 2DG is suggested to have even more powerful therapeutic efficiency *in vivo* than *in vitro.* However, some studies have shown that 2DG alone is not sufficient to eliminate cancer cells *in vivo* (Goldberg et al., 2012, Maschek et al., 2004), Sobhakumari et al. (2016). Instead, combinations of 2DG with other anti-tumour agents result in greater effect in comparison with every single treatment (Goldberg et al., 2012, Maschek et al., 2004).

Moreover, 2DG induced cell death as indicated by Annexin V staining (section 5.3.2.2). 2DG mediates cell death mechanism through the induction of pro-apoptotic protein, Bax (Zagorodna et al., 2011). Besides, 2DG also caused the reduction of intracellular ATP levels seen in chronic lymphocytic leukaemia (Tidmarsh et al., 2004). Reduced ATP level is thought to be the mechanism of 2DG sensitisation in drug combination study. Lack of ATP caused p-glycoprotein to cease its function to

pump out small molecule inhibitor, thus sensitise the cells towards the treatment (Sauna et al., 2001, Tagg et al., 2008). On the contrary, 2DG antileukaemic activity on T-ALL cells was not due to glycolytic inhibition (Gu et al., 2017). Instead, 2DG cell death was induced through N-linked glycosylation and endoplasmic reticulum stress-mediated apoptosis.

The *in vitro* study has shown a possible combination of 2DG and palbociclib, further study on the mechanism should be carried out which include both *in vitro* and *in vivo* platforms. Moreover, palbociclib has the potential therapeutic values and has been used in a combination of clinically available drugs in breast cancer treatment (Finn et al., 2016). Therefore, an ongoing study is being carried out to focus on the resistance side of palbociclib as well as repurposing with other clinically available anti-leukaemic agents.

7.8 Limitation and future work

SLC2A3 and *PFKP* were identified *in vivo* but not *in vitro* in the shRNA screen. This has become quite a challenge in validating these partner genes as there is no proper *in vivo* model for RUNX1/ETO-leukaemia. Furthermore, although we have improved the transplantation capability of Kasumi-1 cells through the intrahepatic injection method in RG mice; however, there were issues with the engraftments involving *SLC2A3* and *PFKP* knockdown cells as clearly indicated in the two experiments described in chapter 3. Furthermore, 2DG inhibition might be of benefit in eradicating leukaemia cells and could provide improved sensitisation for palbociclib treatment.

Additionally, during the labwork phase, I encountered with a lentiviral production problem which lasted approximately eight months until it was improved. This had caused me a delay mainly in the *in vitro* work.

Nevertheless, from this study, several key questions have arisen and provide potential future works.

i. The resistance showed in RUNX1/ETO knockdown in Kasumi-1 cells in hypoxia indicates roles of hypoxia in modulating resistancy. This observation was also

shown previously where the knockdown of RUNX1/ETO did not lead to survival advantage *in vivo* (Mr Hasan's thesis, 2019).This could be a model of relapse in RUNX1/ETO leukaemia which worth an investigation. Future study will emphasise on the roles of HIF-1a in regulating the resistance populations as well as gene expressions profiling to check the enriched pathways. The enrich pathways will be cross-examined with current expressions profile of RUNX1/ETO knockdown in normoxia.

ii. Glutamine deficiency leads to resistance in the palbociclib treated cells which is further evident by low ROS levels. Further investigations on how and why this metabolite caused resistance could provide an insight into how we can manipulate this substance for therapeutic strategy. Moreover, recent publications showed that cancer cells are not only dependent on the glutamine and glucose. Instead, amino acids also play the roles in maintaining LSCs to fuel shunt metabolic pathway as shown in Jones et al. study. Future study will include assays of the leukaemic cells in different nutrient conditions to measure the dependency of the cells toward each nutrient. This will be followed by changes in metabolic activity possibly through Seahorse, ATP and lactic acid assays.

7.9 Concluding remarks and outlook

This study has provided an insight into metabolic rewiring in RUNX1/ETO-leukaemia cells. The *in vivo* study has yet to prove the potential therapeutic value for *SLC2A3*, but *in vitro* analyses showed the variable response towards different nutrient and oxygen conditions. Contrasting findings in this study to the well-documented evidences indicate that targeting metabolic reprogram in cancers is not a straight forward approach, as the cells could shunt to another complex pathway in order to survive. Furthermore, the complexity of rewired metabolism is even further extended by tumour heterogeneity which is present in AML. This requires a better understanding of the underlying genetic and biochemical processes that support tumour development, progression and therapy resistance.

APPENDIX

Appendix 7-1: The E-box protein at the locus of RUNX1/ETO binding site downstream of *SLC2A3* (highlighted in red box).

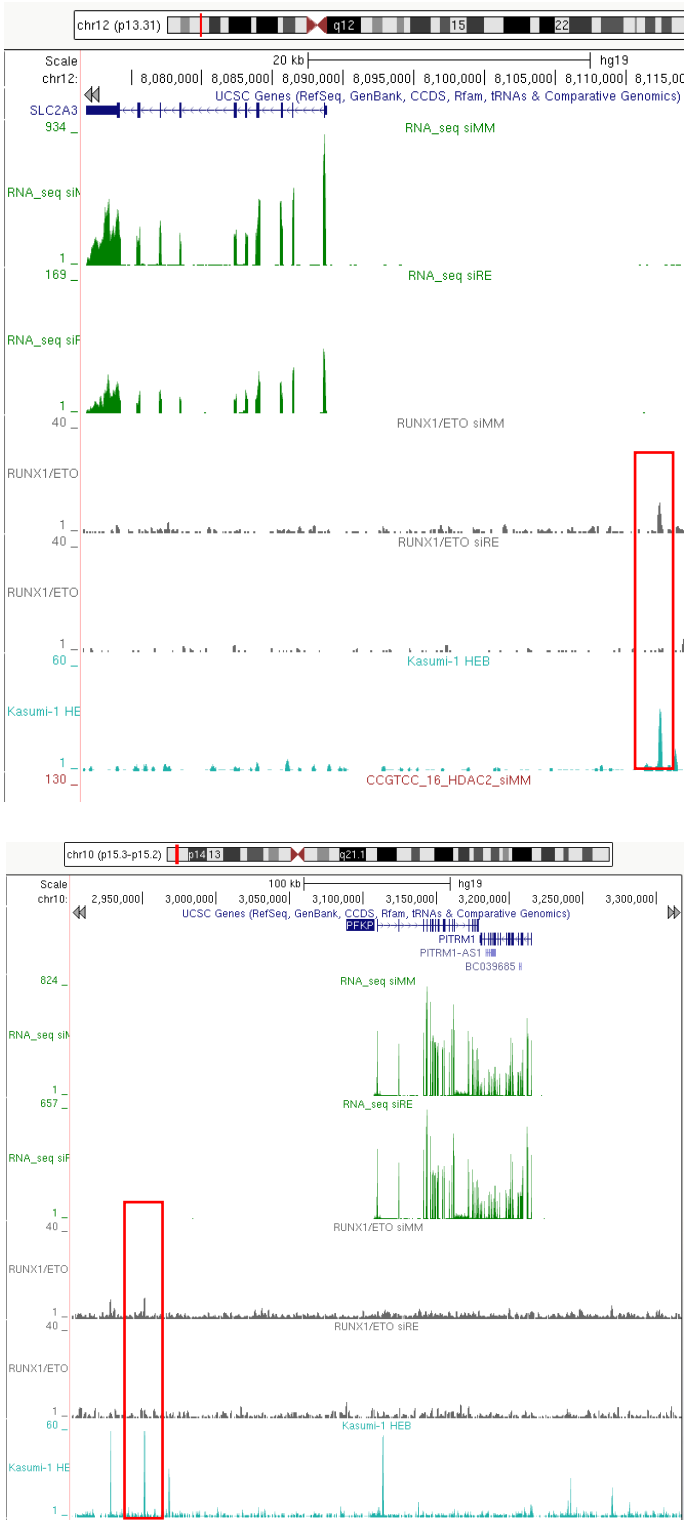

Appendix 7-2: The expressions of *PKM* isoforms upon depletion of *RUNX1/ETO* in Kasumi-1 cells.

REFERENCE

ABRAHAMSSON, J., CLAUSEN, N., GUSTAFSSON, G., HOVI, L., JONMUNDSSON, G., ZELLER, B., FORESTIER, E., HELDRUP, J., HASLE, H., FOR THE NORDIC SOCIETY FOR PAEDIATRIC, H. & ONCOLOGY 2007. Improved outcome after relapse in children with acute myeloid leukaemia. *British Journal of Haematology,* 136**,** 229-236.

AFT, R. L., ZHANG, F. W. & GIUS, D. 2002. Evaluation of 2-deoxy-D-glucose as a chemotherapeutic agent: mechanism of cell death. *British Journal Of Cancer,* 87**,** 805.

AHLER, E., SULLIVAN, W. J., CASS, A., BRAAS, D., YORK, A. G., BENSINGER, S. J., GRAEBER, T. G. & CHRISTOFK, H. R. 2013. Doxycycline alters metabolism and proliferation of human cell lines. *PloS one,* 8**,** e64561-e64561.

AL-ASADI, M. G., CASTELLANOS, M., MAY, S. T., RUSSELL, N. H., SEEDHOUSE, C. H. & PALLIS, M. 2016. Molecular Signature of Dormancy in CD34+CD38- Acute Myeloid Leukaemia Cells. *Blood,* 128**,** 1660-1660.

AL-ISSA, K. & NAZHA, A. 2016. Molecular landscape in acute myeloid leukemia: where do we stand in 2016. *Cancer biology & medicine,* 13**,** 474-482.

AMANN, J. M., NIP, J., STROM, D. K., LUTTERBACH, B., HARADA, H., LENNY, N., DOWNING, J. R., MEYERS, S. & HIEBERT, S. W. 2001. ETO, a Target of t(8;21) in Acute Leukemia, Makes Distinct Contacts with Multiple Histone Deacetylases and Binds mSin3A through Its Oligomerization Domain. *Molecular and Cellular Biology,* 21**,** 6470-6483.

AN, D. S., QIN, F. X.-F., AUYEUNG, V. C., MAO, S. H., KUNG, S. K. P., BALTIMORE, D. & CHEN, I. S. Y. 2006. Optimization and functional effects of stable short hairpin RNA expression in primary human lymphocytes via lentiviral vectors. *Molecular therapy : the journal of the American Society of Gene Therapy,* 14**,** 494-504.

ARBUCKLE, M. I., KANE, S., PORTER, L. M., SEATTER, M. J. & GOULD, G. W. 1996. Structure−Function Analysis of Liver-Type (GLUT2) and Brain-Type (GLUT3) Glucose Transporters: Expression of Chimeric Transporters in

Xenopus Oocytes Suggests an Important Role for Putative Transmembrane Helix 7 in Determining Substrate Selectivity. *Biochemistry,* 35**,** 16519-16527.

ASOU, H., TASHIRO, S., HAMAMOTO, K., OTSUJI, A., KITA, K. & KAMADA, N. 1991. Establishment of a human acute myeloid leukemia cell line (Kasumi-1) with 8;21 chromosome translocation. *Blood,* 77**,** 2031-2036.

ASSI, S. A., IMPERATO, M. R., COLEMAN, D. J. L., PICKIN, A., POTLURI, S., PTASINSKA, A., CHIN, P. S., BLAIR, H., CAUCHY, P., JAMES, S. R., ZACARIAS-CABEZA, J., GILDING, L. N., BEGGS, A., CLOKIE, S., LOKE, J. C., JENKIN, P., UDDIN, A., DELWEL, R., RICHARDS, S. J., RAGHAVAN, M., GRIFFITHS, M. J., HEIDENREICH, O., COCKERILL, P. N. & BONIFER, C. 2019. Subtype-specific regulatory network rewiring in acute myeloid leukemia. *Nature Genetics,* 51**,** 151-162.

AZIMI, I., PETERSEN, R. M., THOMPSON, E. W., ROBERTS-THOMSON, S. J. & MONTEITH, G. R. 2017. Hypoxia-induced reactive oxygen species mediate N-cadherin and SERPINE1 expression, EGFR signalling and motility in MDA-MB-468 breast cancer cells. *Scientific Reports,* 7**,** 15140.

BAGGER, F. O., SASIVAREVIC, D., SOHI, S. H., LAURSEN, L. G., PUNDHIR, S., SØNDERBY, C. K., WINTHER, O., RAPIN, N. & PORSE, B. T. 2016. BloodSpot: a database of gene expression profiles and transcriptional programs for healthy and malignant haematopoiesis. *Nucleic Acids Research,* 44**,** D917-D924.

BAKIRI, L., MATSUO, K., WISNIEWSKA, M., WAGNER, E. F. & YANIV, M. 2002. Promoter Specificity and Biological Activity of Tethered AP-1 Dimers. *Molecular and Cellular Biology,* 22**,** 4952.

BANERJEA, A., LI, M.-J., BAUER, G., REMLING, L., LEE, N.-S., ROSSI, J. & AKKINA, R. 2003. Inhibition of HIV-1 by lentiviral vector-transduced siRNAs in T lymphocytes differentiated in SCID-hu mice and CD34+ progenitor cell-derived macrophages. *Molecular Therapy,* 8**,** 62-71.

BANKER, D. E., RADICH, J., BECKER, A., KERKOF, K., NORWOOD, T., WILLMAN, C. & APPELBAUM, F. R. 1998. The t(8;21) translocation is not consistently associated with high Bcl-2 expression in de novo acute myeloid leukemias of adults. *Clinical Cancer Research,* 4**,** 3051-3062.

BAXTER, M. A., WYNN, R. F., JOWITT, S. N., WRAITH, J. E., FAIRBAIRN, L. J. & BELLANTUONO, I. 2004. Study of Telomere Length Reveals Rapid Aging of Human Marrow Stromal Cells following In Vitro Expansion. *STEM CELLS,* 22**,** 675-682.

BEGHINI, A., PETERLONGO, P., RIPAMONTI, C. B., LARIZZA, L., CAIROLI, R., MORRA, E. & MECUCCI, C. 2000. C-kit mutations in core binding factor leukemias. *Blood,* 95**,** 726-728.

BEN-AMI, O., FRIEDMAN, D., LESHKOWITZ, D., GOLDENBERG, D., ORLOVSKY, K., PENCOVICH, N., LOTEM, J., TANAY, A. & GRONER, Y. 2013. Addiction of t(8;21) and inv(16) Acute Myeloid Leukemia to Native RUNX1. *Cell Reports,* 4**,** 1131-1143.

BENSAAD, K., TSURUTA, A., SELAK, M. A., VIDAL, M. N. C., NAKANO, K., BARTRONS, R., GOTTLIEB, E. & VOUSDEN, K. H. 2006. TIGAR, a p53-Inducible Regulator of Glycolysis and Apoptosis. *Cell,* 126**,** 107-120.

BHATIA, M., WANG, J. C. Y., KAPP, U., BONNET, D. & DICK, J. E. 1997. Purification of primitive human hematopoietic cells capable of repopulating immune-deficient mice. *Proceedings of the National Academy of Sciences,* 94**,** 5320-5325.

BOMKEN, S., BUECHLER, L., REHE, K., PONTHAN, F., ELDER, A., BLAIR, H., BACON, C. M., VORMOOR, J. & HEIDENREICH, O. 2013. Lentiviral marking of patient-derived acute lymphoblastic leukaemic cells allows in vivo tracking of disease progression. *Leukemia,* 27**,** 10.1038/leu.2012.206.

BORTHAKUR, G., KANTARJIAN, H., WANG, X., PLUNKETT, W. K., JR., GANDHI, V. V., FADERL, S., GARCIA-MANERO, G., RAVANDI, F., PIERCE, S. & ESTEY, E. H. 2008. Treatment of core-binding-factor in acute myelogenous leukemia with fludarabine, cytarabine, and granulocyte colony-stimulating factor results in improved event-free survival. *Cancer,* 113**,** 3181-3185.

BORTNER, C. D. & CIDLOWSKI, J. A. 2002. Apoptotic volume decrease and the incredible shrinking cell. *Cell Death And Differentiation,* 9**,** 1307.

BOWEN, D. T., FREW, M. E., HILLS, R., GALE, R. E., WHEATLEY, K., GROVES, M. J., LANGABEER, S. E., KOTTARIDIS, P. D., MOORMAN, A. V., BURNETT, A. K. & LINCH, D. C. 2005. RAS mutation in

acute myeloid leukemia is associated with distinct cytogenetic subgroups but does not influence outcome in patients younger than 60 years. *Blood,* 106**,** 2113.

BRENNER, A. K., NEPSTAD, I. & BRUSERUD, Ø. 2017. Mesenchymal Stem Cells Support Survival and Proliferation of Primary Human Acute Myeloid Leukemia Cells through Heterogeneous Molecular Mechanisms. *Frontiers in immunology,* 8**,** 106-106.

BROWN, R. S., GOODMAN, T. M., ZASADNY, K. R., GREENSON, J. K. & WAHL, R. L. 2002. Expression of hexokinase II and Glut-1 in untreated human breast cancer. *Nuclear Medicine and Biology,* 29**,** 443-453.

BURGESS, D. J. 2013. Glutamine connections. *Nature Reviews Cancer,* 13**,** 293.

BURJANIVOVA, T., MADZO, J., MUZIKOVA, K., MEYER, C., SCHNEIDER, B., VOTAVA, F., MARSCHALEK, R., STARY, J., TRKA, J. & ZUNA, J. 2006. Prenatal origin of childhood AML occurs less frequently than in childhood ALL. *BMC cancer,* 6**,** 100-100.

BURNETT, A. K., HILLS, R. K., MILLIGAN, D., KJELDSEN, L., KELL, J., RUSSELL, N. H., YIN, J. A. L., HUNTER, A., GOLDSTONE, A. H. & WHEATLEY, K. 2010. Identification of Patients With Acute Myeloblastic Leukemia Who Benefit From the Addition of Gemtuzumab Ozogamicin: Results of the MRC AML15 Trial. *Journal of Clinical Oncology,* 29**,** 369-377.

BYRD, J. C., DODGE, R. K., CARROLL, A., BAER, M. R., EDWARDS, C., STAMBERG, J., QUMSIYEH, M., MOORE, J. O., MAYER, R. J., DAVEY, F., SCHIFFER, C. A. & BLOOMFIELD, C. D. 1999. Patients With t(8;21)(q22;q22) and Acute Myeloid Leukemia Have Superior Failure-Free and Overall Survival When Repetitive Cycles of High-Dose Cytarabine Are Administered. *Journal of Clinical Oncology,* 17**,** 3767-3775.

BYRD, J. C., MRÓZEK, K., DODGE, R. K., CARROLL, A. J., EDWARDS, C. G., ARTHUR, D. C., PETTENATI, M. J., PATIL, S. R., RAO, K. W., WATSON, M. S., KODURU, P. R. K., MOORE, J. O., STONE, R. M., MAYER, R. J., FELDMAN, E. J., DAVEY, F. R., SCHIFFER, C. A., LARSON, R. A. & BLOOMFIELD, C. D. 2002. Pretreatment cytogenetic abnormalities are predictive of induction success, cumulative incidence of relapse, and overall

survival in adult patients with de novo acute myeloid leukemia: results from Cancer and Leukemia Group B (CALGB 8461). <*span class="subtitle">Presented in part at the 43rd annual meeting of the American Society of Hematology, Orlando, FL, December 10, 2001, and published in abstract form.⁵⁹ ,* 100**,** 4325-4336.

BYRD, J. C., RUPPERT, A. S., MRÓZEK, K., CARROLL, A. J., EDWARDS, C. G., ARTHUR, D. C., PETTENATI, M. J., STAMBERG, J., KODURU, P. R. K., MOORE, J. O., MAYER, R. J., DAVEY, F. R., LARSON, R. A. & BLOOMFIELD, C. D. 2004. Repetitive Cycles of High-Dose Cytarabine Benefit Patients With Acute Myeloid Leukemia and inv(16)(p13q22) or t(16;16)(p13;q22): Results from CALGB 8461. *Journal of Clinical Oncology,* 22**,** 1087-1094.

CALABI, F., PANNELL, R. & PAVLOSKA, G. 2001. Gene targeting reveals a crucial role for MTG8 in the gut. *Molecular and cellular biology,* 21**,** 5658-5666.

CAMERON, S., TAYLOR, D. S., TEPAS, E. C., SPECK, N. A. & MATHEY-PREVOT, B. 1994. Identification of a critical regulatory site in the human interleukin-3 promoter by in vivo footprinting. *Blood,* 83**,** 2851-2859.

CHENG, G., ZIELONKA, J., DRANKA, B. P., MCALLISTER, D., MACKINNON, A. C., JR., JOSEPH, J. & KALYANARAMAN, B. 2012. Mitochondria-targeted drugs synergize with 2-deoxyglucose to trigger breast cancer cell death. *Cancer research,* 72**,** 2634-2644.

CHOI, Y.-K. & PARK, K.-G. 2018. Targeting Glutamine Metabolism for Cancer Treatment. *Biomolecules & therapeutics,* 26**,** 19-28.

CHOI, Y., ELAGIB, K. E., DELEHANTY, L. L. & GOLDFARB, A. N. 2006. Erythroid Inhibition by the Leukemic Fusion AML1-ETO Is Associated with Impaired Acetylation of the Major Erythroid Transcription Factor GATA-1. *Cancer Research,* 66**,** 2990.

CHOU, T.-C. 2010. Drug Combination Studies and Their Synergy Quantification Using the Chou-Talalay Method. *Cancer Research,* 70**,** 440-446.

CHOU, T.-C. & TALALAY, P. 1984. Quantitative analysis of dose-effect relationships: the combined effects of multiple drugs or enzyme inhibitors. *Advances in Enzyme Regulation,* 22**,** 27-55.

CHRISTENSEN, D. R., CALDER, P. C. & HOUGHTON, F. D. 2015. GLUT3 and PKM2 regulate OCT4 expression and support the hypoxic culture of human embryonic stem cells. *Scientific Reports,* 5**,** 17500.

COLVIN, G. A., BERZ, D., QUESENBERRY, P. J., PAPA, E. & LIU, L. 2009. Short-Term Hematopoietic Stem Cells (ST-HSC) Have Full Long-Term Capacity with Sustained but Reduced Potential Compared with LT-HSC. *Blood,* 114**,** 2550.

COPLEY, M. R., BEER, P. A. & EAVES, C. J. 2012. Hematopoietic Stem Cell Heterogeneity Takes Center Stage. *Cell Stem Cell,* 10**,** 690-697.

COPPÉ, J.-P., DESPREZ, P.-Y., KRTOLICA, A. & CAMPISI, J. 2010. The senescence-associated secretory phenotype: the dark side of tumor suppression. *Annual review of pathology,* 5**,** 99-118.

COSSET, É., ILMJÄRV, S., DUTOIT, V., ELLIOTT, K., VON SCHALSCHA, T., CAMARGO, M. F., REISS, A., MOROISHI, T., SEGUIN, L., GOMEZ, G., MOO, J.-S., PREYNAT-SEAUVE, O., KRAUSE, K.-H., CHNEIWEISS, H., SARKARIA, J. N., GUAN, K.-L., DIETRICH, P.-Y., WEIS, S. M., MISCHEL, P. S. & CHERESH, D. A. 2017. Glut3 Addiction Is a Druggable Vulnerability for a Molecularly Defined Subpopulation of Glioblastoma. *Cancer Cell,* 32**,** 856-868.e5.

CRISAN, M. & DZIERZAK, E. 2016. The many faces of hematopoietic stem cell heterogeneity. *Development,* 143**,** 4571.

CUBITT, C. L., MENTH, J., DAWSON, J., MARTINEZ, G. V., FOROUTAN, P., MORSE, D. L., BUI, M. M., LETSON, G. D., SULLIVAN, D. M. & REED, D. R. 2013. Rapid Screening of Novel Agents for Combination Therapy in Sarcomas. *Sarcoma,* 2013**,** 12.

CURTIS, N. J., MOONEY, L., HOPCROFT, L., MICHOPOULOS, F., WHALLEY, N., ZHONG, H., MURRAY, C., LOGIE, A., REVILL, M., BYTH, K. F., BENJAMIN, A. D., FIRTH, M. A., GREEN, S., SMITH, P. D. & CRITCHLOW, S. E. 2017. Pre-clinical pharmacology of AZD3965, a selective inhibitor of MCT1: DLBCL, NHL and Burkitt's lymphoma anti-tumor activity. *Oncotarget,* 8**,** 69219-69236.

DANG, L., WHITE, D. W., GROSS, S., BENNETT, B. D., BITTINGER, M. A., DRIGGERS, E. M., FANTIN, V. R., JANG, H. G., JIN, S., KEENAN, M. C., MARKS, K. M., PRINS, R. M., WARD, P. S., YEN, K. E., LIAU, L. M.,

RABINOWITZ, J. D., CANTLEY, L. C., THOMPSON, C. B., VANDER HEIDEN, M. G. & SU, S. M. 2009. Cancer-associated IDH1 mutations produce 2-hydroxyglutarate. *Nature,* 462**,** 739.

DAVIS, J. N., MCGHEE, L. & MEYERS, S. 2003. The ETO (MTG8) gene family. *Gene,* 303**,** 1-10.

DE ROOIJ, J. D. E., ZWAAN, C. M. & VAN DEN HEUVEL-EIBRINK, M. 2015. Pediatric AML: From Biology to Clinical Management. *Journal of clinical medicine,* 4**,** 127-149.

DEPREZ, J., VERTOMMEN, D., ALESSI, D. R., HUE, L. & RIDER, M. H. 1997. Phosphorylation and Activation of Heart 6-Phosphofructo-2-kinase by Protein Kinase B and Other Protein Kinases of the Insulin Signaling Cascades. *Journal of Biological Chemistry,* 272**,** 17269-17275.

DEYNOUX, M., SUNTER, N., HÉRAULT, O. & MAZURIER, F. 2016. Hypoxia and Hypoxia-Inducible Factors in Leukemias. *Frontiers in oncology,* 6**,** 41-41.

DICKINS, R. A., HEMANN, M. T., ZILFOU, J. T., SIMPSON, D. R., IBARRA, I., HANNON, G. J. & LOWE, S. W. 2005. Probing tumor phenotypes using stable and regulated synthetic microRNA precursors. *Nature Genetics,* 37**,** 1289.

DINARDO, C. D., RAVANDI, F., AGRESTA, S., KONOPLEVA, M., TAKAHASHI, K., KADIA, T., ROUTBORT, M., PATEL, K. P., MARK, B., PIERCE, S., GARCIA-MANERO, G., CORTES, J. & KANTARJIAN, H. 2015. Characteristics, clinical outcome, and prognostic significance of IDH mutations in AML. *American journal of hematology,* 90**,** 732-736.

DROLLE, H., WAGNER, M., VASOLD, J., KÜTT, A., DENIFFEL, C., SOTLAR, K., SIRONI, S., HEROLD, T., RIEGER, C. & FIEGL, M. 2015. Hypoxia regulates proliferation of acute myeloid leukemia and sensitivity against chemotherapy. *Leukemia Research,* 39**,** 779-785.

DU, X., FU, X., YAO, K., LAN, Z., XU, H., CUI, Q. & YANG, E. 2017. Bcl-2 delays cell cycle through mitochondrial ATP and ROS. *Cell cycle (Georgetown, Tex.),* 16**,** 707-713.

EL MJIYAD, N., CARO-MALDONADO, A., RAMÍREZ-PEINADO, S. & MUÑOZ-PINEDO, C. 2010. Sugar-free approaches to cancer cell killing. *Oncogene,* 30**,** 253.

ELDER, A., BOMKEN, S., WILSON, I., BLAIR, H. J., COCKELL, S., PONTHAN, F., DORMON, K., PAL, D., HEIDENREICH, O. & VORMOOR, J. 2017. Abundant and equipotent founder cells establish and maintain acute lymphoblastic leukaemia. *Leukemia,* 31**,** 2577.

ERMAN, B., CORTES, M., NIKOLAJCZYK, B. S., SPECK, N. A. & SEN, R. 1998. ETS-core binding factor: a common composite motif in antigen receptor gene enhancers. *Molecular and cellular biology,* 18**,** 1322-1330.

FANG, J., ZHOU, S., FAN, J., YAN, S. 2015. Roles of glucose transporter-1 and the phosphatidylinositol 3‑kinase/protein kinase B pathway in cancer radioresistance. *Molecular Medicine Reports,* 11.

FARGE, T., SALAND, E., DE TONI, F., AROUA, N., HOSSEINI, M., PERRY, R., BOSC, C., SUGITA, M., STUANI, L., FRAISSE, M., SCOTLAND, S., LARRUE, C., BOUTZEN, H., FÉLIU, V., NICOLAU-TRAVERS, M.-L., CASSANT-SOURDY, S., BROIN, N., DAVID, M., SERHAN, N., SARRY, A., TAVITIAN, S., KAOMA, T., VALLAR, L., IACOVONI, J., LINARES, L. K., MONTERSINO, C., CASTELLANO, R., GRIESSINGER, E., COLLETTE, Y., DUCHAMP, O., BARREIRA, Y., HIRSCH, P., PALAMA, T., GALES, L., DELHOMMEAU, F., GARMY-SUSINI, B. H., PORTAIS, J.-C., VERGEZ, F., SELAK, M., DANET-DESNOYERS, G., CARROLL, M., RÉCHER, C. & SARRY, J. E. 2017. Chemotherapy Resistant Human Acute Myeloid Leukemia Cells are Not Enriched for Leukemic Stem Cells but Require Oxidative Metabolism. *Cancer Discovery*.

FATHI, A. T., SADRZADEH, H., BORGER, D. R., BALLEN, K. K., AMREIN, P. C., ATTAR, E. C., FOSTER, J., BURKE, M., LOPEZ, H. U., MATULIS, C. R., EDMONDS, K. M., IAFRATE, A. J., STRALEY, K. S., YEN, K. E., AGRESTA, S., SCHENKEIN, D. P., HILL, C., EMADI, A., NEUBERG, D. S., STONE, R. M. & CHEN, Y.-B. 2012. Prospective serial evaluation of 2-hydroxyglutarate, during treatment of newly diagnosed acute myeloid leukemia, to assess disease activity and therapeutic response. *Blood,* 120**,** 4649.

FEI, X., QI, M., WU, B., SONG, Y., WANG, Y. & LI, T. 2012. MicroRNA-195-5p suppresses glucose uptake and proliferation of human bladder cancer T24 cells by regulating GLUT3 expression. *FEBS Letters,* 586**,** 392-397.

FENG, Y., KE, C., TANG, Q., DONG, H., ZHENG, X., LIN, W., KE, J., HUANG, J., YEUNG, S. C. & ZHANG, H. 2014. Metformin promotes autophagy and apoptosis in esophageal squamous cell carcinoma by downregulating Stat3 signaling. *Cell Death &Amp; Disease,* 5**,** e1088.

FERRARI, A., PAPAYANNIDIS, C., BALDAZZI, C., IACOBUCCI, I., PAOLINI, S., PADELLA, A., GUADAGNUOLO, V., PERRICONE, M., ROBUSTELLI, V., VENTURI, C., ABBENANTE, M. C., PARISI, S., SARTOR, C., VOLPATO, F., TESTONI, N., SIMONETTI, G., OTTAVIANI, E. & MARTINELLI, G. 2014. Leukemia Associated TP53 Mutations in AML Patients ARE Strongly Associated with Complex Karyotype and Poor Outcome. *Blood,* 124**,** 2379.

FIDLER, T. P., CAMPBELL, R. A., FUNARI, T., DUNNE, N., BALDERAS ANGELES, E., MIDDLETON, E. A., CHAUDHURI, D., WEYRICH, A. S. & ABEL, E. D. 2017. Deletion of GLUT1 and GLUT3 Reveals Multiple Roles for Glucose Metabolism in Platelet and Megakaryocyte Function. *Cell Reports,* 21**,** 1705.

FINN, R. S., DERING, J., CONKLIN, D., KALOUS, O., COHEN, D. J., DESAI, A. J., GINTHER, C., ATEFI, M., CHEN, I., FOWST, C., LOS, G. & SLAMON, D. J. 2009. PD 0332991, a selective cyclin D kinase 4/6 inhibitor, preferentially inhibits proliferation of luminal estrogen receptor-positive human breast cancer cell lines in vitro. *Breast Cancer Research,* 11**,** R77.

FINN, R. S., MARTIN, M., RUGO, H. S., JONES, S., IM, S.-A., GELMON, K., HARBECK, N., LIPATOV, O. N., WALSHE, J. M., MOULDER, S., GAUTHIER, E., LU, D. R., RANDOLPH, S., DIÉRAS, V. & SLAMON, D. J. 2016. Palbociclib and Letrozole in Advanced Breast Cancer. *New England Journal of Medicine,* 375**,** 1925-1936.

FLAVAHAN, W. A., WU, Q., HITOMI, M., RAHIM, N., KIM, Y., SLOAN, A. E., WEIL, R. J., NAKANO, I., SARKARIA, J. N., STRINGER, B. W., DAY, B. W., LI, M., LATHIA, J. D., RICH, J. N. & HJELMELAND, A. B. 2013. Brain tumor initiating cells adapt to restricted nutrition through preferential glucose uptake. *Nat Neurosci,* 16**,** 1373-1382.

FOWLER, J. S. & IDO, T. 2002. Initial and subsequent approach for the synthesis of 18FDG. *Seminars in Nuclear Medicine,* 32**,** 6-12.

FREDERIKSEN LISA, J., SIEMENS D, R., HEATON JEREMY, P., MAXWELL LORI, R., ADAMS MICHAEL, A. & GRAHAM CHARLES, H. 2003. Hypoxia Induced Resistance to Doxorubicin in Prostate Cancer Cells is Inhibited by Low Concentrations of Glyceryl Trinitrate. *Journal of Urology,* 170**,** 1003-1007.

GARDNER, L. B., LI, Q., PARK, M. S., FLANAGAN, W. M., SEMENZA, G. L. & DANG, C. V. 2001. Hypoxia Inhibits G1/S Transition through Regulation of p27 Expression. *Journal of Biological Chemistry,* 276**,** 7919-7926.

GELMETTI, V., ZHANG, J., FANELLI, M., MINUCCI, S., PELICCI, P. G. & LAZAR, M. A. 1998. Aberrant Recruitment of the Nuclear Receptor Corepressor-Histone Deacetylase Complex by the Acute Myeloid Leukemia Fusion Partner ETO. *Molecular and Cellular Biology,* 18**,** 7185.

GOLDBERG, L., ISRAELI, R. & KLOOG, Y. 2012. FTS and 2-DG induce pancreatic cancer cell death and tumor shrinkage in mice. *Cell Death &Amp; Disease,* 3**,** e284.

GORSKI, D. H., BECKETT, M. A., JASKOWIAK, N. T., CALVIN, D. P., MAUCERI, H. J., SALLOUM, R. M., SEETHARAM, S., KOONS, A., HARI, D. M., KUFE, D. W. & WEICHSELBAUM, R. R. 1999. Blockade of the Vascular Endothelial Growth Factor Stress Response Increases the Antitumor Effects of Ionizing Radiation. *Cancer Research,* 59**,** 3374.

GOYAMA, S., SCHIBLER, J., CUNNINGHAM, L., ZHANG, Y., RAO, Y., NISHIMOTO, N., NAKAGAWA, M., OLSSON, A., WUNDERLICH, M., LINK, K. A., MIZUKAWA, B., GRIMES, H. L., KUROKAWA, M., LIU, P. P., HUANG, G. & MULLOY, J. C. 2013. Transcription factor RUNX1 promotes survival of acute myeloid leukemia cells. *The Journal of clinical investigation,* 123**,** 3876-3888.

GRIESSINGER, E., ANJOS-AFONSO, F., PIZZITOLA, I., ROUAULT-PIERRE, K., VARGAFTIG, J., TAUSSIG, D., GRIBBEN, J., LASSAILLY, F. & BONNET, D. 2014. A niche-like culture system allowing the maintenance of primary human acute myeloid leukemia-initiating cells: a new tool to decipher their chemoresistance and self-renewal mechanisms. *Stem cells translational medicine,* 3**,** 520-529.

GRIMWADE, D., HILLS, R. K., MOORMAN, A. V., WALKER, H., CHATTERS, S., GOLDSTONE, A. H., WHEATLEY, K., HARRISON, C. J. & BURNETT, A. K. 2010. Refinement of cytogenetic classification in acute myeloid leukemia: determination of prognostic significance of rare recurring chromosomal abnormalities among 5876 younger adult patients treated in the United Kingdom Medical Research Council trials. *Blood,* 116**,** 354-365.

GRIMWADE, D., IVEY, A. & HUNTLY, B. J. P. 2016. Molecular landscape of acute myeloid leukemia in younger adults and its clinical relevance. *Blood,* 127**,** 29.

GROWNEY, J. D., SHIGEMATSU, H., LI, Z., LEE, B. H., ADELSPERGER, J., ROWAN, R., CURLEY, D. P., KUTOK, J. L., AKASHI, K., WILLIAMS, I. R., SPECK, N. A. & GILLILAND, D. G. 2005. Loss of Runx1 perturbs adult hematopoiesis and is associated with a myeloproliferative phenotype. *Blood,* 106**,** 494-504.

GRUNDLER, R., BRAULT, L., GASSER, C., BULLOCK, A. N., DECHOW, T., WOETZEL, S., POGACIC, V., VILLA, A., EHRET, S., BERRIDGE, G., SPOO, A., DIERKS, C., BIONDI, A., KNAPP, S., DUYSTER, J. & SCHWALLER, J. 2009. Dissection of PIM serine/threonine kinases in FLT3-ITD-induced leukemogenesis reveals PIM1 as regulator of CXCL12-CXCR4-mediated homing and migration. *The Journal of experimental medicine,* 206**,** 1957-1970.

GU, L., YI, Z., ZHANG, Y., MA, Z., ZHU, Y. & GAO, J. 2017. Low dose of 2-deoxy-D-glucose kills acute lymphoblastic leukemia cells and reverses glucocorticoid resistance via N-linked glycosylation inhibition under normoxia. *Oncotarget,* 8**,** 30978-30991.

GUZY, R. D., HOYOS, B., ROBIN, E., CHEN, H., LIU, L., MANSFIELD, K. D., SIMON, M. C., HAMMERLING, U. & SCHUMACKER, P. T. 2005. Mitochondrial complex III is required for hypoxia-induced ROS production and cellular oxygen sensing. *Cell Metabolism,* 1**,** 401-408.

HANSEN, E., QUIVORON, C., STRALEY, K., LEMIEUX, R. M., POPOVICI-MULLER, J., SADRZADEH, H., FATHI, A. T., GLISER, C., DAVID, M., SAADA, V., MICOL, J.-B., BERNARD, O., DORSCH, M., YANG, H., SU, M., AGRESTA, S., DE BOTTON, S., PENARD-LACRONIQUE, V. & YEN, K. 2014. AG-120, an Oral, Selective, First-in-Class, Potent Inhibitor of Mutant IDH1, Reduces

Intracellular 2HG and Induces Cellular Differentiation in TF-1 R132H Cells and Primary Human IDH1 Mutant AML Patient Samples Treated <em>Ex Vivo</em&gt. *Blood,* 124**,** 3734.

HARAMI-PAPP, H., PONGOR, L. S., MUNKÁCSY, G., HORVÁTH, G., NAGY, Á. M., AMBRUS, A., HAUSER, P., SZABÓ, A., TRETTER, L. & GYŐRFFY, B. 2016. TP53 mutation hits energy metabolism and increases glycolysis in breast cancer. *Oncotarget,* 7**,** 67183-67195.

HATLEN, M. A., WANG, L. & NIMER, S. D. 2012. AML1-ETO driven acute leukemia: insights into pathogenesis and potential therapeutic approaches. *Frontiers of Medicine,* 6**,** 248-262.

HEIDENREICH, O., KRAUTER, J., RIEHLE, H., HADWIGER, P., JOHN, M., HEIL, G., VORNLOCHER, H.-P. & NORDHEIM, A. 2003. AML1/MTG8 oncogene suppression by small interfering RNAs supports myeloid differentiation of t(8;21)-positive leukemic cells. *Blood,* 101**,** 3157-3163.

HIGUCHI, M. 2000. Expression of AML1-ETO immortalizes myeloid progenitors and cooperates with secondary mutations to induce granulocytic sarcoma/acute myeloid leukemia. *Blood,* 96**,** 222a.

HILDEBRAND, D., TIEFENBACH, J., HEINZEL, T., GREZ, M. & MAURER, A. B. 2001. Multiple Regions of ETO Cooperate in Transcriptional Repression. *Journal of Biological Chemistry,* 276**,** 9889-9895.

HOFFMANN, P. R., KENCH, J. A., VONDRACEK, A., KRUK, E., DALEKE, D. L., JORDAN, M., MARRACK, P., HENSON, P. M. & FADOK, V. A. 2005. Interaction between Phosphatidylserine and the Phosphatidylserine Receptor Inhibits Immune Responses In Vivo. *The Journal of Immunology,* 174**,** 1393-1404.

HOHENBERGER, P., FELGNER, C., HAENSCH, W. & SCHLAG, P. M. 1998. Tumor oxygenation correlates with molecular growth determinants in breast cancer. *Breast Cancer Research and Treatment,* 48**,** 97-106.

HOLLANDER, M. C., BLUMENTHAL, G. M. & DENNIS, P. A. 2011. PTEN loss in the continuum of common cancers, rare syndromes and mouse models. *Nature Reviews Cancer,* 11**,** 289.

HOU, Y., ZHOU, M., XIE, J., CHAO, P., FENG, Q. & WU, J. 2017. High glucose levels promote the proliferation of breast cancer cells through GTPases. *Breast Cancer : Targets and Therapy,* 9**,** 429-436.

HSU, Y. C., LAL, D., LAMSON, A., VARGAS, R. & WANG, E. S. 2009. Hypoxia-Induced Chemoresistance to Doxorubicin in Acute Myeloid Leukemia (AML) Cells Occurs Via HIF-1α Independent Mechanism. *Blood,* 114**,** 2749-2749.

HULLEMAN, E., KAZEMIER, K. M., HOLLEMAN, A., VANDERWEELE, D. J., RUDIN, C. M., BROEKHUIS, M. J. C., EVANS, W. E., PIETERS, R. & DEN BOER, M. L. 2009. Inhibition of glycolysis modulates prednisolone resistance in acute lymphoblastic leukemia cells. *Blood,* 113**,** 2014-2021.

HUYHN, A., DOMMERGUES, M., IZAC, B., CROISILLE, L., KATZ, A., VAINCHENKER, W. & COULOMBEL, L. 1995. Characterization of hematopoietic progenitors from human yolk sacs and embryos. *Blood,* 86**,** 4474.

IAN, A. S., DONARD, D., DANIELA, M., KELLE, H. M., ALEXANDER, T. & SUSAN, J. V. 2008. The facilitative glucose transporter GLUT3: 20 years of distinction. *American Journal of Physiology-Endocrinology and Metabolism,* 295**,** E242-E253.

ICHIKAWA, M., ASAI, T., SAITO, T., YAMAMOTO, G., SEO, S., YAMAZAKI, I., YAMAGATA, T., MITANI, K., CHIBA, S., HIRAI, H., OGAWA, S. & KUROKAWA, M. 2004. AML-1 is required for megakaryocytic maturation and lymphocytic differentiation, but not for maintenance of hematopoietic stem cells in adult hematopoiesis. *Nature Medicine,* 10**,** 299.

ICHIKAWA, M., GOYAMA, S., ASAI, T., KAWAZU, M., NAKAGAWA, M., TAKESHITA, M., CHIBA, S., OGAWA, S. & KUROKAWA, M. 2008. AML1/Runx1 Negatively Regulates Quiescent Hematopoietic Stem Cells in Adult Hematopoiesis. *The Journal of Immunology,* 180**,** 4402.

IM, A. P., SEHGAL, A. R., CARROLL, M. P., SMITH, B. D., TEFFERI, A., JOHNSON, D. E. & BOYIADZIS, M. 2014. DNMT3A and IDH mutations in acute myeloid leukemia and other myeloid malignancies: associations with prognosis and potential treatment strategies. *Leukemia,* 28**,** 1774.

ISHIKAWA, F., YOSHIDA, S., SAITO, Y., HIJIKATA, A., KITAMURA, H., TANAKA, S., NAKAMURA, R., TANAKA, T., TOMIYAMA, H., SAITO, N., FUKATA, M., MIYAMOTO, T., LYONS, B., OHSHIMA, K., UCHIDA, N., TANIGUCHI, S., OHARA, O., AKASHI, K., HARADA, M. & SHULTZ, L. D. 2007. Chemotherapy-resistant human AML stem cells home to and engraft within the bone-marrow endosteal region. *Nature Biotechnology,* 25**,** 1315.

ITO, K. & SUDA, T. 2014. Metabolic requirements for the maintenance of self-renewing stem cells. *Nature reviews. Molecular cell biology,* 15**,** 243-256.

IVANOVS, A., RYBTSOV, S., WELCH, L., ANDERSON, R. A., TURNER, M. L. & MEDVINSKY, A. 2011. Highly potent human hematopoietic stem cells first emerge in the intraembryonic aorta-gonad-mesonephros region. *The Journal of experimental medicine,* 208**,** 2417-2427.

IYER, N. V., KOTCH, L. E., AGANI, F., LEUNG, S. W., LAUGHNER, E., WENGER, R. H., GASSMANN, M., GEARHART, J. D., LAWLER, A. M., YU, A. Y. & SEMENZA, G. L. 1998. Cellular and developmental control of O2 homeostasis by hypoxia-inducible factor 1 alpha. *Genes & development,* 12**,** 149-162.

JACOB, B., OSATO, M., YAMASHITA, N., WANG, C. Q., TANIUCHI, I., LITTMAN, D. R., ASOU, N. & ITO, Y. 2010. Stem cell exhaustion due to Runx1 deficiency is prevented by Evi5 activation in leukemogenesis. *Blood,* 115**,** 1610-1620.

JEON, J. Y., KIM, S. W., PARK, K. C. & YUN, M. 2015. The bifunctional autophagic flux by 2-deoxyglucose to control survival or growth of prostate cancer cells. *BMC Cancer,* 15**,** 623.

JIAO, B., WU, C. F., LIANG, Y., CHEN, H. M., XIONG, S. M., CHEN, B., SHI, J. Y., WANG, Y. Y., WANG, J. H., CHEN, Y., LI, J. M., GU, L. J., TANG, J. Y., SHEN, Z. X., GU, B. W., ZHAO, W. L., CHEN, Z. & CHEN, S. J. 2009. AML1-ETO9a is correlated with C-KIT overexpression/mutations and indicates poor disease outcome in t(8;21) acute myeloid leukemia-M2. *Leukemia,* 23**,** 1598.

JOHNSON, M. K., VATHANAYAGAM, R. R. & WANG, E. S. 2011. Hypoxia-Associated Effects on Reactive Oxygen Species Generation by Human Acute Myeloid Leukemia Cells. *Blood,* 118**,** 4998-4998.

JONES, C. L., STEVENS, B. M., D'ALESSANDRO, A., REISZ, J. A., CULP-HILL, R., NEMKOV, T., PEI, S., KHAN, N., ADANE, B., YE, H., KRUG, A., REINHOLD,

D., SMITH, C., DEGREGORI, J., POLLYEA, D. A. & JORDAN, C. T. 2018. Inhibition of Amino Acid Metabolism Selectively Targets Human Leukemia Stem Cells. *Cancer Cell,* 34**,** 724-740.e4.

JONES, R. G. & THOMPSON, C. B. 2009. Tumor suppressors and cell metabolism: a recipe for cancer growth. *Genes & Development,* 23**,** 537-548.

JUN, S. A., SEPIASHVILI, L., KISLINGER, T. & MINDEN, M. D. 2011. Investigating the Potential Use of L-Asparaginase in Myeloid Leukemia. *Blood,* 118**,** 3641.

KADIA, T. M., JAIN, P., RAVANDI, F., GARCIA-MANERO, G., ANDREEF, M., TAKAHASHI, K., BORTHAKUR, G., JABBOUR, E., KONOPLEVA, M., DAVER, N. G., DINARDO, C., PIERCE, S., KANAGAL-SHAMANNA, R., PATEL, K., ESTROV, Z., CORTES, J. & KANTARJIAN, H. M. 2016. TP53 mutations in newly diagnosed acute myeloid leukemia: Clinicomolecular characteristics, response to therapy, and outcomes. *Cancer,* 122**,** 3484-3491.

KANTARJIAN, H. 2016. Acute myeloid leukemia—Major progress over four decades and glimpses into the future. *American Journal of Hematology,* 91**,** 131-145.

KASPERS, G. J. L., ZIMMERMANN, M., REINHARDT, D., GIBSON, B. E. S., TAMMINGA, R. Y. J., ALEINIKOVA, O., ARMENDARIZ, H., DWORZAK, M., HA, S.-Y., HASLE, H., HOVI, L., MASCHAN, A., BERTRAND, Y., LEVERGER, G. G., RAZZOUK, B. I., RIZZARI, C., SMISEK, P., SMITH, O., STARK, B. & CREUTZIG, U. 2013. Improved Outcome in Pediatric Relapsed Acute Myeloid Leukemia: Results of a Randomized Trial on Liposomal Daunorubicin by the International BFM Study Group. *Journal of Clinical Oncology,* 31**,** 599-607.

KAWAUCHI, K., ARAKI, K., TOBIUME, K. & TANAKA, N. 2008. p53 regulates glucose metabolism through an IKK-NF-[kappa]B pathway and inhibits cell transformation. *Nat Cell Biol,* 10**,** 611-618.

KEITH, B., JOHNSON, R. S. & SIMON, M. C. 2011. HIF1α and HIF2α: sibling rivalry in hypoxic tumour growth and progression. *Nature reviews. Cancer,* 12**,** 9-22.

KIM, B., LI, J., JANG, C. & ARANY, Z. 2017a. Glutamine fuels proliferation but not migration of endothelial cells. *The EMBO Journal,* 36**,** 2321-2333.

KIM, N. H., CHA, Y. H., LEE, J., LEE, S.-H., YANG, J. H., YUN, J. S., CHO, E. S., ZHANG, X., NAM, M., KIM, N., YUK, Y.-S., CHA, S. Y., LEE, Y., RYU, J. K.,

PARK, S., CHEONG, J.-H., KANG, S. W., KIM, S.-Y., HWANG, G.-S., YOOK, J. I. & KIM, H. S. 2017b. Snail reprograms glucose metabolism by repressing phosphofructokinase PFKP allowing cancer cell survival under metabolic stress. *Nature Communications,* 8**,** 14374.

KIM, S. J., ZHAO, H., HARDIKAR, S., SINGH, A. K., GOODELL, M. A. & CHEN, T. 2013. A DNMT3A mutation common in AML exhibits dominant-negative effects in murine ES cells. *Blood,* 122**,** 4086.

KIM, Y.-K., KIM, H.-N., LEE, I.-K., BANG, S.-M., JO, D.-Y., WON, J.-H., YIM, C.-Y., YANG, D.-H., LEE, J.-J. & KIM, H.-J. 2007. Prognostic Significance of FLT3/ITD Mutation in AML1/ETO-Associated Acute Myeloid Leukemia. *Blood,* 110**,** 3493.

KITABAYASHI, I., IDA, K., MOROHOSHI, F., YOKOYAMA, A., MITSUHASHI, N., SHIMIZU, K., NOMURA, N., HAYASHI, Y. & OHKI, M. 1998. The AML1-MTG8 leukemic fusion protein forms a complex with a novel member of the MTG8(ETO/CDR) family, MTGR1. *Molecular and cellular biology,* 18**,** 846-858.

KOJIMA, K., MCQUEEN, T., CHEN, Y., JACAMO, R., KONOPLEVA, M., SHINOJIMA, N., SHPALL, E., HUANG, X. & ANDREEFF, M. 2011. p53 activation of mesenchymal stromal cells partially abrogates microenvironment-mediated resistance to FLT3 inhibition in AML through HIF-1α-mediated down-regulation of CXCL12. *Blood,* 118**,** 4431-4439.

KREJCI, O., WUNDERLICH, M., GEIGER, H., CHOU, F.-S., SCHLEIMER, D., JANSEN, M., ANDREASSEN, P. R. & MULLOY, J. C. 2008. p53 signaling in response to increased DNA damage sensitizes AML1-ETO cells to stress-induced death. *Blood,* 111**,** 2190-2199.

KUANG, R., JAHANGIRI, A., MASCHARAK, S., NGUYEN, A., CHANDRA, A., FLANIGAN, P. M., YAGNIK, G., WAGNER, J. R., DE LAY, M., CARRERA, D., CASTRO, B. A., HAYES, J., SIDOROV, M., GARCIA, J. L. I., ERIKSSON, P., RONEN, S., PHILLIPS, J., MOLINARO, A., KOLIWAD, S. & AGHI, M. K. 2017. GLUT3 upregulation promotes metabolic reprogramming associated with antiangiogenic therapy resistance. *JCI insight,* 2**,** e88815-e88815.

KUFE, D. W., MAJOR, P. P., EGAN, E. M. & BEARDSLEY, G. P. 1980. Correlation of cytotoxicity with incorporation of ara-C into DNA. *Journal of Biological Chemistry,* 255**,** 8997-8900.

KUMAR, C. C. 2011. Genetic abnormalities and challenges in the treatment of acute myeloid leukemia. *Genes & cancer,* 2**,** 95-107.

KUMARI, N., DWARAKANATH, B. S., DAS, A. & BHATT, A. N. 2016. Role of interleukin-6 in cancer progression and therapeutic resistance. *Tumor Biology,* 37**,** 11553-11572.

KUNG, J.-C. T. W. B. L. 2012. Incongruity of Imaging Using Fluorescent 2-DG Conjugates Compared to 18F-FDG in Preclinical Cancer Models. *Molecular Imaging and Biology,* 14**,** 553-560.

KUWERT, J. D. P. G. S. 2003. Uptake of [18F]fluorodeoxyglucose in human monocyte-macrophages in vitro. *European Journal of Nuclear Medicine and Molecular Imaging,* 30**,** 267-273.

L. K. PATTERSON, M. A. J., E.L. POWERS (EDS.) 1981. *Oxygen and Oxy-radicals in Chemistry and Biology,* New York, Rodgers, Academic Press.

LACHMANN, N., ACKERMANN, M., FRENZEL, E., LIEBHABER, S., BRENNIG, S., HAPPLE, C., HOFFMANN, D., KLIMENKOVA, O., LÜTTGE, D., BUCHEGGER, T., KÜHNEL, M. P., SCHAMBACH, A., JANCIAUSKIENE, S., FIGUEIREDO, C., HANSEN, G., SKOKOWA, J. & MORITZ, T. 2015. Large-scale hematopoietic differentiation of human induced pluripotent stem cells provides granulocytes or macrophages for cell replacement therapies. *Stem cell reports,* 4**,** 282-296.

LAGADINOU, ELENI D., SACH, A., CALLAHAN, K., ROSSI, RANDALL M., NEERING, SARAH J., MINHAJUDDIN, M., ASHTON, JOHN M., PEI, S., GROSE, V., O'DWYER, KRISTEN M., LIESVELD, JANE L., BROOKES, PAUL S., BECKER, MICHAEL W. & JORDAN, CRAIG T. 2013. BCL-2 Inhibition Targets Oxidative Phosphorylation and Selectively Eradicates Quiescent Human Leukemia Stem Cells. *Cell Stem Cell,* 12**,** 329-341.

LAI, P.-L., LIN, H., CHEN, S.-F., YANG, S.-C., HUNG, K.-H., CHANG, C.-F., CHANG, H.-Y., LU, F. L., LEE, Y.-H., LIU, Y.-C., HUANG, H.-C. & LU, J. 2017.

Efficient Generation of Chemically Induced Mesenchymal Stem Cells from Human Dermal Fibroblasts. *Scientific Reports,* 7**,** 44534.

LAM, K. & ZHANG, D.-E. 2012. RUNX1 and RUNX1-ETO: roles in hematopoiesis and leukemogenesis. *Frontiers in bioscience (Landmark edition),* 17**,** 1120-1139.

LEE, J.-H., LIU, R., LI, J., ZHANG, C., WANG, Y., CAI, Q., QIAN, X., XIA, Y., ZHENG, Y., PIAO, Y., CHEN, Q., DE GROOT, J. F., JIANG, T. & LU, Z. 2017. Stabilization of phosphofructokinase 1 platelet isoform by AKT promotes tumorigenesis. *Nature Communications,* 8**,** 949.

LEE, P., HOCK, A. K., VOUSDEN, K. H. & CHEUNG, E. C. 2015. p53- and p73-independent activation of TIGAR expression in vivo. *Cell death & disease,* 6**,** e1842-e1842.

LEUNG, K. 2004. [18F]Fluoro-2-deoxy-2-D-glucose. In: Molecular Imaging and Contrast Agent Database (MICAD). *2004-2013.* Bethesda (MD): National Center for Biotechnology Information (US).

LI, B., CAO, Y., MENG, G., QIAN, L., XU, T., YAN, C., LUO, O., WANG, S., WEI, J., DING, Y. & YU, D. 2018. Targeting glutaminase 1 attenuates stemness properties in hepatocellular carcinoma by increasing reactive oxygen species and suppressing Wnt/beta-catenin pathway. *EBioMedicine,* 39**,** 239-254.

LIANG, D., MA, Y., LIU, J., TROPE, C. G., HOLM, R., NESLAND, J. M. & SUO, Z. 2012. The hypoxic microenvironment upgrades stem-like properties of ovarian cancer cells. *BMC cancer,* 12**,** 201-201.

LIANG, J., SHAO, S. H., XU, Z.-X., HENNESSY, B., DING, Z., LARREA, M., KONDO, S., DUMONT, D. J., GUTTERMAN, J. U., WALKER, C. L., SLINGERLAND, J. M. & MILLS, G. B. 2007. The energy sensing LKB1–AMPK pathway regulates p27kip1 phosphorylation mediating the decision to enter autophagy or apoptosis. *Nature Cell Biology,* 9**,** 218.

LIN, C.-S., NING, H., LIN, G. & LUE, T. F. 2012. Is CD34 truly a negative marker for mesenchymal stromal cells? *Cytotherapy,* 14**,** 1159-1163.

LIN, L.-I., CHEN, C.-Y., LIN, D.-T., TSAY, W., TANG, J.-L., YEH, Y.-C., SHEN, H.-L., SU, F.-H., YAO, M., HUANG, S.-Y. & TIEN, H.-F. 2005. Characterization of CEBPA Mutations in Acute Myeloid Leukemia: Most

Patients with CEBPA Mutations Have Biallelic Mutations and Show a Distinct Immunophenotype of the Leukemic Cells. *Clinical Cancer Research,* 11**,** 1372.

LIU, L.-Q., ILARIA, R., KINGSLEY, P. D., IWAMA, A., VAN ETTEN, R. A., PALIS, J. & ZHANG, D.-E. 1999. A Novel Ubiquitin-Specific Protease, UBP43, Cloned from Leukemia Fusion Protein AML1-ETO-Expressing Mice, Functions in Hematopoietic Cell Differentiation. *Molecular and Cellular Biology,* 19**,** 3029.

LIU, Y., CHENEY, M. D., GAUDET, J. J., CHRUSZCZ, M., LUKASIK, S. M., SUGIYAMA, D., LARY, J., COLE, J., DAUTER, Z., MINOR, W., SPECK, N. A. & BUSHWELLER, J. H. 2006. The tetramer structure of the Nervy homology two domain, NHR2, is critical for AML1/ETO's activity. *Cancer Cell,* 9**,** 249-260.

LLOYD, P. G., HARDIN, C. D. & STUREK, M. 1999. Examining glucose transport in single vascular smooth muscle cells with a fluorescent glucose analog. *Physiol Res,* 48**,** 401-10.

LUGER, A.-L., SAUER, B., LORENZ, N. I., ENGEL, A. L., BRAUN, Y., VOSS, M., HARTER, P. N., STEINBACH, J. P. & RONELLENFITSCH, M. W. 2018. Doxycycline Impairs Mitochondrial Function and Protects Human Glioma Cells from Hypoxia-Induced Cell Death: Implications of Using Tet-Inducible Systems. *International journal of molecular sciences,* 19**,** 1504.

LUO, M., SHANG, L., BROOKS, M. D., JIAGGE, E., ZHU, Y., BUSCHHAUS, J. M., CONLEY, S., FATH, M. A., DAVIS, A., GHEORDUNESCU, E., WANG, Y., HAROUAKA, R., LOZIER, A., TRINER, D., MCDERMOTT, S., MERAJVER, S. D., LUKER, G. D., SPITZ, D. R. & WICHA, M. S. 2018. Targeting Breast Cancer Stem Cell State Equilibrium through Modulation of Redox Signaling. *Cell Metabolism,* 28**,** 69-86.e6.

LUTTERBACH, B., WESTENDORF, J. J., LINGGI, B., PATTEN, A., MONIWA, M., DAVIE, J. R., HUYNH, K. D., BARDWELL, V. J., LAVINSKY, R. M., ROSENFELD, M. G., GLASS, C., SETO, E. & HIEBERT, S. W. 1998. ETO, a Target of t(8;21) in Acute Leukemia, Interacts with the N-CoR and mSin3 Corepressors. *Molecular and Cellular Biology,* 18**,** 7176-7184.

MANSFIELD, K. D., GUZY, R. D., PAN, Y., YOUNG, R. M., CASH, T. P., SCHUMACKER, P. T. & SIMON, M. C. 2005. Mitochondrial dysfunction resulting from loss of cytochrome c impairs cellular oxygen sensing and hypoxic HIF-α activation. *Cell Metabolism,* 1**,** 393-399.

MANTYCH, G. J., JAMES, D. E., CHUNG, H. D. & DEVASKAR, S. U. 1992. Cellular localization and characterization of Glut 3 glucose transporter isoform in human brain. *Endocrinology,* 131**,** 1270-1278.

MARCUCCI, G., MAHARRY, K., RADMACHER, M. D., MRÓZEK, K., VUKOSAVLJEVIC, T., PASCHKA, P., WHITMAN, S. P., LANGER, C., BALDUS, C. D., LIU, C.-G., RUPPERT, A. S., POWELL, B. L., CARROLL, A. J., CALIGIURI, M. A., KOLITZ, J. E., LARSON, R. A. & BLOOMFIELD, C. D. 2008. Prognostic significance of, and gene and microRNA expression signatures associated with, CEBPA mutations in cytogenetically normal acute myeloid leukemia with high-risk molecular features: a Cancer and Leukemia Group B Study. *Journal of clinical oncology : official journal of the American Society of Clinical Oncology,* 26**,** 5078-5087.

MARDIS, E. R., DING, L., DOOLING, D. J., LARSON, D. E., MCLELLAN, M. D., CHEN, K., KOBOLDT, D. C., FULTON, R. S., DELEHAUNTY, K. D., MCGRATH, S. D., FULTON, L. A., LOCKE, D. P., MAGRINI, V. J., ABBOTT, R. M., VICKERY, T. L., REED, J. S., ROBINSON, J. S., WYLIE, T., SMITH, S. M., CARMICHAEL, L., ELDRED, J. M., HARRIS, C. C., WALKER, J., PECK, J. B., DU, F., DUKES, A. F., SANDERSON, G. E., BRUMMETT, A. M., CLARK, E., MCMICHAEL, J. F., MEYER, R. J., SCHINDLER, J. K., POHL, C. S., WALLIS, J. W., SHI, X., LIN, L., SCHMIDT, H., TANG, Y., HAIPEK, C., WIECHERT, M. E., IVY, J. V., KALICKI, J., ELLIOTT, G., RIES, R. E., PAYTON, J. E., WESTERVELT, P., TOMASSON, M. H., WATSON, M. A., BATY, J., HEATH, S., SHANNON, W. D., NAGARAJAN, R., LINK, D. C., WALTER, M. J., GRAUBERT, T. A., DIPERSIO, J. F., WILSON, R. K. & LEY, T. J. 2009. Recurring mutations found by sequencing an acute myeloid leukemia genome. *The New England journal of medicine,* 361**,** 1058-1066.

MÁRQUEZ, J., ALONSO, F. J., MATÉS, J. M., SEGURA, J. A., MARTÍN-RUFIÁN, M. & CAMPOS-SANDOVAL, J. A. 2017. Glutamine Addiction In Gliomas. *Neurochemical Research,* 42**,** 1735-1746.

MARTINEZ-SORIA, N., MCKENZIE, L., DRAPER, J., PTASINSKA, A., ISSA, H., POTLURI, S., BLAIR, H. J., PICKIN, A., ISA, A., CHIN, P. S., TIRTAKUSUMA, R., COLEMAN, D., NAKJANG, S., ASSI, S., FORSTER, V., REZA, M., LAW, E., BERRY, P., MUELLER, D., ELDER, A., BOMKEN, S. N., PAL, D., ALLAN, J. M., VEAL, G. J., COCKERILL, P. N., WICHMANN, C., VORMOOR, J., LACAUD, G., BONIFER, C. & HEIDENREICH, O. 2018. The Oncogenic Transcription Factor RUNX1/ETO Corrupts Cell Cycle Regulation to Drive Leukemic Transformation. *Cancer Cell,* 34**,** 626-642.e8.

MARTINEZ, N., DRESCHER, B., RIEHLE, H., CULLMANN, C., VORNLOCHER, H.-P., GANSER, A., HEIL, G., NORDHEIM, A., KRAUTER, J. & HEIDENREICH, O. 2004. The oncogenic fusion protein RUNX1-CBFA2T1 supports proliferation and inhibits senescence in t(8;21)-positive leukaemic cells. *BMC Cancer,* 4**,** 44.

MASCHEK, G., SAVARAJ, N., PRIEBE, W., BRAUNSCHWEIGER, P., HAMILTON, K. & TIDMARSH, G. F. 2004. 2-deoxy-D-glucose increases the efficacy of adriamycin and paclitaxel in human osteosarcoma and non-small cell lung cancers in vivo. *Cancer Res,* 64.

MASIN, M., VAZQUEZ, J., ROSSI, S., GROENEVELD, S., SAMSON, N., SCHWALIE, P., DEPLANCKE, B., FRAWLEY, L., GOUTTENOIRE, J., MORADPOUR, D., OLIVER, T. & MEYLAN, E. 2014. GLUT3 is induced during epithelial-mesenchymal transition and promotes tumor cell proliferation in non-small cell lung cancer. *Cancer & Metabolism,* 2**,** 11.

MATHUPALA, S. P., KO, Y. H. & PEDERSEN, P. L. 2006. Hexokinase II: cancer's double-edged sword acting as both facilitator and gatekeeper of malignancy when bound to mitochondria. *Oncogene,* 25**,** 4777-4786.

MATOZAKI, S., NAKAGAWA, T., KAWAGUCHI, R., AOZAKI, R., TSUTSUMI, M., MURAYAMA, T., KOIZUMI, T., NISHIMURA, R., ISOBE, T. & CHIHARA, K. 1995. Establishment of a myeloid leukaemic cell line (SKNO-1) from a patient

with t(8;21) who acquired monosomy 17 during disease progression. *British Journal of Haematology,* 89**,** 805-811.

MCBRIDE, J. L., BOUDREAU, R. L., HARPER, S. Q., STABER, P. D., MONTEYS, A. M., MARTINS, I., GILMORE, B. L., BURSTEIN, H., PELUSO, R. W., POLISKY, B., CARTER, B. J. & DAVIDSON, B. L. 2008. Artificial miRNAs mitigate shRNA-mediated toxicity in the brain: implications for the therapeutic development of RNAi. *Proceedings of the National Academy of Sciences of the United States of America,* 105**,** 5868-5873.

MCGOWAN, J. V., CHUNG, R., MAULIK, A., PIOTROWSKA, I., WALKER, J. M. & YELLON, D. M. 2017. Anthracycline Chemotherapy and Cardiotoxicity. *Cardiovascular drugs and therapy,* 31**,** 63-75.

MEHTA, H. M., MALANDRA, M. & COREY, S. J. 2015. G-CSF and GM-CSF in Neutropenia. *Journal of immunology (Baltimore, Md. : 1950),* 195**,** 1341-1349.

MILLS, C. C., KOLB, E. A. & SAMPSON, V. B. 2018. Development of Chemotherapy with Cell-Cycle Inhibitors for Adult and Pediatric Cancer Therapy. *Cancer research,* 78**,** 320-325.

MIMURA, I., NANGAKU, M., KANKI, Y., TSUTSUMI, S., INOUE, T., KOHRO, T., YAMAMOTO, S., FUJITA, T., SHIMAMURA, T., SUEHIRO, J.-I., TAGUCHI, A., KOBAYASHI, M., TANIMURA, K., INAGAKI, T., TANAKA, T., HAMAKUBO, T., SAKAI, J., ABURATANI, H., KODAMA, T. & WADA, Y. 2012. Dynamic Change of Chromatin Conformation in Response to Hypoxia Enhances the Expression of GLUT3 (SLC2A3) by Cooperative Interaction of Hypoxia-Inducible Factor 1 and KDM3A. *Molecular and Cellular Biology,* 32**,** 3018-3032.

MIWA, H., SUGANUMA, K., SHIKAMI, M., IMAI, N., SAKAI, M., HIRAMATSU, A., YAMAMOTO, H., WAKABAYASHI, M., WATARAI, M., HANAMURA, I., IMAMURA, A., MIHARA, H. & NITTA, M. 2008. Energy Metabolism of Leukemia Cells: Glycolysis Vs Oxidative Phosphorylation. *Blood,* 112**,** 2935-2935.

MIYOSHI, H., KOZU, T., SHIMIZU, K., ENOMOTO, K., MASEKI, N., KANEKO, Y., KAMADA, N. & OHKI, M. 1993. The t(8;21) translocation in acute myeloid

leukemia results in production of an AML1-MTG8 fusion transcript. *The EMBO Journal,* 12**,** 2715-2721.

MIYOSHI, H., SHIMIZU, K., KOZU, T., MASEKI, N., KANEKO, Y. & OHKI, M. 1991. t(8;21) breakpoints on chromosome 21 in acute myeloid leukemia are clustered within a limited region of a single gene, AML1. *Proceedings of the National Academy of Sciences of the United States of America,* 88**,** 10431-10434.

MOELLER, B. J., CAO, Y., LI, C. Y. & DEWHIRST, M. W. 2004. Radiation activates HIF-1 to regulate vascular radiosensitivity in tumors: Role of reoxygenation, free radicals, and stress granules. *Cancer Cell,* 5**,** 429-441.

MOLENAAR, R. J., MACIEJEWSKI, J. P., WILMINK, J. W. & VAN NOORDEN, C. J. F. 2018. Correction: Wild-type and mutated IDH1/2 enzymes and therapy responses. *Oncogene,* 37**,** 5810-5810.

MONDESIR, J., WILLEKENS, C., TOUAT, M. & DE BOTTON, S. 2016. IDH1 and IDH2 mutations as novel therapeutic targets: current perspectives. *Journal of blood medicine,* 7**,** 171-180.

MORENO-ASSO, A., CASTAÑO, C., GRILLI, A., NOVIALS, A. & SERVITJA, J. M. 2013. Glucose regulation of a cell cycle gene module is selectively lost in mouse pancreatic islets during ageing. *Diabetologia,* 56**,** 1761-1772.

MORRISON, S. J., WANDYCZ, A. M., HEMMATI, H. D., WRIGHT, D. E. & WEISSMAN, I. L. 1997. Identification of a lineage of multipotent hematopoietic progenitors. *Development,* 124**,** 1929.

MRÓZEK, K. & BLOOMFIELD, C. D. 2012. Acute myeloid leukemia with adverse cytogenetic risk. *Oncology (Williston Park, N.Y.),* 26**,** 714-723.

MULLOY, J. C., CAMMENGA, J., BERGUIDO, F. J., WU, K., ZHOU, P., COMENZO, R. L., JHANWAR, S., MOORE, M. A. S. & NIMER, S. D. 2003. Maintaining the self-renewal and differentiation potential of human CD34⁺ hematopoietic cells using a single genetic element. *Blood,* 102**,** 4369-4376.

MULLOY, J. C., CAMMENGA, J., MACKENZIE, K. L., BERGUIDO, F. J., MOORE, M. A. S. & NIMER, S. D. 2002. The AML1-ETO fusion protein promotes the expansion of human hematopoietic stem cells. *Blood,* 99**,** 15.

MURPHY, M. P. 2012. Modulating Mitochondrial Intracellular Location as a Redox Signal. *Science Signaling,* 5**,** pe39.

MUZ, B., DE LA PUENTE, P., AZAB, F. & AZAB, A. K. 2015. The role of hypoxia in cancer progression, angiogenesis, metastasis, and resistance to therapy. *Hypoxia (Auckland, N.Z.),* 3**,** 83-92.

NAGAMATSU, S., KORNHAUSER, J. M., BURANT, C. F., SEINO, S., MAYO, K. E. & BELL, G. I. 1992. Glucose transporter expression in brain. cDNA sequence of mouse GLUT3, the brain facilitative glucose transporter isoform, and identification of sites of expression by in situ hybridization. *Journal of Biological Chemistry,* 267**,** 467-472.

NAGARAJAN, A., MALVI, P. & WAJAPEYEE, N. 2016. Oncogene-directed alterations in cancer cell metabolism. *Trends in cancer,* 2**,** 365-377.

NANCOLAS, B., GUO, L., ZHOU, R., NATH, K., NELSON, D. S., LEEPER, D. B., BLAIR, I. A., GLICKSON, J. D. & HALESTRAP, A. P. 2016. The anti-tumour agent lonidamine is a potent inhibitor of the mitochondrial pyruvate carrier and plasma membrane monocarboxylate transporters. *The Biochemical journal,* 473**,** 929-936.

NELSON, C. A., WANG, J. Q., LEAV, I. & CRANE, P. D. 1996. The interaction among glucose transport, hexokinase, and glucose-6-phosphatase with respect to 3H-2-deoxyglucose retention in murine tumor models. *Nuclear Medicine and Biology,* 23**,** 533-541.

NELSON, R. 2010. *Gemtuzumab Voluntarily Withdrawn From US Market* [Online]. MedSCape. [Accessed].

NESTEROV, A., LU, X., JOHNSON, M., MILLER, G. J., IVASHCHENKO, Y. & KRAFT, A. S. 2001. Elevated Akt Activity Protects the Prostate Cancer Cell Line LNCaP from TRAIL-induced Apoptosis. *Journal of Biological Chemistry,* 276**,** 10767-10774.

NICK, H. J., KIM, H.-G., CHANG, C.-W., HARRIS, K. W., REDDY, V. & KLUG, C. A. 2012a. Distinct classes of c-Kit-activating mutations differ in their ability to promote RUNX1-ETO-associated acute myeloid leukemia. *Blood,* 119**,** 1522-1531.

NICK, H. J., KIM, H.-G., CHANG, C.-W., HARRIS, K. W., REDDY, V. & KLUG, C. A. 2012b. Distinct classes of c-Kit–activating mutations differ in their ability to promote RUNX1-ETO–associated acute myeloid leukemia. *Blood,* 119**,** 1522-1531.

NOBLE, R. A., BELL, N., BLAIR, H., SIKKA, A., THOMAS, H., PHILLIPS, N., NAKJANG, S., MIWA, S., CROSSLAND, R., RAND, V., TELEVANTOU, D., LONG, A., KEUN, H. C., BACON, C. M., BOMKEN, S., CRITCHLOW, S. E. & WEDGE, S. R. 2017. Inhibition of monocarboxyate transporter 1 by AZD3965 as a novel therapeutic approach for diffuse large B-cell lymphoma and Burkitt lymphoma. *Haematologica,* 102**,** 1247.

NORTH, T., GU, T. L., STACY, T., WANG, Q., HOWARD, L., BINDER, M., MARIN-PADILLA, M. & SPECK, N. A. 1999. Cbfa2 is required for the formation of intra-aortic hematopoietic clusters. *Development,* 126**,** 2563-2575.

NUCHPRAYOON, I., MEYERS, S., SCOTT, L. M., SUZOW, J., HIEBERT, S. & FRIEDMAN, A. D. 1994. PEBP2/CBF, the murine homolog of the human myeloid AML1 and PEBP2 beta/CBF beta proto-oncoproteins, regulates the murine myeloperoxidase and neutrophil elastase genes in immature myeloid cells. *Molecular and cellular biology,* 14**,** 5558-5568.

O'NEIL, R. G., WU, L. & MULLANI, N. 2005. Uptake of a Fluorescent Deoxyglucose Analog (2-NBDG) in Tumor Cells. *Molecular Imaging and Biology,* 7**,** 388-392.

OGIHARA, H., KANNO, T., MORII, E., KIM, D.-K., LEE, Y.-M., SATO, M., KIM, W.-Y., NOMURA, S., ITO, Y. & KITAMURA, Y. 1999. Synergy of PEBP2/CBF with mi transcription factor (MITF) for transactivation of mouse mast cell protease 6 gene. *Oncogene,* 18**,** 4632.

OKUDA, T., CAI, Z., YANG, S., LENNY, N., LYU, C.-J., VAN DEURSEN, J. M. A., HARADA, H. & DOWNING, J. R. 1998. Expression of a Knocked-In AML1-ETO Leukemia Gene Inhibits the Establishment of Normal Definitive Hematopoiesis and Directly Generates Dysplastic Hematopoietic Progenitors. *Blood,* 91**,** 3134.

OKUDA, T., VAN DEURSEN, J., HIEBERT, S. W., GROSVELD, G. & DOWNING, J. R. 1996. AML1, the Target of Multiple Chromosomal Translocations in Human

Leukemia, Is Essential for Normal Fetal Liver Hematopoiesis. *Cell,* 84**,** 321-330.

PABST, T., MUELLER, B. U., HARAKAWA, N., SCHOCH, C., HAFERLACH, T., BEHRE, G., HIDDEMANN, W., ZHANG, D.-E. & TENEN, D. G. 2001a. AML1-ETO downregulates the granulocytic differentiation factor C/EBP[alpha] in t(8;21) myeloid leukemia. *Nat Med,* 7**,** 444-451.

PABST, T., MUELLER, B. U., HARAKAWA, N., SCHOCH, C., HAFERLACH, T., BEHRE, G., HIDDEMANN, W., ZHANG, D.-E. & TENEN, D. G. 2001b. AML1–ETO downregulates the granulocytic differentiation factor C/EBPα in t(8;21) myeloid leukemia. *Nature Medicine,* 7**,** 444.

PAL, D., BLAIR, H. J., ELDER, A., DORMON, K., RENNIE, K. J., COLEMAN, D. J. L., WEILAND, J., RANKIN, K. S., FILBY, A., HEIDENREICH, O. & VORMOOR, J. 2016. Long-term in vitro maintenance of clonal abundance and leukaemia-initiating potential in acute lymphoblastic leukaemia. *Leukemia,* 30**,** 1691.

PAN, M., REID, M. A., LOWMAN, X. H., KULKARNI, R. P., TRAN, T. Q., LIU, X., YANG, Y., HERNANDEZ-DAVIES, J. E., ROSALES, K. K., LI, H., HUGO, W., SONG, C., XU, X., SCHONES, D. E., ANN, D. K., GRADINARU, V., LO, R. S., LOCASALE, J. W. & KONG, M. 2016. Regional glutamine deficiency in tumours promotes dedifferentiation through inhibition of histone demethylation. *Nature Cell Biology,* 18**,** 1090.

PANG, Y.-Y., WANG, T., CHEN, F.-Y., WU, Y.-L., SHAO, X., XIAO, F., HUANG, H.-H., ZHONG, H. & ZHONG, J.-H. 2015. Glycolytic inhibitor 2-deoxy-d-glucose suppresses cell proliferation and enhances methylprednisolone sensitivity in non-Hodgkin lymphoma cells through down-regulation of HIF-1α and c-MYC. *Leukemia & Lymphoma,* 56**,** 1821-1830.

PARK, S. H., CHI, H.-S., MIN, S.-K., PARK, B. G., JANG, S. & PARK, C.-J. 2011. Prognostic impact of c-KIT mutations in core binding factor acute myeloid leukemia. *Leukemia Research,* 35**,** 1376-1383.

PARSONS, D. W., JONES, S., ZHANG, X., LIN, J. C.-H., LEARY, R. J., ANGENENDT, P., MANKOO, P., CARTER, H., SIU, I. M., GALLIA, G. L., OLIVI, A., MCLENDON, R., RASHEED, B. A., KEIR, S., NIKOLSKAYA, T.,

NIKOLSKY, Y., BUSAM, D. A., TEKLEAB, H., DIAZ, L. A., JR., HARTIGAN, J., SMITH, D. R., STRAUSBERG, R. L., MARIE, S. K. N., SHINJO, S. M. O., YAN, H., RIGGINS, G. J., BIGNER, D. D., KARCHIN, R., PAPADOPOULOS, N., PARMIGIANI, G., VOGELSTEIN, B., VELCULESCU, V. E. & KINZLER, K. W. 2008. An integrated genomic analysis of human glioblastoma multiforme. *Science (New York, N.Y.),* 321**,** 1807-1812.

PASCHKA, P., MARCUCCI, G., RUPPERT, A. S., MRÓZEK, K., CHEN, H., KITTLES, R. A., VUKOSAVLJEVIC, T., PERROTTI, D., VARDIMAN, J. W., CARROLL, A. J., KOLITZ, J. E., LARSON, R. A. & BLOOMFIELD, C. D. 2006. Adverse Prognostic Significance of KIT Mutations in Adult Acute Myeloid Leukemia With inv(16) and t(8;21): A Cancer and Leukemia Group B Study. *Journal of Clinical Oncology,* 24**,** 3904-3911.

PAVLOVA, N. N. & THOMPSON, C. B. 2016. The Emerging Hallmarks of Cancer Metabolism. *Cell metabolism,* 23**,** 27-47.

PEARCE, D. J., TAUSSIG, D., ZIBARA, K., SMITH, L.-L., RIDLER, C. M., PREUDHOMME, C., YOUNG, B. D., ROHATINER, A. Z., LISTER, T. A. & BONNET, D. 2006. AML engraftment in the NOD/SCID assay reflects the outcome of AML: implications for our understanding of the heterogeneity of AML. *Blood,* 107**,** 1166.

PENG, T., GOLUB, T. R. & SABATINI, D. M. 2002. The immunosuppressant rapamycin mimics a starvation-like signal distinct from amino acid and glucose deprivation. *Molecular and cellular biology,* 22**,** 5575-5584.

PETERSON, L. F., BOYAPATI, A., AHN, E.-Y., BIGGS, J. R., OKUMURA, A. J., LO, M.-C., YAN, M. & ZHANG, D.-E. 2007a. Acute myeloid leukemia with the 8q22;21q22 translocation: secondary mutational events and alternative t(8;21) transcripts. *Blood,* 110**,** 799-805.

PETERSON, L. F., YAN, M. & ZHANG, D.-E. 2007b. The p21(Waf1) pathway is involved in blocking leukemogenesis by the t(8;21) fusion protein AML1-ETO. *Blood,* 109**,** 4392-4398.

PETIT, C., GOUEL, F., DUBUS, I., HEUCLIN, C., ROGET, K. & VANNIER, J. P. 2016. Hypoxia promotes chemoresistance in acute lymphoblastic leukemia cell lines by modulating death signaling pathways. *BMC cancer,* 16**,** 746-746.

POTTER, H. & HELLER, R. 2003. Transfection by Electroporation. *Current protocols in molecular biology / edited by Frederick M. Ausubel ... [et al.],* CHAPTER**,** Unit-9.3.

POTTER, H., WEIR, L. & LEDER, P. 1984. Enhancer-dependent expression of human kappa immunoglobulin genes introduced into mouse pre-B lymphocytes by electroporation. *Proceedings of the National Academy of Sciences of the United States of America,* 81**,** 7161-7165.

PTASINSKA, A., ASSI, S. A., MANNARI, D., JAMES, S. R., WILLIAMSON, D., DUNNE, J., HOOGENKAMP, M., WU, M., CARE, M., MCNEILL, H., CAUCHY, P., CULLEN, M., TOOZE, R. M., TENEN, D. G., YOUNG, B. D., COCKERILL, P. N., WESTHEAD, D. R., HEIDENREICH, O. & BONIFER, C. 2012. Depletion of RUNX1/ETO in t(8;21) AML cells leads to genome-wide changes in chromatin structure and transcription factor binding. *Leukemia,* 26**,** 1829-1841.

PTASINSKA, A., ASSI, SALAM A., MARTINEZ-SORIA, N., IMPERATO, MARIA R., PIPER, J., CAUCHY, P., PICKIN, A., JAMES, SALLY R., HOOGENKAMP, M., WILLIAMSON, D., WU, M., TENEN, DANIEL G., OTT, S., WESTHEAD, DAVID R., COCKERILL, PETER N., HEIDENREICH, O. & BONIFER, C. 2014. Identification of a Dynamic Core Transcriptional Network in t(8;21) AML that Regulates Differentiation Block and Self-Renewal. *Cell Reports,* 8**,** 1974-1988.

PUI, C.-H., CAMPANA, D., PEI, D., BOWMAN, W. P., SANDLUND, J. T., KASTE, S. C., RIBEIRO, R. C., RUBNITZ, J. E., RAIMONDI, S. C., ONCIU, M., COUSTAN-SMITH, E., KUN, L. E., JEHA, S., CHENG, C., HOWARD, S. C., SIMMONS, V., BAYLES, A., METZGER, M. L., BOYETT, J. M., LEUNG, W., HANDGRETINGER, R., DOWNING, J. R., EVANS, W. E. & RELLING, M. V. 2009. Treating childhood acute lymphoblastic leukemia without cranial irradiation. *The New England journal of medicine,* 360**,** 2730-2741.

QUEK, L., OTTO, G. W., GARNETT, C., LHERMITTE, L., KARAMITROS, D., STOILOVA, B., LAU, I. J., DOONDEEA, J., USUKHBAYAR, B., KENNEDY, A., METZNER, M., GOARDON, N., IVEY, A., ALLEN, C., GALE, R., DAVIES, B., STERNBERG, A., KILLICK, S., HUNTER, H., CAHALIN, P., PRICE, A., CARR, A., GRIFFITHS, M., VIRGO, P., MACKINNON, S., GRIMWADE, D.,

FREEMAN, S., RUSSELL, N., CRADDOCK, C., MEAD, A., PENIKET, A., PORCHER, C. & VYAS, P. 2016. Genetically distinct leukemic stem cells in human CD34- acute myeloid leukemia are arrested at a hemopoietic precursor-like stage. *The Journal of experimental medicine,* 213**,** 1513-1535.

R WISE, D., DEBERARDINIS, R., MANCUSO, A., SAYED, N., ZHANG, X.-Y., K PFEIFFER, H., NISSIM, I., DAIKHIN, E., YUDKOFF, M., MCMAHON, S. & B THOMPSON, C. 2008. *Myc regulates a transcriptional program that stimulates mitochondrial glutaminolysis and leads to glutamine addiction*.

RAEZ, L. E., PAPADOPOULOS, K., RICART, A. D., CHIOREAN, E. G., DIPAOLA, R. S., STEIN, M. N., ROCHA LIMA, C. M., SCHLESSELMAN, J. J., TOLBA, K., LANGMUIR, V. K., KROLL, S., JUNG, D. T., KURTOGLU, M., ROSENBLATT, J. & LAMPIDIS, T. J. 2013. A phase I dose-escalation trial of 2-deoxy-d-glucose alone or combined with docetaxel in patients with advanced solid tumors. *Cancer Chemotherapy and Pharmacology,* 71**,** 523-530.

RATHMELL, J. C., FOX, C. J., PLAS, D. R., HAMMERMAN, P. S., CINALLI, R. M. & THOMPSON, C. B. 2003. Akt-directed glucose metabolism can prevent Bax conformation change and promote growth factor-independent survival. *Molecular and cellular biology,* 23**,** 7315-7328.

RECZEK, C. R. & CHANDEL, N. S. 2017. The Two Faces of Reactive Oxygen Species in Cancer. *Annual Review of Cancer Biology,* 1**,** 79-98.

REEDIJK, A. M. J., KLEIN, K., COEBERGH, J. W. W., KREMER, L. C., DINMOHAMED, A. G., DE HAAS, V., VERSLUIJS, A. B., OSSENKOPPELE, G. J., BEVERLOO, H. B., PIETERS, R., ZWAAN, C. M., KASPERS, G. J. L. & KARIM-KOS, H. E. 2018. Improved survival for children and young adolescents with acute myeloid leukemia: a Dutch study on incidence, survival and mortality. *Leukemia*.

REID, MICHAEL A., WANG, W.-I., ROSALES, KIMBERLY R., WELLIVER, MENG X., PAN, M. & KONG, M. 2013. The B55α Subunit of PP2A Drives a p53-Dependent Metabolic Adaptation to Glutamine Deprivation. *Molecular Cell,* 50**,** 200-211.

REIKVAM, H., HATFIELD, K. J., KITTANG, A. O., HOVLAND, R. & BRUSERUD, Ø. 2011. Acute Myeloid Leukemia with the t(8;21) Translocation: Clinical Consequences and Biological Implications. *Journal of Biomedicine and Biotechnology,* 2011**,** 23.

REITMAN, Z. J., PARSONS, D. W. & YAN, H. 2010. IDH1 and IDH2: not your typical oncogenes. *Cancer cell,* 17**,** 215-216.

RESHKIN, S. J., BELLIZZI, A., CALDEIRA, S., ALBARANI, V., MALANCHI, I., POIGNEE, M., ALUNNI-FABBRONI, M., CASAVOLA, V. & TOMMASINO, M. 2000. Na+/H+ exchanger-dependent intracellular alkalinization is an early event in malignant transformation and plays an essential role in the development of subsequent transformation-associated phenotypes. *The FASEB Journal,* 14**,** 2185-2197.

RHOADES, K. L., HETHERINGTON, C. J., HARAKAWA, N., YERGEAU, D. A., ZHOU, L., LIU, L.-Q., LITTLE, M.-T., TENEN, D. G. & ZHANG, D.-E. 2000. Analysis of the role of AML1-ETO in leukemogenesis, using an inducible transgenic mouse model. *Blood,* 96**,** 2108.

ROBEY, R. B. & HAY, N. 2009. Is Akt the "Warburg kinase"?-Akt-energy metabolism interactions and oncogenesis. *Seminars in cancer biology,* 19**,** 25-31.

ROESCH, A., VULTUR, A., BOGESKI, I., WANG, H., ZIMMERMANN, KATHARINA M., SPEICHER, D., KÖRBEL, C., LASCHKE, MATTHIAS W., GIMOTTY, PHYLLIS A., PHILIPP, STEPHAN E., KRAUSE, E., PÄTZOLD, S., VILLANUEVA, J., KREPLER, C., FUKUNAGA-KALABIS, M., HOTH, M., BASTIAN, BORIS C., VOGT, T. & HERLYN, M. 2013. Overcoming Intrinsic Multidrug Resistance in Melanoma by Blocking the Mitochondrial Respiratory Chain of Slow-Cycling JARID1Bhigh Cells. *Cancer Cell,* 23**,** 811-825.

RÖNNSTRAND, L. 2004. Signal transduction via the stem cell factor receptor/c-Kit. *Cellular and Molecular Life Sciences CMLS,* 61**,** 2535-2548.

ROUAULT-PIERRE, K., LOPEZ-ONIEVA, L., FOSTER, K., ANJOS-AFONSO, F., LAMRISSI-GARCIA, I., SERRANO-SANCHEZ, M., MITTER, R., IVANOVIC, Z., DE VERNEUIL, H., GRIBBEN, J., TAUSSIG, D., REZVANI, HAMID R., MAZURIER, F. & BONNET, D. 2013. HIF-2α Protects Human Hematopoietic Stem/Progenitors and Acute Myeloid Leukemic Cells from

Apoptosis Induced by Endoplasmic Reticulum Stress. *Cell Stem Cell,* 13**,** 549-563.

ROWE, J. M. & LÖWENBERG, B. 2013. Gemtuzumab ozogamicin in acute myeloid leukemia: a remarkable saga about an active drug. *Blood,* 121**,** 4838.

ROWLEY, J. D. 1973. Identification of a translocation with quinacrine fluorescence in a patient with acute leukemia. *Annales de Genetique,* 16**,** 109-112.

ROY, A. & SIL, P. C. 2012. Tertiary butyl hydroperoxide induced oxidative damage in mice erythrocytes: Protection by taurine. *Pathophysiology,* 19**,** 137-148.

RUNDQVIST, H. & JOHNSON, R. S. 2013. Tumour oxygenation: implications for breast cancer prognosis. *Journal of Internal Medicine,* 274**,** 105-112.

RYNINGEN, A., ERSVÆR, E., ØYAN, A. M., KALLAND, K.-H., VINTERMYR, O. K., GJERTSEN, B. T. & BRUSERUD, Ø. 2006. Stress-induced in vitro apoptosis of native human acute myelogenous leukemia (AML) cells shows a wide variation between patients and is associated with low BCL-2:Bax ratio and low levels of heat shock protein 70 and 90. *Leukemia Research,* 30**,** 1531-1540.

SACCHI, N., TAMANINI, F., WILLEMSEN, R., DENIS-DONINI, S., CAMPIGLIO, S. & HOOGEVEEN, A. T. 1998. Subcellular localization of the oncoprotein MTG8 (CDR/ETO) in neural cells. *Oncogene,* 16**,** 2609.

SAITO, Y., CHAPPLE, RICHARD H., LIN, A., KITANO, A. & NAKADA, D. 2015. AMPK Protects Leukemia-Initiating Cells in Myeloid Leukemias from Metabolic Stress in the Bone Marrow. *Cell Stem Cell,* 17**,** 585-596.

SALEEM, A., DVORZHINSKI, D., SANTANAM, U., MATHEW, R., BRAY, K. & STEIN, M. 2012. Effect of dual inhibition of apoptosis and autophagy in prostate cancer. *Prostate,* 72.

SALPETER, S. J., KLOCHENDLER, A., WEINBERG-COREM, N., PORAT, S., GRANOT, Z., SHAPIRO, A. M. J., MAGNUSON, M. A., EDEN, A., GRIMSBY, J., GLASER, B. & DOR, Y. 2011. Glucose regulates cyclin D2 expression in quiescent and replicating pancreatic β-cells through glycolysis and calcium channels. *Endocrinology,* 152**,** 2589-2598.

SATOH, Y., MATSUMURA, I., TANAKA, H., EZOE, S., FUKUSHIMA, K., TOKUNAGA, M., YASUMI, M., SHIBAYAMA, H., MIZUKI, M., ERA, T., OKUDA, T. & KANAKURA, Y. 2008. AML1/RUNX1 works as a negative

regulator of c-Mpl in hematopoietic stem cells. *The Journal of biological chemistry,* 283**,** 30045-30056.

SAUNA, Z. E., SMITH, M. M., MÜLLER, M., KERR, K. M. & AMBUDKAR, S. V. 2001. The Mechanism of Action of Multidrug-Resistance-Linked P-Glycoprotein. *Journal of Bioenergetics and Biomembranes,* 33**,** 481-491.

SCHNITTGER, S., DICKER, F., KERN, W., WENDLAND, N., SUNDERMANN, J., ALPERMANN, T., HAFERLACH, C. & HAFERLACH, T. 2011. RUNX1 mutations are frequent in de novo AML with noncomplex karyotype and confer an unfavorable prognosis. *Blood,* 117**,** 2348.

SCHOCH, C., KERN, W., KRAWITZ, P., DUGAS, M., SCHNITTGER, S., HAFERLACH, T. & HIDDEMANN, W. 2001. Dependence of age-specific incidence of acute myeloid leukemia on karyotype. *Blood,* 98**,** 3500.

SCHOSSERER, M., GRILLARI, J. & BREITENBACH, M. 2017. The Dual Role of Cellular Senescence in Developing Tumors and Their Response to Cancer Therapy. *Frontiers in oncology,* 7**,** 278-278.

SCHWARTZENBERG-BAR-YOSEPH, F., ARMONI, M. & KARNIELI, E. 2004. The Tumor Suppressor p53 Down-Regulates Glucose Transporters GLUT1 and GLUT4 Gene Expression. *Cancer Research,* 64**,** 2627.

SEMENZA, G. L. 2017. Hypoxia-inducible factors: coupling glucose metabolism and redox regulation with induction of the breast cancer stem cell phenotype. *The EMBO Journal,* 36**,** 252-259.

SESSO, A., FUJIWARA, D. T., JAEGER, M., JAEGER, R., LI, T. C., MONTEIRO, M. M. T., CORREA, H., FERREIRA, M. A., SCHUMACHER, R. I., BELISÁRIO, J., KACHAR, B. & CHEN, E. J. 1999. Structural elements common to mitosis and apoptosis. *Tissue and Cell,* 31**,** 357-371.

SGARBI, G., GORINI, G., LIUZZI, F., SOLAINI, G. & BARACCA, A. 2018. Hypoxia and IF_1 Expression Promote ROS Decrease in Cancer Cells. *Cells,* 7**,** 64.

SINGH, D., ARORA, R., KAUR, P., SINGH, B., MANNAN, R. & ARORA, S. 2017. Overexpression of hypoxia-inducible factor and metabolic pathways: possible targets of cancer. *Cell & bioscience,* 7**,** 62-62.

SINGH, R., LILLARD, J. W., JR. & SINGH, S. 2011. Chemokines: key players in cancer progression and metastasis. *Frontiers in bioscience (Scholar edition),* 3**,** 1569-1582.

SOBHAKUMARI, A., ORCUTT, K. P., LOVE-HOMAN, L., KOWALSKI, C. E., PARSONS, A. D., KNUDSON, C. M. & SIMONS, A. L. 2016. 2-Deoxy-d-glucose Suppresses the In Vivo Antitumor Efficacy of Erlotinib in Head and Neck Squamous Cell Carcinoma Cells. *Oncology research,* 24**,** 55-64.

SONVEAUX, P., VÉGRAN, F., SCHROEDER, T., WERGIN, M. C., VERRAX, J., RABBANI, Z. N., DE SAEDELEER, C. J., KENNEDY, K. M., DIEPART, C., JORDAN, B. F., KELLEY, M. J., GALLEZ, B., WAHL, M. L., FERON, O. & DEWHIRST, M. W. 2008. Targeting lactate-fueled respiration selectively kills hypoxic tumor cells in mice. *The Journal of clinical investigation,* 118**,** 3930-3942.

SOOD, R., KAMIKUBO, Y. & LIU, P. 2017. Role of RUNX1 in hematological malignancies. *Blood,* 129**,** 2070.

SOONTARARAK, S., CHOW, L., JOHNSON, V., COY, J., WHEAT, W., REGAN, D. & DOW, S. 2018. Mesenchymal Stem Cells (MSC) Derived from Induced Pluripotent Stem Cells (iPSC) Equivalent to Adipose-Derived MSC in Promoting Intestinal Healing and Microbiome Normalization in Mouse Inflammatory Bowel Disease Model. *STEM CELLS Translational Medicine,* 7**,** 456-467.

SORIA, N. M., TUSSIWAND, R., ZIEGLER, P., MANZ, M. G. & HEIDENREICH, O. 2008. Transient depletion of RUNX1/RUNX1T1 by RNA interference delays tumour formation in vivo. *Leukemia,* 23**,** 188.

SPENCER, J. A., FERRARO, F., ROUSSAKIS, E., KLEIN, A., WU, J., RUNNELS, J. M., ZAHER, W., MORTENSEN, L. J., ALT, C., TURCOTTE, R., YUSUF, R., CÔTÉ, D., VINOGRADOV, S. A., SCADDEN, D. T. & LIN, C. P. 2014. Direct measurement of local oxygen concentration in the bone marrow of live animals. *Nature,* 508**,** 269-273.

STAMATERIS, R. E., SHARMA, R. B., KONG, Y., EBRAHIMPOUR, P., PANDAY, D., RANGANATH, P., ZOU, B., LEVITT, H., PARAMBIL, N. A., O'DONNELL, C. P., GARCÍA-OCAÑA, A. & ALONSO, L. C. 2016. Glucose Induces Mouse β-Cell Proliferation via IRS2, MTOR, and Cyclin D2 but Not the Insulin Receptor. *Diabetes,* 65**,** 981-995.

STARSKA, K., FORMA, E., JÓŹWIAK, P., BRYŚ, M., LEWY-TRENDA, I., BRZEZIŃSKA-BŁASZCZYK, E. & KRZEŚLAK, A. 2015. Gene and protein expression of glucose transporter 1 and glucose transporter 3 in human laryngeal cancer—the relationship with regulatory hypoxia-inducible factor-1α expression, tumor invasiveness, and patient prognosis. *Tumour Biology,* 36**,** 2309-2321.

STEGMEIER, F., HU, G., RICKLES, R. J., HANNON, G. J. & ELLEDGE, S. J. 2005. A lentiviral microRNA-based system for single-copy polymerase II-regulated RNA interference in mammalian cells. *Proceedings of the National Academy of Sciences of the United States of America,* 102**,** 13212-13217.

STEIN, M., LIN, H., JEYAMOHAN, C., DVORZHINSKI, D., GOUNDER, M., BRAY, K., EDDY, S., GOODIN, S., WHITE, E. & DIPAOLA, R. S. 2010. TargetingTumor MetabolismWith 2-Deoxyglucose in Patients With Castrate-Resistant Prostate Cancer and Advanced Malignancies. *The Prostate,* 70**,** 1388-1394.

STEINBACH, J. P., WOLBURG, H., KLUMPP, A., PROBST, H. & WELLER, M. 2003. Hypoxia-induced cell death in human malignant glioma cells: energy deprivation promotes decoupling of mitochondrial cytochrome c release from caspase processing and necrotic cell death. *Cell Death And Differentiation,* 10**,** 823.

STOJAK, M., ŁUKAWSKA, M., OSZCZAPOWICZ, I., OPYDO-CHANEK, M. & MAZUR, L. 2014. Cell-cycle Disturbance and Induction of Programmed Death by New Formamidine Analogs of Daunorubicin. *Anticancer Research,* 34**,** 7151-7158.

SUBRAMANIAN, A., TAMAYO, P., MOOTHA, V. K., MUKHERJEE, S., EBERT, B. L., GILLETTE, M. A., PAULOVICH, A., POMEROY, S. L., GOLUB, T. R., LANDER, E. S. & MESIROV, J. P. 2005. Gene set enrichment analysis: A

knowledge-based approach for interpreting genome-wide expression profiles. *Proceedings of the National Academy of Sciences,* 102**,** 15545-15550.

SUDA, T., TAKUBO, K. & SEMENZA, GREGG L. 2011. Metabolic Regulation of Hematopoietic Stem Cells in the Hypoxic Niche. *Cell Stem Cell,* 9**,** 298-310.

SULLIVAN, R., PARÉ, G. C., FREDERIKSEN, L. J., SEMENZA, G. L. & GRAHAM, C. H. 2008. Hypoxia-induced resistance to anticancer drugs is associated with decreased senescence and requires hypoxia-inducible factor-1 activity. *Molecular Cancer Therapeutics,* 7**,** 1961.

SUN, W., GRAVES, B. J. & SPECK, N. A. 1995. Transactivation of the Moloney murine leukemia virus and T-cell receptor beta-chain enhancers by cbf and ets requires intact binding sites for both proteins. *Journal of virology,* 69**,** 4941-4949.

TAGG, S. L. C., FOSTER, P. A., LEESE, M. P., POTTER, B. V. L., REED, M. J., PUROHIT, A. & NEWMAN, S. P. 2008. 2-Methoxyoestradiol-3,17-O,O-bis-sulphamate and 2-deoxy-D-glucose in combination: a potential treatment for breast and prostate cancer. *British Journal of Cancer,* 99**,** 1842-1848.

TAJAN, M., HOCK, A. K., BLAGIH, J., ROBERTSON, N. A., LABUSCHAGNE, C. F., KRUISWIJK, F., HUMPTON, T. J., ADAMS, P. D. & VOUSDEN, K. H. 2018. A Role for p53 in the Adaptation to Glutamine Starvation through the Expression of SLC1A3. *Cell Metabolism,* 28**,** 721-736.e6.

TAKAHASHI, A., SATAKE, M., YAMAGUCHI-IWAI, Y., BAE, S. C., LU, J., MARUYAMA, M., ZHANG, Y. W., OKA, H., ARAI, N. & ARAI, K. 1995. Positive and negative regulation of granulocyte-macrophage colony- stimulating factor promoter activity by AML1-related transcription factor, PEBP2. *Blood,* 86**,** 607.

TAKAHASHI, S. 2011. Current findings for recurring mutations in acute myeloid leukemia. *Journal of hematology & oncology,* 4**,** 36-36.

TAKAKURA, N., WATANABE, T., SUENOBU, S., YAMADA, Y., NODA, T., ITO, Y., SATAKE, M. & SUDA, T. 2000. A Role for Hematopoietic Stem Cells in Promoting Angiogenesis. *Cell,* 102**,** 199-209.

TAO, W., WANG, M., VOSS, E. D., COCKLIN, R. R., SMITH, J. A., COOPER, S. H. & BROXMEYER, H. E. 2004. Comparative Proteomic Analysis of Human

CD34+ Stem/Progenitor Cells and Mature CD15+ Myeloid Cells. *STEM CELLS,* 22**,** 1003-1014.

TAVIAN M., B. K., SINKA L., VALLET J., PÉAULT B. 2010. Embryonic origin of human hematopoiesis. *Int. J. Dev. Biol.,* 54**,** 1061-1065.

TELFER, J. C. & ROTHENBERG, E. V. 2001. Expression and Function of a Stem Cell Promoter for the Murine CBFα2 Gene: Distinct Roles and Regulation in Natural Killer and T Cell Development. *Developmental Biology,* 229**,** 363-382.

THAKKAR, A. D., RAJ, H., CHAKRABARTI, D., RAVISHANKAR, SARAVANAN, N., MUTHUVELAN, B., BALAKRISHNAN, A. & PADIGARU, M. 2010. Identification of Gene Expression Signature in Estrogen Receptor Positive Breast Carcinoma. *Biomarkers in Cancer,* 2**,** 1-15.

THOMAS, D. & MAJETI, R. 2017. Biology and relevance of human acute myeloid leukemia stem cells. *Blood,* 129**,** 1577-1585.

TIDMARSH, G. F., TANNER, L. I., O'CONNOR, J., ENG, C. & MORDEC, K. 2004. Effect of 2-Deoxyglucose, a Glycolytic Inhibitor, on the ATP Levels and Viability of B Lymphocytes from Subjects with Chronic Lymphocytic Leukemia (CLL). *Blood,* 104**,** 4810.

TRAGGIAI, E., CHICHA, L., MAZZUCCHELLI, L., BRONZ, L., PIFFARETTI, J.-C., LANZAVECCHIA, A. & MANZ, M. G. 2004. Development of a Human Adaptive Immune System in Cord Blood Cell-Transplanted Mice. *Science,* 304**,** 104-107.

TRAN, T. Q., ISHAK GABRA, M. B., LOWMAN, X. H., YANG, Y., REID, M. A., PAN, M., O'CONNOR, T. R. & KONG, M. 2017. Glutamine deficiency induces DNA alkylation damage and sensitizes cancer cells to alkylating agents through inhibition of ALKBH enzymes. *PLOS Biology,* 15**,** e2002810.

TSUZUKI, S., HONG, D., GUPTA, R., MATSUO, K., SETO, M. & ENVER, T. 2007. Isoform-specific potentiation of stem and progenitor cell engraftment by AML1/RUNX1. *PLoS medicine,* 4**,** e172-e172.

VANCE, J. E. & TASSEVA, G. 2013. Formation and function of phosphatidylserine and phosphatidylethanolamine in mammalian cells. *Biochimica et Biophysica Acta (BBA) - Molecular and Cell Biology of Lipids,* 1831**,** 543-554.

VANGALA, R. K., HEISS-NEUMANN, M. S., RANGATIA, J. S., SINGH, S. M., SCHOCH, C., TENEN, D. G., HIDDEMANN, W. & BEHRE, G. 2003. The myeloid master regulator transcription factor PU.1 is inactivated by AML1-ETO in t(8;21) myeloid leukemia. *Blood,* 101**,** 270.

VARDIMAN, J. W., HARRIS, N. L. & BRUNNING, R. D. 2002. The World Health Organization (WHO) classification of the myeloid neoplasms. *Blood,* 100**,** 2292.

VELASCO-HERNANDEZ, T., HYRENIUS-WITTSTEN, A., REHN, M., BRYDER, D. & CAMMENGA, J. 2014. HIF-1α can act as a tumor suppressor gene in murine acute myeloid leukemia. *Blood,* 124**,** 3597-3607.

VELASCO-HERNANDEZ, T., SONEJI, S., HIDALGO, I., ERLANDSSON, E., CAMMENGA, J. & BRYDER, D. 2018. Hif-1α Deletion May Lead to Adverse Treatment Effect in a Mouse Model of MLL-AF9-Driven AML. *Stem cell reports,* 12**,** 112-121.

VELASCO-HERNANDEZ, T., SONEJI, S., HIDALGO, I., ERLANDSSON, E., CAMMENGA, J. & BRYDER, D. 2019. Hif-1α Deletion May Lead to Adverse Treatment Effect in a Mouse Model of MLL-AF9-Driven AML. *Stem Cell Reports,* 12**,** 112-121.

VEUGER, M. J. T., HEEMSKERK, M. H. M., HONDERS, M. W., WILLEMZE, R. & BARGE, R. M. Y. 2002. Functional role of alternatively spliced deoxycytidine kinase in sensitivity to cytarabine of acute myeloid leukemic cells. *Blood,* 99**,** 1373.

VIJAYARAGHAVAN, S., KARAKAS, C., DOOSTAN, I., CHEN, X., BUI, T., YI, M., RAGHAVENDRA, A. S., ZHAO, Y., BASHOUR, S. I., IBRAHIM, N. K., KARUTURI, M., WANG, J., WINKLER, J. D., AMARAVADI, R. K., HUNT, K. K., TRIPATHY, D. & KEYOMARSI, K. 2017. CDK4/6 and autophagy inhibitors synergistically induce senescence in Rb positive cytoplasmic cyclin E negative cancers. *Nature communications,* 8**,** 15916-15916.

VUKOVIC, M., GUITART, A. V., SEPULVEDA, C., VILLACRECES, A., O'DUIBHIR, E., PANAGOPOULOU, T. I., IVENS, A., MENENDEZ-GONZALEZ, J., IGLESIAS, J. M., ALLEN, L., GLYKOFRYDIS, F., SUBRAMANI, C., ARMESILLA-DIAZ, A., POST, A. E. M., SCHAAK, K., GEZER, D., SO, C. W.

E., HOLYOAKE, T. L., WOOD, A., O'CARROLL, D., RATCLIFFE, P. J. & KRANC, K. R. 2015. Hif-1α and Hif-2α synergize to suppress AML development but are dispensable for disease maintenance. *The Journal of experimental medicine,* 212**,** 2223-2234.

WAHDAN-ALASWAD, R., FAN, Z., EDGERTON, S. M., LIU, B., DENG, X.-S., ARNADOTTIR, S. S., RICHER, J. K., ANDERSON, S. M. & THOR, A. D. 2013. Glucose promotes breast cancer aggression and reduces metformin efficacy. *Cell Cycle,* 12**,** 3759-3769.

WAKITA, S., YAMAGUCHI, H., MIYAKE, K., MITAMURA, Y., KOSAKA, F., DAN, K. & INOKUCHI, K. 2011. Importance of c-kit mutation detection method sensitivity in prognostic analyses of t(8;21)(q22;q22) acute myeloid leukemia. *Leukemia,* 25**,** 1423.

WANG, H., NICOLAY, B. N., CHICK, J. M., GAO, X., GENG, Y., REN, H., GAO, H., YANG, G., WILLIAMS, J. A., SUSKI, J. M., KEIBLER, M. A., SICINSKA, E., GERDEMANN, U., HAINING, W. N., ROBERTS, T. M., POLYAK, K., GYGI, S. P., DYSON, N. J. & SICINSKI, P. 2017a. The metabolic function of cyclin D3–CDK6 kinase in cancer cell survival. *Nature,* 546**,** 426-430.

WANG, L., GURAL, A., SUN, X.-J., ZHAO, X., PERNA, F., HUANG, G., HATLEN, M. A., VU, L., LIU, F., XU, H., ASAI, T., XU, H., DEBLASIO, T., MENENDEZ, S., VOZA, F., JIANG, Y., COLE, P. A., ZHANG, J., MELNICK, A., ROEDER, R. G. & NIMER, S. D. 2011a. The leukemogenicity of AML1-ETO is dependent on site-specific lysine acetylation. *Science (New York, N.Y.),* 333**,** 765-769.

WANG, Q., STACY, T., MILLER, J. D., LEWIS, A. F., GU, T.-L., HUANG, X., BUSHWELLER, J. H., BORIES, J.-C., ALT, F. W., RYAN, G., LIU, P. P., WYNSHAW-BORIS, A., BINDER, M., MARÍN-PADILLA, M., SHARPE, A. H. & SPECK, N. A. 1996. The CBFβ Subunit Is Essential for CBFα2 (AML1) Function In Vivo. *Cell,* 87**,** 697-708.

WANG, T., YU, H., HUGHES, N. W., LIU, B., KENDIRLI, A., KLEIN, K., CHEN, W. W., LANDER, E. S. & SABATINI, D. M. 2017b. Gene Essentiality Profiling Reveals Gene Networks and Synthetic Lethal Interactions with Oncogenic Ras. *Cell,* 168**,** 890-903.e15.

WANG, Y., LIU, Y., MALEK, SAMI N., ZHENG, P. & LIU, Y. 2011b. Targeting HIF1α Eliminates Cancer Stem Cells in Hematological Malignancies. *Cell Stem Cell,* 8**,** 399-411.

WARBURG, O. 1956a. On respiratory impairment in cancer cells. *Science,* 124.

WARBURG, O. 1956b. On respiratory impairment in cancer cells. *Science,* 10**,** 269-70.

WARD, P. S., PATEL, J., WISE, D. R., ABDEL-WAHAB, O., BENNETT, B. D., COLLER, H. A., CROSS, J. R., FANTIN, V. R., HEDVAT, C. V., PERL, A. E., RABINOWITZ, J. D., CARROLL, M., SU, S. M., SHARP, K. A., LEVINE, R. L. & THOMPSON, C. B. 2010. The Common Feature of Leukemia-Associated IDH1 and IDH2 Mutations Is a Neomorphic Enzyme Activity Converting α-Ketoglutarate to 2-Hydroxyglutarate. *Cancer Cell,* 17**,** 225-234.

WICHMANN, C., QUAGLIANO-LO COCO, I., YILDIZ, Ö., CHEN-WICHMANN, L., WEBER, H., SYZONENKO, T., DÖRING, C., BRENDEL, C., PONNUSAMY, K., KINNER, A., BRANDTS, C., HENSCHLER, R. & GREZ, M. 2015. Activating c-KIT mutations confer oncogenic cooperativity and rescue RUNX1/ETO-induced DNA damage and apoptosis in human primary CD34+ hematopoietic progenitors. *Leukemia,* 29**,** 279-289.

WICK, A. N., DRURY, D. R., NAKADA, H. I., WOLFE, J. B., WITH THE TECHNICAL ASSISTANCE OF BARBARA, B. & RUTH, G. 1957. LOCALIZATION OF THE PRIMARY METABOLIC BLOCK PRODUCED BY 2-DEOXYGLUCOSE. *Journal of Biological Chemistry,* 224**,** 963-969.

WIEMELS, J. L., XIAO, Z., BUFFLER, P. A., MAIA, A. T., MA, X., DICKS, B. M., SMITH, M. T., ZHANG, L., FEUSNER, J., WIENCKE, J., PRITCHARD-JONES, K., KEMPSKI, H. & GREAVES, M. 2002. In utero origin of t(8;21) AML1-ETO translocations in childhood acute myeloid leukemia. *Blood,* 99**,** 3801.

WISE, D. R. & THOMPSON, C. B. 2010. Glutamine Addiction: A New Therapeutic Target in Cancer. *Trends in biochemical sciences,* 35**,** 427-433.

WLODKOWIC, D., SKOMMER, J. & DARZYNKIEWICZ, Z. 2009. Flow cytometry-based apoptosis detection. *Methods in molecular biology (Clifton, N.J.),* 559**,** 19-32.

WOLFORD, J. K. & PROCHAZKA, M. 1998. Structure and expression of the human MTG8/ETO gene1The sequences reported in this manuscript were deposited with the GenBank Database under Accession Nos AF018270–AF018283.1. *Gene,* 212**,** 103-109.

WONG, T.-K. & NEUMANN, E. 1982. Electric field mediated gene transfer. *Biochemical and Biophysical Research Communications,* 107**,** 584-587.

WU, D., OZAKI, T., YOSHIHARA, Y., KUBO, N. & NAKAGAWARA, A. 2013. Runt-related transcription factor 1 (RUNX1) stimulates tumor suppressor p53 protein in response to DNA damage through complex formation and acetylation. *The Journal of biological chemistry,* 288**,** 1353-1364.

WU, H., ZHU, H., LIU, D. X., NIU, T. K., REN, X. & PATEL, R. 2009. Silencing of elongation factor-2 kinase potentiates the effect of 2-deoxy-D-glucose against human glioma cells through blunting of autophagy. *Cancer Res,* 69.

YAMAGUCHI, R., JANSSEN, E., PERKINS, G., ELLISMAN, M., KITADA, S. & REED, J. C. 2011. Efficient elimination of cancer cells by deoxyglucose-ABT-263/737 combination therapy. *PloS one,* 6**,** e24102-e24102.

YAMAMOTO, T., TAKANO, N., ISHIWATA, K., OHMURA, M., NAGAHATA, Y., MATSUURA, T., KAMATA, A., SAKAMOTO, K., NAKANISHI, T., KUBO, A., HISHIKI, T. & SUEMATSU, M. 2014. Reduced methylation of PFKFB3 in cancer cells shunts glucose towards the pentose phosphate pathway. *Nature communications,* 5**,** 3480-3480.

YAN, J.-S., LI, Y.-D., LIU, S.-H., YIN, Q.-Q., LIU, X.-Y., XIA, L. & LU, Y. 2017. The t(8;21) fusion protein RUNX1-ETO downregulates PKM2 in acute myeloid leukemia cells. *Leukemia & Lymphoma,* 58**,** 1985-1988.

YAN, M., BUREL, S. A., PETERSON, L. F., KANBE, E., IWASAKI, H., BOYAPATI, A., HINES, R., AKASHI, K. & ZHANG, D.-E. 2004. Deletion of an AML1-ETO C-terminal NcoR/SMRT-interacting region strongly induces leukemia development. *Proceedings of the National Academy of Sciences of the United States of America,* 101**,** 17186-17191.

YAN, S., WANG, Y., CHEN, M., LI, G. & FAN, J. 2015. Deregulated SLC2A1 Promotes Tumor Cell Proliferation and Metastasis in Gastric Cancer. *International journal of molecular sciences,* 16**,** 16144-16157.

YAN, X.-J., XU, J., GU, Z.-H., PAN, C.-M., LU, G., SHEN, Y., SHI, J.-Y., ZHU, Y.-M., TANG, L., ZHANG, X.-W., LIANG, W.-X., MI, J.-Q., SONG, H.-D., LI, K.-Q., CHEN, Z. & CHEN, S.-J. 2011. Exome sequencing identifies somatic mutations of DNA methyltransferase gene DNMT3A in acute monocytic leukemia. *Nature Genetics,* 43**,** 309.

YANG, L., BRYDER, D., ADOLFSSON, J., NYGREN, J., MÅNSSON, R., SIGVARDSSON, M. & JACOBSEN, S. E. W. 2005. Identification of Lin[–]Sca1⁺kit⁺CD34⁺Flt3[–] short-term hematopoietic stem cells capable of rapidly reconstituting and rescuing myeloablated transplant recipients. *Blood,* 105**,** 2717.

YASSIN, M., AQAQE, N., YASSIN, A. A., VAN GALEN, P., KUGLER, E., BERNSTEIN, B. E., KOREN-MICHOWITZ, M., CANAANI, J., NAGLER, A., LECHMAN, E. R., DICK, J. E., WIENHOLDS, E., IZRAELI, S. & MILYAVSKY, M. 2019. A novel method for detecting the cellular stemness state in normal and leukemic human hematopoietic cells can predict disease outcome and drug sensitivity. *Leukemia*.

YEN, K., TRAVINS, J., WANG, F., DAVID, M. D., ARTIN, E., STRALEY, K., PADYANA, A., GROSS, S., DELABARRE, B., TOBIN, E., CHEN, Y., NAGARAJA, R., CHOE, S., JIN, L., KONTEATIS, Z., CIANCHETTA, G., SAUNDERS, J. O., SALITURO, F. G., QUIVORON, C., OPOLON, P., BAWA, O., SAADA, V., PACI, A., BROUTIN, S., BERNARD, O. A., DE BOTTON, S., MARTEYN, B. S., PILICHOWSKA, M., XU, Y., FANG, C., JIANG, F., WEI, W., JIN, S., SILVERMAN, L., LIU, W., YANG, H., DANG, L., DORSCH, M., PENARD-LACRONIQUE, V., BILLER, S. A. & SU, S.-S. M. 2017. AG-221, a First-in-Class Therapy Targeting Acute Myeloid Leukemia Harboring Oncogenic IDH2 Mutations. *Cancer Discovery,* 7**,** 478.

YERGEAU, D. A., HETHERINGTON, C. J., WANG, Q., ZHANG, P., SHARPE, A. H., BINDER, M., MARÍN-PADILLA, M., TENEN, D. G., SPECK, N. A. & ZHANG, D.-E. 1997. Embryonic lethality and impairment of haematopoiesis in mice heterozygous for an AML1-ETO fusion gene. *Nature Genetics,* 15**,** 303-306.

YI, W., CLARK, P. M., MASON, D. E., KEENAN, M. C., HILL, C., GODDARD, W. A., 3RD, PETERS, E. C., DRIGGERS, E. M. & HSIEH-WILSON, L. C. 2012. Phosphofructokinase 1 glycosylation regulates cell growth and metabolism. *Science (New York, N.Y.),* 337**,** 975-980.

YOUNG, V. R. & AJAMI, A. M. 2001. Glutamine: The Emperor or His Clothes? *The Journal of Nutrition,* 131**,** 2449S-2459S.

YU, J., LI, J., ZHANG, S., XU, X., ZHENG, M., JIANG, G. & LI, F. 2012. IGF-1 induces hypoxia-inducible factor 1α-mediated GLUT3 expression through PI3K/Akt/mTOR dependent pathways in PC12 cells. *Brain Research,* 1430**,** 18-24.

YUAN, Y., ZHOU, L., MIYAMOTO, T., IWASAKI, H., HARAKAWA, N., HETHERINGTON, C. J., BUREL, S. A., LAGASSE, E., WEISSMAN, I. L., AKASHI, K. & ZHANG, D.-E. 2001. AML1-ETO expression is directly involved in the development of acute myeloid leukemia in the presence of additional mutations. *Proceedings of the National Academy of Sciences,* 98**,** 10398.

ZAGORODNA, O., MARTIN, S. M., RUTKOWSKI, D. T., KUWANA, T., SPITZ, D. R. & KNUDSON, C. M. 2011. 2-Deoxyglucose-induced toxicity is regulated by Bcl-2 family members and is enhanced by antagonizing Bcl-2 in lymphoma cell lines. *Oncogene,* 31**,** 2738.

ZHANG, D., FEI, Q., LI, J., ZHANG, C., SUN, Y., ZHU, C., WANG, F. & SUN, Y. 2016. 2-Deoxyglucose Reverses the Promoting Effect of Insulin on Colorectal Cancer Cells In Vitro. *PLOS ONE,* 11**,** e0151115.

ZHANG, J., KALKUM, M., YAMAMURA, S., CHAIT, B. T. & ROEDER, R. G. 2004a. E Protein Silencing by the Leukemogenic AML1-ETO Fusion Protein. *Science,* 305**,** 1286.

ZHANG, J., KALKUM, M., YAMAMURA, S., CHAIT, B. T. & ROEDER, R. G. 2004b. E Protein Silencing by the Leukemogenic AML1-ETO Fusion Protein. *Science,* 305**,** 1286-1289.

ZHANG, S.-L., HE, Y. & TAM, K. Y. 2018a. Targeting cancer metabolism to develop human lactate dehydrogenase (hLDH)5 inhibitors. *Drug Discovery Today,* 23**,** 1407-1415.

ZHANG, Y., CHEN, X., GUEYDAN, C. & HAN, J. 2017. Plasma membrane changes during programmed cell deaths. *Cell Research,* 28**,** 9.

ZHANG, Y. & DERYNCK, R. 2000. Transcriptional regulation of the TGF-β-inducible mouse germ-line Ig α constant region gene by functional cooperation of Smad, CREB and AML family members. *Journal of Biological Chemistry*.

ZHANG, Y., GAO, S., XIA, J. & LIU, F. 2018b. Hematopoietic Hierarchy – An Updated Roadmap. *Trends in Cell Biology,* 28**,** 976-986.

ZHANG, Y. & ROWLEY, J. D. 2013. Chapter 75 - Leukemias, Lymphomas, and Other Related Disorders. *In:* RIMOIN, D., PYERITZ, R. & KORF, B. (eds.) *Emery and Rimoin's Principles and Practice of Medical Genetics.* Oxford: Academic Press.

ZHELEV, Z., IVANOVA, D., AOKI, I., SAGA, T. & BAKALOVA, R. 2015. 2-Deoxy-D-glucose Sensitizes Cancer Cells to Barasertib and Everolimus by ROS-independent Mechanism(s). *Anticancer Research,* 35**,** 6623-6632.

ZHONG, D., XIONG, L., LIU, T., LIU, X., LIU, X., CHEN, J., SUN, S.-Y., KHURI, F. R., ZONG, Y., ZHOU, Q. & ZHOU, W. 2009. The Glycolytic Inhibitor 2-Deoxyglucose Activates Multiple Prosurvival Pathways through IGF1R. *The Journal of Biological Chemistry,* 284**,** 23225-23233.

ZHOU, J.-H., ZHANG, T.-T., SONG, D.-D., XIA, Y.-F., QIN, Z.-H. & SHENG, R. 2016. TIGAR contributes to ischemic tolerance induced by cerebral preconditioning through scavenging of reactive oxygen species and inhibition of apoptosis. *Scientific Reports,* 6**,** 27096.

ZILFOU, J. T. & LOWE, S. W. 2009. Tumor suppressive functions of p53. *Cold Spring Harbor perspectives in biology,* 1**,** a001883-a001883.

ZUNDEL, W., SCHINDLER, C., HAAS-KOGAN, D., KOONG, A., KAPER, F., CHEN, E., GOTTSCHALK, A. R., RYAN, H. E., JOHNSON, R. S., JEFFERSON, A. B., STOKOE, D. & GIACCIA, A. J. 2000. Loss of PTEN facilitates HIF-1-mediated gene expression. *Genes & development,* 14**,** 391-396.